SEARCH FOR PHYSICS BEYOND THE STANDARD MODEL AT PARTICLE COLLIDERS USING MACHINE LEARNING TECHNIQUES

Inauguraldissertation
zur
Erlangung der Würde eines Doktors der Philosophie
vorgelegt der
Philosophisch-Naturwissenschaftlichen Fakultät
der Universität Basel

von

Ahmed Hammad
Basel, 2021

Genehmigt von der Philosophisch-Naturwissenschaftlichen Fakultät auf Antrag von Prof. Dr. Stefan Antusch, Dr. Oliver Fischer, Prof. Dr. Bernd Krusche und Prof. Dr. Tao Han.

Basel, 22.06.2021

Prof. Dr. Marcel Mayor
Dekan

Dedicated to my wife and my lovely twins
Omar & Mariam

ABSTRACT

Both ATLAS and CMS collaborations have reported the discovery of a resonance with a mass around 125 GeV, immediately associated with the long sought after Higgs boson. With this discovery, the standard model (SM) of particle physics is considered to be complete. However, non-vanishing neutrino masses provide the first confirmed hint towards physics beyond the SM. Extending the SM by sterile neutrinos can naturally explain the smallness of neutrino masses as observed by neutrino oscillation. Moreover, the problem of naturalness and the meta stability of the SM vacuum are hints for extending the SM scalar potential. A well motivated framework to naturally extend the SM scalar sector is to add $SU(2)_L$ complex scalar singlet, doublet or triplet to the SM Lagrangian. These hypothetical particles, the additional neutrinos or scalars, can give rise to a testable phenomenology when they have masses around the electroweak scale. They are actively searched for at the current colliders such as the Large Hadron Collider (LHC). The proposed future colliders, which are currently in the design phase, will be more powerful than the operated colliders to date.

In this dissertation, we investigate various aspects of sterile neutrino and heavy scalar phenomenology as well as the prospects of the current and future colliders searches for them. In particular, we investigate the prospects of searching for sterile neutrinos in low scale seesaw scenarios via the lepton flavor violating (but lepton number conserving) dilepton dijet signature at the high luminosity phase of the current LHC and the proposed Large Hadron electron Collider (LHeC). For part of the parameter space where the sterile neutrino is long lived, where the sterile neutrino mass is less than the W boson mass, we investigate the LHeC sensitivity to the displaced vertex search. For sterile neutrino mass above $\mathcal{O}(TeV)$ we investigate the LHeC sensitivity to the charged lepton flavor violation processes that can be generated at one loop level. We show that for all sterile neutrino mass range, from 5 GeV up to $\mathcal{O}(10^5)$ GeV, the LHeC could already probe the LFV signatures beyond the current experimental bounds.

In the second part of this dissertation, various aspects for heavy scalars extending the SM Lagrangian and various searches for heavy scalars at colliders are investigated. We start with studying the prospects of the LHeC search for heavy neutral scalars within the minimal extension of the SM Lagrangian with one additional complex scalar field. The mixing between the singlet and the SM doublet scalar fields gives rise to a SM like Higgs and a heavy scalar. Moreover, it induces phenomenological signatures for the heavy Higgs, analogously to the SM Higgs boson, that can be tested at the LHeC. Using multivariate analysis and machine learning techniques we show that the LHeC could probe the heavy signatures for masses between 200 and 800 GeV beyond the current LHC and its future high luminosity phase sensitivity.
Also, the prospect signature of the spontaneous CP violation are investigated

via the angular distribution of tau lepton pair produced from heavy scalar decays. For this purpose, we focus on the Two Higgs Doublet Model, as an example model, which can offer a source for CP violation in its scalar potential. Considering a benchmark point that is compatible with the current constraints but within reach of the high luminosity LHC, we study the prospects of determining the CP property of a heavy neutral Higgs state. We show that CP conservation in the scalar sector can be excluded at the 90% CL for a benchmark point with maximal CP violation if the background can be controlled with a relative accuracy of 0.5%, which could be the accuracy target for future LHC measurements.

Finally, we study the phenomenology of the minimal extension of the SM Lagrangian with a scalar triplet field. The precedence of this scenario over any other consideration that after the symmetry breaking, when the components of the triplet field have masses around the electroweak scale, the model features a rich phenomenology. We discuss the current allowed parameter space taking into account all relevant constraints, including charged lepton flavour violation as well as collider search. In part of the parameter space the triplet components can be long lived, with displaced distance, in the range of cm, potentially leading to a characteristic displaced vertex signature where the doubly charged component decays into same sign charged leptons. The fact that the LHC is looking for doubly charged scalars via track only analysis or charged stable particles, makes this part of the parameter space still untested by the current LHC measurements. By performing a detailed analysis at the reconstructed level we show that already at the current run of the LHC a discovery would be possible for the considered parameter point, via dedicated searches for displaced vertex signatures.

PUBLICATIONS

This dissertation is based on research that lead to various publications [1–10] to which the author contributed during his PhD studies conducted under the supervision of Prof. Dr. Stefan Antusch and Dr. Oliver Fischer at the Department of Physics of the University of Basel from October 2017 to October 2021. This dissertation entails figures and tables that are taken from these publications:

[1] Stefan Antusch, Oliver Fischer, A. Hammad, and Christiane Scherb. "Testing CP Properties of Extra Higgs States at the HL-LHC." In: *JHEP* 03 (2021), p. 200. DOI: 10.1007/JHEP03(2021)200. arXiv: 2011.10388 [hep-ph].

[2] Stefan Antusch, A. Hammad, and Ahmed Rashed. "Searching for charged lepton flavor violation at ep colliders." In: *JHEP* 03 (2021), p. 230. DOI: 10.1007/JHEP03(2021)230. arXiv: 2010.08907 [hep-ph].

[3] Stefan Antusch, A. Hammad, and Ahmed Rashed. "Probing Z′ mediated charged lepton flavor violation with taus at the LHeC." In: *Phys. Lett. B* 810 (2020), p. 135796. DOI: 10.1016/j.physletb.2020.135796. arXiv: 2003.11091 [hep-ph].

[4] Stefan Antusch, Oliver Fischer, and A. Hammad. "Lepton-Trijet and Displaced Vertex Searches for Heavy Neutrinos at Future Electron-Proton Colliders." In: *JHEP* 03 (2020), p. 110. DOI: 10.1007/JHEP03(2020)110. arXiv: 1908.02852 [hep-ph].

[5] W. Abdallah, A. Hammad, S. Khalil, and S. Moretti. "Dark matter spin characterization in mono-Z channels." In: *Phys. Rev. D* 100.9 (2019), p. 095006. DOI: 10.1103/PhysRevD.100.095006. arXiv: 1907.08358 [hep-ph].

[6] Stefan Antusch, Oliver Fischer, A. Hammad, and Christiane Scherb. "Low scale type II seesaw: Present constraints and prospects for displaced vertex searches." In: *JHEP* 02 (2019), p. 157. DOI: 10.1007/JHEP02(2019)157. arXiv: 1811.03476 [hep-ph].

[7] Luigi Delle Rose, Oliver Fischer, and A. Hammad. "Prospects for Heavy Scalar Searches at the LHeC." In: *Int. J. Mod. Phys. A* 34.23 (2019), p. 1950127. DOI: 10.1142/S0217751X19501276. arXiv: 1809.04321 [hep-ph].

[8] W. Abdallah, A. Hammad, S. Khalil, and S. Moretti. "Searching for Charged Higgs Bosons in the B − L Supersymmetric Standard Model at the High Luminosity Large Hadron Collider." In: *Phys. Lett. B* 788 (2019), pp. 65–69. DOI: 10.1016/j.physletb.2018.10.065. arXiv: 1806.03585 [hep-ph].

[9] Stefan Antusch, Eros Cazzato, Oliver Fischer, A. Hammad, and Kechen Wang. "Lepton Flavor Violating Dilepton Dijet Signatures from Sterile Neutrinos at Proton Colliders." In: *JHEP* 10 (2018), p. 067. DOI: 10.1007/JHEP10(2018)067. arXiv: 1805.11400 [hep-ph].

[10] W. Abdallah, A. Hammad, A. Kasem, and S. Khalil. "Long-lived B-L symmetric SSM particles at the LHC." In: *Phys. Rev. D* 98.9 (2018), p. 095019. DOI: 10.1103/PhysRevD.98.095019. arXiv: 1804.09778 [hep-ph].

ACKNOWLEDGEMENTS

I would like to thank all of those people who helped make this dissertation possible. First, I wish to thank my supervisor Prof. Dr. Stefan Antusch and Dr. Oliver Fischer for all their guidance, encouragement, support, and patience. their sincere interest in various areas of particle physics has been a great inspiration to me throughout working on this dissertation. I am so grateful that I learned a lot from you not only in physics but also from your way of working.
I want to thank Dr. Ahmed Rashed for the very pleasant collaboration and fruitful discussions.
Thanks to my MSc. supervisors Prof. Dr. Stefan Moretti and Prof. Dr. Shaaban Khalil for the continues collaboration and fruitful work.
I would like to thank Waleed Abdallah, Eros Cazzoto, Christiane Schreb, Kechen Wang, Johannes Rosskopp for their collaboration and discussions.
I express my sincere thanks to Waleed Esmail and Vasja Susic, Ahmed Moursi and Mustafa Ashri for the very pleasant and fruitful discussions. Last but not least, I would like to thank my understanding and patient wife for her support.

CONTENTS

Part I

INTRODUCTION

1 INTRODUCTION

1.1 INTRODUCTION

The Standard Model (SM) [11–13] is the Quantum Field Theory that rules the world of the elementary particles at the energy scales explored so far, when gravitational interactions can be neglected. The model is based on the gauge groups $SU(3)_c \times SU(2)_L \times U(1)_Y$. The SM recognizes two types of elementary fermions: quarks and leptons. Fermions are arranged under the $SU(2)_L$ in six left-handed families: three families consist of left-handed quark doublets, and three families consist of left-handed lepton doublets. Each left-handed fermion has a corresponding right-handed one that does not participate in the doublets. In the leptonic section, electron, muon and tau (which are referred to as different flavors of the lepton), are associated with neutral fermions called neutrinos. Neutrions in the SM come with left-handed doublets only, thus they remain massless in the SM framework. The SM successfully describes an impressive amount of data, but there are experimental and theoretical evidences that call for some extensions.

First, on the experimental side, the SM is inadequate for describing the experimentally observed pattern of neutrino oscillation [14–16]. If we insist in keeping the field content of the minimal SM, the only way to account for neutrino oscillation is to add to the SM Lagrangian some renormalizable operators which, after the spontaneous breaking of the gauge symmetry, generate mass terms for left-handed neutrinos. Neutrinos in the SM come in three massless[1] flavors, which is in conflict with the neutrino oscillation phenomenon. Beside the neutrino oscillation phenomenon, further experiments have confirmed that neutrinos can convert their flavors [17]. These phenomena can only be explained when neutrinos have masses and mixing which requires extensions of the SM contents. There are wide range of models that explain the tiny neutrino masses. Within the class of renormalizable models that can provide neutrino mass terms, adding right-handed neutrinos to the SM content is the most elegant solution. The additional right-handed neutrinos are singlets under the SM gauge symmetry where they couple only to the left-handed neutrinos and the Higgs field via small Yukawa couplings. The smallness of the neutrino masses can be explained by small values for the Yukawa couplings; this mechanism is known as type-I seesaw mechanism [18–28]. However, this mechanism does not fix completely the overall scale of the right-handed neutrino mass as well the neutrino mixing parameters that remain arbitrary. For instance, values for the mass scale of the heavy neutrinos can be motivated from the eV range up to way above the Grand Unification scale. Neutrino oscillation experiment can test some of the parameters like the mass squared difference between the light neutrino mass states, but it can not determine the absolute neutrino mass

[1] *The masslessness of three neutrinos corresponds to the lepton number conservation*

scale. Furthermore, with the current measurements, different arrangements of the neutrino mass states are allowed for the ordering of the neutrino masses, namely the normal hierarchy (NH) or the inverted hierarchy (IH). Other experiments like Neutrino Ettore Majorana Observatory (NEMO3) detector is devoted to the search for neutrinoless double beta decay $(0\nu\beta\beta)$ [29, 30]. Neutrinoless double beta decay is dedicated to study the intrinsic neutrino nature; its observation could prove the neutrino is its own anti-particle: if it is Majorana fermion. Moreover, $(0\nu\beta\beta)$ experiments are sensitive to the half life of the isotope involved in the neutrinoless decay which leads to bounds on the effective Majorana mass and the neutrinos mixing elements [31, 32][2] . Cosmological data can also be used to test neutrino properties, in particular their masses. The cosmic neutrino background has not been detected yet, but the accurate agreement between the calculated and observed primordial abundances of light elements, as well as the analysis of the power spectrum of the cosmic microwave background set an upper bound on the sum of neutrino masses [33–36]. Lepton Flavor Violation (LFV) is one of the main phenomena that test, indirectly, the existence of heavy neutrinos. The current LVF experiments [37–41] are sensitive to neutrinos mixing [1] which set sever bounds in the mixing parameters[2]. The enormous data delivered by the Large Hadron Collider (LHC) makes it able to cover the heavy neutrino searches at mass scale in the TeV range. In the last years, CMS and ATALS carried out extensive searches for heavy neutrinos in a wide range of its possible decay products [45–48]. The fact that no signal has been observed above the background enables the LHC to set bounds on the mixing parameters and the neutrino mass.

[2] *Theoretically, the half life time is expressed in terms of the phase space factor as well as the nuclear matrix element which, in principle, set bounds on the combination of effective Majorana mass and neutrino mixing*

Second, on the theoretical side, the scale difference between the mass of the electroweak Higgs boson and the Planck mass is a big puzzle. The calculations of the Higgs mass using the quantum field theory of the SM show that it receives contributions from all energy scales, all the way up to the highest energy scale at which the Standard Model is valid. The most obvious choice is thus the Plank energy scale. This difference of many orders of magnitude between Plank scale and electroweak scale is referred to as the "The Hierarchy Problem". The electrically neutral part of the Standard Model Higgs field is a complex scalar H with a classical potential

$$V = \mu^2 |H|^2 + \lambda |H|^4 \ .$$

The SM requires a non-vanishing vacuum expectation value (VEV) at the minimum of the potential. This will occur if $\lambda > 0$ and $\mu^2 < 0$, resulting $v = \langle H \rangle = \sqrt{\mu^2/2\lambda}$. The problem is that Higgs mass receives enormous quantum corrections from the virtual effects of every particle that couples, directly or indirectly, to the Higgs field. The largest contribution comes from the top quark correction. Fortunately, the cancellation of the top quark correction can

1 The reason why the LFV measurements constrain the neutrinos mixing parameters is that heavy neutrinos can mediate the LFV processes at one loop level and the form factors of the loop are proportional to the mixing parameters squared. Therefore the sensitivity to the neutrino mass is rather poor.

2 The current limit on the neutrino mixing parameters are $\mathcal{O}(10^{-6})$ while future upgrades are expected to increase the current sensitivity by one or two orders of magnitude [42–44].

take place by adding extra scalar[3] to the SM Higgs potential. In general, extra scalars contribute to the Higgs mass correction with an opposite sign to the top quark contribution. Another aspect that motivates the extension of the scalar sector is the possible improvement of the metastable SM vacuum. The observed Higgs mass $m_H = 125.09 \pm 0.24$ GeV [49] leads to a negative value of the Higgs quartic coupling λ at some energy scale below the Planck scale, making the Higgs vacuum metastable. Extending the scalar sector of the SM with extra scalars retains the stability of the SM potential at higher energies [50]. In general, the Higgs sector is very sensitive to any new physics and can be easily captured at colliders. Extending the scalar sector of the SM can lead to three main observational effects;

[3] *For solving the problem, the additional scalar can be either an $SU(2)_L$ singlet, doublet or triplet*

- Modifications of the SM Higgs boson properties, i. e.couplings, decay rates and the CP properties.
- Existence of additional electrically neutral or charged scalars, which can be produced and tested at colliders.
- Additional scalars can have new decay modes with final state particles that are absent in the SM which could be studied at the collider.

So far, all measurements of the 125 GeV Higgs boson properties are (within the current experimental precision) in agreement with the SM predictions, and searches for additional scalar states have not found any convincing hints of new particles. All these experimental searches constrain the parameters of the additional scalars. Extending the SM scalar sector can be done by adding $SU(2)_L$ signlet, doublet or triplet scalars as follow

- Adding a complex scalar filed, which is a singlet under the SM gauge symmetry, is one of the simplest extension of the SM Higgs potential. The scalar sector is thus described by the potential

$$V(H,S) = m_1^2 H^\dagger H + m_2^2 S^\dagger S + \lambda_1 (H^\dagger H)^2 + \lambda_2 (S^\dagger S)^2 + \lambda_3 (H^\dagger H)(S^\dagger S)\,,$$

  which is the most general renormalizable scalar potential of the SM $SU(2)_L$ with Higgs doublet H and the complex scalar $SU(2)_L$ singlet S. The mixing between the two scalars form two physical neutral states h_1^{SM} and h_2. In here it is necessary to fix the mass of h_1^{SM} to the observed 125 GeV scalar while the mass of the second scalar, h_2, is controlled by the measurements. The mixing between the two scalars leads to interesting collider signatures; (i) the signal strength[4] of h_1^{SM} are universally suppressed by the mixing angle; (ii) the additional scalar, h_2, can be searched for at the colliders, produced and decay in the same way as the h_1^{SM}, but with different signal rate; (iii) if h_2 is heavier than the h_1^{SM}, it can decay to two h_1^{SM} bosons creating a unique signature for new physics; (iiii) if the mixing between the two scalars is neglected then h_2 can be considered as dark matter candidate.

[4] *The signal strength is the ratio of the SM couplings to the measured Higgs couplings*

- A minimal prototype for an extended scalar sector is the Two Higgs Doublet Model (THDM) where the scalar sector of the SM is extended by an

additional scalar $SU(2)_L$ doublet field. One of the main motivations of the THDM is the ability to explain the baryon asymmetry of the universe with an additional source of CP violation in the scalar potential [51]. The possibilities for explicit or spontaneous CP violation constitute one of the attractive features of THDM. According to the current measurements, the discovered scalar resonance is compatible with the CP even SM-like Higgs boson but the possibility of a more complex scalar potential that includes CP violation is not ruled out yet. As there is no additional scalar resonances have been found to date the additional scalar doublets are tightly constrained. In general, the THDM potential is very rich and contains 14 free parameters that can introduce Flavor Changing Neutral Currents (FCNCs) at the tree level. As there is no hint for FCNC yet, the THDM potential receives additional constraints. Similar to the SM Higgs boson, the scalar particles in the THDM can be studied at particle colliders such as the LHC and its future high luminosity phase, HL-LHC. Once another scalar is discovered, its CP properties have to be studied similar to the SM Higgs boson. The CP properties can be studied via the spin correlation of the final state leptons from the scalar decays to Z boson pair [52], the angular correlation of tau lepton pairs from the scalar decays [53] or in the top quark associated production with the scalar [54].

- Extending the SM Lagrangian with a $SU(2)_L$ triplet is an attractive possibility to generate the observed light neutrino masses. This mechanism for neutrino mass generation is usually referred to as the type-II seesaw. After the electroweak symmetry breaking the induced vacuum expectation value of the scalar triplet gives mass to the SM massless neutrino via its coupling to the lepton $SU(2)_L$ doublets. Adding a scalar triplet to the SM potential was initially introduced as a mechanism for generating neutrino masses but when the components of the triplet field have masses around the electroweak scale, the model features a rich phenomenology that can be studied at the particle colliders. The low energy scale version of the type-II seesaw mechanism has implications for various well known observables at different energy scales [55, 56]. The triplet field is defined as,

$$\Delta = \begin{pmatrix} \frac{\Delta^+}{\sqrt{2}} & \Delta^{++} \\ \Delta^0 & \frac{\Delta^+}{\sqrt{2}} \end{pmatrix}, \tag{1}$$

  with its doubly charged component being of particular importance for phenomenological studies. It can decay into a pair of same sign charged leptons via its coupling with non-diagonal Yukawa matrix to the $SU(2)_L$ lepton doublets. The importance of this kind of decay is that it does not have any SM background contribution. This signature has been searched for at different colliders: The LHC [57–60], the Large Electon Positron collider (LEP) [61–63] and at the Tevatron [64–67]. Without any hint for new physics, these experiments provide stringent constraints from their direct searches that requires the mass of the doubly charged scalar to be above 600 GeV for the part of the parameter space where the Yukawa coupling

is not too small such that the doubly charged can decay promptly. Moreover, the part of the parameter space where the Yukawa coupling is too small is of particular interest while the doubly charged scalar is no longer decaying promptly but rather long lived or even stable charged particle that can skip from the detector parts before it decays. Considering the doubly charged scalar as long lived particle has important consequences for the LHC searches where the above mentioned mass limit from the prompt searches can no longer be applied. If the doubly charged has a very long life time such that it can pass through all detector parts one might consider it as stable charged particles with characteristic energy deposition in the different sub detectors. In general, massive doubly charged scalars leave a unique track inside the pixel tracker that can be easily seen [68–70]. Moreover, when the decays of long lived doubly charged can occur inside the detector, one might also search for the displaced secondary vertices. This possibility has recently been discussed in ref. [71], where it has been claimed that the HL-LHC can probe a broad part of the parameter space via such displaced vertex searches, restricted however by the heavy stable charged particles measurements.

Although most of the current collider studies in high energy particle physics focus on the current enormous data delivered from the LHC, the various proposed future colliders with their envisaged high energies and high luminosity are also interesting for testing new physics signatures. There are several future colliders that are being proposed from different organizations with the prime goal to precisely test the SM and to search for BSM physics [72–75]. One of the proposed future colliders is the Large Hadron electron Collider (LHeC) [76] which is proposed to operate concurrenting to the LHC period using one of the proton beams and a new electron beam. The LHeC is proposed to collide 7 TeV proton beam with 60 GeV electron beam with 1.3 TeV center of mass energy. Accordingly, all non-QED physics is expected to be boosted in the forward direction of the detector.[5] . Its unique kinematics together with its clear environment and low pile up, make the LHeC one of the most sensitive future colliders for new physics searches.

[5] *The forward direction of the detector is planned to be the proton direction*

1.2 OUTLINE

This dissertation is organised as follows: The introduction is given in Part I. Part II discusses the basics of neutrino and Higgs physics. In Chapter 2, we first discuss the origin of neutrino masses and mixing in the presence of additional right-handed neutrinos. We also discuss the different types of neutrinos, Weyl, Dirac or Majorana, and how to arrange a four component neutrino spinor such that it can be massive. Chapter 3 briefly discusses different models beyond the SM for neutrino mass generation. Chapter 4 discusses the Higgs physics beyond the SM. We focus on models that minimally extend the SM Lagrangian by $SU(2)_L$ singlet, doublet and triplet scalars. In chapter 5, we discuss the methodology of performing a collider analysis using machine learning methods as the Boosted Decision Trees (BDT). We also briefly discuss some of the statistical methods as the maximum likelihood method for limits on the physi-

cal parameters. Part III is concerned with the electroweak scale sterile neutrino and Higgs phenomenology with their searches at the current and future colliders. Chapter 6 discusses the prospects of searching for sterile neutrinos in the low scale seesaw model with lepton number conserving symmetry via the lepton flavor violation dilepton plus dijets signature. The study focuses on the final state $e^{\pm}\mu^{\pm}jj$ at the HL-LHC and its future upgrade, the Future Circular Collider (FCC-hh). Chapter 7 discusses the analysis of the lepton flavor violating lepton plus trijet signature and the displaced veterx signature of sterile neutrino at the LHeC within the low scale seesaw model with protected lepton number symmetry (SPSS). In chapter 8, we investigate the sensitivity of electron proton colliders for charged lepton flavor violation (cLFV) in an effective theory approach. We also consider the symmetry protected seesaw scenario where such lepton flavor violation processes exist at the loop level. In chapter 9, we discuss the prospects of the LHeC search for a complex heavy scalar singlet extended the SM scalar potential. For the search, three different decay channels are considered and multivariate techniques are used. Chapter 10 discusses the possibility to discover CP violation in the THDM at the HL-LHC. The study first evaluates the currently allowed parameter region in the THDM. For a benchmark point, the prospects of determining the CP properties of an extra neutral Higgs state are investigated. Chapter 11 discusses the status of extending the SM Lagrangian with scalar triplet forming the minimal type-II seesaw model. The study evaluates the currently allowed parameter space of the model as well as signatures from prompt and displaced decays are considered. Summary of the dissertation is given in chapter 12.

Part II

BACKGROUND

2

INRODUCTION TO MASSIVE NEUTRINOS AND NEUTRINO MIXING

The origin of the small neutrino masses is still mystery. However, it is believed that neutrino masses are a low energy manifestation of physics beyond the Standard Model and thus their smallness is due to a suppression generated by a new higher energy scale. On this front, adding right-handed Majorana (sterile) neutrinos to the SM is considered as the simplest natural mechanism for massive neutrinos, which mix with the left-handed SM neutrinos via the interaction with the SM field generating a so called "Dirac mass term". The smallness of the Dirac neutrino masses is ensured, unnaturally, by the smallness of the Yukawa coupling while Majorana neutrino mass is large compared to the weak scale. Due to the mixing between Majorana and Dirac neutrinos, the mass eigenstates are mixture of both of them, and we end up with light and heavy neutrinos. The light neutrinos satisfy the measured neutrino mass difference while the heavy ones can be of $\mathcal{O}(TeV)$ or above. In this chapter we investigate the properties of Dirac and Majorana neutrinos and the most general case for neutrino mixing.

2.1 DIRAC OR MAJORANA NEUTRINOS

The general solution of the Dirac equation is not an irreducible representation of the Lorentz group.[6] The proper Lorentz algebra is isomorphic to $SU(2) \times SU(2)$ so that a left chiral fermion would be a doublet under one of the $SU(2)$'s and singlet under the other. A left chiral fermion, χ_L, is represented by $(\frac{1}{2}, 0)$ while right chiral fermion, χ_R, is represented by $(0, \frac{1}{2})$. The problem with assigning a frame-independent helicity to a fermion disappears if the fermion is massless. Moreover, in the massless fermion limit, γ_5 commutes with the mass-independent term in the Dirac Hamiltonian. Without any ambiguity, massless fermions have their helicity and chirality states being the same. Each of them has a two component spinor and is called Weyl fermion. In fact, space inversion transforms χ_L into χ_R and vice versa, implying that parity conservation requires the existence of both chiral components. However, the discovery of parity violation validates the possibility to describe massless particles with Weyl fermions. At the time when there was no indication of the existence of neutrino masses and it was likely the neutrinos participate in weak interactions through its left handed chiral component, Salam proposed to describe the neutrino with a left handed Weyl spinor. This is the so called two component theory of massless neutrinos, which has been incorporated in the SM, where neutrinos are massless and described by left-handed Weyl spinors only. The reducible representation for a fermion field is $(\frac{1}{2}, 0) + (0, \frac{1}{2})$ which tells us that a general fermion field can be described by two massless

[6] *This can be seen by the commutation of γ_5 with all generators of the representation*

Weyl fields. To this end we can ask how Majorana or Dirac fields can be built from Weyl fermions ?

Massive Majorana fermions must have both left and right chiral components. While it is clear that we need both chiralities, the question now is how to arrange the two chiralities such that the Majorana condition is satisfied[1]. A left chiral Weyl field satisfies the equation

$$(1+\gamma_5)\chi_L = 0\,, \tag{2}$$

with χ_L is the two component Weyl fermion field and $\gamma_5 = i\gamma^0\gamma^1\gamma^2\gamma^3$, while left and right-chiral operators defined as $L/R = \frac{1}{2}(1 \mp \gamma_5)$. Taking the complex conjugate and multiplying by γ_0 gives

$$\gamma_0 C(1+\gamma_5)\chi_L^* = 0\,, \tag{3}$$

with C the charge conjugate matrix. With $C\gamma_5^\top = \gamma_5 C$ and using the anti-commutation of the Gamma matrices we get

$$(1-\gamma_5)\gamma_0 C\chi_L^* = 0\,. \tag{4}$$

The last equation shows that right-chiral Weyl fermion field is the charge conjugated left-chiral field with right-chiral Weyl fermion satisfies the equation

$$(1-\gamma_5)\hat{\chi}_L = 0 \tag{5}$$

Accordingly, the four component Majorana spinor can be constructed from two component left-handed Weyl spinors as

$$\psi = \chi_L + \hat{\chi}_L\,, \tag{6}$$

which satisfies the reality condition for Majorana field [77]. It is important to stress here that a four component Majorana fermion can be constructed from one Weyl fermion and its charge conjugate.

Massive Dirac fermions should also contain both chiralities and they are complex fields in general. The Majorana reality condition requires the righ-chiral field to be the charge conjugated left-chiral field which is not the case for Dirac fermions. Thus, unlike the Majorana four component spinor, the Dirac four component spinor can be constructed from two different Weyl fermions as

$$\psi = \chi_L + \chi_R\,. \tag{7}$$

Now, we have the right arrangement for both Dirac and Majorana fields such that they can be massive.

2.1.1 *massive neutrinos*

Back to the SM Lagrangian, charged leptons, quarks and gauge bosons acquire their masses via the spontaneous symmetry breaking. However, the SM can not account for non-zero neutrino masses.[7] Since with the particle content

[7] *The current implementation of the SM particle content contains only left-handed neutrinos*

1 Majorana condition implies that the particle is identical to its antiparticle, i.e. a Majorana fermion is its own antiparticle [77]

of the SM there are no possible gauge invariant and renormalisable terms for neutrino masses, new particles can be added to the SM particle content. The extension of the SM that is needed is the introduction of right-handed components $\chi_{\alpha R}$, with $\alpha = e, \mu, \tau$. The essential characteristic of these fields is that they are singlets under the SM gauge groups. In this dissertation we follow the usual convention of calling the new right-handed fields sterile neutrinos in order to distinguish them from the active neutrino fields of the SM which participate in weak interactions through their left-handed components. Dirac mass term can be generated by adding three right-handed neutrinos[8] that minimally extend the SM Lagrangian by Yukawa term as

[8] *The additional three right-handed neutrinos correspond to the lepton flavors, e, μ and τ*

$$\mathcal{L}_{Y,lep} = -\left(\sum_{\alpha,\beta=e,\mu,\tau} Y^{l}_{\alpha\beta} \overline{L_{\alpha L}} \Phi l_{\beta R} + \sum_{\alpha,\beta=e,\mu,\tau} Y^{\nu}_{\alpha\beta} \overline{L_{\alpha L}} \widetilde{\Phi} N_{\beta R} \right) + \text{H.c.}\,, \quad (8)$$

where Y^{l} and Y^{ν} are the charged lepton and neutrino Yukawa matrix, $N_{\beta R}$ are the right handed neutrinos, $L_{\alpha L}$ are the $SU(2)$ lepton doublets, $l_{\beta} R$ are the right handed charged leptons. The Higgs field in the the unitary gauge $\Phi = \begin{pmatrix} 0 \\ \frac{v+h}{\sqrt{2}} \end{pmatrix}$, where h is the SM Higgs and v is the Higgs vacuum expectation value. The first term in eq. 8 is the normal SM Yukawa term that generates masses for the charged lepton while the second term is the new Yukawa term that generates neutrino masses. The lepton Yukawa Lagrangian can be written in matrix form[9] as

[9] *Given that Y^{ν} is a complex $3 \times n$ matrix, with n the number of the right handed neutrinos*

$$\mathcal{L}_{Y,lep} = -\left(\frac{v+h}{\sqrt{2}} \right) \left(\overline{l_L} Y^{l} l_R + \overline{\nu_L} Y^{\nu} N_R \right) + \text{H.c.}\,, \quad (9)$$

where l_L, l_R, ν_L and N_R are vectors with dimension three. In the SM framework the charged lepton Yukawa matix, Y^{l}, can be diagonalized through a bi-unitary transformation

$$V^{l\dagger}_{L} Y^{l} V^{l}_{R} = y^{l}\,, \quad (10)$$

where y^{l} is the diagonal 3×3 Yukawa matrix and V^{l}_{L} and V^{l}_{R} are two 3×3 unitary matrices.[10] The neutrino Yukawa matrix, Y^{ν}, is not diagonal and thus the involved neutrinos are not in the mass basis. Following the same procedure as for the charged lepton Yukawa matrix, the neutrino Yukawa matrix can be diagonalized by two unitary matrices

[10] *Unitary matrices satisfy $V^{l\dagger}_{L} = (V^{l}_{L})^{-1}$ and $V^{l\dagger}_{R} = (V^{l}_{R})^{-1}$*

$$V^{\nu\dagger}_{L} Y^{\nu} V^{\nu}_{R} = y^{\nu}\,, \quad (11)$$

where y^{ν} is the diagonal neutrino Yukawa matrix and the neutrino mass eigenstates are defined as

$$\nu'_{\alpha L} = V^{\nu\dagger}_{L} \nu_{\alpha L} \quad \text{and} \quad N'_{\beta R} = V^{\nu\dagger}_{R} N_{\beta R}\,, \quad (12)$$

where $\nu'_{\alpha L}$ and $N'_{\beta R}$ are the neutrino mass eigenstates with $\alpha, \beta = 1, 2, 3$. The diagonalized lepton Yukawa Lagrangian now reads

$$\mathcal{L}_{Y,lep} = -\left(\frac{v+h}{\sqrt{2}} \right) \left(\sum_{\alpha=e,\mu,\tau} \overline{l_{\alpha L}} y^{l}_{\alpha} l_{\alpha R} + \sum_{k=1}^{3} \overline{\nu'_{kL}} y^{\nu}_{k} N'_{kR} \right) + \text{H.c.} \quad (13)$$

Using eq. 7, massive Dirac neutrinos can be defined as

$$\nu_k = \nu'_{kL} + N'_{kR}, \quad \text{with } k = 1,2,3\,, \tag{14}$$

we finally obtain

$$\mathcal{L}_{Y,lep} = -\sum_{\alpha=e,\mu,\tau} \frac{y^l_\alpha v}{\sqrt{2}} \overline{l_\alpha} l_\alpha - \sum_{k=1}^{3} \frac{y^\nu_k v}{\sqrt{2}} \overline{\nu_k} \nu_k\,, \tag{15}$$

with the Dirac neutrino mass defined by the SM Higgs VEV and the Yukawa neutrino matrix as

$$m_k = \frac{y^\nu_k v}{\sqrt{2}}, \quad \text{with } k = 1,2,3\,. \tag{16}$$

In order to reproduce achieve the measured neutrino masses, fixing the $v = 246$ GeV, the elements of Yukawa matrix have to be small.[2]

The fact that Majorana fermions are singlets under the SM gauge transformations means that they are allowed to have a Majorana mass term without the restriction of EWSB as the only source for giving mass. Thus the Lagrangian density may contain a term

$$\mathcal{L}_M = -\sum_{\alpha\beta} \frac{M_{\alpha\beta}}{2} \left(\overline{\nu^c_{\alpha L}} \nu_{\beta L} + \overline{\nu_{\beta L}} \nu^c_{\alpha L} \right)\,, \tag{17}$$

with $M_{\alpha\beta}$ a non diagonal Majorana mass matrix and α, β denoting the number of additional Majorana neutrinos. The factor of $\frac{1}{2}$ is necessary to remove the double counting of the degrees of freedom while Majorana fermions are their own antiparticles. The fact that the SM contains only left-handed neutrino raises an important question if it is possible that SM neutrinos can have Majorana mass term, as in eq. 17. The answer is no, because such a Mjorana term is not allowed by the SM gauge symmetry.[11] Thus, such a term can not be obtained in the SM content at the renormalizable level but it can be constructed as a higher dimensional non-renormalizable term as [78]

[11] *Majorana term, $\overline{\nu^c_L}\nu_L$, has weak isospin $I_3 = 1$ and hypercharge $Y = -2$. Since the SM does not contain any weak isospin triplet with $Y = 2$, the constructed Majorana term is not renormalizable*

$$\mathcal{L}_5 = \frac{\kappa_{\alpha\beta}}{2m_{\alpha\beta}} \left(\overline{L^c_\alpha} \sigma_2 \Phi \right) \left(\overline{L_\beta} \sigma_2 \Phi \right) + \text{H.c.}\,, \tag{18}$$

where $\kappa_{\alpha\beta}$ is a dimensionless coupling and $m_{\alpha\beta}$ is a constant with dimension of mass. The non-renormalizable term, $\mathcal{L}_5$, is not acceptable in the framework of the SM because it contains a product of fields with mass dimension larger than four. It is important, however, to realize that the SM can not be considered as a fundamental theory but only as an effective theory which is the low energy product of the symmetry breaking of a high energy theory. After the electroweak symmetry breaking, a Majorana mass can be generated

$$\mathcal{L}_M = -\sum_{\alpha\beta} \frac{\kappa_{\alpha\beta} v^2}{2m_{\alpha\beta}} \left(\overline{\nu^c_{\alpha L}} \nu_{\beta L} + \overline{\nu_{\beta L}} \nu^c_{\alpha L} \right)\,, \tag{19}$$

2 The smallness of the Yukawa couplings still unresolved which opens up the suggestions that the SM is an effective model stemmed from new physics that decouple at higher energy scale

with effective Majorana mass $M_{\alpha\beta} = \frac{\kappa_{\alpha\beta} v^2}{m_{\alpha\beta}}$, which is the non-diagonal Majorana mass matrix in eq. 17. As in the Dirac case, the Majorana mass matrix, $M_{\alpha\beta}$, is in general non-diagonal and in order to express the neutrinos in the mass eigenstates the mass matrix has to be diagonalized. The Majorana mass matrix can be diagonlaized by Takagi decomposition [79] using only one unitary matrix

$$(V_L^\nu)^\top \, M \, V_L^\nu = m^\nu \,, \tag{20}$$

with m_ν is the diagonal Majorana mass matrix. The mass eigenstates is obtained by the transformation

$$\nu'_{kL} = (V_L^\nu)^\dagger \, \nu_{kL} \,, \tag{21}$$

where ν'_{kL} are the diagonal mass eigenstates and k denotes the number of the additional Majorana neutrinos. The diagonalized Majorana mass term reads

$$\mathcal{L}_M = -\frac{1}{2} m_k^\nu \overline{\nu'^c_{kL}} \nu'_{kL} + \text{H.c.} \tag{22}$$

Using eq. 6, massive Majorana field can be defined as

$$N_k = \nu'_{kL} + \nu'^c_{kL} \,, \tag{23}$$

and we can finally obtain Majorana Lagrangian in the mass basis as

$$\mathcal{L}_M = -\frac{1}{2} \sum_k m_k^\nu \overline{N_k} N_k \,. \tag{24}$$

2.2 LEPTONIC MIXING AND MIXING PARAMETERS

The leptonic mixing can be derived in analogy to the SM quarks. In general, any unitary $N \times N$ matrix depends on $N(N-1)/2$ mixing angles and $N(N+1)/2$ phases. In Dirac neutrinos case, with three active neutrinos, the mixing matrix can be written in terms of three mixing angles and six phases. However, not all phases are physical observables while some of them can be absorbed by proper phase transformations. The leptonic Lagrangian is invariant under global phase transformation of the lepton fields as

$$\nu_\alpha = e^{i\phi_\alpha^\nu} \nu_\alpha, \quad l_\alpha = e^{i\phi_\alpha^l} l_\alpha \,. \tag{25}$$

Physical phases can be obtained from their effect on the leptonic mixing in the weak charged current

$$J_{cc}^\mu = \sum_{\alpha=e,\mu,\tau} \frac{g_2}{\sqrt{2}} \overline{\nu'_{\alpha L}} \gamma^\mu l'_{\alpha L} = \sum_{\alpha=e,\mu,\tau} \sum_{\beta=1,2,3} \frac{g_2}{\sqrt{2}} \overline{\nu_{\beta L}} \gamma^\mu V_L^{\nu\dagger} V_L^l l_{\alpha L} \,, \tag{26}$$

with the matrix product, $V_L^{\nu\dagger} V_L^l = U_{PMNS}$, defining the PMNS leptonic mixing matrix. Performing the global phase transformation, the weak charged current becomes

$$J_{cc}^\mu = 2 e^{-i(\phi_2^\nu - \phi_\mu^2)} \sum_{\alpha,\beta} \frac{g_2}{\sqrt{2}} \overline{\nu_{\beta L}} \gamma^\mu e^{-i(\phi_\beta^\nu - \phi_2^\nu)} V_L^{\nu\dagger} V_L^l e^{i(\phi_\alpha^l - \phi_\mu^l)} l_{\alpha L} \,. \tag{27}$$

It is clear that from the global phase transformation of the lepton fields we have five arbitrary phases which can be used to eliminate five phase from the leptonic mixing matrix, U_{PMNS}. Thus, after the phase redefinition of the lepton fields, the leptonic mixing matrix can be parametrised by three mixing angles $(\theta_{12}, \theta_{13}, \theta_{13})$ and one complex physical Dirac phase δ_D as[80]

$$U_{PMNS} = \begin{pmatrix} c_{12}c_{12} & c_{12}c_{12} & s_{13}e^{-i\delta_D} \\ -s_{12}c_{23} - c_{12}s_{23}s_{13}e^{i\delta_D} & c_{12}c_{23} - s_{12}s_{13}s_{23}e^{i\delta_D} & s_{23}C_{13} \\ s_{12}2_{23} - c_{12}c_{23}s_{13}e^{i\delta_D} & -s_{23}c_{12} - c_{23}s_{13}s_{12}e^{i\delta_D} & c_{23}C_{13} \end{pmatrix}, \tag{28}$$

where s_{ij} and c_{ij} indicate $\sin\theta_{ij}$ and $\cos\theta_{ij}$. A salient feature of massive Dirac neutrinos is the lepton number conservation. Table 1 lists the lepton number L and the lepton flavor (family) number L_α of every lepton. To see why massive Dirac neutrinos are lepton number conserving, we first make the global phase transformations as in eq. 25. Because of the Dirac mass term, the kinetic term and the charged current interaction term are all invariant, the lepton number must be conserved for Dirac neutrinos. Although the Lepton number is conserved, lepton flavors are violated due to the non-diagonal elements of U_{PMNS}. In other words, the leptonic mixing leads to lepton flavor violation but lepton number conservation.

Table 1: Lepton number L and lepton flavor number L_α of charged leptons and neutrinos (for $\alpha = e, \mu, \tau$).

	e	ν_e	e^+	$\overline{\nu}_e$	μ	ν_μ	μ^+	$\overline{\nu}_\mu$	τ	ν_τ	τ^+	$\overline{\nu}_\tau$
L	+1	+1	−1	−1	+1	+1	−1	−1	+1	+1	−1	−1
L_e	+1	+1	−1	−1	0	0	0	0	0	0	0	0
L_μ	0	0	0	0	+1	+1	−1	−1	0	0	0	0
L_τ	0	0	0	0	0	0	0	0	+1	+1	−1	−1

As in Dirac case, the charged weak current with massive Majorana fermions can be written in the mass basis after rotating the interaction fields by U^M_{PMNS} as in eq. 21. However, unlike the Dirac case, massive Majorana neutrinos are not invariant under the global phase transformation, 25. This fact leads to both lepton and flavor numbers being violated which leads to interesting phenomena such as the neutrinoless double beta decay and same sign leptons final states. Moreover, the leptonic mixing matrix, U^M_{PMNS}, contains two independent phases that can not be eliminated simultaneously.[12] The leptonic mixing matrix for Majorana neutrinos is then written as [80]

[12] *Usually called Majorana phases*

$$U^M_{PMNS} = \begin{pmatrix} c_{12}c_{12}e^{i\alpha_1} & c_{12}c_{12} & s_{13}e^{-i\delta_D} \\ -s_{12}c_{23} - c_{12}s_{23}s_{13}e^{i\delta_D} & c_{12}c_{23} - s_{12}s_{13}s_{23}e^{i\delta_D}e^{i\alpha_2} & s_{23}C_{13} \\ s_{12}2_{23} - c_{12}c_{23}s_{13}e^{i\delta_D} & -s_{23}c_{12} - c_{23}s_{13}s_{12}e^{i\delta_D} & c_{23}C_{13} \end{pmatrix}, \tag{29}$$

where α_1 and α_2 are the two physical Majorana phases.

3

NEUTRINO MASSES BEYOND THE SM

The SM gauge groups $SU(3)_c \times SU(2)_L \times U(1)_Y$ define the gauge bosons of the model, while fermions have to be chosen somewhat arbitrarily. These choices are made such that the SM structure maintains two properties that forbid massive neutrinos. First, the SM is a renormalizable theory, in which higher dimensional operators that may give each neutrino a Majorana mass do not exist. Second, There are no right-handed neutrinos, so a Dirac neutrino mass term con not be constructed. There is only one Higgs doublet, so a gauge invariant Majorana mass term is also forbidden.[13] In order to generate tiny neutrino masses, one of the above mentioned conditions of the SM has to be ignored. Within the framework of the SM as a consistent field theory, its particle content can be extended or its renormalizability can be abandoned to accommodate massive neutrinos. There are several ways to this goal. For simplicity, we roughly classify the viable ideas about neutrino mass generation into seesaw and non-seesaw mechanisms.

[13] *In other words, one can say that the SM possesses a $B - L$ symmetry which assures the neutrinos to be massless*

One of the most interesting non-seesaw mechanisms for neutrino mass generation is through extending the SM with higher dimensions non-renormalizable operators. the non-renormalizable operators can extend the SM Lagrangian as

$$\mathcal{L}_{eff} = \mathcal{L}_{SM} + \frac{\mathcal{L}_{d=5}}{\Lambda} + \frac{\mathcal{L}_{d=6}}{\Lambda^2} + \cdots , \tag{30}$$

where Λ denotes the cut off scale for theory. The lowest dimension operator that violates the lepton number, L, is the unique dimension five operator [14] that was first invented by Weinberg [78]. After the Spontaneous symmetry breaking the Weinberg operator generates masses for neutrinos as described in eq. 18. The generated neutrino mass can be sufficiently small, $\mathcal{O}(GeV)$, if Λ is not far away from the energy scale of the possible grand unified theories, $\sim 10^{13}$ GeV. Accordingly, it is suggested that neutrino masses can serve as a low energy window for new physics at very high energy scale.

[14] *It is found that only one dimension five operator exist that conserves all the known symmetries and is known as Weinberg operator*

The essential spirit of seesaw mechanisms is to add new fermions to the SM allowing for Dirac neutrino masses with lepton number conservation as well as Majorana neutrino masses with lepton number violation. There are three typical seesaw mechanisms distinguished by the properties of the additional fields to the SM.

3.1 SEESAW MODELS

The seesaw mechanism provides an attractive explanation of the smallness of the neutrino masses compared to the masses of the charged fermions of the same generation through the extension of the SM Lagrangian by extra fermions or scalars. However, this mechanism does not fix completely the overall scale of the light neutrino masses since the mass scale of Majorana neutrinos, though

is expected to be large, is not precisely known. Moreover, the ratios of the light neutrino masses as well as the lepton mixing parameters remain arbitrary; one can easily obtain any desired values of these parameters by properly choosing the elements of the neutrino Yukawa matrix. Therefore by itself, without any additional assumptions, this mechanism has limited predictive power. To gain more predictivity one has to invoke additional assumptions.

3.1.1 *Seesaw type I*

In the type I seesaw (c.f e.g. [3, 9] and refs herein), three right handed neutrinos are added to the SM. After the symmetry breaking Dirac mass terms are generated through the small Yukawa coupling to the SM Higgs field. Also, a Majorana mass term is introduced and the leptonic Lagrangian is written as

$$\mathcal{L}^{I}_{lep} = -\overline{l_L} Y^l \Phi l_R - \overline{l_L} Y^\nu \widetilde{\Phi} N_R - \frac{M_R}{2} \overline{N^c_R} N_R + H.c.\,, \tag{31}$$

where M_R is the non diagonal Majorana mass matrix. Moreover, it is important to stress here that Majorana mass term can be built from left-handed or right-handed neutrinos with their charge conjugate such that they violate the lepton number.

3.1.2 *Seesaw type II*

In type II seesaw (c.f e.g. [6] and refs herein), instead of extending the SM by adding right-handed singlet neutrinos as in type I seesaw, one can make use of the fact that the neutrino mass term, $\overline{l^c_L} l_L$[15] is a $SU(2)_L$ triplet. Accordingly, a renormalizable neutrino mass term can be formed by adding a scalar triplet[16] , Δ, to the SM Lagrangian. The leptonic Lagrangian can be written as

$$\mathcal{L}^{II}_{lep} = -\overline{l_l} Y^l \Phi l_R - Y^\nu_\Delta \overline{l_L} i\sigma_2 \Delta l^c_L + H.c.\,, \tag{32}$$

where Y^ν_Δ is the non diagonal Yukawa matrix and Δ is the scalar triplet, defined as

$$\Delta = \begin{pmatrix} \frac{\Delta^+}{\sqrt{2}} & \Delta^{++} \\ \Delta^0 & \frac{\Delta^+}{\sqrt{2}} \end{pmatrix}. \tag{33}$$

[15] *With* l *the* $SU(2)_L$ *doublet defined as* $l_L = \begin{pmatrix} \nu_L \\ l_L \end{pmatrix}$

[16] *The additional triplet must have* $Y = -2$ *such that the mass term* $\overline{l^c_L} l_L$ *is invariant under the SM gauge symmetry*

3.1.3 *Seesaw type III*

Type III seesaw (c.f e.g. [81–84] and refs herein), can be performed by adding a $SU(2)_L$ triplet fermion to the SM content, which couples to the SM lepton doublets via Yukawa term. In this scenario the scalar sector is not modified and the leptonic Lagrangian can be written as

$$\mathcal{L}^{III}_{lep} = -\overline{l_l} Y^l \Phi l_R - Y^\nu_\Xi \overline{l_L} i\sigma_2 \Phi \Xi + H.c.\,, \tag{34}$$

where Y_Ξ^ν is the non diagonal Yukawa matrix and Ξ is the fermion triplet that defined as

$$\Xi = \begin{pmatrix} \Xi^- & \frac{\Xi^0}{\sqrt{2}} \\ \frac{\Xi^0}{\sqrt{2}} & \Xi^+ \end{pmatrix} . \tag{35}$$

3.2 MINIMAL SYMMETRY PROTECTED LOW SCALE SEESAW MODEL (SPSS)

In this scenario (c.f e.g. [3] and refs herein), a pair of sterile neutrinos N_R^1 and N_R^2 is added under a global $U(1)$ symmetry, lepton number like symmetry, that forces the two sterile neutrons to have opposite lepton number assignments. The leptonic Lagrangian is given by

$$\mathcal{L}_{lep}^{SPSS} = -\overline{l_l} Y^l \Phi l_R - Y_\alpha^\nu \overline{N_R^1} \widetilde{\Phi}^\dagger l^\alpha - \frac{M_R}{2} \overline{N_R^1} N_R^{2c} + \text{H.c.} + \cdots , \tag{36}$$

with the dots indicate that the SPSS scenario can be extended with additional sterile neutrinos. The additional neutrinos are assumed to either be comparatively heavy or to be uncharged under the lepton number like symmetry. In the limit of intact symmetry they can neither mix with N_R^1 and N_R^2 nor participate in the Yukawa interaction with the lepton doublets, and thus they would be decoupled from other particles. Accordingly, in this limit, the relevant parameters for collider phenomenology are the neutrino Yukawa matrix y_α^ν and the sterile neutrinos masses. After electroweak symmetry breaking, the Dirac mass and the sterile neutrino mass construct a 5×5 mass matrix as

$$\mathcal{L}_m^{SPSS} = \begin{pmatrix} \overline{\nu_{eL}^c} \\ \overline{\nu_{\mu L}^c} \\ \overline{\nu_{\tau L}^c} \\ \overline{N_R^1} \\ \overline{N_R^2} \end{pmatrix}^T \begin{pmatrix} 0 & 0 & 0 & m_{\nu e} & 0 \\ 0 & 0 & 0 & m_{\nu \mu} & 0 \\ 0 & 0 & 0 & m_{\nu \tau} & 0 \\ m_{\nu e} & m_{\nu \mu} & m_{\nu \tau} & 0 & M \\ 0 & 0 & 0 & M & 0 \end{pmatrix} \begin{pmatrix} \nu_{eL} \\ \nu_{\mu L} \\ \nu_{\tau L} \\ N_R^{1c} \\ N_R^{2c} \end{pmatrix} + \text{H.c.} , \tag{37}$$

with Dirac neutrino masses $m_{\nu\alpha} = \frac{v\, y_\alpha^\nu}{\sqrt{2}}$. In the case where the limit is intact, the sterile neutrino N_R^2 does not couple to the lepton doublets via the Yukawa coupling. Accordingly, the cancellation of the contributions to the light neutrino mass matrix is exact and the three light neutrinos are massless. This allows for the neutrino Yukawa couplings to be large, which makes this scenario accessible at colliders when the sterile neutrino mass are of order of the EW scale. The mass matrix can be diagonalized by unitary 5×5 leptonic matrix defined as

$$\mathcal{U} = \begin{pmatrix} \theta_{e1} & \theta_{e2} & \theta_{e3} & -\frac{i\theta_e}{\sqrt{2}} & \frac{1\theta_e}{\sqrt{2}} \\ \theta_{\mu 1} & \theta_{\mu 2} & \theta_{\mu 3} & -\frac{i\theta_\mu}{\sqrt{2}} & \frac{1\theta_\mu}{\sqrt{2}} \\ \theta_{\tau 1} & \theta_{\tau 2} & \theta_{\tau 3} & -\frac{i\theta_\tau}{\sqrt{2}} & \frac{1\theta_\tau}{\sqrt{2}} \\ 0 & 0 & 0 & \frac{i}{\sqrt{2}} & \frac{1}{\sqrt{2}} \\ \theta_e^* & \theta_\mu^* & \theta_\tau^* & \frac{-i}{\sqrt{2}}\left(1 - \frac{1}{2}\theta^2\right) & \frac{1}{\sqrt{2}}\left(1 - \frac{1}{2}\theta^2\right) \end{pmatrix} , \tag{38}$$

with the active sterile mixing parameters $\theta_\alpha = \frac{y_\alpha^{*\nu} v}{\sqrt{2}M}$, $\alpha = e, \mu$ and τ. The upper left 3×3 block are the parameters for the effective PMNS matrix with its elements

$$\theta_{\alpha i} = \left(\delta_{\alpha\beta} - \frac{1}{2}\theta_\alpha \theta_\beta^*\right) U_{\beta i}^\nu \,, \quad \alpha, \beta = e, \mu, \tau \text{ and } i = 1, 2, 3 \tag{39}$$

where $U_{\beta i}^\nu$ is a unitary 3×3 matrix and $\theta_\alpha, \theta_\beta^*$ are the active-sterile mixing parameters. The neutrino mass eigenstates can be obtained by diagonalizing the mass matrix as

$$U^T M U = \text{Diag } (0, 0, 0, M, M) \,. \tag{40}$$

The diagonalization is accurate up to $\mathcal{O}(\theta^2)$ correction to the heavy neutrino masses which can be safely neglected. The neutrino eigenstates are admixtures of the active and sterile neutrinos and can be obtained by

$$n_i = U_{i\alpha}^\dagger n'_\alpha = (\nu_1, \nu_2, \nu_3, N_1, N_2) \,, \tag{41}$$

with ν_i and N_α are the light and heavy neutrinos. Both light and heavy neutrinos participate in the weak interactions, and the strength of the weak interactions is suppressed by the active-sterile mixing for the heavy neutrinos. The gauge interactions of the charged weak currents, $j_\mu^\pm$, and the neutral weak currents, j_μ^0, can be expressed in the mass basis as

$$j_\mu^\pm = \frac{g}{\sqrt{2}} \left[\sum_{\alpha=e,\mu,\tau} \sum_{i=1,2,3} \theta_{\alpha i} \overline{l_\alpha} \gamma_\mu P_L \nu_i + \sum_{\alpha=e,\mu,\tau} \theta_\alpha \overline{l_\alpha} \gamma_\mu P_L \frac{1}{\sqrt{2}} (-iN_1 + N_2) \right] + \text{H.c.} \tag{42}$$

$$j_\mu^0 = \frac{g}{2\cos\theta_W} \left[\sum_{i,j=1}^{3} \theta_{\alpha i} \overline{\nu_i} \gamma_\mu \nu_j + \sum_{i=1}^{3} (\theta_{i4} \overline{\nu_i} \gamma_\mu N_1 + \theta_{i5} \overline{\nu_i} \gamma_\mu N_2) \right] + \text{H.c.} \,, \tag{43}$$

with

$$\theta_{i4} = \sum_{\alpha=e,\mu,\tau} -i\theta_{i\alpha}^* \frac{\theta_\alpha}{\sqrt{2}} \quad \text{and} \quad \theta_{i5} = \sum_{\alpha=e,\mu,\tau} \theta_{i\alpha}^* \frac{\theta_\alpha}{\sqrt{2}} \,.$$

4

HIGGS PHYSICS BEYOND THE SM

Understanding the mechanism of electroweak symmetry breaking and generating masses for the known elementary particles has been one of the fundamental endeavours in particle physics for decades. The discovered scalar in 2012 with mass of approximately 125 GeV is compatible with the Higgs boson of the SM. The electroweak symmetry breaking mechanism provides a general framework to keep the structure of the gauge interactions at high energies untouched and it generates the observed masses for the gauge bosons, $W^{\pm}$ and Z^0. The SM Higgs potential reads

$$V(\Phi) = m^2\Phi^\dagger\Phi + \lambda(\Phi^\dagger\Phi)^2\,, \tag{44}$$

with the SM Higgs field Φ being a self-interacting $SU(2)_L$ doublet. $V(\Phi)$ is the most general renormalizable scalar potential and if the quadratic term is negative, the neutral component of the SM Higgs field acquires a non-zero vacuum expectation value

$$\langle\Phi\rangle = \frac{1}{\sqrt{2}}\begin{pmatrix} 0 \\ v + H \end{pmatrix}. \tag{45}$$

The SM Higgs boson couples to the $SU(2)_L \times U(1)_Y$ gauge bosons through the covariant derivative, D_μ, appearing in the kinetic term of the Lagrangian as

$$\mathcal{L} = (D_\mu\Phi)^\dagger(D^\mu\Phi)\,. \tag{46}$$

After EWSB, the neutral and the charged massless Goldstone bosons mix with the gauge fields corresponding to the broken generators of $SU(2)_L \times U(1)_Y$ and become the longitudinal components of the massive gauge bosons, Z and $W^{\pm}$. The acquired gauge bosons mass squared is

$$m_W^2 = \frac{g_2^2 v}{4} \quad \text{and} \quad \frac{(g_1 + g_2)^2 v}{4}\,, \tag{47}$$

where g_2, g_1 are the gauge couplings of $SU(2)_L$ and $U(1)_Y$ respectively. The fourth generator remains unbroken, massless, since it is associated with the conserved electromagnetic symmetry. Fermions in the SM acquire masses through renormalizable Yukawa interactions with the SM Higgs field as

$$\mathcal{L}_Y = -Y^d_{ij}\overline{q_{Li}}\Phi d_{Rj} - Y^u_{ij}\overline{q_{Li}}\tilde{\Phi} d_{Rj} - Y^l_{ij}\overline{l_{Li}}\Phi e_{Rj} + \text{H.c.}\,, \tag{48}$$

with $\tilde{\Phi} = i\sigma_2\Phi^*$ and q_L (l_L) and $d_R, u_R (e_R)$ are the quark (lepton) $SU(2)_L$ doublets and singlets, respectively. As already discussed, the neutrino mass term is forbidden in the SM and can be generated for models beyond the SM framework. The SM Higgs boson coupling to massive gauge bosons and fermions are given by

$$\kappa_{H\bar{f}f} = \frac{m_f}{v} \quad \text{and} \quad \kappa_{HVV} = \frac{2m_V^2}{v}\,, \tag{49}$$

with $V = W^{\pm}$ and Z bosons.

The observed SM Higgs boson is compatible with the current Higgs measurements, but there are some hints in ATLAS and CMS data that can be interpreted as 270 GeV neutral scalar resonance [85–87]. These anomalies in LHC Run I and Run II can be explained by the "Madala hypothesis" [88]. It is also woth mentioning that CMS has reported a 2.8 sigma deviation from the SM background for neutral scalar resonance at 90 GeV to diphoton final state [89]. Such a resonance can be explained by the existence of light scalar particle from the broken $U(1)_{B-L}$ symmetry [90]. In the following, we discuss the basic construction of extending the SM scalar sector by singlet, doublet and triplet $SU(2)_L$ complex scalar.

4.1 SM EXTENSION WITH SCALAR SINGLET

Extending the SM scalar potential with $SU(2)_L$ singlet is the simplest way of extending the SM gauge groups by $U(1)_X$ which can be broken by a scalar singlet, S, that acquires a vacuum expectation value v', (c.f e.g. [7] and refs herein). In some scenarios the scalar singlet can act as a portal to the SM neutral field in dark sectors, which otherwise would remain unobserved. It can also play a major role in models of electroweak baryogenesis as they represent one of the most economical possibilities to realize the first order electroweak phase transition. The mass scale of the scalar singlet is controlled by the vacuum expectation value of the broken $U(1)_X$ while the direct collider search for extra scalar resonances set a lower bound in its mass. The most general potential for a complex scalar singlet extending the SM is

$$V(\Phi, S) = m^2\Phi^\dagger\Phi + \mu^2 S^\dagger S + \lambda_1(\Phi^\dagger\Phi)^2 + \lambda_2(S^\dagger S)^2 + \lambda_3 S^\dagger S\Phi^\dagger\Phi\,, \tag{50}$$

where m^2, μ^2 are the masses of the SM Higgs boson and the scalar singlet and λ_i are free real parameters that control the mixing between the scalar fields. The stability of $V(\Phi, S)$ can be achieved with restricting the value of the free potential couplings as

$$\lambda_3 > -2\sqrt{\lambda_1\lambda_2} \quad \text{and} \quad \lambda_1, \lambda_2 > 0\,. \tag{51}$$

Solving the tadpole equations to get the value of the VEVs as

$$\frac{\partial V(\Phi, S)}{\partial v} = m^2 + \lambda_1 v^2 + \frac{\lambda_3}{2} v'^2 = 0, \tag{52}$$

$$\frac{\partial V(\Phi, S)}{\partial v'} = \mu^2 + \lambda_2 v'^2 + \frac{\lambda_3}{2} v^2 = 0. \tag{53}$$

From the solution of the tadpole equations the two VEVs can be written as

$$v^2 = \frac{4\lambda_2\mu^2 - 2\lambda_3 m^3}{\lambda_3^2 - 4\lambda_1\lambda_2} \quad \text{and} \quad v'^2 = -\frac{2(m^2 + \lambda_1 v^2)}{\lambda_3}\,. \tag{54}$$

The VEV of the Higgs doublet is constrained to the measured 246 GeV while v' has only a lower bound from the lower limit imposed on the mass of the

singlet scalar from the direct collider searches. The mass matrix squared can be obtained from the scalar potential, $V(\Phi, S)$, as

$$M^2(H,S) = \begin{pmatrix} 2\lambda_1 v^2 & \lambda_3 v v' \\ \lambda_3 v v' & 2\lambda_2 v'^2 \end{pmatrix} . \tag{55}$$

The mass matrix can be diagonalized by 2×2 unitary matrix U^s as

$$U^{s\dagger} M^2(H,S) U^s = M^2(H,S)_{diag} . \tag{56}$$

Consequently, the Higgs fields can be rotated to their mass eignstates by the transformation

$$U^{s\dagger} \begin{pmatrix} H \\ S \end{pmatrix} = \begin{pmatrix} \cos\alpha & -\sin\alpha \\ \sin\alpha & \cos\alpha \end{pmatrix}^\dagger \begin{pmatrix} H \\ S \end{pmatrix} = \begin{pmatrix} h_1^{SM} \\ h_2 \end{pmatrix} , \tag{57}$$

with h_1^{SM}, h_2 are the physcial SM-like Higgs and the extra scalar respectively and the mixing angle is defined as

$$\tan 2\alpha = \frac{|\lambda_3| v v'}{\lambda_1 v^2 - \lambda_2 v'^2} . \tag{58}$$

The squared masses for the physical Higgs states are given by

$$m^2_{h_1^{SM}, h_2} = \lambda_1 v^2 + \lambda_2 v'^2 \mp \sqrt{(\lambda_1 v^2 - \lambda_2 v'^2)^2 + \lambda_3^2 v^2 v'^2} , \tag{59}$$

where $m_{h_1^{SM}}$ is set to the measured Higgs boson mass while m_{h_2} has a lower bound from the direct collider searches.

For phenomenological studies, one can express the parameters in the potential with the physical parameters, m_{h_1}, m_{h_2} and α as

$$\lambda_1 = \frac{m^2_{h_2}}{4v^2}(1 - \cos 2\alpha) + \frac{m^2_{h_1}}{4v^2}(1 + \cos 2\alpha) , \tag{60}$$

$$\lambda_2 = \frac{m^2_{h_1}}{4v'^2}(1 - \cos 2\alpha) + \frac{m^2_{h_2}}{4v'^2}(1 + \cos 2\alpha) , \tag{61}$$

$$\lambda_3 = \sin 2\alpha \left(\frac{m^2_{h_2} - m^2_{h_1}}{2 v v'} \right) . \tag{62}$$

For nonvanishing mixing angle, α, the mixing between the two Higgs fields induces couplings of the physical scalar states, h_1^{SM}, h_2 with the SM particles. The coupling of the Higgs bosons to the SM fermions and gauge bosons are given by

$$\kappa_{h_1 \bar{f} f} = \frac{m_f}{v} \cos\alpha , \qquad \kappa_{h_2 \bar{f} f} = \frac{m_f}{v} \sin\alpha , \tag{63}$$

$$\kappa_{h_1 VV} = \frac{2m_V^2}{v} \cos\alpha \quad \text{and} \quad \kappa_{h_2 VV} = \frac{2m_V^2}{v} \sin\alpha . \tag{64}$$

4.2 SM EXTENSION WITH SCALAR DOUBLET

Extending the SM scalar potential with extra scalar $SU(2)_L$ doublet form what is called the Two Higgs Doublet Model (THDM), (c.f e.g. [1] and refs herein). Therefore, its most general form should allow for global transformations which mix these fields and change the relative phases. The most generic potential for the THDM can be written as:

$$V = m_{11}^2(\phi_1^\dagger\phi_1) + m_{22}^2(\phi_2^\dagger\phi_2) + \lambda_1(\phi_1^\dagger\phi_1)^2 + \lambda_2(\phi_2^\dagger\phi_2)^2 + \lambda_3(\phi_1^\dagger\phi_1)(\phi_2^\dagger\phi_2) + \lambda_4(\phi_1^\dagger\phi_2)(\phi_2^\dagger\phi_1) + \frac{1}{2}\left[-m_{12}^2(\phi_1^\dagger\phi_2) + \lambda_5(\phi_1^\dagger\phi_2)^2 + \lambda_6(\phi_1^\dagger\phi_1)(\phi_1^\dagger\phi_2) + \lambda_7(\phi_2^\dagger\phi_2)(\phi_1^\dagger\phi_2) + \text{H.c.}\right], \tag{65}$$

with ϕ_1 and ϕ_2 are doublet $SU(2)_L$ scalr fields defined as

$$\phi_1 = \begin{pmatrix} \eta_1^+ \\ (v_1 + h_1 + ih_3)/\sqrt{2} \end{pmatrix} \quad \text{and} \quad \phi_2 = \begin{pmatrix} \eta_2^+ \\ (v_2 + h_2 + ih_4)/\sqrt{2} \end{pmatrix}. \tag{66}$$

The THDM potential has the freedom to generate Flavor Changing the Neutral Currents (FCNCs) at tree level. The fact that there is no hint for FCNCs in the current measurement sets severe bounds on the parameters. Glashow and Weinberg [91] found that the FCNCs can be naturally suppressed by imposing a Z_2 symmetry, which transform the scalar fields as

$$\phi_1 \to \phi_1, \qquad \phi_2 \to -\phi_2\,. \tag{67}$$

According to the fields transformation under the Z_2 symmetry one can classify the THDM into three types

- Exact Z_2 symmetry. In this case the Higgs potential can be written such that $\lambda_6 = \lambda_7 = m_{12}^2 = 0$. Thus the potential free parameters are taken to be real while only λ_5 can be complex. The complex phase of λ_5 can lead to CP violation of the potential but with proper field redefinition one can absorb the complex phase ending up with a CP conserving potential. In this case the THDM potential is similar to the Minimal Supersymmetric Model (MSSM) potential.

- Softly broken Z_2 symmetry. In this case the potential respects the Z_2 symmetry at small distances, much smaller than $1/M$[17] , in all orders of perturbation theory, i. e.for $M^2 \to \infty$ the transition $\phi_1 \to \phi_2$ disappears.[18] Thus we have $\lambda_6 = \lambda_7 = 0$ and we end up with two complex parameters, m_{12}^2 and λ_5. Accordingly, with two independent complex phases, we cannot rotate the fields to absorb the two phases simultaneously. The phases vanish only if
$$\eta(\lambda_5) = 2\eta(m_{12}^2)\,, \tag{68}$$
with $\eta(\lambda_5), \eta(m_{12}^2)$ are the complex phases of λ_5 and the soft mass m_{12}^2 respectively. In the following we consider the THDM with softly broken Z_2 where the complex phase leads to spontenous CP violation.

- Hard broken Z_2 symmetry. In this case the scalar potential has all freedom as eq. 65. This potential is not favored for collider studies while it leads to a strong FCNC and spontenous CP violation.

[17] *With M the mass scale of the soft breaking appear in the potential*

[18] *Hence the name of "softly" broken* Z_2

In the following, from the aforementioned THDM types, we focus on a softly broken Z_2 symmetry, where in addition to the complex λ_5 parameter the soft mass m_{12}^2 parameter is also taken to be complex. The scalar potential is then given by

$$\begin{aligned} V_\phi = {} & m_{11}^2(\phi_1^\dagger\phi_1) + m_{22}^2(\phi_2^\dagger\phi_2) - \left[m_{12}^2(\phi_1^\dagger\phi_2) + \text{H.c}\right] + \lambda_1(\phi_1^\dagger\phi_1)^2 + \lambda_2(\phi_2^\dagger\phi_2)^2 \\ & + \lambda_3(\phi_1^\dagger\phi_1)(\phi_2^\dagger\phi_2) + \lambda_4(\phi_1^\dagger\phi_2)(\phi_2^\dagger\phi_1) + \frac{1}{2}\left[\lambda_5(\phi_1^\dagger\phi_2)^2 + \text{H.c}\right]. \end{aligned} \tag{69}$$

We parametrize the two complex-valued parameters as, $m_{12}^2 = |m_{12}^2|e^{i\eta(m_{12}^2)}$, $\lambda_5 = |\lambda_5|e^{i\eta(\lambda_5)}$, introducing the two phases $\eta(m_{12}^2)$ and $\eta(\lambda_5)$.

Minimizing the Higgs potential after electroweak symmetry breaking to find the unknown soft masses

$$\begin{aligned} \frac{\partial V}{\partial h_1} &= \frac{1}{2}v_1v_2^2\Re(\lambda_5) - v_2\Re(m_{12}^2) + \lambda_1 v_1^3 + m_{11}^2 v_1 + \frac{1}{2}\lambda_3 v_1 v_2^2 + \frac{1}{2}\lambda_4 v_1 v_2^2 = 0\,, \\ \frac{\partial V}{\partial h_2} &= \frac{1}{2}v_1^2v_2\Re(\lambda_5) - v_1\Re(m_{12}^2) + \frac{1}{2}\lambda_3 v_1^2 v_2 + \frac{1}{2}\lambda_4 v_1^2 v_2 + \lambda_2 v_2^3 + m_{22}^2 v_2 = 0\,, \\ \frac{\partial V}{\partial h_3} &= -\frac{1}{2}v_1v_2^2\Im(\lambda_5) + v_2\Im(m_{12}^2) = 0\,, \\ \frac{\partial V}{\partial h_4} &= \frac{\partial V}{\partial h_3} \times \left(-\frac{v_1}{v_2}\right) = 0\,, \end{aligned} \tag{70}$$

with v_1 and v_2 denoting the two (by convention real and positive) vacuum expectation values of the two scalar fields ϕ_1 and ϕ_2. The two VEVs satisfy $v = \sqrt{v_1^2 + v_2^2}$, with v denoting the SM VEV $v \approx 246$ GeV, and we define $\tan\beta := v_2/v_1$.

Solving the first two equations one can eliminate m_{11}^2 and m_{22}^2 as

$$\begin{aligned} m_{11}^2 &= \frac{-v_1v_2^2\Re(\lambda_5) + 2v_2\Re(m_{12}^2) - 2\lambda_1 v_1^3 - \lambda_3 v_1 v_2^2 - \lambda_4 v_1 v_2^2}{2v_1}, \\ m_{22}^2 &= \frac{-v_1^2v_2\Re(\lambda_5) + 2v_1\Re(m_{12}^2) - 2\lambda_2 v_2^3 - \lambda_3 v_1^2 v_2 - \lambda_4 v_1^2 v_2}{2v_1}, \end{aligned} \tag{71}$$

while from the third equation we get the condition

$$\Im(m_{12}^2) = \frac{1}{2}v_1v_2\Im(\lambda_5)\,. \tag{72}$$

In the following we will use this relation to remove $\Im(m_{12}^2)$ from all equations, leaving

$$\Re(m_{12}^2) \quad \text{and} \quad \lambda_5 = |\lambda_5|\, e^{i\eta(\lambda_5)}\,, \tag{73}$$

as the remaining independent parameters. In this sense, the phase parameter $\eta(\lambda_5)$ of λ_5 governs CP violation in V_ϕ. The scalar squared mass matrix given by

$$M^2 = \begin{pmatrix} D_1 & O_1 & O_2 & O_3 \\ O_1 & D_2 & O_4 & O_5 \\ O_2 & O_4 & D_3 & O_6 \\ O_3 & O_5 & O_6 & D_4 \end{pmatrix}, \tag{74}$$

with the diagonal elements

$$\begin{aligned} D_1 &= 3\lambda_1 v_1^2 + \tfrac{v_2^2\lambda_3}{2} + \tfrac{v_2^2\lambda_4}{2} + m_{11}^2 + \tfrac{1}{2}v_2^2\Re(\lambda_5)\,, \\ D_2 &= \tfrac{\lambda_3 v_1^2}{2} + \tfrac{\lambda_4 v_1^2}{2} + \tfrac{1}{2}\Re(\lambda_5)v_1^2 + 3v_2^2\lambda_2 + m_{22}^2)\,, \\ D_3 &= \lambda_1 v_1^2 + \tfrac{v_2^2\lambda_3}{2} + \tfrac{v_2^2\lambda_4}{2} + m_{11}^2 - \tfrac{1}{2}v_2^2\Re(\lambda_5)\,, \\ D_4 &= \tfrac{\lambda_3 v_1^2}{2} + \tfrac{\lambda_4 v_1^2}{2} - \tfrac{1}{2}\Re(\lambda_5)v_1^2 + v_2^2\lambda_2 + m_{22}^2\,, \end{aligned} \tag{75}$$

and the off-diagonal elements

$$\begin{aligned} O_1 &= v_1 v_2\lambda_3 + v_1 v_2\lambda_4 + v_1 v_2\Re(\lambda_5) - \Re(m_{12}^2)\,, \\ O_2 &= -\tfrac{1}{2}v_2^2\Im(\lambda_5)\,, \\ O_3 &= \tfrac{1}{2}v_1 v_2\Im(\lambda_5)\,, \\ O_4 &= -O_3\,, \\ O_5 &= \tfrac{1}{2}v_1^2\Im(\lambda_5)\,, \\ O_6 &= v_1 v_2\Re(\lambda_5) - \Re(m_{12}^2)\,. \end{aligned} \tag{76}$$

Diagonalizing the mass matrix in eq. (175) by 4×4 unitary matrix, R_{ij},

$$R^\dagger M^2 R = Diag(0, M_{H_1}^2, M_{H_2}^2, M_{H_3}^2)\,, \tag{77}$$

with the neutral Higgs mass eigenstates $H_i (i = 0,1,2,3)$ are related to the interaction fields h_i via the rotation

$$h_i = \sum_i R_{ij}^\dagger H_j\,. \tag{78}$$

Due to the existence of the complex $\Im(\lambda_5)$ the three phyiscal scalars are not definite CP even or odd eignstates but a mixing between both states. It is pretty clear that if $\Im(\lambda_5) = 0$ we retrieve the CP conservation of of the scalar potential and the squared mass matrix now reads

$$M^2 = \begin{pmatrix} D_1 & O_1 & 0 & 0 \\ O_1 & D_2 & 0 & 0 \\ 0 & 0 & D_3 & O_6 \\ 0 & 0 & O_6 & D_4 \end{pmatrix}\,. \tag{79}$$

The upper left 2×2 block can be diagonalized by a 2×2 unitary matrix, as in eq. 57, leading to CP even eigenstates $h^S M_1, h_2$ with the mixing angle, α, defined as

$$\alpha = \frac{2\chi}{2v_1^2\lambda_1\cos^2\beta + \Re(m_{12}^2)\tan\beta - \chi}\,, \tag{80}$$

with $\chi = v_1^2\cos\beta\sin\beta\left(\lambda_3 + \lambda_4 + \Re(\lambda_5) - \Re(m_{12}^2)\right)$. The lower right 2×2 gives the massless Goldstone boson and a massive CP odd scalar, A. In the following, we consider the scalar coupling to fermions and gauge bosons in the case of CP conserving and CP violating the scalar potential.

- Scalar fermions coupling (CP conservation).

$$\kappa_{h_1\bar{f}f} = \frac{-Y^l \cos\alpha(P_L + P_R)}{\sqrt{2}}, \quad \kappa_{h_2\bar{f}f} = \frac{-Y^l \sin\alpha(P_L + P_R)}{\sqrt{2}},$$
$$\kappa_{A\bar{f}f}\frac{iY^l \cos\rho(P_L - P_R)}{\sqrt{2}}, \quad \kappa_{H^+\bar{f}f} = -Y^l \cos\rho P_R, \quad \kappa_{H^-\bar{f}f} = -Y^l \cos\rho P_L\,, \tag{81}$$

  with $H^\pm$ are the charged Higgs bosons and α, ρ are the angles used to diagonlaized the CP even and CP odd states respectively.

- Scalar gague bosons coupling (CP conservation).

$$\kappa_{h_1W^+W^-} = -\frac{1}{2}v\cos(\alpha-\beta)g_2^2, \quad \kappa_{h_2W^+W^-} = -\frac{1}{2}v\sin(\alpha-\beta)g_2^2$$
$$\kappa_{h_1ZZ} = \frac{1}{2}v\cos(\alpha-\beta)(g_1^2+g_2^2), \quad \kappa_{h_2ZZ} = \frac{1}{2}v\sin(\alpha-\beta)(g_1^2+g_2^2)\,. \tag{82}$$

  It is important to mention that in the case of CP conservation the coupling between the CP odd state, A, and gauge bosons is induced at the one loop level only.

- Scalar fermions coupling (CP violation).

$$\kappa_{H_i\bar{f}f} = -\frac{Y^l}{\sqrt{2}}\left[(R_{i,1} - iR_{i,3})\,P_L + (R_{i,1} + iR_{i,3})\,P_R\right], \quad i = 1,2,3\,. \tag{83}$$

- Scalar gague bosons coupling (CP violation).

$$\kappa_{H_iVV} = \frac{2m_V^2}{v_1}\left(R_{i,1}\cos\beta - R_{i,2}\sin\beta\right), \quad i = 1,2,3\,. \tag{84}$$

  with $V = W^\pm, Z$.

4.3 SM EXTENSION WITH SCALAR TRIPLET

Extending the SM Lagrangian with $SU(2)_L$ scalar triplet, Δ, is called "Type II seesaw" model, (c.f e.g. [6] and refs herein). The type II seesaw is one of the most appealing scenarios for generating neutrino masses. The scalar triplet develops an induced vacuum expectation value after the electroweak symmetry breaking, giving masses to neutrinos via its coupling to the $SU(2)_L$ lepton doublets. The matrix representations for the scalar fields are given by:

$$\Phi = \begin{pmatrix} \Phi^+ \\ \Phi^0 \end{pmatrix} \text{ and } \Delta = \begin{pmatrix} \frac{\Delta^+}{\sqrt{2}} & \Delta^{++} \\ \Delta^0 & -\frac{\Delta^+}{\sqrt{2}} \end{pmatrix}. \tag{85}$$

The $SU(3)_C \times SU(2)_L \times U(1)_Y$ invariant Lagrangian for the scalar fields is

$$\mathcal{L} = (D_\mu\Phi)^\dagger(D^\mu\Phi) + Tr((D_\mu\Delta)^\dagger(D^\mu\Delta)) - V(\Phi,\Delta) - \mathcal{L}_{Yukawa} \tag{86}$$

with the covariant derivaties

$$D_\mu \Phi = \partial_\mu \Phi + i g T^a W_\mu^a \Phi + i \frac{g'}{2} B_\mu \Phi \tag{87}$$

$$D_\mu \Delta = \partial_\mu \Delta + i g [T_\mu^a, \Delta] + i \frac{g'}{2} B_\mu \Delta, \tag{88}$$

and the scalar potential

$$\begin{aligned} V(\Phi, \Delta) = & \mu^2 \Phi^\dagger \Phi - M_T^2 Tr(\Delta^\dagger \Delta) - \frac{\lambda}{4} |\Phi^\dagger \Phi|^2 \\ & - \lambda_{HT} \Phi^\dagger \Phi Tr(\Delta^\dagger \Delta) - \lambda_T (Tr(\Delta^\dagger \Delta))^2 \\ & - \lambda'_T Tr((\Delta^\dagger \Delta)^2) - \lambda'_{HT} \Phi^\dagger \Delta \Delta^\dagger \Phi \\ & - (\kappa \Phi^\top i \sigma^2 \Delta^\dagger \Phi + H.c.) \end{aligned} \tag{89}$$

while the new Yukawa term is

$$\mathcal{L}_{Y_\Delta} = Y_\Delta \bar{\ell^c} i \sigma^2 \Delta \ell + H.c.\,. \tag{90}$$

After electroweak symmetry breaking the scalar fields acquire their vacuum expectation values as

$$\langle \Phi \rangle = \frac{1}{\sqrt{2}} \begin{pmatrix} 0 \\ v \end{pmatrix} \text{ and } \langle \Delta \rangle = \frac{1}{\sqrt{2}} \begin{pmatrix} 0 & 0 \\ v_T & 0. \end{pmatrix}, \tag{91}$$

where $v_T \ll v$ to naturally explain the small neutrino masses. Evolving the scalar fields around their VEVs and minimizing the potential leads to seven physical massive eigenstates: $H^{\pm\pm}, H^\pm, h, H, A$. The three massless Goldstone bosons $G^\pm$ and G^0 are absorbed by the SM gauge bosons $W^\pm$ and Z. The scalar potential and the new Yukawa term contain the following parameters: five coupling parameters $\lambda, \lambda_{HT}, \lambda_T, \lambda'_T$ and λ'_{HT}, two mass parameters μ and M_T, the seesaw parameter κ (with mass dimension = 1), the VEVs v and v_T and the new Yukawa matrix $(Y_\Delta)_{ij}$. The tadpole equations allow us to express μ and M_T in terms of the couplings and κ:

$$\mu^2 = -\sqrt{2} \kappa v_T + \frac{1}{2} (\lambda_{HT} + \lambda'_{HT}) v_T + \frac{1}{4} \lambda v^2\,, \tag{92}$$

$$M_T^2 = -(\lambda_T + \lambda'_T) v_T^2 - \frac{1}{2} (\lambda_{HT} + \lambda'_{HT}) v^2 + \frac{\kappa v^2}{\sqrt{2} v_T}. \tag{93}$$

The mass matrix squared for the CP even scalars reads

$$M^2 = \begin{pmatrix} -4 v_T \kappa + 2 v_T^2 \left(\lambda_{HT} + \lambda'_{HT}\right) + 3 \lambda v^2 - 4 \mu & v\, v_T \left(\lambda_{HT} + \lambda'_{HT}\right) - v\, \kappa \\ v\, v_T \left(\lambda_{HT} + \lambda'_{HT}\right) - v\, \kappa & 3 \left(\lambda_T + \lambda'_T\right) v_T^2 + v^2 \left(\lambda_{HT} + \lambda'_{HT}\right) + M_T \end{pmatrix} \tag{94}$$

which can be diagonalized by a unitary 2×2 matrix as in eq. 57. The masses for the physical Higgs bosons are

$$m_{H^{\pm\pm}}^2 = \frac{\kappa v^2}{\sqrt{2} v_T} + \frac{\lambda'_{HT} v^2}{2} + \lambda'_T v_T^2 \tag{95}$$

$$m^2_{H^\pm} = \frac{\kappa v^2}{\sqrt{2}v_T} + \frac{\lambda'_{HT} v^2}{4} + \frac{\lambda'_{HT} v_T^2}{2} + \sqrt{2}\kappa v_T \tag{96}$$

$$m^2_h = \frac{1}{2}(A + C - \sqrt{(A-C)^2 + 4B^2}) \tag{97}$$

$$m^2_H = \frac{1}{2}(A + C + \sqrt{(A-C)^2 + 4B^2}), \tag{98}$$

with $A = -\frac{\lambda}{2}v^2$, $B = -(\lambda_{HT} + \lambda'_{HT})v_T v - \sqrt{2}\kappa v$ and $C = \frac{\kappa v^2}{\sqrt{2}v_T} - 2(\lambda_T + \lambda'_T)v_T^2$, and

$$m^2_{A^0} = \frac{\kappa v^2}{\sqrt{2}v_T} + 2\sqrt{2}\kappa v_T. \tag{99}$$

The coupling of the neutral scalar fields to the SM gauge bosons and fermions are the same as in eq. 63 while the doubly charged coupling to gauge bosons and fermions read

$$\kappa_{H^{++}ff} = (Y_\Delta)_{ij}, \qquad \kappa_{H^{++}W^-W^-} = \sqrt{2}g_2^2 v_T\,. \tag{100}$$

5 METHODELOGY OF COLLIDER SIMULATION

Investigating the phenomenology of sterile neutrinos and heavy Higgs at the current and future colliders is the main goal of this thesis. For the subsequent investigations, simulation of collider phenomenology for sterile neutrinos and heavy Higgses are performed in the framework of different models beyond the SM. For collider simulation one has to generate events that mimic the real events produced at the colliders. For this purpose, a long chain of numerical tools has to be used such that we start with a written Lagrangian and end with simulated events at the so called reconstructed level.[19] The process of generating reconstructed events can be classified as follow

[19] *The reconstructed level events are those events simulated with taken into account the collider effect such that the parent particle (new physics) can be constructed from the final state particles*

1. Starting from beyond SM Lagrangian in the gauge bases, FeynRules [92] and SARAH [93] programs can be used to calculate all vertices in the physical basis. These programs write the vertices in different model file outputs such as the Universal FeynRules Output (UFO) [94] which can be used as input for Monte Carlo event generator programs.
2. Monte Carlo event generator programs, such as MadGraph [92], using the UFO model files generate events at the parton level.
3. We use Pythia8 [95] to simulate the initial and final state radiation of the partons, hadronization, beam reminant and multiple interactions.
4. Events from Pythia8 are produced at the hadron level. For jets reconstruction we use FastJet simulator program [96].
5. The detector effects are included by using the fast detector simulation tool, Delphes [97].

To this end, the simulated events with final state particles at the reconstructed level which can be used to analyze the properties of the new physics.

5.1 BOOSTED DECISION TREES (BDT)

The enormous data delivered from the current experiments allow us to constrain the new physics parameters e.g. the production probability of heavy new particles at colliders.[20] Thus the need for utilizing Machine Learning Algorithms (MLAs) for collider searches becomes essential. MLAs are the paradigm for automated learning from data, using computing algorithms. The main goal of MLAs is to exploit the large data sets in order to reduce the complexity of the data and find features of new physics hidden in the data. The current most frequently used MLAs are the Boosted Decision Trees (BDT) and the Deep Neural Networks (DNN). Although many different models for machine learning exist, still all of them[21] have a common way of dealing with the problem of extracting new physics signatures from the large background contributions.

[20] *It also constrains the heavy new physics masses to very high values, above the current collider energy*

[21] *As supervised learning algorithms*

5.1.1 *BDT objectives*

One of the BDT objectives is its ability to probe the signatures of heavy particles at colliders with high accuracy. Achieving high accuracy, e.g, in discriminating signatures of a heavy resonant particle from the SM background, can not be reached by simple cut and count analysis, the invariant mass distribution, which are of most important variables for new physics study, has a wide resonance and can not be distinguished from the relevant backgrounds. The discriminating power of the BDT relies on the fact that the signal and the background may be characterized by different features that can be entangled in several distributions. When these features are not clearly manifest in some specific observable (like the wide resonance of the invariant mass distribution in our case), it could be difficult, in principle, to identify the most relevant distributions that allow us to efficiently separate the signal from the background events. The output of each decision tree is called "BDT classifier" which is produced after combining many weak observables.[22]

[22] *Weak observables are those kinematic distributions that cannot be distinguished well from the background*

5.1.2 *BDT classification*

The BDT classification, or the supervised ML in general, first divides the data sample, signal and background, into two parts. The first part is used to train the decision trees with given labels for both signal events and background events. This data sample is called "training data sample". The second part of the data is used to "blindly" test the trained data. This data sample is called "test data sample". The hard work is all done in the training part where the decision trees try to understand the features of the data and create an efficient classifier distinguishes between the signal and background events. Optimizing the classifier efficiency is done by minimizing an error function between the decision trees predictions and the true value. The determination of the final classifier is done by a sequential growing of binary trees that can be constructed as follows:

- Picking up random sample events creating the *root node*.
- The algorithm finds the optimal threshold that gives the best separation between signal and background events by calculating the error function.
- Once the optimal threshold is determined the root node is split into two *branches*. Each branch is labeled as mostly signal events or mostly background events.
- Branches that not mostly signal or background (impure) considered as a new node, and split again.
- Considering each impure branch as a new node, the algorithm continues splitting until all branches are labeled as either pure signal *leaves* or pure background *leaves*.
- The algorithm repeats all the above steps until the desired accuracy is achieved.

The threshold for splitting the branches is based on the purity of each branch. The branch which gives the lowest purity is chosen to be the next splitted one. The purity at each branch is defined as

$$P = \frac{N_s}{N_S + N_B}, \tag{101}$$

with N_S and N_B are the number of signal and background events in each branch. Once the purity in each branch is calculated the threshold is optimized by minimizing the error function (Gini index function) which is defined as

$$G_i = \sum_i^n W_i P(1-P), \tag{102}$$

with n is the number of events in each branch and W_i is the weight given to each event. If the sample is pure signal then $G_i = 0$ with $P = 1$. For pure background sample $G_i = 0$ with $P = 0$. Thus minimizing the Gini index indicates a branch with either pure signal or background events. Based on the purity one can identify the branch that is mostly like signal events with $P = 1$ (signal leaf) or mostly like background events with $P = 0$ (background leaf). Events are classified as signal or background according to the leaf where they landed on. If a training event is mis-classified, i.e. a signal event lands on a background leaf or the reverse then the weight of that event is increased (boosted). Thereafter a second tree is built using the new weights. Hence repeating the procedure considering only missclassified events with their weights boosted. Several decision trees can be built and then combined into a forest where the final output BDT discriminant is determined by the majority vote of all trees. The final BDT classifier ranges between -1 and 1, where the events with discriminant value near 1 is considered as signal-like events and those near to -1 are considered as background-like events.

5.2 STATISTICAL EVALUATION OF THE CONSTRUCTED CLASSIFIER

After the BDT classifier is determined, the signal to background yield can be maximized via the ratio $N_s/(N_S + N_B)$. Given the number of the remaining signal and background events; in order to claim the existence or exclusion of a new physics, a statistical test has to be performed. In this manner the null hypothesis is tested against the alternative hypothesis. Based on which test we want to perform i.e. significance or exclusion test, the null and the alternative hypothesis can be defined. For the purpose of excluding the existence of new physics the two hypotheses can be defined as:

- Null hypothesis H_0, which hypothesizes that the data contains both signal plus background events; usually referred to as $S + B$ hypothesis.
- Alternative hypothesis H_1, which hypothesizes that the data contains only background events; usually referred to as B hypothesis.

Historically it was agreed that to make an inference one has to reject the null hypothesis. The expected number of events in the i^{th} bin of the BDT classifier histogram can be defined as

$$E[n^i] = \mu N_S^i + N_B^i \,, \tag{103}$$

with μ the signal strength modifier, with $\mu = 0$ rejecting the $(S+B)$ hypothesis while for $\mu = 1$ rejecting the B hypothesis.

5.2.1 *Maximum likelihood estimate*

The likelihood function is constructed as Poisson probabilities for all bins as:

$$\mathcal{L}(\mu, \theta) = \sum_i^n \frac{(\mu N_S^i + N_B^i)^{n_i}}{n_i} e^{(\mu N_S^i + N_B^i)} . \sum_i X(\tilde{\theta}_i|\theta_i) \,, \tag{104}$$

with $X(\tilde{\theta}_i|\theta_i)$ the probability density function of the nuisance parameter θ_i. The value of $(\tilde{\theta_i})$ is an approximation of the true value of θ_i which can be estimated. For the statistical test one can construct the profile log likelihood as

$$q(\mu) = -2 \ln \lambda(\mu) \,, \tag{105}$$

with $\lambda(\mu)$ is the maximum likelihood estimate. To measure the level of rejecting the null hypothesis[23] we compute the P-value as:

[23] *Measuring how far the null hypothesis is not compatible with the data*

$$P = \int_{q(\mu)}^{\infty} F\left[q(\mu)|\mu\right] dq(\mu) \,, \tag{106}$$

with $F\left[q(\mu)|\mu\right]$ being the probability distribution function that measures the incompatibility between data and our hypothesis, while higher values of $q(\mu)$ correspond to high disagreement between data and hypothesis. Finally, the confidence level, $(1-\alpha)$, for signal exclusion can be obtained as:

$$CL_s = \frac{P\left[q(\mu)|\mu N_S + N_B\right]}{P\left[q(\mu)|N_B\right]} < \alpha \,, \tag{107}$$

where the upper limit on μ is the largest value for μ with $P < \alpha$. Thus one can simply get the upper exclusion limit at different confidence levels by

$$\mu_{\text{upper bound}} = \hat{\mu} + \sigma \Phi^{-1}(1-\alpha) \,, \tag{108}$$

with $\hat{\mu}$ being the estimated expected median and Φ is a cumulative distribution function. In this thesis we use the 5 σ which corresponds to $(1-\alpha) = 0.9999$.

Part III

BEYOND THE STANDARD MODEL PHENOMENOLOGY

6

LEPTON FLAVOR VIOLATING DILEPTON DIJET SIGNATURES FROM STERILE NEUTRINOS AT PROTON COLLIDERS

Published in: 10.1007/JHEP10(2018)067 [9]

Lepton Flavor Violating Dilepton Dijet Signatures from Sterile Neutrinos at Proton Colliders

Stefan Antusch[a] , **Eros Cazzato**[a] , **Oliver Fischer**[b] , **A. Hammad**[a] , **Kechen Wang**[c,d]

[a] *Department of Physics, University of Basel, Klingelbergstr. 82, CH-4056 Basel, Switzerland*

[b] *Institute for Nuclear Physics, Karlsruhe Institute of Technology, Hermann-von-Helmholtz-Platz 1, D-76344 Eggenstein-Leopoldshafen, Germany*

[c] *DESY, Notkestrae 85, D-22607 Hamburg, Germany*

[d] *Center for Future High Energy Physics, Institute of High Energy Physics, Chinese Academy of Sciences, Beijing, 100049, China*

ABSTRACT

In this article we investigate the prospects of searching for sterile neutrinos in lowscale seesaw scenarios via the lepton flavour violating (but lepton number conserving) dilepton dijet signature. In our study, we focus on the final state $e^{\pm}\mu^{\mp}jj$ at the HL-LHC and the FCC-hh (or the SppC). We perform a multivariate analysis at the detector level including the dominant SM backgrounds from di-top, di-boson, and tri-boson. Under the assumption of the active-sterile neutrino mixings $|V_{lN}|^2 = |\theta_e|^2 = |\theta_\mu|^2$ and $|V_{\tau N}|^2 = |\theta_\tau|^2 = 0$, the sensitivities on the signal production cross section times branching ratio $\sigma(pp \to l^{\pm}N) \times BR(N \to l^{\mp}jj)$ and on $|V_{lN}|^2$ for sterile neutrino mass M_N between 200 and 1000 GeV are derived. For the benchmark $M_N = 500$ GeV, when ignoring systematic uncertainties at the HL-LHC (FCC-hh/SppC) with 3 (20) ab^{-1} luminosity, the resulting 2-σ limits on $|V_{lN}|^2$ are 4.9×10^{-3} (7.0×10^{-5}), while the 2 -σ limit on $\sigma \times BR$ are 4.4×10^{-2} (1.6×10^{-2}) fb, respectively. The effect of the systematic uncertainty is also studied and found to be important for sterile neutrinos with smaller masses. We also comment on searches with $\tau^{\pm}\mu^{\mp}jj$ and $\tau^{\pm}e^{\mp}jj$ final states.

6.1 INTRODUCTION

The observation of neutrino oscillations provides evidence that at least two of the involved neutrinos are massive. The absolute mass scale of the light neutrino masses has not been measured but it is bound to lie below about 0.2 eV from neutrinoless double beta decay experiments and cosmological constraints, see for instance Ref. [98, 99] for recent reviews. The origin of the neutrino masses is a prominent puzzle of today's elementary particle physics, since it is not possible within the Standard Model (SM) to account for it in a renormalisable way. Thus neutrino oscillations are evidence from the laboratory for physics beyond the SM.

In the following, we shall focus on the class of SM extensions with neutral fermions, which are gauge singlets and therefore often referred to as "sterile" neutrinos, and can provide mass terms for the light neutrinos to explain the observed oscillations. In particular, the addition of sterile neutrinos allows for a Majorana-type mass term as well as for Dirac-type masses via Yukawa couplings with the SM active neutrino fields. The sterile and active neutrinos mix when the electroweak symmetry is broken, resulting in light and heavy mass eigenstates. This mass generating mechanism goes by the name of type-I seesaw and is highly searched for by the particle physics community, cf. e.g. Refs. [100–102]. Prominent signatures are the likes of neutrinoless double beta decay and same-sign dilepton searches at proton colliders. Furthermore, this class of models can give an explanation for the observed baryon asymmetry of our universe via leptogenesis and of dark matter, for a recent review see e.g. Ref. [103] and references therein.

In type-I seesaw, one often assumes either tiny neutrino Yukawa couplings or a very high mass scale for the heavy neutrinos in order to explain the smallness of the light neutrinos' masses. This assumption makes it, however, nearly impossible to produce these particles at collider experiments.

Alternatively, one may impose a protective ("lepton number"-like) symmetry, where a slight breaking from this symmetry is responsible for the small mass of the light neutrinos. Various types of symmetry protected seesaw models have been constructed in the literature, cf. for instance [104–109]. In this framework neither tiny neutrino Yukawa couplings nor large masses for the heavy neutrinos are required to explain the smallness of the light neutrino masses. Thus heavy neutrinos with masses around the electroweak scale with unsuppressed Yukawa couplings (and thus unsuppressed active-sterile neutrino mixings) are possible, and their effects can be studied at colliders (cf. Ref. [110] for an overview).

Regardless of the underlying model, especially at proton colliders the signatures from sterile neutrinos are often hidden behind comparably enormous rates of SM background for most processes. There are a few processes at high-energy colliders where the background does not pose an unsurmountable problem, the most prominent ones being the lepton number violating (LNV) same sign dilepton $\ell_\alpha^\pm \ell_\alpha^\pm$ final states in the dilepton-dijet channel. However the signal strength of this type of signature is suppressed together with

the LNV by the smallness of the neutrino masses, as discussed for instance in Refs. [107, 111–113].

On the other hand, as was suggested in Ref. [111], the lepton flavour violating (LFV) (but lepton number conserving (LNC)) dilepton signature, with the final state $\ell_\alpha^\pm \ell_\beta^\mp$ ($\alpha \neq \beta$) (and to some extent also the LFV trilepton signature) has reducible background only while its signal strength is unsuppressed by the light neutrino masses.

Previous collider studies have focused mostly on same-sign dileptons for the LHC, e.g. [114–122]. Some studies of this channel can also be found for future accelerators such as the Future Circular Collider (FCC) [123]. Also the trilepton channel has gotten attention recently and triggered some studies of LHC discovery prospects [124–126]. Very little attention has been given to the LFV (but LNC) dilepton-dijet channel so far, despite the promising sensitivity obtained from a "first look" at the parton level in Refs. [111, 127].

The goal of this article is therefore to present a thorough investigation of the LFV (but LNC) dilepton-dijet channel as a signature from sterile neutrino extensions of the Standard Model, especially the $e^\pm \mu^\mp jj$ final state. Our study goes beyond previous works by discussing relevant backgrounds, performing a fast simulation of the detector response for the signal and background, applying multivariate analysis techniques to separate the signal from the background, as well as including a discussion for the statistical and systematic errors. We provide sensitivities not only for the high-luminosity Large Hadron Collider (HL-LHC) but also for the FCC in the hadron colliding mode (FCC-hh). Our results are also applicable to the Super proton-proton Collider (SppC) [128] depending of course on the final design and the corresponding detector performance.

The article is organized as follows. In section 6.2, we briefly describe the theory model we used. In section 7.3, we present the search strategy for LFV dilepton-dijet signals from heavy sterile neutrinos. The results at HL-LHC and FCC-hh are shown in section 6.4. We conclude in section 6.5.

6.2 THE THEORY MODEL

We use a specific realisation which captures the relevant features of the symmetry protected seesaw models for the collider phenomenology as our benchmark model. This realisation involves two heavy neutrinos that supposes a "lepton number"-like symmetry (an extended version of the usual lepton number), which can be found in e.g. [129]. For this collider study it is sufficient to focus on the limit of intact protective symmetry, i.e. symmetry limit, since the signal is lepton number conserving and the light neutrino masses are for collider purposes effectively zero, see below.[1]

1 When the symmetry is approximate, viz. slightly broken, non-degenerate heavy neutrino masses induce LNV.

The benchmark model includes one pair of sterile neutrinos N_R^1 and N_R^2 which are relevant for the collider phenomenology. The resulting Lagrangian density is given by:

$$\mathscr{L} = \mathscr{L}_{SM} - \overline{N_R^1} M_N N_R^{2\,c} - y_{\nu_\alpha} \overline{N_R^1} \widetilde{\phi}^\dagger L^\alpha + \text{H.c.} + \dots \,, \tag{109}$$

where $\mathscr{L}_{SM}$ contains the usual SM field content and with L^α, $(\alpha = e, \mu, \tau)$, and ϕ being the lepton and Higgs doublets, respectively, y_{ν_α} are the complex-valued neutrino Yukawa couplings, and M_N the sterile neutrino mass. The ellipses indicate terms for additional sterile neutrinos which are decoupled from collider phenomenology.

The symmetric mass matrix $\mathcal{M}$ of the active and sterile neutrinos is obtained from Eq. (147) after electroweak symmetry breaking $\mathscr{L}$ contains $-1/2\,\overline{n^c}\,\mathcal{M}\,n + \text{H.c}$, with $n = \left(\nu_{e_L}, \nu_{\mu_L}, \nu_{\tau_L}, (N_R^1)^c, (N_R^2)^c\right)^T$. It can be diagonalized by the unitary 5×5 leptonic mixing matrix U:

$$U^T \mathcal{M}\, U \cong \text{Diag}\,(0, 0, 0, M_N, M_N) \,. \tag{110}$$

The mass eigenstates $\tilde{n}_j = (\nu_1, \nu_2, \nu_3, N_4, N_5)_j^T = U_{j\alpha}^\dagger n_\alpha$ are the three light neutrinos, which are massless in the symmetry limit, and two heavy neutrinos with degenerate mass eigenvalues M_N in the symmetric limit. The leptonic mixing matrix U in Eq. (110) can be expressed explicitly, cf. [129]. Its entries are governed by the active-sterile neutrino mixing angles which are quantified via

$$\theta_\alpha = \frac{y_{\nu_\alpha}^*}{\sqrt{2}} \frac{v_{EW}}{M_N} \,, \qquad |\theta|^2 := \sum_\alpha |\theta_\alpha|^2 \,, \tag{111}$$

with $v_{EW} = 246.22$ GeV the vacuum expectation value of the Higgs field.

Since the light and heavy neutrino mass eigenstates are admixtures of the active and sterile neutrinos, the weak currents, cast into the mass basis, are given by

$$j_\mu^\pm = \sum_{i=1}^{5} \sum_{\alpha=e,\mu,\tau} \frac{g}{\sqrt{2}} \bar{\ell}_\alpha \gamma_\mu P_L U_{\alpha i} \tilde{n}_i + \text{H.c.} \,, \tag{112}$$

$$j_\mu^0 = \sum_{i,j=1}^{5} \sum_{\alpha=e,\mu,\tau} \frac{g}{2\,c_W} \overline{\tilde{n}_j} U_{j\alpha}^\dagger \gamma_\mu P_L U_{\alpha i} \tilde{n}_i \,, \tag{113}$$

with U the leptonic mixing matrix, g being the weak coupling constant, c_W the cosine of the Weinberg angle and $P_L = \frac{1}{2}(1 - \gamma^5)$ the left-chiral projection operator. The resulting heavy neutrino interactions can be summarized as

$$j_\mu^\pm \supset \frac{g}{2} \theta_\alpha \bar{\ell}_\alpha \gamma_\mu P_L \left(-i N_4 + N_5\right) + \text{H.c.} \,, \tag{114}$$

$$j_\mu^0 = \frac{g}{2\,c_W} \sum_{i,j=1}^{5} \vartheta_{ij} \overline{\tilde{n}_i} \gamma_\mu P_L \tilde{n}_j \,, \tag{115}$$

$$\mathscr{L}_{\text{Yuk.}} \supset \frac{M_N}{v_{EW}} \sum_{i=1}^{3} \left(\vartheta_{i4}^* \overline{N_4^c} + \vartheta_{i5}^* \overline{N_5^c}\right) h\, \nu_i + \text{H.c.} \,, \tag{116}$$

with $h = \sqrt{2}\,\mathrm{Re}(\phi^0)$ being the real scalar Higgs boson and $\vartheta_{ij} = \sum_{\alpha=e,\mu,\tau} U^{\dagger}_{i\alpha} U_{\alpha j}$.

In the limit of the protective symmetry being exact, the benchmark model adds seven parameters to the SM, the moduli of the neutrino Yukawa couplings ($|y_{\nu_e}|$, $|y_{\nu_\mu}|$, $|y_{\nu_\tau}|$), their respective phase, or equivalently, the active-sterile mixing angles from Eq. (148), and the mass M_N. The phases may be accessible in neutrino oscillation experiments (see e.g. [130, 131]). We restrict ourselves to the four parameters $|\theta_e|$, $|\theta_\mu|$, $|\theta_\tau|$ and M_N. In the following, we also use the neutrino mixing matrix elements $|V_{\alpha N}|^2$ to present our results, which are commonly used in the literature to quantify the active-sterile neutrino mixing. For a fixed flavor α (usually identified via the charged lepton l_α) this notation relates to the one introduced above in the following way:

$$|V_{\alpha N}|^2 = |U_{\alpha 4}|^2 + |U_{\alpha 5}|^2 = |\theta_\alpha|^2 \,. \tag{117}$$

6.3 SEARCH STRATEGY

Proton colliders provide an environment where the SM can be tested at highest center-of-mass energies. For what follows we consider the HL-LHC with 14 TeV center-of-mass energy and a total integrated luminosity of 3 ab^{-1} [132]. We also consider the discussed FCC-hh [133–135] and the SppC [128], with envisaged center-of-mass energies of 100 TeV and target integrated luminosities of around 20 ab^{-1} [136]. For brevity, we will only refer to the FCC-hh in the following.

6.3.1 *Signal: Mixed-flavor Dilepton Plus Jets from Heavy Neutrinos*

Heavy neutrinos can be produced from proton-proton collisions via Drell-Yan processes, Higgs boson decays, and gauge boson fusion, cf. [137–139]. We focus here on charged current Drell-Yan production of a heavy neutrino with an associated charged lepton yielding $pp \to \ell^{\pm}_{\alpha} N$, cf. Fig. 1. It is the dominant production mechanism for heavy neutrino masses around the electroweak scale and the considered center-of-mass energies. It is worth noting that the $W\gamma$ fusion production process is the next most important process in the mass range from 200 GeV to ~1 TeV, and it becomes more important and even surpasses the charged current Drell-Yan production for larger heavy neutrino masses [123]. The contribution from $W\gamma$ adds about 20~30% to the LO cross section, cf. Ref. [123]. Due to its limited enhancement on the final discovery limits for the here considered mass range, the $W\gamma$ contributions to the signal are not considered in this study.

As shown in Fig. 1, the charged current decays of the Drell-Yan produced heavy neutrinos together with the hadronic decay of the final state W boson yield the semileptonic final state $\ell^{\pm}_{\alpha}\ell^{\mp}_{\beta}jj$. To discriminate between these two final state leptons, we label the lepton from the Drell-Yan off-shell $W^{*\pm}$ as $l^{\pm}_{W^*}$ (i.e. $l^{\pm}_{\alpha}$ or $l^{\pm}$), while the lepton from the heavy neutrino as $l^{\mp}_{N}$ (i.e. $l^{\mp}_{\beta}$ or $l'^{\mp}$). We note that for the signal these two leptons can have different flavors. The event rate is sensitive to the mixing angle combination of $|\theta_\alpha|^2$ and $|\theta_\beta|^2/|\theta|^2$ through the production and decay channel, respectively. Here the flavor indices $\alpha, \beta =$

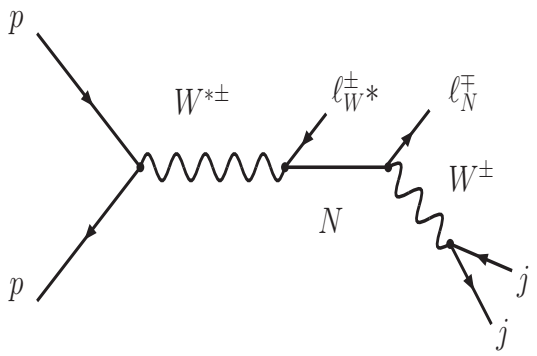

Figure 1: The Feynman diagram depicting the dominant signal production mechanism for heavy neutrino masses and center-of-mass energies as considered in this article.

e, μ, τ can be inferred from the charged leptons. For $\alpha \neq \beta$, this final state yields a signal for lepton flavour violation, because there is no SM background process at the parton level as discussed in Refs. [111, 127]. We emphasize that we study the LNC process with leptons of opposite charge since there the signal strength is not suppressed by the smallness of the neutrino masses.[2]

The signal for our study is $e^{\pm}\mu^{\mp}jj$ with $\alpha = e\,(\mu)$ and $\beta = \mu\,(e)$, which tests the mixing angle combination $|\theta_e\theta_\mu|^2/|\theta|^2$ or equivalently, $|V_{eN}V_{\mu N}|^2/\sum_\alpha |V_{\alpha N}|^2$. For practical reasons we make the following assumption and discuss the special case for the active-sterile mixing angles:

$$|V_{lN}|^2 = |\theta_e|^2 = |\theta_\mu|^2 \neq 0 \qquad \text{and} \qquad |V_{\tau N}|^2 = |\theta_\tau|^2 = 0\,, \tag{118}$$

which implies that $|V_{eN}V_{\mu N}|^2/\sum_{\alpha=e,\mu,\tau}|V_{\alpha N}|^2 = \frac{1}{2}|V_{lN}|^2$. The results derived below are valid for this case only, but they can be translated to any of the other possible set of active-sterile mixing angles with a numerical overall factor.

In Fig. 2, we show the production cross section times branching ratio $\sigma(pp \to l^{\pm}N) \times \mathrm{BR}(N \to l^{\mp}jj)$ in fb at the HL-LHC and FCC-hh when $|V_{lN}|^2 = 10^{-2}$ and $|V_{\tau N}| = 0$. We note that here $l = e, \mu$. Besides the mixed flavor lepton pair $e^{\pm}\mu^{\mp}$, the cross sections in this figure also include the production of the same flavor lepton pairs e^+e^- and $\mu^+\mu^-$. The cross sections for a few mass points can be also calculated from the initial number of events in Table 2 and 3.

It is worth noting that the signal process may feature two jets with an invariant mass around the W boson mass with possible further hadronic activity. We remark that in scenarios where the heavy neutrino mass is large its decay products can be strongly boosted, such that the hadronic decays of the W bosons may be collimated, giving rise to a single jet instead of two.

2 Breaking of the protective symmetry can induce LNV by heavy neutrino oscillations as discussed in Refs. [113, 140–142], but even in a optimistic case the fraction of LNV events is negligible (for $\theta^2 \lesssim 10^{-5}$) [113].

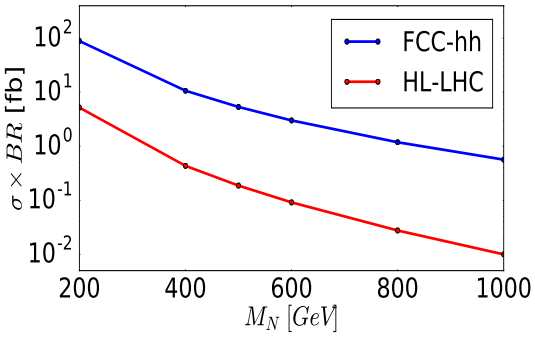

Figure 2: Production cross section times branching ratio $\sigma(pp \to l^{\pm}N) \times BR(N \to l^{\mp}jj)$ in fb for heavy neutrino mass eigenstates via the Drell-Yan processes $pp \to W^* \to \ell^{\pm}N \to \ell^{\pm}\ell^{\mp}jj$ at leading order. Here, $l = e, \mu$ and the cross section includes di-leptons with all flavor combinations (i.e., $e^{\pm}\mu^{\mp}$, e^+e^-, and $\mu^+\mu^-$). The active-sterile mixings are fixed as $|V_{lN}|^2 = |V_{eN}|^2 = |V_{\mu N}|^2 = 10^{-2}$, $|V_{\tau N}| = 0$.

6.3.2 *Standard Model Backgrounds*

The dominant SM backgrounds contributing to the $e^{\pm}\mu^{\mp}jj$ signature arise for instance from the di-lepton final state with additional missing momentum due to processes with light neutrinos, or from the di-tau final state with both tau's decaying leptonically. In principle, these backgrounds can be rejected with high signal efficiency by requiring the amount of missing energy in the final state to be small. However, due to effects like the finite resolution of the missing momentum, some backgrounds may still survive after such cuts. Thus, we expect that a full detector simulation, which is beyond the scope of the present analysis, can be important.

The background processes considered in our analysis are

1. di-top in fully leptonical decays:
   1.1. $pp \to t\bar{t} \to (bW^+)(\bar{b}W^-) \to (b\,l^+\nu)(\bar{b}\,l^-\bar{\nu})$, where both l can be either e or μ ;
2. di-boson with di-tau di-jet final states:
   2.1. $pp \to WZ \to (jj)(\tau^+\tau^-)$;
   2.2. $pp \to ZZ \to (jj)(\tau^+\tau^-)$;
3. tri-boson with at least 2 jets and at least 2 leptons (including taus):
   3.1. $pp \to WWZ \to (l\nu)(l\nu)(jj)$;
   3.2. $pp \to WWZ \to (jj)(jj)(\tau^+\tau^-)$;
   3.3. $pp \to WWZ \to (jj)(l\nu)(\tau^+\tau^-)$;
   3.4. $pp \to WWZ \to (jj)(l\nu)(l^+l^-)$.

For the tri-boson, if both taus decay leptonically, the final state will have 3 leptons. When one lepton is out of the detector range or mis-identified, it can

still contribute to the backgrounds. The other decay channels of W or Z bosons will either have no $e^{\pm}\mu^{\mp}$ final states or are lacking of jets. Therefore, they are not included in our analysis. The production cross sections corresponding to $t\bar{t}$, WZ, ZZ, WWZ with decaying into the final states listed above are about 3432 (1.37×10^5), 1787 (5654), 468 (4483), 6.83 (95.5) fb at the HL-LHC (FCC-hh), respectively.

Furthermore, we checked many other possible background processes, including for instance all the processes listed above with one additional gluon jet or photon (γ) in the final state, and also the processes $VVgg$, $\gamma\mu\mu V$ with $V = Z, W$, and $\gamma\mu\nu W$. We used an estimated rate of misidentifying γ, g as an electron at FCC-hh of $\sim 10^{-3}$, comparable to the one at the LHC. We found that especially the requirement of large transverse momenta of the g, γ, renders the cross sections of these processes much smaller than the ones listed above, and we decided not to include them into our analysis.

6.3.3 *Simulation, Pre-selection and Analysis*

For the simulation of signal and background samples, we use MadGraph5 version 2.4.3 [143] as the event generator. The parton shower and hadronization is done by Pythia6 [144], while the detector simulations are completed by Delphes [97] with the ATLAS configuration card file (version 3.4.1) for the HL-LHC and with the FCC-hh configuration card file (October 2016 version) for the FCC-hh.

Based on the kinematics of the signal and backgrounds, in order to generate the events more effectively, we apply the following cuts at the simulation level: a minimal transverse momentum $p_T(j) > 20$ GeV, $p_T(l) > 20$ GeV and the range of the pseudorapidity $|\eta(j)| < 10$, $|\eta(l)| < 7$ for jets (including b-jets) and leptons; a maximal missing energy $\not{E}_T < 30$ GeV. The cuts on $|\eta|$ do not affect the analysis because the detector geometry limits this range to be $|\eta| \lesssim 5$. The cut on the missing energy are motivated from the prior knowledge that the signal does not produce missing energy at the parton level and only a limited amount can be created during reconstruction [111]. These cuts at the parton level enhance the quality of the background events and thus save the simulation time.

The following pre-selection cuts are then applied on the simulation events:

1. Exactly 1 muon, exactly 1 electron, with opposite charges (i.e. $e^{\pm}\mu^{\mp}$); at least 2 jets; no b-jet and no taus;

2. Both jets and leptons with threshold cuts of $p_T > 30$ GeV;

3. Missing energy $\not{E}_T < 20$ GeV.

After the pre-selection cuts, the final state will have at least 2 light jets, 1 muon and 1 electron. The first two leading jets j_1 and j_2 are considered to be the jets from the final state W decay (see Fig. 1). To identify the lepton l_N from the sterile neutrino decay, we combine the first two leading jets with each lepton and calculate the invariant masses corresponding to two combinations.

The combination with invariant mass closer to the sterile neutrino mass indicates l_N, while the other lepton will be identified as the lepton l_{W^*} from the off-shell W^* decay.

Once the l_{W^*} and l_N are identified, the following 40 observables are input into the TMVA package [145] to perform the Multi-Variate Analysis (MVA):

1. global observables:
   - 1.1. the missing energy $\not{E}_T$;
   - 1.2. the scalar sum of the transverse momentum p_T of all jets H_T;
   - 1.3. the scalar sum of p_T of all visible objects p_T^{vis}.
2. observables for the jets and leptons:
   - 2.1. p_T and the pseudorapidity η of the first two leading jets j_1 and j_2: $p_T(j_1)$, $\eta(j_1)$, $p_T(j_2)$, $\eta(j_2)$;
   - 2.2. p_T, η and the invariant mass M of the system of j_1 and j_2: $p_T(j_1 + j_2)$, $\eta(j_1 + j_2)$, $M(j_1 + j_2)$;
   - 2.3. p_T and η of the lepton from the off-shell W decay l_{W^*} and the lepton from the heavy neutrino N decay l_N: $p_T(l_{W^*})$, $\eta(l_{W^*})$, $p_T(l_N)$, $\eta(l_N)$;
   - 2.4. M of the system of l_{W^*} and l_N: $M(l_{W^*} + l_N)$;
   - 2.5. the pseudorapidity difference $\Delta\eta$ between jet and lepton: $\Delta\eta(j_1, l_{W^*})$, $\Delta\eta(j_2, l_{W^*})$, $\Delta\eta(j_1, l_N)$, $\Delta\eta(j_2, l_N)$;
   - 2.6. the azimuthal angle difference $\Delta\phi$: $\Delta\phi(j_1, l_{W^*})$, $\Delta\phi(j_2, l_{W^*})$, $\Delta\phi(j_1, l_N)$, $\Delta\phi(j_2, l_N)$;
   - 2.7. the angular distance difference ΔR: $\Delta R(j_1, l_{W^*})$, $\Delta R(j_2, l_{W^*})$, $\Delta R(j_1, l_N)$, $\Delta R(j_2, l_N)$.
3. observables for the reconstructed N system:
   - 3.1. p_T, η, and M of the system: $p_T(j_1 + j_2 + l_N)$, $\eta(j_1 + j_2 + l_N)$, $M(j_1 + j_2 + l_N)$;
   - 3.2. $\Delta\eta$, $\Delta\phi$ and ΔR between the system of jets and l_N: $\Delta\eta(j_1 + j_2, l_N)$, $\Delta\phi(j_1 + j_2, l_N)$, $\Delta R(j_1 + j_2, l_N)$.
4. observables for the reconstructed off-shell W^* system:
   - 4.1. M of the system: $M(j_1 + j_2 + l_N + l_{W^*})$;
   - 4.2. p_T, η, and M of the system of jets and l_{W^*}: $p_T(j_1 + j_2 + l_{W^*})$, $\eta(j_1 + j_2 + l_{W^*})$, $M(j_1 + j_2 + l_{W^*})$;
   - 4.3. $\Delta\eta$, $\Delta\phi$ and ΔR between the system of jets and l_{W^*}: $\Delta\eta(j_1 + j_2, l_{W^*})$, $\Delta\phi(j_1 + j_2, l_{W^*})$, $\Delta R(j_1 + j_2, l_{W^*})$.

The details of the multivariate and statistical analysis are explained in the Appendix 6.6.

6.4 RESULTS

In this section, we present the analysis results for the HL-LHC and for the 100 TeV proton collider FCC-hh, which is also valid for the SppC with the same detector performance. We remind ourselves that the HL-LHC (FCC-hh) has center-of-mass energy $\sqrt{s} = 14$ (100) TeV and that we consider a total integrated luminosity of 3 (20) ab^{-1}.

6.4.1 *Results at HL-LHC and FCC-hh*

To illustrate our results, we show the distributions of some selected observables after applying the pre-selection cuts for the signal with benchmark mass M_N = 500 GeV (S, black with filled area), and SM backgrounds of $t\bar{t}$ (red), WZ (blue), ZZ (cyan), and WWZ (green) in Appendix 6.7. The Fig. 8 and Fig. 9 are for the HL-LHC and FCC-hh, respectively.

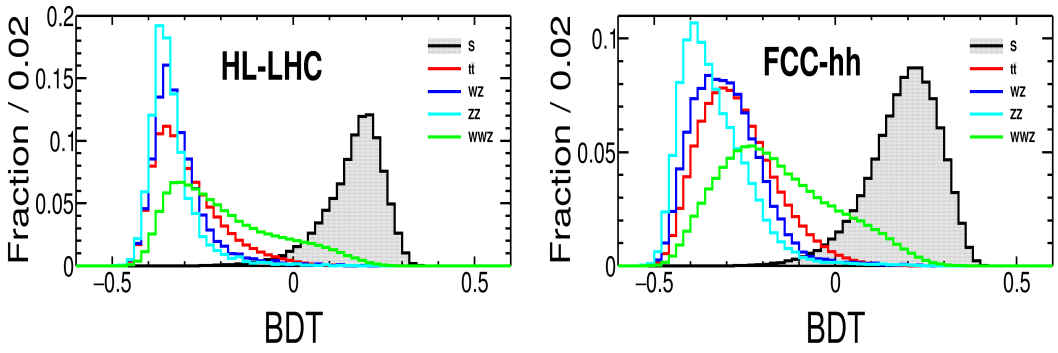

Figure 3: Distributions of BDT response at the HL-LHC (left) and FCC-hh (right) for signal with M_N = 500 GeV (S, black with filled area), and for SM backgrounds including $t\bar{t}$ (red), WZ (blue), ZZ (cyan), and WWZ (green).

One can see from Fig. 8 that the distributions of signal and SM background are very different for the given examples. For brevity, we describe here only a few of them at the HL-LHC: The distributions of the $M(j_1 + j_2 + l_N)$ of the signal peaks sharply around the sterile neutrino mass 500 GeV, while all backgrounds peak below 250 GeV; In the di-jet invariant mass $M(j_1 + j_2)$ plot, the signal and WZ peaks around the W boson mass, while ZZ and WWZ peak around the Z boson mass and $t\bar{t}$ has a flat peak around 110 GeV; In the dilepton invariant mass $M(l_{W^*} + l_N)$ plot, the backgrounds WZ and ZZ peak around 70 GeV, and $t\bar{t}$ and WWZ peak around 100 GeV, while the signal has a very flat peak around 400 GeV; For the distributions of $M(j_1 + j_2 + l_N + l_{W^*})$, $p_T(l_N)$, $p_T(j_1 + j_2)$ and p_T^{vis}, the signal peaks at larger values compared to the backgrounds. Other useful distributions to distinguish signal from background exist, for instance $\not{E}_T$ and angular observables, which we list in section 6.3.3.

As described in section 6.3.3, all the 40 observables listed in that section are input into the TMVA. We utilize the Boosted Decision Trees (BDT) method to perform the multivariate analysis. The distributions of the BDT response

Cuts		M_N [GeV]						Background			
		200	400	500	600	800	1000	$t\bar{t}$	WZ	ZZ	WWZ
initial		1.56×10^4	1307	563	275	83.2	30.7	1.03×10^7	5.36×10^6	1.40×10^6	2.05×10^4
pre-sel.	cut 1	2545	260	109	50.6	14.1	5.0	3.26×10^5	2.63×10^4	6008	343
	cut 2	1830	229	97.7	45.2	12.4	4.4	1.83×10^5	1462	337	164
	cut 3	1376	130	46.9	18.5	3.7	0.99	5.44×10^4	265	64	58
BDT	> 0.2013	111	-	-	-	-	-	19.1	0.10	0.027	0.56
	> 0.2162	-	37.8	-	-	-	-	2.3	-	0.027	0.41
	> 0.2148	-	-	13.9	-	-	-	0.63	-	0.014	0.16
	> 0.2263	-	-	-	3.6	-	-	0.13	-	0.014	0.046
	> 0.2264	-	-	-	-	0.63	-	0.0068	-	-	0.013
	> 0.2348	-	-	-	-	-	0.15	0.00012	-	-	0.0041

Table 2: Numbers of events at each cut stage for signals with fixed $|V_{lN}|^2 = 10^{-2}$ and different sterile neutrino masses M_N and for background processes. The numbers correspond to an integrated luminosity of 3 ab^{-1} at the HL-LHC.

for the signal with M_N = 500 GeV (S, black with filled area), and for the SM backgrounds including $t\bar{t}$ (red), WZ (blue), ZZ (cyan), and WWZ (green) are shown in Fig. 27 for the HL-LHC (left) and the FCC-hh (right). The BDT response shows that a very good separation between the signal and background is possible. For WWZ background process, although it has larger mixing with the signal, due to its relatively small initial production cross section, its final contributions to the backgrounds after the optimized BDT cut are still limited, cf. Table 2 and Table 3.

Cuts		M_N [GeV]						Background			
		200	400	500	600	800	1000	$t\bar{t}$	WZ	ZZ	WWZ
initial		1.78×10^6	2.14×10^5	1.07×10^5	6.03×10^4	2.38×10^4	1.13×10^4	2.75×10^9	1.13×10^8	8.97×10^7	1.91×10^6
pre-sel.	cut 1	3.84×10^5	5.98×10^4	3.03×10^4	1.70×10^4	6347	2856	6.08×10^7	1.96×10^6	1.46×10^6	5.45×10^4
	cut 2	3.39×10^5	5.76×10^4	2.95×10^4	1.66×10^4	6257	2824	3.61×10^7	6.20×10^4	4.24×10^4	1.96×10^4
	cut 3	2.90×10^5	4.36×10^4	2.10×10^4	1.12×10^4	3722	1484	9.08×10^6	7090	5497	6657
BDT	> 0.2935	6611	-	-	-	-	-	238.4	0.6	0.5	15.9
	> 0.2827	-	5762	-	-	-	-	81.5	0.9	0.7	20.3
	> 0.2654	-	-	4666	-	-	-	53.8	0.3	0.5	16.4
	> 0.2611	-	-	-	2701	-	-	33.9	-	-	8.9
	> 0.2428	-	-	-	-	1261	-	27.1	0.3	-	6.7
	> 0.2262	-	-	-	-	-	693	27.6	0.3	-	6.7

Table 3: Numbers of events at each cut stage for signals with fixed $|V_{lN}|^2 = 10^{-2}$ and different sterile neutrino masses M_N and for background processes. The numbers correspond to an integrated luminosity of 20 ab^{-1} at the FCC-hh.

In Table 2, we show the numbers of events at each cut stage for signals with $|V_{lN}|^2 = 10^{-2}$ and different sterile neutrino masses M_N and for background processes of $t\bar{t}$, WZ, ZZ, and WWZ at the HL-LHC with 3 ab^{-1} integrated luminosity. The numbers of events at the FCC-hh with 20 ab^{-1} integrated luminosity are presented in Table 3. Since the kinematical distributions vary with M_N, the BDT cuts are optimized for different masses.

Based on our analysis, the prospects for sterile neutrino searches via the opposite sign mixed-flavor dilepton plus di-jet (i.e. $e^{\pm}\mu^{\mp}jj$) including a systematic uncertainty of $\delta_{sys} = 10\%$ on the background are derived, using the Higgs Analysis-Combined Limit tool [146], for details see the explanations in

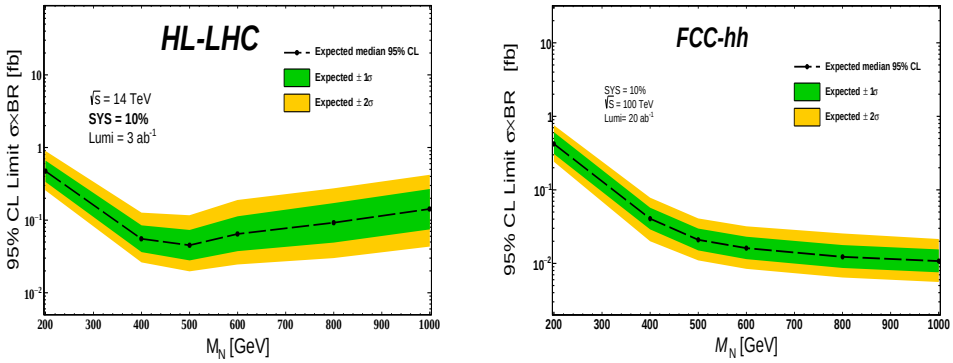

Figure 4: Expected limits on the production cross section times branching ratio $\sigma(pp \to l^{\pm}N) \times BR(N \to l^{\mp}jj)$ in fb when testing the signal hypothesis at the HL-LHC (left) with $\sqrt{s} = 14$ TeV and 3 ab^{-1} and at the FCC-hh (right) with $\sqrt{s} = 100$ TeV and 20 ab^{-1}, including the 1 and 2-σ confidence interval. These limits have been derived based on the analysis of the $e^{\pm}\mu^{\mp}jj$ final state.

the Appendix 6.6. In Fig. 4, we show the expected limit on the production cross section times branching ratio $\sigma(pp \to l^{\pm}N) \times BR(N \to l^{\mp}jj)$ in fb when testing the signal hypothesis at the HL-LHC (left) with $\sqrt{s} = 14$ TeV and 3 ab^{-1} and at the FCC-hh (right) with $\sqrt{s} = 100$ TeV and 20 ab^{-1}, including the 1 and 2-σ confidence interval. The figure shows that the total production cross section for this final state can be tested at the HL-LHC and FCC-hh for values of $\mathcal{O}(0.1)$ and $\mathcal{O}(0.01)$ fb, respectively. It is worthy of note that the decline of the production cross section for increasing masses is (at least partially) compensated for by the increased BDT efficiency, such that the limits on the total cross section remain more or less flat.

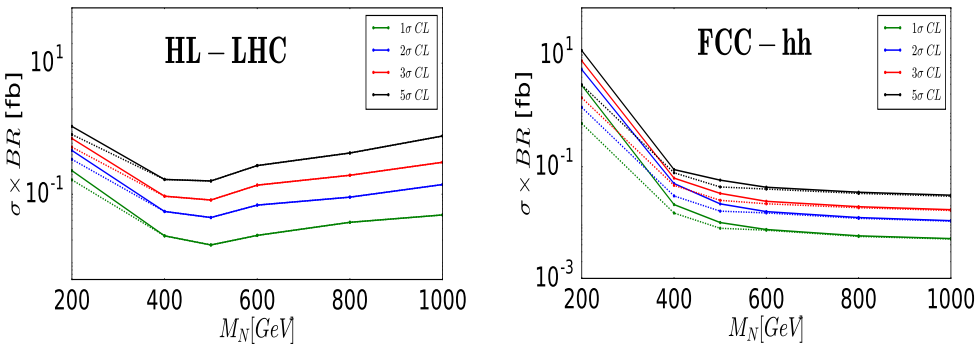

Figure 5: Same as Fig. 4, including the 1, 2, 3 and 5-σ median expected limits on the production cross section times branching ratio $\sigma(pp \to l^{\pm}N) \times BR(N \to l^{\mp}jj)$ in fb at the HL-LHC (left) with 3 ab^{-1} luminosity and at the FCC-hh (right) with $\sqrt{s} = 100$ TeV and 20 ab^{-1} luminosity. In both panels the solid (dashed) line denotes that a 10% (0%) systematic uncertainty on the background is considered.

In Fig. 5, we show the 1, 2, 3 and 5-σ median expected limits on the production cross section times branching ratio $\sigma(pp \to l^{\pm}N) \times BR(N \to l^{\mp}jj)$ in

fb at the HL-LHC (left) with $\sqrt{s} = 14$ TeV and 3 ab^{-1} luminosity and at the FCC-hh (right) with $\sqrt{s} = 100$ TeV and 20 ab^{-1} luminosity. In this figure, the solid (dashed) line denotes that 10% (0%) systematic uncertainty on the background is considered. Comparing the solid and dashed curves, one can see that as sterile neutrino mass M_N decreases, the effects of the systematic uncertainty on the background become more obvious. This is because that the number of background events after the BDT cut will increase as M_N decreases (cf. Table 2 and Table 3). When $M_N = 500$ GeV, with 0% systematic uncertainty on background, the 2 (5)-σ limit on the $\sigma \times$ BR is $4.4 \times 10^{-2}(1.5 \times 10^{-1})$ fb at the HL-LHC, while it is $1.6 \times 10^{-2}(4.3 \times 10^{-2})$ fb at the FCC-hh.

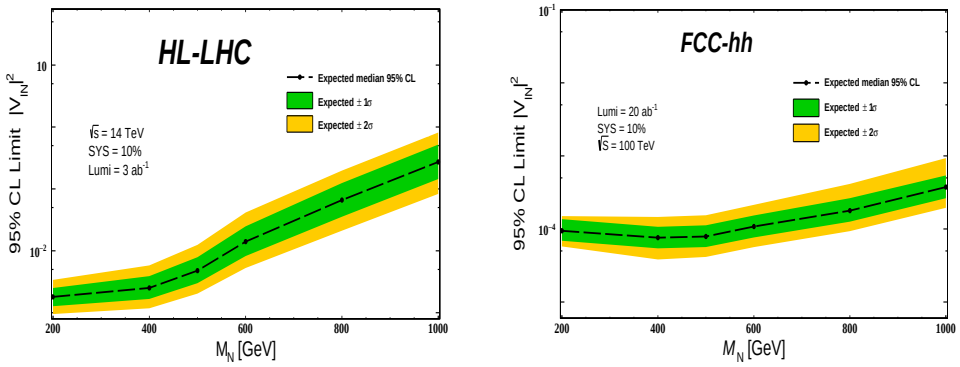

Figure 6: Expected limits on the parameter $|V_{lN}|^2$ when testing the signal hypothesis for $|V_{lN}|^2 = |V_{eN}|^2 = |V_{\mu N}|^2$ and $|V_{\tau N}|^2 = 0$, including the 1 and 2-σ confidence interval. The left (right) panel denotes the limit for the HL-LHC (FCC-hh) with $\sqrt{s} = 14$ (100) TeV and 3 (20) ab^{-1} luminosity. These limits have been derived based on the analysis of the $e^{\pm}\mu^{\mp}jj$ final state.

Using the assumption in Eq. (118) for the active-sterile mixing angles, we can convert the limits from Fig. 5 into limits on $|V_{lN}|^2$, cf. the definition in Eq. (117). We show the resulting expected median limit on the total active-sterile mixing $|V_{lN}|^2$ in Fig. 6 for the HL-LHC (left) with $\sqrt{s} = 14$ TeV and 3 ab^{-1} and at the FCC-hh (right) with $\sqrt{s} = 100$ TeV and 20 ab^{-1}, including the 1 and 2σ confidence interval. When extracting these limits, a systematic uncertainty of 10% on the background has been considered. It is worthwhile to point out that these results are quantitatively close to the first estimates from Ref. [111].

In Fig. 7, we show the 1, 2, 3 and 5-σ median expected limits on the total active-sterile mixing squared $|V_{lN}|^2$ for the HL-LHC (left panel) and the FCC-hh (right panel), including a systematic uncertainty of 0% (dashed) and 10% (solid) on the background. Comparing the solid and dashed curves, one can see that at the HL-LHC (FCC-hh), when $M_N < 400$ (600) GeV, the effects of 10% systematic uncertainty on the background become visible. For 200 GeV mass point, due to much larger background events after the BDT cut, the systematic uncertainty can weaken the limits greatly. Therefore, to enhance the discovery power for sterile neutrino with small masses, controlling the systematic uncertainty at such future colliders will be very important. When $M_N = 500$ GeV, with 0% systematic uncertainty on the background, the 2 (5)-σ limit on the $|V_{lN}|^2$ are $4.9 \times 10^{-3}(1.7 \times 10^{-2})$ at the HL-LHC, while it is $7.0 \times 10^{-5}(1.9 \times 10^{-4})$ at the FCC-hh.

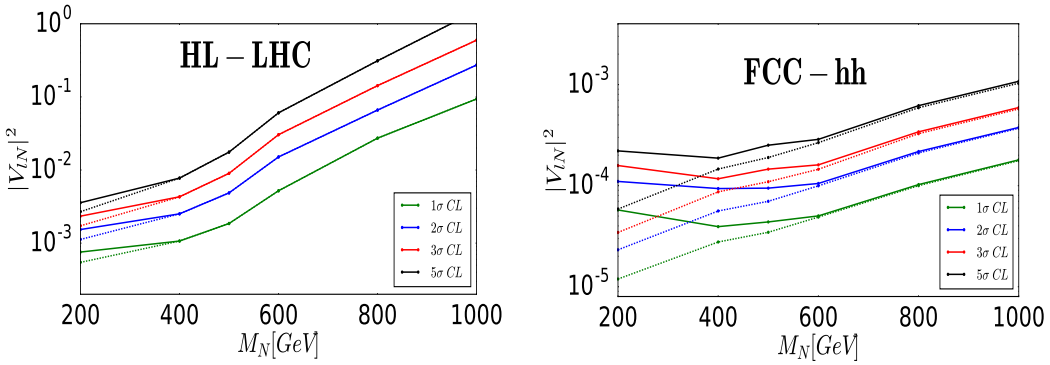

Figure 7: Same as Fig. 6, including the 1, 2, 3 and 5-σ median expected limits on the parameter $|V_{lN}|^2$ for $|V_{lN}|^2 = |V_{eN}|^2 = |V_{\mu N}|^2$ and $|V_{\tau N}|^2 = 0$, at the HL-LHC (left) with 3 ab^{-1} luminosity and at the FCC-hh (right) with $\sqrt{s} = 100$ TeV and 20 ab^{-1} luminosity. In both panels the solid (dashed) line denotes that a 10% (0%) systematic uncertainty on the background is considered.

6.4.2 *Discussion*

We note that our results on the sensitivity of the proton-proton colliders are qualitatively identical to those in Ref. [111]. Moreover, the sensitivity is comparable to the analyses that consider lepton-number violating final states, cf. e.g. [147].

An important low energy constraint exists, that also tests the here considered active-sterile mixings: the $\mu \to e\gamma$ measurement from the Mu to E Gamma (MEG) collaboration. Via the null result in their searches for the process $\mu \to e\gamma$ [148] they put stringent limits on the combination $|V_{eN}V_{\mu N}|$ (which is equal to $|\theta_e^*\theta_\mu|$) [129, 149]. Indeed, finding a signal in the $e^\pm\mu^\mp jj$ channel at the HL-LHC or the FCC would be in tension with the present constraints from MEG.

It is interesting to consider the LFV dilepton dijet signature with one tau lepton in the final state. The relevant active-sterile mixing parameters that are tested in this way are then $|V_{eN}V_{\tau N}|$ and $|V_{\mu N}V_{\tau N}|$, respectively. The present constraints on these mixing angle combinations are much weaker compared to those derived from the MEG result, cf. e.g. Ref. [149] and references therein. This could mean a great discovery potential in these channels, if our results for the sensitivities would also hold, at least approximately, for the $e^\pm\tau^\mp jj$ and $\mu^\pm\tau^\mp jj$ final states.

However, including the tau flavor necessitates to reconstruct the tau lepton either from a muon or an electron, which requires the finding of a non-vanishing impact parameter and inserts additional missing momentum from the neutrino associated to a tau decay. More promising is the reconstruction of a tau from its hadronic decays, which, on the other hand, introduces many additional backgrounds involving heavy quarks.

Heavy neutrinos with masses above 1 TeV are produced dominantly via the $W\gamma$ fusion processes. The kinematics of the final state particles is very similar to the ones studied in our analysis. We therefore assume, that for $M > 1$ TeV, the sensitivity via $W\gamma$ fusion becomes better compared to our results, such that the latter comprise a conservative limit on these parameters.

6.5 CONCLUSIONS

Low scale seesaw scenarios allow for large active-sterile neutrino mixings and heavy neutrinos with masses that are kinematically accessible at particle colliders. Due to the approximate symmetry, lepton number violation is suppressed in these scenarios, which motivates the study of lepton flavour violating (LFV) but lepton number conserving (LNC) signal channels.

In this article we investigated the most promising sterile neutrino signature of this type, based on parton level studies from previous works, the LFV but LNC final state $e^{\pm}\mu^{\mp}jj$. This final state does not have SM backgrounds at the parton level, such that the signal and backgrounds can be well separated via a thorough analysis of the distributions from a number of kinematic observables.

For the active-sterile neutrino mixings we assumed, for definiteness, $|V_{lN}|^2 = |\theta_e|^2 = |\theta_\mu|^2$ and $|V_{\tau N}|^2 = |\theta_\tau|^2 = 0$. We remark that the $e^{\pm}\mu^{\mp}jj$ signature is sensitive to $|V_{eN}V_{\mu N}|^2/\sum_\alpha |V_{\alpha N}|^2$, which means that it is suppressed if one of the two active-sterile mixing parameters is much larger than the other ones, while the signal rate is maximal for the case we assumed (for fixed $\sum_\alpha |V_{\alpha N}|^2$).

We considered the HL-LHC (FCC-hh/SppC) with $\sqrt{s} = 14$ (100) TeV and a total integrated luminosity of 3 (20) ab^{-1}. We simulated large event samples for the signal and for the dominant SM backgrounds processes (di-top, di-boson, and tri-boson) including parton shower, hadronization and fast detector simulation. Forty kinematic observables are constructed from each event and are fed into a multivariate analysis tool to perform a BDT analysis. We derive the 1, 2, 3, and 5-σ limits on the production cross section times branching ratio $\sigma(pp \to l^{\pm}N) \times BR(N \to l^{\mp}jj)$, and recast it as a limit on the active-sterile mixing parameter $|V_{lN}|^2$. The result is comparable to the previous estimates obtained in Ref. [111], but more robust.

We find that, under our assumptions and for the benchmark $M_N = 500$ GeV, when ignoring systematic uncertainties at the HL-LHC and the FCC-hh/SppC, the resulting 2 (5)-σ sensitivities on $|V_{lN}|^2$ are 4.9×10^{-3} (1.7×10^{-2}) and 7.0×10^{-5} (1.9×10^{-4}), while the 2 (5)-σ limits on the production cross section times branching ratio $\sigma \times BR$ are 4.4×10^{-2}(1.5×10^{-1}) fb and 1.6×10^{-2} (4.3×10^{-2}) fb, respectively. At the FCC-hh, the reduced production rate for larger masses is partially compensated by the signal efficiency, such that the limits on the cross section are not strongly dependent on the mass.

It is worth noting that the systematic uncertainties affect smaller heavy neutrino masses more than larger ones. In particular, this effect is relevant when $M_N < 400$ (600) GeV at the HL-LHC (FCC-hh). For 200 GeV mass, the limits can be weakened greatly by adding a 10% systematic uncertainty on the background. Therefore, controlling the systematic uncertainty at the future pp colliders will be very important to enhance the discovery power for sterile neutrinos with small masses.

The results presented here can also be representative for final states with the τ flavor. In this case, additional backgrounds have to be included, and the difficulty of reconstructing the tau lepton has to be taken into account. Consequently, we expect the sensitivities of the LNC-LFV $\tau^{\pm}\mu^{\mp}jj$ and $\tau^{\pm}e^{\mp}jj$ final states to be weaker. However, also the present constraints on the combinations

$|V_{eN}V_{\tau N}|$ and $|V_{\mu N}V_{\tau N}|$ are much weaker compared to those from MEG on $|V_{eN}V_{\mu N}|$. The $\tau^{\pm}\mu^{\mp}jj$ and $\tau^{\pm}e^{\mp}jj$ channels could therefore mean great discovery potential, but require a dedicated analysis which is left for future studies.

Acknowledgements

We thank the members of the FCC study collaboration for many useful discussions. K.W. also wants to thank Christophe Grojean and Cai-dian Lü for helpful discussions and their support. This work has been supported by the Swiss National Science Foundation. K.W. acknowledges support from the International Postdoctoral Exchange Fellowship Program (No.90 Document of OCPC, 2015). O.F. acknowledges support from the "Fund for promoting young academic talent" from the University of Basel under the internal reference number DPA2354 and has received funding from the European Unions Horizon 2020 research and innovation program under the Marie Sklodowska-Curie grant agreement No 674896 (Elusives).

6.6 APPENDIX: MULTIVARIATE AND STATISTICAL ANALYSIS

In this section we describe our setup of the Multivariate analysis (MVA), which is a statistical analysis of large data sets based on machine learning techniques to discriminate between two sets of data. Here we use the Tool for MultiVariate Analysis (TMVA) [145], employing the Boosted Decision Tree (BDT).

We perform a frequentist test which uses the profile Likelihood ratio as test statistics. In addition to the parameters of interest for the limit calculation such as, the total cross section of the process and the integrated luminosity, we include nuisance parameters for background of 10% to account for the unknown systematics at future colliders, assuming a logarithmic-normal distribution.

We construct an upper expected limit for the signal with upper/lower one and two sigma error bands using Higgs Analysis-Combined Limit tool [150]. The limits can be set via the level of agreement between the data collected and a given hypothesis by computing the probability of finding the observed data incompatible with the prediction for a given hypothesis, this probability is referred to as the p-value.

The expected value of finding the number of events in the ith bin of the BDT distribution is given by

$$E[n_i] = \mu S_i + B_i \,, \tag{119}$$

where the parameter μ is called the signal strength. When a hypothesis with $\mu = 0$ is rejected a discovery can be established, while rejecting the hypothesis with $\mu = 1$ defines our limit for the calculation. The likelihood function is constructed as Poisson probabilities for all bins as:

$$\mathcal{L}(\mu, \theta) = \sum_{i=1}^{n} \frac{(\mu S_i + B_i)^{n_i}}{n_i!} e^{-(\mu S_i + B_i)}. \tag{120}$$

The profile likelihood ratio can be constructed by the Maximum-Likelihood Estimate (MLE) as:

$$\lambda(\mu) = \frac{\mathcal{L}(\mu, \hat{\theta})}{\mathcal{L}(\hat{\mu}, \hat{\theta})} \tag{121}$$

with $\hat{\theta}$ and $\hat{\mu}$ are the estimated parameters for θ and μ that maximize the likelihood function, i.e., for a given μ and pseudo data at $\hat{\theta}$, the combined $\hat{\mu}$ with $\hat{\theta}$ define the point for which the likelihood reaches its global maximum. The fact that the profile likelihood ratio depends on systematical errors broaden the estimate of the maximum likelihood, thus large systematical errors lead to weaker limits. For the statistical test one can construct the profile log likelihood as:

$$q(\mu) = -2 \ln \lambda(\mu) \tag{122}$$

To measure the level of incompatibility we compute $p-$value as:

$$p = \int_{q(\mu)}^{\infty} F[q(\mu)|\mu] dq(\mu), \tag{123}$$

with $F[q(\mu)|\mu]$ being the probability distribution function that measures the incompatibility between data and our hypothesis, while higher values of $q(\mu)$ correspond to high disagreement between data and hypothesis. The signal is excluded at $(1-\alpha)$ confidence level if

$$CL_s = \frac{P\left(q(\mu)|\mu S + B\right)}{P\left(q(\mu)|B\right)} < \alpha, \tag{124}$$

where the upper limit on μ is the largest value for μ with $P < \alpha$, i.e., if $\alpha = 0.05$ then the signal is excluded with 95% confidence level. Thus one can simply get the upper exclusion limit at different confidence levels by

$$\mu_{up} = \hat{\mu} + \sigma \Phi^{-1}(1-\alpha) \tag{125}$$

with $\hat{\mu}$ being the estimated expected median and Φ^{-1} being a cumulative distribution function. We use the following confidence levels: $(1-\alpha) = 0.6827$ corresponds to the $1-\sigma$ confidence level; $(1-\alpha) = 0.9545$ corresponds to the $2-\sigma$ confidence level; $(1-\alpha) = 0.997$ corresponds to the $3-\sigma$ confidence level and $(1-\alpha) = 0.9999$ corresponds to the $5-\sigma$ confidence level. Finally, the error bands can be obtained by

$$\text{Band}_{(1-\alpha)} = \hat{\mu} \pm \frac{\sigma \Phi^{-1}(1-\alpha)}{N} \,. \tag{126}$$

In fact if we restrict the number of events for the signal and the background to be large and ignore the correlation effect between bins, one can calculate the limit from the following formula for the significance

$$\sigma_{\text{stat+syst}} = \left[2 \left((N_s + N_b) \ln \frac{(N_s + N_b)(N_b + \sigma_b^2)}{N_b^2 + (N_s + N_b)\sigma_b^2} - \frac{N_b^2}{\sigma_b^2} \ln \left(1 + \frac{\sigma_b^2 N_s}{N_b (N_b + \sigma_b^2)}\right) \right) \right]^{1/2} \tag{127}$$

with N_s, N_b being the number of signal and background events, respectively, and σ_b parametrising the systematic uncertainty.

6.7 APPENDIX: DISTRIBUTIONS OF INPUT OBSERVABLES

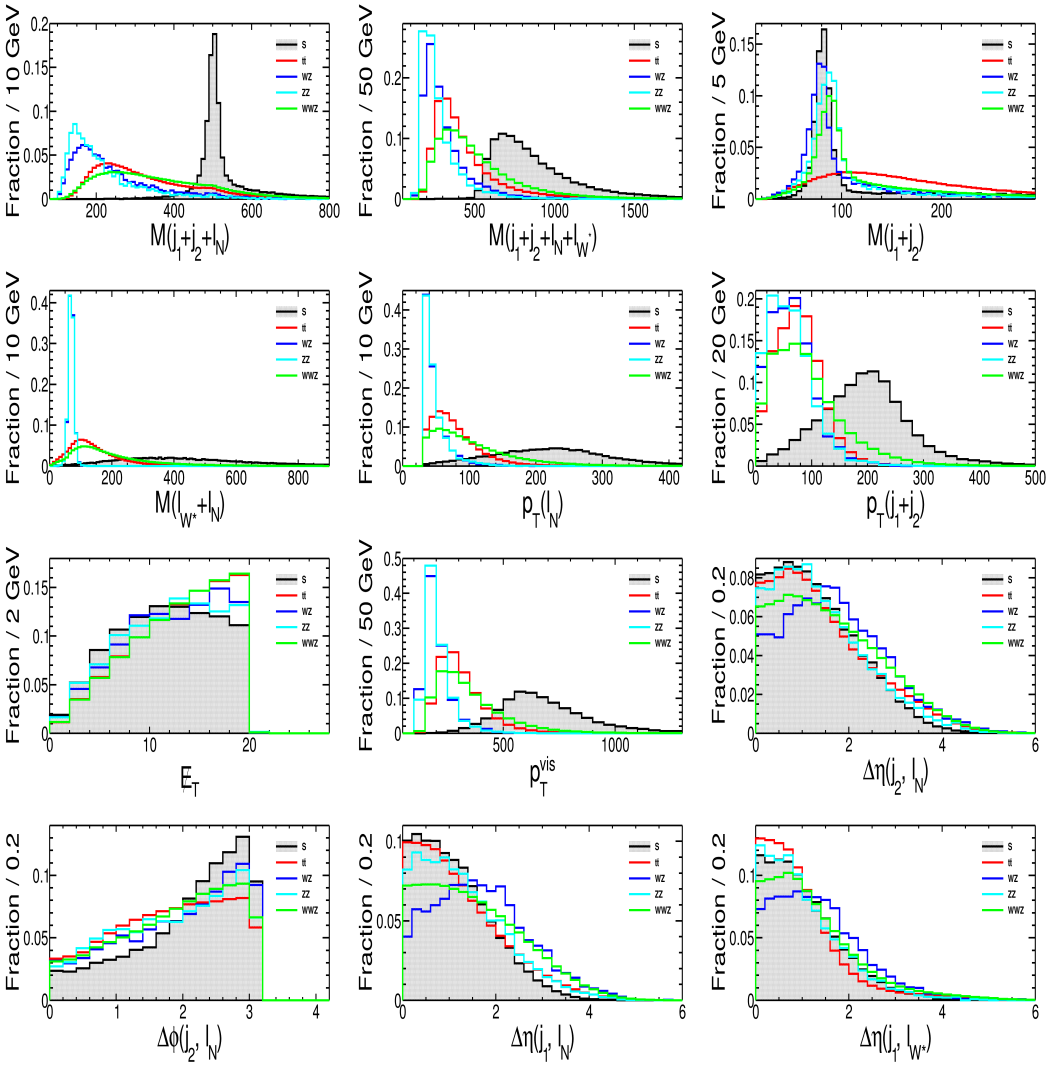

Figure 8: Kinematic distributions of some selected observables for the signal with M_N = 500 GeV (S, black with filled area), and for SM background processes of $t\bar{t}$ (red), WZ (blue), ZZ (cyan), and WWZ (green) after applying the pre-selection cuts at the HL-LHC.

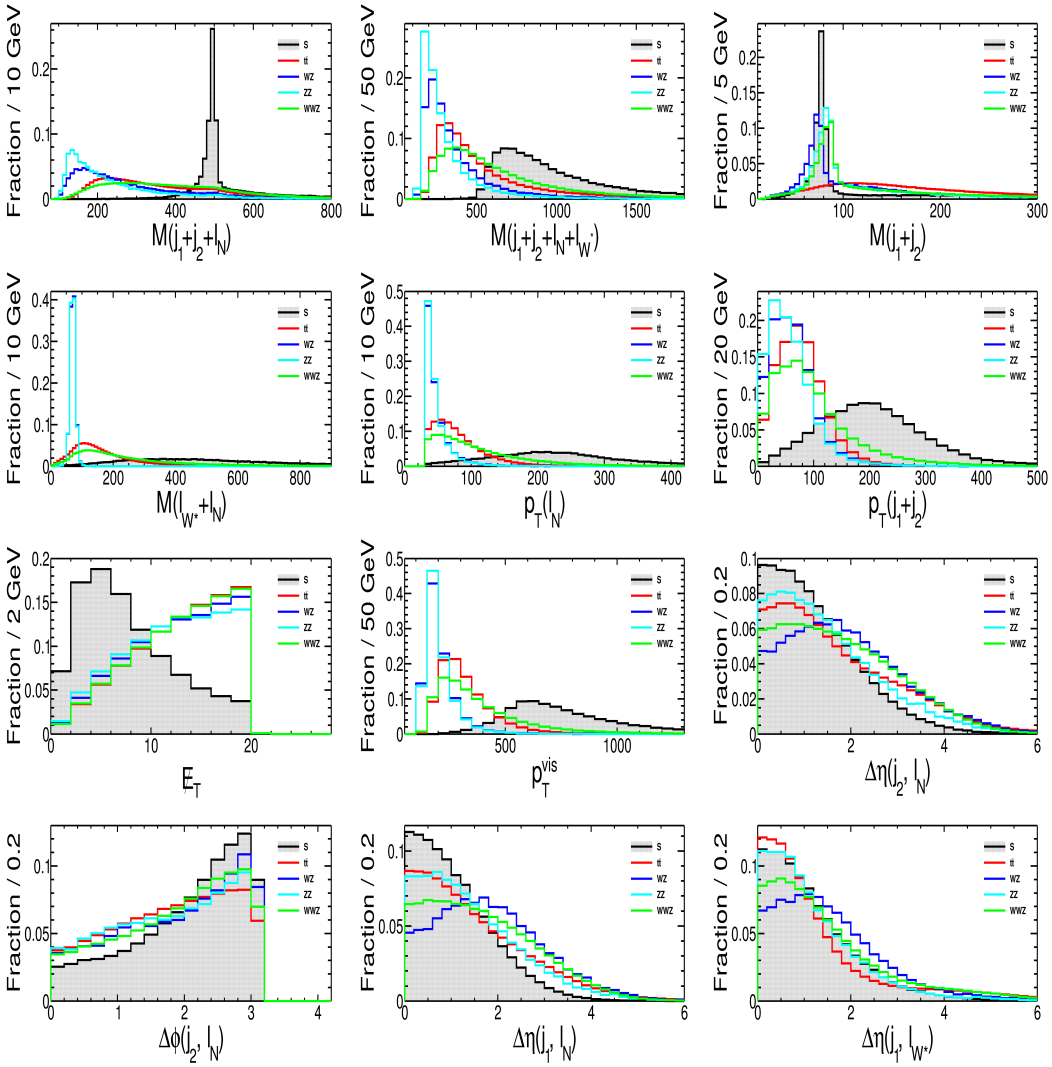

Figure 9: Kinematic distributions of some selected observables for the signal with M_N = 500 GeV (S, black with filled area), and for SM background processes of $t\bar{t}$ (red), WZ (blue), ZZ (cyan), and WWZ (green) after applying the pre-selection cuts at the FCC-hh.

7

LEPTON-TRIJET AND DISPLACED VERTEX SEARCHES FOR HEAVY NEUTRINOS AT FUTURE ELECTRON-PROTON COLLIDERS

Published in: 10.1007/JHEP03(2020)110 [4]

Lepton-Trijet and Displaced Vertex Searches for Heavy Neutrinos at Future Electron-Proton Colliders

Stefan Antusch*[1], Oliver Fischer†[2], A. Hammad‡[1]

[1] *Department of Physics, University of Basel, Klingelbergstr. 82, CH-4056 Basel, Switzerland*

[2] *Institute for Nuclear Physics, Karlsruhe Institute of Technology Hermann-von-Helmholtz-Platz 1, D-76344 Eggenstein-Leopoldshafen, Germany*

ABSTRACT

Electron proton (ep) colliders could provide particle collisions at TeV energies with large data rates while maintaining the clean and pile up-free environment of lepton colliders, which makes them very attractive for heavy neutrino searches. Heavy (mainly sterile) neutrinos with masses around the electroweak scale are proposed in low scale seesaw models for neutrino mass generation. In this paper, we analyse two of the most promising signatures of heavy neutrinos at ep colliders, the lepton-flavour violating (LFV) lepton-trijet signature and the displaced vertex signature. In the considered benchmark model, we find that for heavy neutrino masses around a few hundred GeV, the LFV lepton-trijet signature at ep colliders yields the best sensitivity of all currently discussed heavy neutrino signatures (analysed at the reconstructed level) up to now.

7.1 INTRODUCTION

The observation of neutrino flavour oscillations implies that the neutrino degrees of freedom of the Standard Model (SM) of elementary particles are not massless. At least two of them must obtain a small mass in order to explain the experimental results. Generating such masses requires physics beyond the SM, either an extended Higgs sector or the addition of extra fermions with neutral components. When these fermions are simply introduced as total singlets under the gauge group of the SM, they are often referred to as "sterile" neutrinos.

In addition to a Majorana mass term, the singlet fermions can also have a Yukawa-type interaction which couples them to the SM neutrinos contained in the lepton $SU(2)_L$-doublets and the SM Higgs doublet. After electroweak symmetry breaking, this term leads to a coupling of the neutral fermions to the SM Higgs boson as well as to a mixing in the neutral lepton mass matrix between the sterile neutrinos and the SM neutrinos. This mixing results in heavy and light mass eigenstates, the latter of which are mostly active neutrinos and observed in neutrino oscillation experiments, while the former are mostly sterile but have suppressed interactions with the weak gauge bosons. It is these suppressed interactions which allows for various production and decay channels of the new neutral heavy fermions and many aspects of the resulting signatures at particle colliders have been studied, see e.g. [111] and references therein.

In the past, the Large Electron Positron collider (LEP) searched for heavy neutral leptons, i.e. "heavy neutrinos", and provides limits which are still very relevant, for instance via direct searches [151], or also via precision tests [149]. Searches for heavy neutrinos at the LHC used to focus on lepton number violating signatures, see e.g. [9] and references therein. Recently the CMS collaboration investigated the trilepton signature [152], and ATLAS the displaced vertex signature [153]. The discovery prospects for heavy neutrinos at the LHC via lepton number conserving signatures are limited due to the large backgrounds and the tiny production cross section for larger masses. Furthermore, in typical low scale seesaw models, and in benchmark models like the "Symmetry Protected Seesaw Scenario" (SPSS) [129] which captures their main features in a "simplified model", lepton number violation is not to be expected at observable rates (cf. figure 3 of [113]).

An interesting way to improve the prospects for discovering heavy neutrinos at the LHC may be the Large Hadron electron Collider (LHeC) [154, 155], envisioned to be operated simultaneously, and without interference with the hadron-hadron collisions, at ~1.3 TeV centre-of-mass energy and could provide a total integrated luminosity of 1 ab^{-1}. It would provide valuable improvements to the PDF sets [156] and thus reduce the PDF-associated systematic uncertainties, and also significantly improve some of the Higgs measurements to the subpercent level [157, 158]. First discussions of searches for heavy neutrinos at an LHeC-like collider include lepton number violating signatures [159–161], while ref. [162] focuses on the lepton number conserving final states including electrons. A systematic assessment of sterile neutrino signatures at

ep colliders and first sensitivity estimates in the SPSS benchmark model are given in [111]. More generally, electron proton colliders offer unique opportunities with respect to certain Beyond the SM (BSM) physics searches, cf. e.g. [111, 160, 163–165], see also ref. [166] for an overview. Furthermore, the Future Circular Collider (FCC) design study also includes an electron-proton collider mode, the FCC-he, which could collide the same 60 GeV electron beam from the LHeC electron linac with the 50 TeV proton beam from the FCC-hh, giving rise to a centre of mass energy of about 3.5 TeV [74, 167].

In this article we study in depth two of the most promising direct search channels for sterile neutrinos at ep colliders, based e.g. on the sensitivity estimates in ref. [111]. In section 2 we recapitulate the model, and in section 3 we analyse the prospects for the lepton flavor violating lepton-trijet signature at the reconstructed level including the dominant backgrounds, and we carry out an improved analysis for the displaced vertex searches with the full detector geometry and event kinematics. In section 4 we summarize our results and conclude.

7.2 THE MODEL

For our analysis, we will use the "Symmetry Protected Seesaw Scenario" (SPSS) benchmark model [129], which includes two sterile neutrinos with opposite charges under a "lepton number"-like symmetry, an extended version of the usual lepton number. The small observed neutrino masses are generated when the "lepton number"-like symmetry is slightly broken. For the context of this study, we will treat the protective symmetry as being exact, which is referred to as the "symmetry limit" of the model. In this limit, lepton number (LN) is conserved. When the symmetry is slightly broken (or only approximate), lepton number violation (LNV) is induced. A discussion for which parameter regions the LNV effects can be observable in the SPSS benchmark model with small symmetry breaking can be found in [113].

The Lagrangian density of the benchmark model, including the sterile neutrino pair N_R^1 and N_R^2 is given by:

$$\mathscr{L} = \mathscr{L}_{SM} - \overline{N_R^1} M_N N_R^{2\,c} - y_{\nu_\alpha} \overline{N_R^1} \widetilde{\phi}^\dagger L^\alpha + \text{H.c.} + \dots \,, \tag{128}$$

where $\mathscr{L}_{SM}$ contains the usual SM field content and with L^α, $(\alpha = e, \mu, \tau)$, and ϕ being the lepton and Higgs doublets, respectively. The parameters y_{ν_α} are the complex-valued neutrino Yukawa couplings, and M_N is the sterile neutrino (Majorana) mass. The ellipses indicate additional terms with sterile neutrinos that are decoupled from collider phenomenology as well as possible terms which slightly break the "lepton number"-like symmetry.

Electroweak symmetry breaking yields a symmetric mass matrix of the active and sterile neutrinos, which can be diagonalized by a unitary 5×5 leptonic mixing matrix U, cf. [129]. The mass eigenstates $\tilde{n}_j = (\nu_1, \nu_2, \nu_3, N_4, N_5)_j^T = U_{j\alpha}^\dagger n_\alpha$ are the three light neutrinos (which are massless in the symmetry limit) and two *heavy neutrinos* with degenerate mass eigenvalues M_N (in the symme-

try limit). The leptonic mixing matrix governs the interactions of the heavy neutrinos, which is quantified by the active-sterile neutrino mixing angles

$$\theta_\alpha = \frac{y^*_{\nu_\alpha}}{\sqrt{2}} \frac{v_{EW}}{M_N}\,, \qquad |\theta|^2 := \sum_\alpha |\theta_\alpha|^2\,, \tag{129}$$

with $v_{EW} = 246.22$ GeV being the vacuum expectation value of the Higgs field. This allows the heavy neutrino mass eigenstates to participate in the weak current interactions, with

$$j^\pm_\mu \supset \frac{g}{2}\,\theta_\alpha\,\bar{\ell}_\alpha\,\gamma_\mu P_L\,(-iN_4 + N_5) + \text{H.c.}\,, \tag{130}$$

$$j^0_\mu = \frac{g}{2\,c_W} \sum_{i,j=1}^{5} \vartheta_{ij}\overline{\tilde{n}_i}\gamma_\mu P_L \tilde{n}_j\,, \tag{131}$$

$$\mathscr{L}_{\text{Yuk.}} \supset \frac{M_N}{v_{EW}} \sum_{i=1}^{3} \left(\vartheta^*_{i4}\overline{N^c_4} + \vartheta^*_{i5}\overline{N^c_5}\right) h\,\nu_i + \text{ H.c.}\,, \tag{132}$$

and where g is the weak coupling constant, c_W the cosine of the Weinberg angle, $P_L = \frac{1}{2}(1-\gamma^5)$ the left-chiral projection operator, $h = \sqrt{2}\,\text{Re}(\phi^0)$ the real scalar Higgs boson and $\vartheta_{ij} := \sum_{\alpha=e,\mu,\tau} U^\dagger_{i\alpha} U_{\alpha j}$.

In the symmetry limit of the benchmark model, only the moduli of the complex neutrino Yukawa couplings ($|y_{\nu_e}|$, $|y_{\nu_\mu}|$, $|y_{\nu_\tau}|$), or equivalently of the active-sterile mixing angles from Eq. (148), ($|\theta_e|$, $|\theta_\mu|$, $|\theta_\tau|$), and the (w.l.o.g. real and positive) mass parameter M_N are physical. Via the relation

$$|V_{\alpha N}|^2 = |\theta_\alpha|^2\,, \tag{133}$$

one can readily translate our results in terms of the neutrino mixing matrix elements $V_{\alpha N}$ often used in the literature.

7.3 SEARCH STRATEGY

Electron-proton colliders provide an environment where the SM can be tested at higher centre-of-mass energies compared to electron-positron colliders, with comparably low rates of background. In the following we consider the Large Hadron electron Collider (LHeC) [154, 155, 168] and the Future Circular Collider in hadron-electron collision mode (FCC-he) [156, 169] for the search of the heavy neutrinos. The LHeC makes utilizes the 7-TeV proton beam of the LHC and a 60-GeV electron beam with up to 80% polarization, to achieve a centre-of-mass energy close to 1.3 TeV with a total of 1 ab^{-1} integrated luminosity, while the FCC-he would collide the same electron beam with the 50-TeV proton beam from the FCC, resulting in the centre-of-mass energy close to 3.5 TeV reaching 3 ab^{-1} integrated luminosity.

7.3.1 *Heavy neutrino production at electron-proton colliders*

At electron-proton colliders, heavy neutrinos can be produced via t-channel exchange of a W boson together with a jet, or via $W\gamma$-fusion, which gives rise

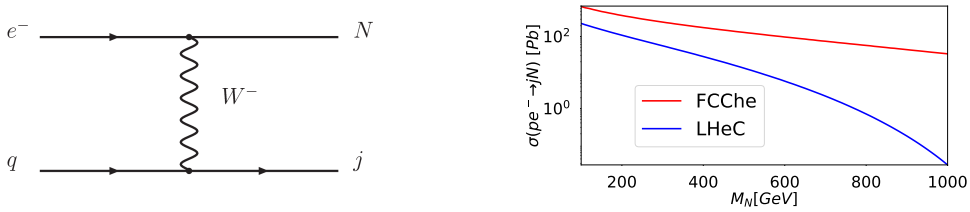

Figure 10: *Left:* Feynman diagram representing the leading order production channel for heavy neutrinos in electron-proton scattering. *Right:* Cross section for heavy neutrino production in electron-proton collisions, divided by the active-sterile mixing paramter $|\theta_e|^2$.

to a heavy neutrino and a W^- boson. The latter channel, though suppressed by the parton distribution function of the photon within the proton, becomes increasingly important for larger centre-of-mass energies and sterile neutrino masses. Both production channels are sensitive on the active-sterile mixing parameter θ_e only. We show the Feynman diagram for the production mechanism via t-channel exchange of a W boson and the production cross section in the left panel of fig. 10.

It is instructive to consider the differential cross section in the centre of mass frame, which can be expressed as:

$$\frac{d\sigma}{d\Omega} = \frac{g^4 |V_{ij}|^2 |\theta_e|^2}{32S\pi^2((Q^2 - m_W^2)^2 + m_W^2\Gamma_W^2)} \times \left[\frac{S(S - M_N^2)}{4} - \frac{M_N^2(xE_pE_N + xE_p|K_N|\cos\theta)}{2} + (xE_pE_N)^2 + 2xE_p|K_N|\cos\theta\right]$$

with the squared transferred momentum $Q^2 = -M_N^2 + 2E_e(E_N - |K_N|\cos\theta)$ and the energy $S = 4xE_eE_p$. The differential cross section depends on the energy S and the two kinematic variables Q^2 and the Bjorken variable x. At electron proton colliders the Bjorken x can be obtained from the measurement of the inelasticity y_e as [170]:

$$x = \frac{Q^2}{Sy_e} \qquad \text{with} \qquad y_e = 1 - \frac{E_N - K_N^z}{2E_e} \tag{134}$$

with K_N^z being the momentum of the scattered neutrino in Z-direction. The scattering angle θ is defined between the direction of the outgoing particles and the proton beam. For a large region of the parameter space with $x \lesssim E_e/E_p$, the energy of the scattered neutrino is approximately equal to the electron beam, which causes the cross section to peak in the direction of large θ (i.e. backwards). For more massive scattered neutrinos with $M_N \gtrsim 60$ GeV a comparatively large momentum transfer is required, which causes the heavy neutrino to scatter in the very forward direction[170, 171].

The cross section in eq. (134) allows us to understand the kinematics of heavy neutrino production as a function of its mass, as shown in fig. 11, displayed as scattering angle of the heavy neutrino with respect to the beam axis versus the Lorentz boost factor γ. The figures were obtained from data samples with 10^4 events and show the interpolated density contours where 68%,

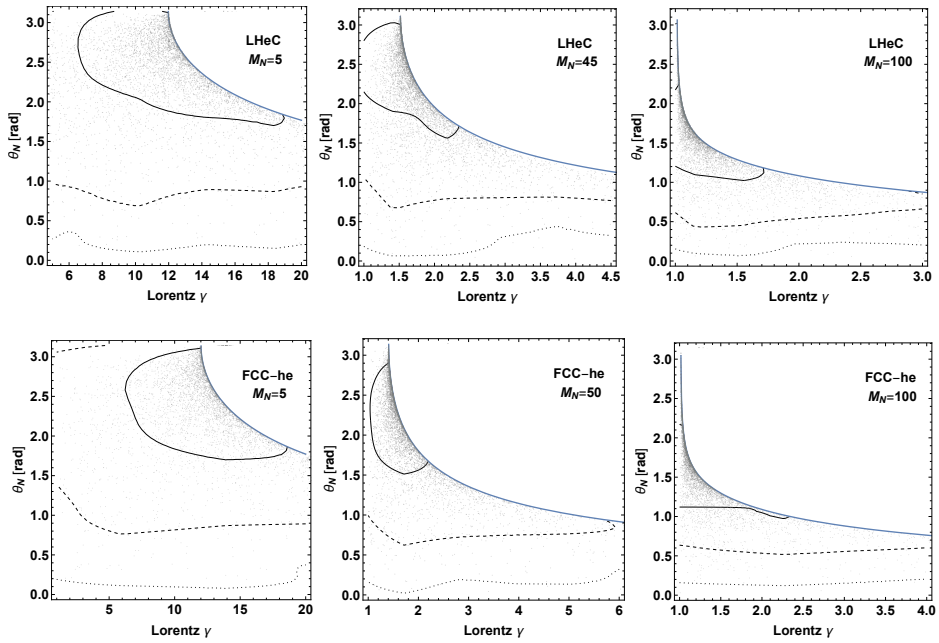

Figure 11: Kinematics of the heavy neutrino produced in electron-proton collisions at the LHeC (upper row) and at the FCC-he (lower row). All masses are in GeV, the proton is in direction of $\theta = 0$. The plots show the distribution of the scattering angle θ_N (10^4 events, shown as black dots) of the heavy neutrino with respect to the beam axis versus the Lorentz boost factor γ. The black solid, dashed, and dotted line show the density contours with 68%, 95%, and 99% of the points inside the contour lines.

95%, and 99% of the points are inside the black solid, dashed, and dotted contour lines, respectively. The correlation between the kinematical parameters γ and θ stems from the cross section (134), and can be understood from the inelasticity condition above together with the fact that $Q^2 = m_W^2$ maximises the interaction rate[1]:

$$1 - \frac{E_N - K_N^z}{2E_e} = \frac{m_W^2}{xS}\,. \tag{135}$$

From this relation it follows directly, for instance, that for $\theta = \pi$ and $xS \gg m_W^2$ the momentum $K_N = E_e$, while for $\theta \sim 0$ it follows that $K_N \gg E_e$. One can identify the unphysical region for θ and γ via $x > 1$, which is given by the region above the blue curves in fig. 11.

We notice that the kinematics at LHeC and FCC-he produce on average similar Lorentz boosts despite the different proton beam momenta, which stems from the fact that the heavy neutrino is produced from the electron. For $M_N \leqslant 50$ GeV a typical Lorentz boost factor can be estimated heuristically with E_e/M_N. We find it interesting that the kinematical distributions are very different for the different masses M_N, which might allow to infer the mass of the heavy neutrino indirectly.

1 Here we consider the case $M_N < m_W$. For $M_N > m_W$ this is more complicated due to suppression from the phase space versus the W boson going off-shell.

7.3.2 *Prompt Searches: Lepton-Trijets from Heavy Neutrinos*

In the following we discuss the prospects of heavy neutrino detection via lepton flavor violating processes. We consider the signal from the process chain

$$p\, e^- \to N + j \to \mu^- + W^+ + j \to \mu^- + 3j\,, \tag{136}$$

where the heavy neutrino decays via the charged current into a muon and a W^+, which in turn decays into two jets. The branching ratio for the decay of N into a muon is proportional to $|\theta_\mu|^2/|\theta|^2$, such that the rate for the process $p\, e^- \to \mu^- + 3j$ via heavy neutrinos is proportional to $|\theta_e|^2|\theta_\mu|^2/|\theta|^2$ (cf. [111]).

For concreteness, we will perform our analysis assuming the relation

$$|\theta_e|^2 = |\theta_\mu|^2 \gg |\theta_\tau|^2\,, \tag{137}$$

setting θ_τ to zero. This allows to present them later in the results section together with the existing bounds on $\mu \to e + \gamma$, as functions of $|\theta_e\theta_\mu|$. Our results of course hold general: one simply has to replace $|\theta_e\theta_\mu|$ by $2|\theta_e|^2|\theta_\mu|^2/|\theta|^2$ on the y-axis of the plots showing the results for the sensitivities.

This lepton-trijet final state yields an "unambiguous signal" for lepton flavour violation, which means there exists no SM background process at the parton level with this final state, as discussed in [111, 127]. SM backgrounds, as will be discussed below, of course exist due to possible misidentification or, e.g., from SM final states which only differ by additional light neutrinos. For the latter type of backgrounds, one expects that the kinematical distributions of the muon can be used as a powerful discriminator between signal and background. The sensitivity prospects for the LHeC and the FCC-he have been estimated in ref. [111] at the parton level (with not optimised cuts). In this work, we will improve these sensitivity estimates.

7.3.2.1 *Considered Standard Model Backgrounds*

Backgrounds	$\sigma_{(\mathrm{LHeC})}$[Pb]	$\sigma_{(\mathrm{FCChe})}$[Pb]
$pe^- \to je^-VV$, where $VV \to jj\mu^-\mu^+$	0.00616	2.40
$pe^- \to je^-VV$, where $VV \to jj\mu^-\bar{\nu}_\mu$	0.00185	0.45
$pe^- \to j\nu_e VV$, where $VV \to jj\mu^-\mu^+$	0.00606	2.30
$pe^- \to j\nu_e VV$, where $VV \to jj\mu^-\bar{\nu}_\mu$	0.00180	0.44

Table 4: Dominant background processes considered in our analysis and their total cross sections. The samples have been produced with the following cuts: $P_T(j) \geqslant 5$ GeV, $P_T(l) \geqslant 2$ GeV and $|\eta(l/j)| \leqslant 4.5$.

The dominant SM backgrounds for the $jjj\mu^-$ signature considered in our analysis, and their total cross sections, are summarized in table 4.

One very important background arises from di-vector boson production associated with jet and a neutrino, e.g $pe^- \to j\nu_e VV$ with $V = W^-, W^+, Z$. Especially when one of the V is a W^-, decaying into $\mu^-\nu_\mu$, then the final

state only differs from the signal by two additional neutrinos. Nevertheless, the light neutrino in the final state gives rise to missing energy and allows for efficient separation of this process from the signal, which comes without missing energy.

Another important class of background comes from di-vector boson production associated with a jet and an electron, e.g $pe^- \to je^- VV$ with $V = W^-W^+Z$. While the signal does not have hard electrons, it contains many soft electrons due to radiative processes. Therefore one cannot simply reject events that contain electrons without decreasing the signal efficiency. For $m_N \leqslant 200$ GeV, the distance $\Delta R(W, \mu) = \sqrt{(\Delta\eta)^2 + (\Delta\phi)^2}$ between the W^- and the muon is a very good discriminator, since in the background the muons always come from vector boson decays. For higher masses $m_N \geqslant 400$ GeV, the muons from heavy neutrino decays are highly boosted and can be distinguished from the background muons.

The background that arises from single vector boson production with radiated jets can be reduced very well since the radiated jets are very soft and can be easily distinguished from signal jets. Also, background with single vector boson production that decays to a tau lepton pair that gives raise to $jj\mu^- + \text{MET}$ final state is highly reduced because of the missing energy and low momentum of the final state fermions that come from the tau decay. Finally, the three vector boson production is not considered since its cross section is much smaller compared to the two vector boson production processes.

7.3.2.2 *Pre-selection and analysis*

For the simulation of the signal and background event samples, the Monte Carlo event generator MadGraph5 version 2.4.3[143] is employed. The parton shower and hadronisation are done by Ptyhia6[144]. For fast detector simulation we use Delphes[97]. We note that Pythia needs to be patched[172] in order to achieve a reasonable event generation efficiency and that it is crucial that the first (second) beam, as inputted in the MadGraph run card, corresponds to the proton (electron) to correctly match the asymmetric detector setup implemented in the Delphes card.

For signal reconstruction (at reconstruction level after detector simulation) we require at least one muon with $P_T \geqslant 2$ GeV and three jets with $P_T \geqslant 5$ GeV. We reconstruct the W boson from the possible combinations of the three jets and adopt a mass window of $60 \leqslant m_W \leqslant 100$ GeV. This allows to fix the beam jet via the one with the highest pseudo rapidity and highest momentum remaining. We construct 18 kinematical distributions as input to the package TMVA[145] to perform the Multi-Variate Analysis, employing a Boosted Decision Tree (BDT). The discriminating power of the BDT relies on the fact that the signal and the background may be characterized by different features that can be entangled.

The BDT algorithm ranks the input variables according to its ability to separate between signal events and background events. To illustrate the results we show, for the LHeC, the 18 variable distributions for the 6 signal benchmark points and all backgrounds summed in Fig.12. The invariant mass distribution of the heavy neutrino is classified as the highest ranking for all mass points

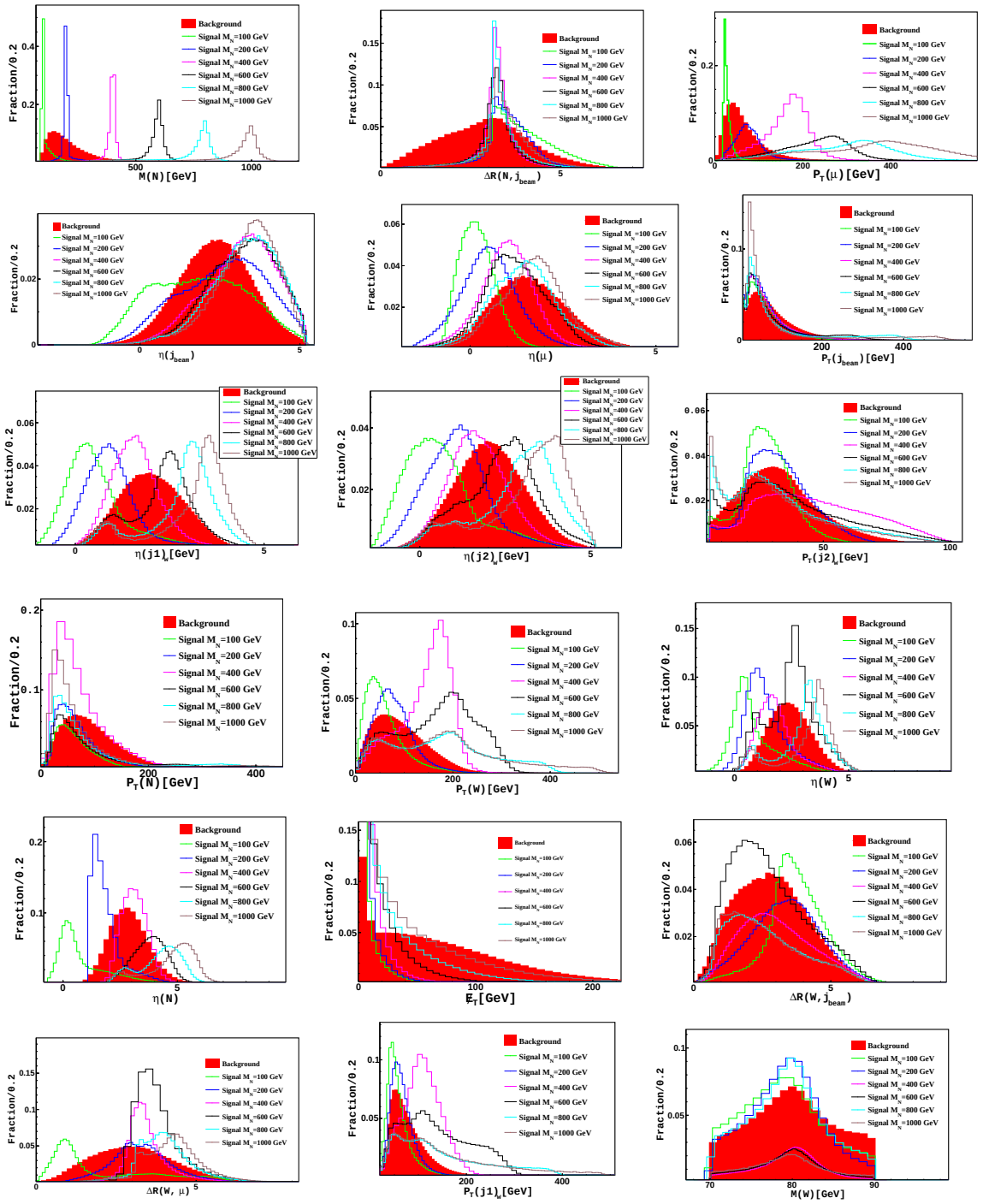

Figure 12: Kinematical distributions for the 6 signal benchmark points and all the backgrounds summed at the LHeC.

with $m_N \geqslant 200$ GeV, while for smaller mass transverse missing energy is the most important one. Other variables like muon transverse momentum, $P_T(\mu)$, and the distance between heavy neutrino and the beam jet, $\Delta R(N, j_{beam})$, have high rank in separating the signal events from background events especially for $m_N \geqslant 400$ GeV. All the other variables have fluctuating rank according to the different mass points.

We remark that the large asymmetry in the beam energies at an electron-proton collider leads to a strong boost of the final states particles into the direction of the proton beam, which in general shifts the angular observables towards larger η values and affects the angular correlations. This effect is kinematically fixed for the known SM background processes, but shows an interesting dependency on the heavy neutrino mass for the signal process. In particular for masses of a few hundred GeV the jets from the decay chain $N \to W^+\mu^- \to jj\mu^-$ feature a peak at large η values, while for small masses of a few tens of GeV the heavy neutrinos and their decay products tend to reside in the backward direction at small negative η values, cf. fig. 11.

7.3.2.3 *Results*

We show the resulting BDT distributions for the LHeC and FCC-he with $m_N = 400$ GeV and $\theta_e = \theta_\mu = 0.01$, $|\theta_\tau| = 0$ in fig. 13. It reflects the clear separability of signal and background for moderate efficiency losses on the signal side. The resulting limits on the cross section at 95% confidence level are shown in the left column of fig. 14. The right column shows the resulting sensitivity on the active sterile mixing parameter combination $|\theta_e\theta_\mu|$ as a function of the heavy neutrino mass m_N.

Fig. 13 (*left*) shows in blue the resulting BDT response for the LHeC and FCC-he with trained events (shown by the data points) and tested events (shown by the shaded areas) superimposed. We note that in order to avoid over-training, we require that the Kolmogorov-Smirnov classifier is around and below 0.5. The BDT discriminator ranges from -1 to 1, events with discriminant value near 1 is classified as signal-like events (blue) and those near -1 is considered as background-like events (red).

The optimization of signal significance as a function of signal and background cut efficiency is shown in fig. 13 (*right*). At the LHeC, the maximum cut efficiency is at BDT $\geqslant 0.17$ that correspond to signal significance $\simeq 16\sigma$ with signal efficiency 0.78 and background rejection efficiency 0.004. For the FCC-he the cut efficiency has been maximized by requiring BDT $\geqslant 0.189$ to obtain a signal significance $\simeq 37.8\sigma$, with signal cut efficiency 0.6 and background rejection efficiency 0.0001.

Based on the BDT analysis, the sensitivity for heavy neutrino searches via the lepton flavour violating process $3j + \mu$ is derived using the Higgs Analysis Combined Limit tool[146]. To extract the limits we preformed a frequentist test which uses the profile likelihood as test statistics corresponding to the remaining number of signal/background events after the BDT cut. At the LHeC, for the benchmark point with $\theta_e = \theta_\mu = 0.01$, $|\theta_\tau| = 0$ and $M = 400$ GeV, the number of signal events is 330 and background events 64. For the FCC-he, the number of signal events is 1743 and background events 376.

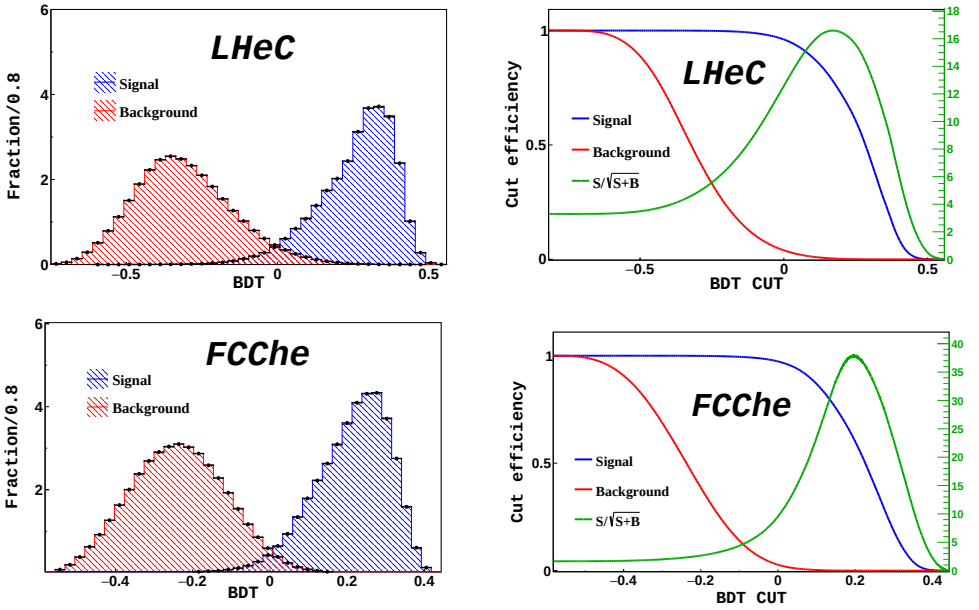

Figure 13: All the plots use $M_N = 400$ GeV and $\theta_e = \theta_\mu = 0.01$, $|\theta_\tau| = 0$. *Upper left*: BDT distribution at the LHeC for both train and test samples superimposed. *Bottom left*: BDT distribution at the FCC-he for both train (black dotted distributions) and test (filled blue and red distributions) samples superimposed for both signal and background events. *Upper right*: Cut efficiency at the LHeC with BDT cut $\geqslant 0.17$ one can get $S/\sqrt{S+B} = 16\sigma$ with number of signal events = 330 and background events = 64. The cut efficiency for the signal is 0.78 and for the background 0.004. *Bottom right*: Cut efficiency at the FCC-he with BDT cut $\geqslant 0.189$ one can get $S/\sqrt{S+B} = 37.87\sigma$ with number of signal events = 1743 and background events = 376. The cut efficiency for the signal is 0.6 and for the background 0.0001.

In fig. 14 we show the expected median limit at 95% CL with the one and two sigma bands on the total cross section (*left*). The right panel shows the resulting sensitivity on the related mixing angles $|\theta_e\theta_\mu|$ (with $\theta_e = \theta_\mu$ and $|\theta_\tau| = 0$, cf. discussion in section 3.1). Besides the parameters of interest, such as the total cross section and the integrated luminosity, we consider an uncertainty parameter of 2% for the background events as logarithmic-normal distribution to account for the unknown systematic uncertainties. Further background information on the used statistical methods can be found, e.g., in the appendix of [9].

7.3.3 *Displaced vertex searches*

Heavy neutrinos with masses below the W boson mass threshold and with $|\theta|^2 \leqslant 10^{-5}$ naturally develop lifetimes that are macroscopic, i.e. that allow them to travel a finite and measurable distance in the detector before they decay. Such decays at a distance from the interaction point are reconstructed as displaced secondary vertices, which is a very exotic signature that has no irreducible SM backgrounds. We consider the process chain $pe^- \to j(N \to$

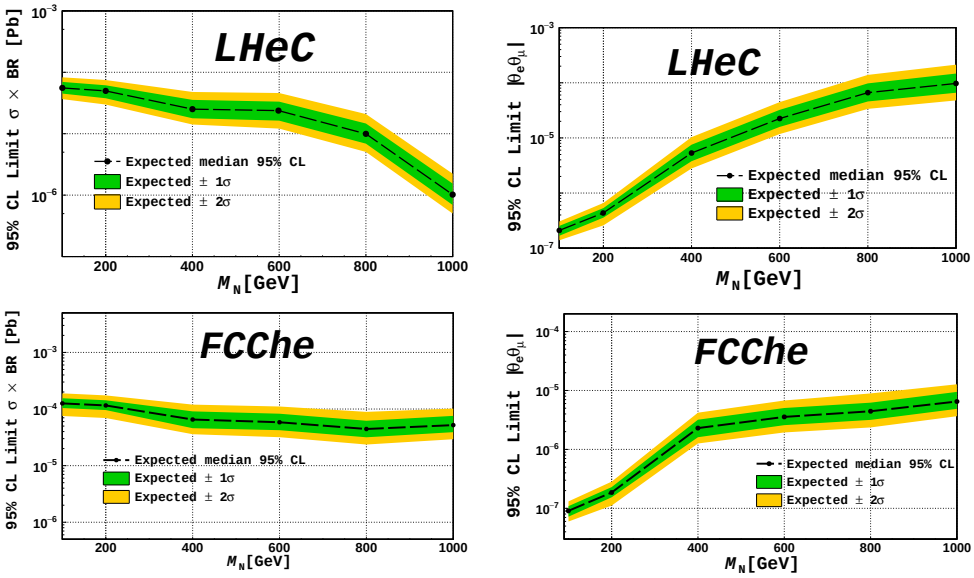

Figure 14: *Left*: Expected limit on the production section times branching ratio of $\sigma(pe^- \to Nj) \times BR(N \to \mu^- jj)$ when testing the signal hypotheses (for $|\theta_e| = |\theta_\mu|$ and $|\theta_\tau| = 0$) at LHeC (up) and FCChe(down). *Right*: Corresponding expected limit on the mixing parameters $|\theta_e\theta_\mu|$ when testing the signal hypotheses at the LHeC (up) and the FCChe (down).

visible$|_{\text{displaced}}$) as our signal, where we exclude the $\sim 5\%$ branching fraction of $N \to 3\nu$ and decays inside the detector are considered to yield unmistakable signatures. We do not discuss here the prospects of identifying or reconstructing the heavy neutrino properties from this signature.

7.3.3.1 *The detector*

We use description of the LHeC detector from the CDR [155]. The interaction point (IP) fixes the centre of our cylindrical coordinate system, the z axis is fixed by the proton beam. The tracker has a radius of 88 cm around the z axis, its z extension in forward and backward directions is about 390 cm and 190 cm, respectively. The HCAL has a radius of 260 cm and extends an additional 217 cm and 187 cm in forward and backward direction, respectively, and the muon system adds 178 cm to the radial extension. The total detector length is 1316 cm.

7.3.3.2 *Vertexing*

The primary vertex can be obtained from the intersection of the charged track and the interaction region. The interaction region has a root mean square transverse extension of $\sim 7\mu$m, and a longitudinal extension of ~ 0.6 mm. The tracking resolution is $\sim 8\mu$m, and the impact parameter resolution is comparable for charged particles with kinetic energy above 10 GeV with angles above 10 degrees. We assume therefore, that a displacement of $\sim 40\mu$m from the primary vertex will yield a sufficient degree of confidence that the secondary vertex is not identical to the primary vertex [155]. We emphasize that the considered

displacement is not confined to the transverse plane since the precision of the primary vertex is known with $\mathcal{O}(10)\mu m$ in all directions. Thus, the minimal vertex displacement is given by $40\mu m$ and the maximal vertex displacement is given by the extension of the muon system, which is 4.38 m in radial direction and 5.3 m (7.5 m) in backward (forward) direction.

7.3.3.3 *Backgrounds*

We discuss backgrounds only for the LHeC, the situation is very similar for the FCC-he. Possible backgrounds come from SM particles that have a finite lifetime and are incorrectly reconstructed. Natural candidates for such backgrounds are for instance tau leptons, which can be produced via the process $e^- p \to \nu\nu j \tau^-$ with a cross section of

$$\sigma(e^- p \to \nu\nu j \tau^-) = 0.34 \text{ pb}, \tag{138}$$

and they have typical displacements of $\sim$ mm. However, tau leptons only decay either into charged leptons plus neutrinos or into hadrons plus a neutrino and will not be easily confused with the signal signature. We therefore assume that they can be effectively vetoed against by existing tau tags, provided that $m_N \gg m_\tau$.

Another candidate for SM backgrounds are B mesons, for which we obtain an estimate via the final states νb, $\nu \bar{b}$, and $\nu, j, b\bar{b}$, with the following cross sections:

$$\sigma(e^- p \to \nu b) = 144 |V_{ub}|^2 \text{ pb}, \tag{139}$$

$$\sigma(e^- p \to \nu j b\bar{b}) = 0.54 \text{ pb}. \tag{140}$$

With $|V_{ub}| = 0.004$ [173] about $\sim 10^6$ singly and doubly produced b mesons with lifetimes of $\sim$ 1 ps are to be expected, most of which decay typically inside the beam pipe and within a few mm from the IP. The doubly produced b mesons can be vetoed against with B-tag filters and the fact that there is more hadronic activity (a second b jet) close to the IP. A more important discriminator against all B mesons is their characteristic mass around 5 GeV. We will assume that this allows for complete suppression of this background when $m_N > 5$ GeV.

One more possible background process is given by cosmic muons, which may coincide with a bunch crossing and might be misidentified as two back-to-back muons. In the following, we assume that the cosmic muons and the above mentioned SM background can be vetoed without efficiency loss via appropriate preselection criteria on the final state, even when the displacement is as small as $\sim 40\mu m$. This is optimistic as we have to expect that in a real experiment the rejection of possible backgrounds, signal reconstruction, and further unknown detector effects will reduce the signal efficiency below 100%, reducing the experimental sensitivity. Estimating this effect requires a full simulation and real data, which is beyond the scope of the present analysis. However, we expect that the use of all the kinematic information on the event will enable background suppression that is at least as effective as in the previous section.

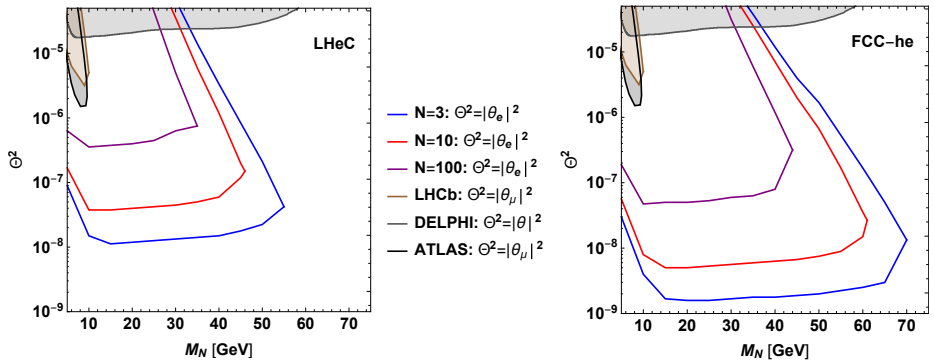

Figure 15: Parameter space giving rise to N = 3, , 10, 100 heavy neutrino decays with a displaced secondary vertex at the LHeC (left) and the FCC-he (right). The gray area denotes the best exclusion limits from the experiments from ATLAS [153], LHCb [174], LEP [151], and MEG [175]. In this figure, $|\theta_\alpha| = 0$ for $\alpha \neq e$. Notice that each experiment is sensitive to a different set of active-sterile mixing parameters, as indicated in the legend.

7.3.3.4 *Analysis and results*

We quantify the expected number of heavy neutrino decays with given displacement according to the formalism presented in ref. [174]:

$$N_{dv}(E_p, \mathcal{L}, m_N, |\theta_e|) = \sigma(E_p, m_N, |\theta_e|)\,\mathcal{L} \times \int D_N(\vartheta, \gamma)\, P_{dv}(x_{min}(\vartheta), x_{max}(\vartheta), \Delta x_{lab}(\tau, \gamma))\, d\vartheta d\gamma\,. \tag{141}$$

In the above equation, σ labels the production cross section and depends and the proton beam energy E_p, $\mathcal{L}$ the integrated luminosity, $D_N(\vartheta, \gamma)$ is the probability distribution for N with an angle ϑ between momentum p and beam axis, P_{dv} is the probability distribution of a decay, and τ is the proper life time. The probability of decays with a displacement $x_{min} \leqslant \Delta x_{lab} \leqslant x_{max}$ is

$$P_{dv} = \text{Exp}\left(\frac{-x_{min}}{\Delta x_{lab}}\right) - \text{Exp}\left(\frac{-x_{max}}{\Delta x_{lab}}\right)\,. \tag{142}$$

We take the asymmetric set up of the detector and the full angular and momentum distributions into account and choose for our analysis the 95% confidence level, corresponding to the number of displaced vertices being $N_{dv} \geqslant 3.09$. We show the corresponding exclusion sensitivity contour at 95% confidence, labelled "N = 3" in fig. 15. The figure also contains the contour lines for the number of expected displaced vertices being N = 10, 100 for comparison. It is worth noticing that most of the decays enclosed inside the contour yield events in the backward hemisphere of the detector, i.e. into the direction of the electron beam, where there is indeed no background to be expected, cf. fig. 11.

7.3.4 *Discussion*

To put our results into a general context we show a combination of the leading search prospects for heavy neutrinos (at 95% confidence level) in fig. 16, together with present constraints from the MEG experiment [175] as computed

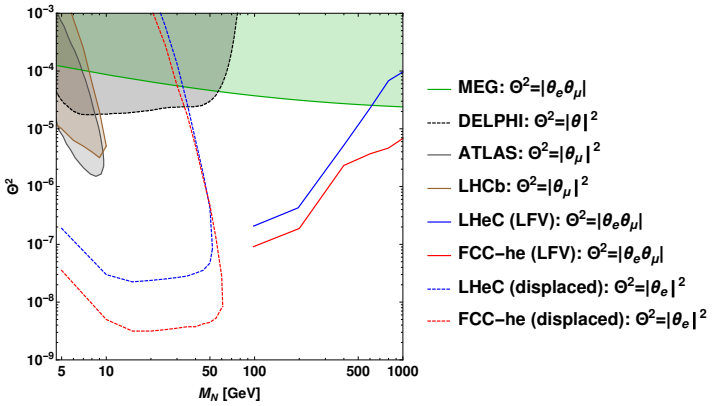

Figure 16: Sensitivity of the LFV lepton-trijet searches (at 95% C.L.) and the displaced vertex searches (at 95% C.L.) compared to the current exclusion limits from ATLAS [153], LHCb [174], LEP [151], and MEG [175]. The sensitivity of the lepton-trijet searches at ep colliders can be generalized to its full θ_α-dependence by replacing $|\theta_e\theta_\mu|$ with $2|\theta_e|^2|\theta_\mu|^2/|\theta|^2$. Notice that each experiment is sensitive to a different set of active-sterile mixing parameters, as indicated in the legend.

in ref. [129], the LEP experiment Delphi [151], and the recent result from ATLAS [153]. In comparison, the searches for lepton number conserving and lepton flavor violating final states at the HL-LHC and FCC-hh can only test active-sterile mixings that are much larger [9].

It is worthwhile to compare the results of this study with previous ones from ref. [111], which was a first look at the parton level and considered only a single background process. Here we performed an analysis at the reconstructed level, including hadronization and a number of backgrounds, and the obtained results – optimised by the use of the BDT – are more robust than the previous ones. It turns out that the new results have a better sensitivity to active-sterile mixing for any given mass compared to the previous result; as an illustration, the sensitivity for $M_N = 200$ GeV at 1σ parton level was 2×10^{-6} while here it is 2×10^{-7} at 95% confidence. This is because the previous results were on purpose very conservative in employing only a single cut on the missing energy. In this light it would be very interesting to compare our results with other promising signatures in ref. [111], such as the dilepton-jet final state in the high-mass regime or some of the signatures from $W\gamma$ fusion at high energies.

Let us comment on the impact of the flavor structure of active-sterile mixing. In the scenario that is complementary to our choice above, where $|\theta_\mu| \ll |\theta_e|, |\theta_\tau|$, the LFV final state $\tau^- jjj$ is the most prominent. We expect that our results are indicative also for this case because the tau reconstruction should benefit from the clean and pile up-free environment of the electron-proton collision, such that the reduction of the signal efficiency due to reconstruction losses should be small. Therefore our results should hold in more generality, unless unless $|\theta_e| \gg |\theta_\mu|, |\theta_\tau|$, in which case the lepton flavor conserving signatures become most relevant.

While in our model lepton number violation (LNV) is effectively absent for masses of $\mathcal{O}(100)$ GeV [113] it is interesting to consider the possibility of the

LNV final states at lower masses. The lepton trijet signature with an anti-lepton is also free of background and can be detectable with a significance that is similar to the lepton number conserving lepton trijet. This is important for the investigation of heavy neutrino-antineutrino oscillations, a phenomenon that can arise naturally in our model when the heavy neutrino pair is almost mass-degenerate and has macroscopic lifetimes. This phenomenon is rooted in the interference between the two Majorana-like heavy neutrinos and suppresses or allows lepton number violation (LNV) as a function of the displacement of the secondary vertex (or more precisely of the heavy neutrino lifetime). When the heavy neutrino production and decay vertices are separable in the detector these oscillations can be observed experimentally at ep colliders via the unambiguous LNV signature $N \to \ell^+ J$, where J denotes a number of hadrons. Therefore this signature could be observable at the LHeC and FCC-he within the contour lines shown in fig. 15 and with sufficient statistics even a determination of the oscillation length could be possible, which allows for instance to infer the mass splitting and thereby contribute to testing the conditions for leptogenesis.

7.4 CONCLUSIONS

In this paper we have analysed two of the most promising signatures of heavy neutrinos at ep colliders: the lepton-flavour violating (LFV) lepton-trijet signature $p\ e^- \to \mu^- + 3j$ and the displaced vertex signature. The latter is particularly relevant for heavy neutrino masses below m_W, where the heavy neutrinos can have macroscopic lifetimes. The lepton-trijet signature has been identified e.g. in ref. [111] as one of the most promising signatures among the many possible search channels for all collider types in the mass region above m_W up to some hundreds of GeV.

To capture the heavy neutrino properties of low scale seesaw models, we have used the "Symmetry Protected Seesaw Scenario" (SPSS) benchmark model [129], which includes two sterile neutrinos with opposite charges under a "lepton number"-like symmetry. We have performed our analysis for the choice $\theta_e = \theta_\mu$ and $\theta_\tau = 0$ for the active-sterile mixing angles. However, e.g. for the lepton-trijet signature, replacing $|\theta_e\theta_\mu|$ by $2|\theta_e|^2|\theta_\mu|^2/|\theta|^2$, one can easily recover the full parameter dependence.

We also note that we have used the "symmetry limit" of the benchmark model for our analysis, such that all final states are lepton number conserving. When the light neutrino masses are introduced via a small breaking of the protective symmetry, this can in principle (depending on the induced small mass splitting of the quasi-degenerate heavy neutrino pair) lead to observable lepton number violation via heavy neutrino-antineutrino oscillations. For displaced vertices the heavy neutrino-antineutrino oscillations might even be resolved via an oscillatory lifetime-dependence of $\mathrm{Br}(N \to \mu^- + 2j)/\mathrm{Br}(N \to \mu^+ + 2j)$, as discussed in [113].

Regarding the displaced vertex signatures, we have improved previous estimates by including the full detector geometry and the distribution of the relativistic velocity of the heavy neutrinos. We found that LHeC and FCC-he

can reach remarkable exclusion sensitivities down to $\mathcal{O}(10^{-8})$ and $\mathcal{O}(10^{-9})$ for $|\theta_e\theta_\mu|$, respectively, at the 95% confidence level (cf. figs. 15 and 16) . For the LFV lepton-trijet signature at ep colliders, we improved on previous estimates by including SM background processes and separating signal from background signatures at the reconstructed level with a Boosted Decision Tree (BDT). Our statistical evaluation shows that this channel can reach exclusion sensitivities to active-sterile mixing parameters $|\theta_e\theta_\mu|$ as small as 10^{-7} for FCC-he and 2×10^{-7} for LHeC at the 95% confidence level. For the considered benchmark model, this is the best sensitivity of all currently discussed heavy neutrino signatures in this mass range. For the whole mass region between about 5 GeV and up to $\mathcal{O}(1$ TeV) the sensitivity prospects for these signatures are reaching deeply into the currently unconstrained region.

In summary, our results demonstrate that ep colliders, such as the LHeC and the FCC-he, are excellent facilities for discovering heavy neutrinos in a large mass window around the electroweak scale. They are particularly good in the mass region above m_W up to some hundreds of GeV, where the LFV lepton-trijet signature could be a "golden channel" for heavy neutrino searches. A discovery of heavy neutrinos would have far-reaching consequences, opening up the possibility to resolve the origin of the observed neutrino masses, which is one of the great open questions in particle physics.

Acknowledgements

We thank Max and Uta Klein, Monica D'Onofrio, and Georges Azuelos for useful discussions. This work has been supported by the Swiss National Science Foundation. O.F. received funding from the European Unions Horizon 2020 research and innovation program under the Marie Sklodowska-Curie grant agreement No 674896 (Elusives).

8

SEARCHING FOR CHARGED LEPTON FLAVOR VIOLATION AT ep COLLIDERS

Published in: 10.1007/JHEP03(2021)230 [2]

Searching for charged lepton flavor violation at ep colliders

Stefan Antusch[†], A. Hammad[†] and Ahmed Rashed[‡]

[†]Department of Physics, University of Basel, Klingelbergstr. 82, CH-4056 Basel, Switzerland
[‡] Department of Physics, Shippensburg University of Pennsylvania,
Franklin Science Center, 1871 Old Main Drive, Pennsylvania, 17257, USA

ABSTRACT

We investigate the sensitivity of electron-proton ($e\,p$) colliders for charged lepton flavor violation (cLFV) in an effective theory approach, considering a general effective Lagrangian for the conversion of an electron into a muon or a tau via the effective coupling to a neutral gauge boson or a neutral scalar field. For the photon, the Z boson and the Higgs particle of the Standard Model, we present the sensitivities of the LHeC for the coefficients of the effective operators, calculated from an analysis at the reconstructed level. As an example model where such flavor changing neutral current (FCNC) operators are generated at loop level, we consider the extension of the Standard Model by sterile neutrinos. We show that the LHeC could already probe the LFV conversion of an electron into a muon beyond the current experimental bounds, and could reach more than an order of magnitude higher sensitivity than the present limits for LFV conversion of an electron into a tau. We discuss that the high sensitivities are possible because the converted charged lepton is dominantly emitted in the backward direction, enabling an efficient separation of the signal from the background.

8.1 INTRODUCTION

Experimental searches for charged lepton flavor violation (cLFV) are among the most sensitive probes of new physics beyond the Standard Model (SM) of elementary particles. In the SM, such flavor changing neutral current interactions in the lepton sector are absent at tree level and with massless neutrinos, and even when neutrino masses are introduced in an effective theory approach via the dimension five neutrino mass operator, they only get induced at loop level at tiny rates far below envisioned observational possibilities.

As an indirect probe of new physics, cLFV is known to be sensitive to extensions of the SM at scales far beyond the reach of direct searches at present and currently discussed future colliders. At present, particularly strong limits on LFV $\mu - e$ transitions come from $\mathrm{Br}(\mu \to e\gamma) \leqslant 4.2 \times 10^{-13}$ [37], and on LFV $\tau - e$ transitions from $\mathrm{Br}(\tau \to e\gamma) \leqslant 3.3 \times 10^{-8}$ [38] and $\mathrm{Br}(\tau \to 3e) \leqslant 2.7 \times 10^{-8}$ [39]. Planned experiments to extend the cLFV searches beyond these limits include MEG II [42], which could reach a sensitivity for $\mathrm{Br}(\mu \to e\gamma)$ down to 6×10^{-14}. Furthermore, the Mu3e experiment plans to reach a sensitivity for $\mathrm{Br}(\mu \to 3e)$ down to 2×10^{-15} [40] and the Mu2e experiment has the goal to increase the sensitivity for the $\mu - e$ conversion rate by four orders of magnitude down to 8×10^{-17} [176]. Both B-factories BABAR and BELLE II aim to improve the sensitivity on LFV τ decays by more than an order of magnitude down to $\mathrm{Br}(\tau \to e\gamma) < 3 \times 10^{-9}$ and $\mathrm{Br}(\tau \to 3e) < 1.2 \times 10^{-9}$ [41, 43, 44].

In this paper, we show that future electron-proton (ep) colliders such as the LHeC would be excellent facilities for probing the cLFV conversion of an electron into a muon or a tau via the effective coupling to a neutral gauge boson or a neutral scalar. To explore the potential for discovering cLFV induced by heavy new physics in a model-independent way, we consider a general effective Lagrangian for our sensitivity calculations via collider simulations at the reconstructed level. In addition, as an example model where flavor changing neutral current (FCNC) operators inducing cLFV are generated at loop level, we consider the extension of the Standard Model by sterile neutrinos. There we show that the LHeC could probe the LFV conversion of an electron into a muon beyond the current experimental bounds, and could reach more than an order of magnitude higher sensitivity for the LFV conversion of an electron into a tau.

8.2 HIGH SENSITIVITY TO CLFV AT ep COLLIDERS

Compared to electron-positron colliders, the high center-of-mass energy at ep colliders can provide an environment to test the SM at high energies with comparably low rates of background. Two examples of possible future ep colliders are the Large Hadron electron Collider (LHeC) [76, 154, 155, 168] and the ep mode of the Future Circular Collider (FCC). At the LHeC, the center-of-mass energy of 1.3 TeV with a total of 3 ab^{-1} integrated luminosity would be achieved by the use of the 7 TeV proton beam of the LHC in addition to a 60 GeV electron beam with up to 80% polarization. Moreover, the proposed

electron-proton experiment at the FCC (FCC-eh) is designed with the same energy level of the electron beam from the LHeC electron linac, but with the upgraded proton beam with energy of 50 TeV from the FCC-hh. This will achieve a center of mass energy of 3.5 TeV. This environment can be employed for significantly improving the PDF measurements and lower the associated systematic uncertainties. At the same time, an impact on the precision of some Higgs measurements is anticipated. In general, electron-proton colliders would be a great environment for testing certain types of new physics beyond the Standard Model, as has been explored in various studies (cf. e.g. [3, 4, 7, 177–179]).

8.2.1 *cLFV via effective vertices at* ep *colliders*

Charged lepton flavor violating (cLFV) processes can occur at the LHeC through an effective vertex that couples the incoming electron to a muon or a tau and a neutral scalar or vector boson. With the neutral scalar or vector boson in the t-channel, the effective flavor changing neutral current (FCNC) interactions can lead to $e-\mu$ or $e-\tau$ flavor transitions, as shown in Fig. 17. The processes have a specific kinematics that can be used to efficiently discriminate the signal from the SM background. A particularly useful feature, as we will discuss blow in section 8.2.2, is that at low momentum transfer the final state lepton, i.e. the μ or τ, is dominantly emitted in the backward region of the detector (cf. [76, 155]). At the LHeC, we will show that this allows to almost completely suppress the relevant SM backgrounds in some cases.

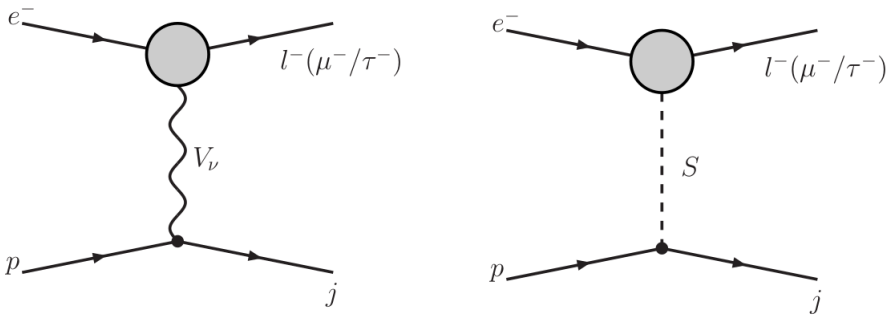

Figure 17: Feynman diagrams for cLFV processes at the LHeC induced by effective operators (represented by blobs in the diagrams) that couple the incoming electron to a muon or a tau and a vector bosons V_ν (left) or a scalar S (right).

The effective FCNC Lagrangian for charged leptons contains effective operators coupling the charged leptons to neutral scalars and neutral vector bosons. The effective Lagrangian for the couplings to neutral scalars is given by

$$\mathcal{L}_{\text{eff}}^{\text{scalar}} = \bar{\ell}_\alpha P_{L,R} \ell_\beta S \, N_{L,R}, \tag{143}$$

with $\ell_\beta, \ell_\alpha, S$ representing the incoming and outgoing charged leptons and the neutral scalar boson of the effective vertex, respectively. $N_{L,R}$ represents the left and right form factors of the effective scalar operator and $P_{L,R}$ are the chiral projection operators. We note that expressions like $P_{L,R}N_{L,R}$ are shorthand notations for the sum over both combinations, $P_L N_L + P_R N_R$. The part of the

effective Lagrangian for the coupling to vector bosons can be expressed in terms of monopole and dipole operators. The effective Lagrangian containing the monopole operators is given by

$$\mathcal{L}_{\text{eff}}^{\text{monopole}} = \bar{\ell}_\alpha \gamma_\mu P_{L,R} \ell_\beta \left[A_{L,R}\ g^{\mu\nu} + B_{L,R}(g^{\mu\nu} q^2 - q^\mu q^\nu) \right] V_\nu, \tag{144}$$

where q is the momentum of the gauge boson V_ν and where in the SM V_ν is either Z or γ. $A_{L,R}$ and $B_{L,R}$ are the form factors of the monopole operators. The effective Lagrangian containing the dipole operator is given by

$$\mathcal{L}_{\text{eff}}^{\text{dipole}} = \bar{\ell}_\alpha \sigma^{\mu\nu} P_{L,R} \ell_\beta\ q_\mu V_\nu\ D_{L,R}, \tag{145}$$

with $\sigma^{\mu\nu} = \frac{i}{2}[\gamma^\mu, \gamma^\nu]$ and $D_{L,R}$ denoting the left and right form factors of the dipole operator.

8.2.2 *Low background for cLFV due to specific kinematics*

The differential cross sections of the cLFV processes (cf. Fig. 17) depend on the center of mass energy s and the two kinematic variables q^2 and the Bjorken variable x. At the electron-proton colliders, the Bjorken x can be obtained from the measurement of the inelasticity y_e as [170]

$$x = \frac{q^2}{s\ y_e}, \qquad \text{with} \qquad y_e = 1 - \frac{E_\mu}{2E_e}\,(1 - \cos\theta)\,, \tag{146}$$

with E_μ, E_e being the energies of the scattered muon and the incoming electron, respectively. The scattering angle θ is defined between the direction of the outgoing particles and the proton beam. For the region of the parameter space with $x \approx E_e/E_p$, the energy of the scattered muon is approximately equal to the electron beam, which causes the cross section to peak in the backward direction of the detector. For larger q^2, x is larger due to the larger energy transfer from the proton beam that pushes the scattered muons somewhat more in the forward direction [155].

The SM background processes take place through the charged and neutral currents with $W^\pm$ and Z/H bosons exchange. For the charged current, a (t-channel) W boson can radiate a Z/γ^* which then generates a $\ell\bar{\ell}$ pair. For the neutral currents, a (t-channel) Z/H boson can generate charged leptons via radiating weak gauge bosons which then decay leptonically. Other backgrounds come from the decay of the on-shell produced bosons, e.g. $pe^- \to Ze^-j, Z \to \mu^\pm\mu^\mp$. The production of the on-shell Z boson requires a large energy transfer, and thus the dimuons will be detected mainly in the forward region of the detector. Accordingly, the cLFV process at the LHeC through an effective vertex can provide a unique signal in the backward direction which is almost background free.

In Fig. 18, we show examples for the angular distribution of the scattered muons at the LHeC, for the case of exchanged photons, Z bosons, and SM Higgs particles (showing as examples the form factors $A_{L,R}^{Z/\gamma}$ and $N_{L,R}^{H}$). As one can see, the scattered muons are dominantly emitted in the backward direction. For the massive mediators (Z, H), the cross section maximizes at

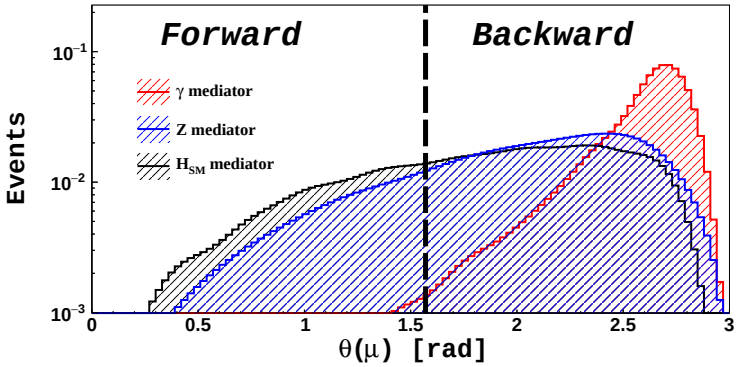

Figure 18: Examples for the muon angular distributions at the reconstructed level for the photon (red), Z boson (blue) and Higgs boson (black) mediated cLFV processes shown in Fig. 17. The distributions in the plot correspond to the contributions from the form factors $A_{L,R}^{Z/\gamma}$ and $N_{L,R}^{H}$, with total number of events normalized to one. Note that the y-axis has a logarithmic scale. The forward direction is the proton beam direction and the backward direction is the electron beam direction.

$q^2 = M^2$ and thus the peak shifts towards the forward direction compared to the photon case. A similar effect occurs for the form factors with momentum dependence, $B_{L,R}^{Z/\gamma}$ and $D_{L,R}^{Z/\gamma}$, which will be discussed in section 4 (with angular distributions shown in Fig. 7).

For the simulation, we have implemented the effective vertices in MadGraph [143]. After generating the events by MadGraph, Pythia [144] is used for showering and hadronization. For fast LHeC detector simulation we use Delphes [97]. The event reconstruction has been done by MadAnalysis5 [180] with the requirement that the scattered muons have to be hard, with $P_T > 25$ GeV.

8.3 LHEC SENSITIVITY TO CLFV FROM HEAVY NEUTRAL LEPTONS

In this section, before we turn to the model-independent analysis, we investigate the sensitivity of the LHeC for cLFV induced by heavy neutral leptons (also referred to as "heavy neutrinos" or "sterile neutrinos"). In particular, we will explore the LHeC sensitivity to the combinations $|\theta_e\theta_\mu^*|$ and $|\theta_e\theta_\tau^*|$ of active-sterile neutrino mixing angles within the "Symmetry Protected Seesaw Scenario" (SPSS) benchmark scenario (cf. [111, 129]), and compare it with the current bounds from non-collider experiments. The most relevant present constraints on the mixing parameters come from the two body decays, e.g. $\ell_\alpha \to \ell_e\gamma$ [37, 38], and the three body decays $\ell_\alpha \to 3\,\ell_e$ [39, 181, 182] of taus and muons ($\alpha = \mu, \tau$). For final state muons we also consider the constraint from the $\mu - e$ conversion search at SINDRUM II [183].

8.3.1 *Benchmark scenario: SPSS*

For the analysis of the LHeC sensitivities and the comparison to the present experimental constraints, we consider the SPSS benchmark model. In this subsec-

tion, we will only give a brief summary to the SPSS and refer for details to [111, 129]. Beyond the particle content of the SM, the scenario includes two sterile neutrinos with opposite charges under an approximate "lepton number"-like symmetry. The small observed neutrino masses arise from the small breaking of the "lepton number"-like symmetry. For the study of cLFV, we can treat the protective "lepton number"-like symmetry as being exact, such that lepton number is conserved. A discussion for which parameter regions the lepton number violating effects can be observable in the SPSS benchmark model with small symmetry breaking can be found in [113].

The Lagrangian density of the SPSS benchmark model, including the sterile neutrino pair N_R^1 and N_R^2, is given by:

$$\mathcal{L} = \mathcal{L}_{SM} - \overline{N_R^1} M_N N_R^{2\,c} - y_{\nu_\alpha} \overline{N_R^1} \widetilde{\phi}^\dagger L^\alpha + \text{H.c.} + \dots \,, \tag{147}$$

where L^α ($\alpha = e, \mu, \tau$) and ϕ are the lepton and Higgs doublets, respectively, and the parameters y_{ν_α} denote the complex-valued neutrino Yukawa couplings. M_N is the heavy neutral lepton (Majorana) mass parameter. The dots indicate additional terms which can be neglected in this study. They may contain additional heavy neutral leptons that are decoupled from collider phenomenology and indirect searches as well as the terms which slightly break the "lepton number"-like symmetry.

After electroweak symmetry breaking the neutral leptons (i.e. the active and sterile neutrinos) have a symmetric mass matrix, which can be diagonalized by a unitary 5×5 matrix U, cf. [129]. The mass eigenstates are $\tilde{n}_j = (\nu_1, \nu_2, \nu_3, N_4, N_5)_j^T = U_{j\alpha}^\dagger n_\alpha$. They include the three light neutrinos (which are actually massless in the symmetry limit) and two heavy neutrinos with (in the symmetry limit) degenerate mass eigenvalues M_N. The off-diagonal block of the mixing matrix U governs the interactions of the heavy neutrinos. It can be quantified by the active-sterile neutrino mixing angles θ_α related to the neutrino Yukawa couplings y_{ν_α} via

$$\theta_\alpha = \frac{y_{\nu_\alpha}^*}{\sqrt{2}} \frac{v_{EW}}{M_N} \,, \qquad |\theta|^2 := \sum_\alpha |\theta_\alpha|^2 \,, \tag{148}$$

where $v_{EW} = 246.22$ GeV denotes the vacuum expectation value of the Higgs field. Due to the mixing of the active and sterile neutrinos, the heavy neutrino mass eigenstates participate in the weak interactions as

$$j_\mu^\pm \supset \frac{g}{2} \theta_\alpha \bar{\ell}_\alpha \gamma_\mu P_L \left(-iN_4 + N_5\right) + \text{H.c.} \,, \tag{149}$$

$$j_\mu^0 = \frac{g}{2\, c_W} \sum_{i,j=1}^{5} \vartheta_{ij} \overline{\tilde{n}_i} \gamma_\mu P_L \tilde{n}_j \,, \tag{150}$$

$$\mathcal{L}_{\text{Yuk.}} \supset \frac{M_N}{v_{EW}} \sum_{i=1}^{3} \left(\vartheta_{i4}^* \overline{N_4^c} + \vartheta_{i5}^* \overline{N_5^c}\right) H \nu_i + \text{ H.c.} \,. \tag{151}$$

g is the weak coupling constant, c_W the cosine of the Weinberg angle and $P_L = \frac{1}{2}(1 - \gamma^5)$ is the left-chiral projection operator. H denotes the real scalar Higgs boson and $\vartheta_{ij} := \sum_{\alpha=e,\mu,\tau} U_{i\alpha}^\dagger U_{\alpha j}$.

Finally, we note that in the symmetry limit of the SPSS benchmark model, only the moduli $|\theta_e|$, $|\theta_\mu|$ and $|\theta_\tau|$ of the active-sterile mixing angles and the (w.l.o.g. real and positive) mass parameter M_N are physical. Furthermore, we remark that via the relation $|V_{\alpha N}|^2 = |\theta_\alpha|^2$, one can readily translate our results (which we will give in terms of the active-sterile neutrino mixing angles θ_α) to the neutrino mixing matrix elements $V_{\alpha N}$ often used in the literature.

8.3.2 *Calculation of the form factors for the cLFV operators*

To calculate the form factors for the cLFV operators within the SPSS from the respective penguin diagrams (cf. Fig. 19), we use the package Peng4BSM@LO [184]. Peng4BSM@LO is a Mathematica package that calculates the contributions of the form factors of certain effective operators originating from one-loop penguin Feynman diagrams. In order to allow for generic finite form factors, the package calculates the form factors as the first order expansion of the small masses and momenta of the external fermions. We remark that all cLFV penguin processes have no tree level amplitude, and are thus finite at the one-loop level. The UV-divergence vanishes when we sum up over all diagrams and apply the unitarity condition of the leptonic mixing matrix U.

We find (using Peng4BSM@LO [184]) that the form factors in the SM extension by heavy neutral leptons (within the SPSS benchmark scenario) are given by

$$\begin{aligned} B_L^\gamma = \sum_{k=1}^{5} \frac{e^2|\theta_e\theta_\alpha^*|}{1152\pi^2 M_W^3 \sin^3\theta_W (1-x_k^2)^4} \big[&(x_k^2-1)(3e\, v_{EW}\, x_k^2(2x_k^4+5x_k^2-1) \\ &- M_W \sin\theta_W (11x_k^6 - 27x_k^4 + 90x_k^4 - 20)) \\ &+ 12(M_W \sin\theta_W x_k^4 (x_k^4 - 4x_k^2 + 12) - 3e\, v_{EW}\, x_k^6)\ln(x_k)\big]\,, \end{aligned}$$

$$D_L^\gamma = \frac{-i\, e^2\, M_e |\theta_e\theta_\alpha^*|}{384\pi^2\, M_W^2 \sin_W^2} \sum_{k=1}^{5} \left(\frac{7 - 34x_k^2 + 63x_k^4 - 34x_k^6 - 2x^8 - (48x_k^6 - 12x_k^4)\ln(x_k)}{(1-x_k^2)^4} \right),$$

$$D_R^\gamma = \frac{-i\, e^2\, M_\alpha |\theta_e\theta_\alpha^*|}{384\pi^2\, M_W^2 \sin_W^2} \sum_{k=1}^{5} \left(\frac{7 - 34x_k^2 + 63x_k^4 - 34x_k^6 - 2x^8 - (48x_k^6 - 12x_k^4)\ln(x_k)}{(1-x_k^2)^4} \right),$$

$$\begin{aligned} A_L^Z = &\frac{e^2|\theta_e\theta_\alpha^*|}{16\pi^2\, M_W\, \cos\theta_W \sin^3\theta_W} \\ &\times \sum_{k=1}^{5} \left(\frac{1}{(1-x_k^2)^4} \big[(x_k^2-1)(M_W(8x_k^2\sin^2\theta_W - 9x_k^2 - 1) - 4e\sin\theta_W\, v_{EW} x_k^2) \right. \\ &\left. + 4(M_W(5 - 4\sin^2\theta_W) + 2e\sin\theta_W v_{EW}) x_k^4 \ln(x_k)\big] \right), \end{aligned}$$

$$
\begin{aligned}
B_L^Z = &-\sum_{k=1}^{5} \frac{ie^2|\theta_e\theta_\alpha^*|}{2304\pi^2\cos\theta_W M_W^3\sin^3\theta_W(1-x_k^2)^4} \\
&\times\big[(x_k^2-1)(6x_k^2 e\ \sin\theta_W v_{EW}(2x_k^4+5x_k^2-1)+M_W(-12-2(\sin^2\theta_W-12)x_k^2 \\
&+(7\sin^2\theta_W-12)x_k^4-11x_k^6\sin^2\theta_W+\cos^2\theta_W(11x_k^6-47x_k^4+178x_k^2-40))) \\
&-12(6x_k^2 e\ \sin\theta_W v_{EW}x_k^6+M_W(4-14x_k^2+8(2+3\cos^2\theta_W)x_k^4-2x_k^6(3+4\cos^2\theta_W) \\
&+(\cos^2\theta_W-\sin^2\theta_W)x_k^8))\ln(x_k)\big]\,,
\end{aligned}
$$

$$
\begin{aligned}
D_L^Z = &-\sum_{k=1}^{5} \frac{ie^2 M_e|\theta_e\theta_\alpha^*|}{768\pi^2\cos\theta_W M_W^2\sin^3\theta_W(1-x_k^2)^4} \\
&\times\big[(x_k^2-1)(8+x_k^2(\sin^2\theta_W-24)+x_k^4(16-5\sin^2\theta_W) \\
&-2x_k^6\sin^2\theta_W\cos^2\theta_W(14-53x_k^2+67x_k^4+2x^6))-4x_k^2(2-2x_k^2(4+3\cos^2\theta_W) \\
&+3x_k^4(2+7\cos^2\theta_W-\sin^2\theta_W)\ln(x_k))\big]\,,
\end{aligned}
$$

$$
\begin{aligned}
D_R^Z = &-\sum_{k=1}^{5} \frac{ie^2 M_\alpha|\theta_e\theta_\alpha^*|}{768\pi^2\cos\theta_W M_W^2\sin^3\theta_W(1-x_k^2)^4} \\
&\times\big[(x_k^2-1)(8+x_k^2(\sin^2\theta_W-24)+x_k^4(16-5\sin^2\theta_W) \\
&-2x_k^6\sin^2\theta_W\cos^2\theta_W(14-53x_k^2+67x_k^4+2x^6)) \\
&-4x_k^2(2-2x_k^2(4+3\cos^2\theta_W)+3x_k^4(2+7\cos^2\theta_W-\sin^2\theta_W)\ln(x_k))\big]\,,
\end{aligned}
$$

$$
B_R^\gamma = A_R^Z = B_R^Z = A_{L,R}^\gamma = 0\,.
$$

In the above equations, we have defined $x_k := \frac{M_{\tilde{n}_k}}{M_W}$. e is the electric charge, M_α is the mass of the charged lepton ℓ_α (with $\alpha = \mu, \tau$) and θ_W denotes the weak mixing angle.

We note that the lepton self energy diagrams with virtual photon exchange do not contribute to the amplitude since they cancel out with terms from W boson and Goldstone boson diagrams. The monopole term that is proportional to $q_\mu q_\nu$, cf. Eq. (144), vanishes as ist should because it would violate quark current conservation. For the case of Z boson exchange the dipole form factors, $D_{L,R}^Z$, flip the chirality of the outgoing fermions. They are suppressed since they are proportional to the lepton mass [185–187]. We have neglected the contributions from the effective operators with the SM Higgs boson, because they are suppressed by the small couplings of the Higgs to the beam quarks.

8.3.3 *Method for obtaining the cLFV sensitivity at the LHeC*

In the following, we assume that the heavy neutral leptons have sufficiently large masses that they cannot be directly produced at the LHeC. With this con-

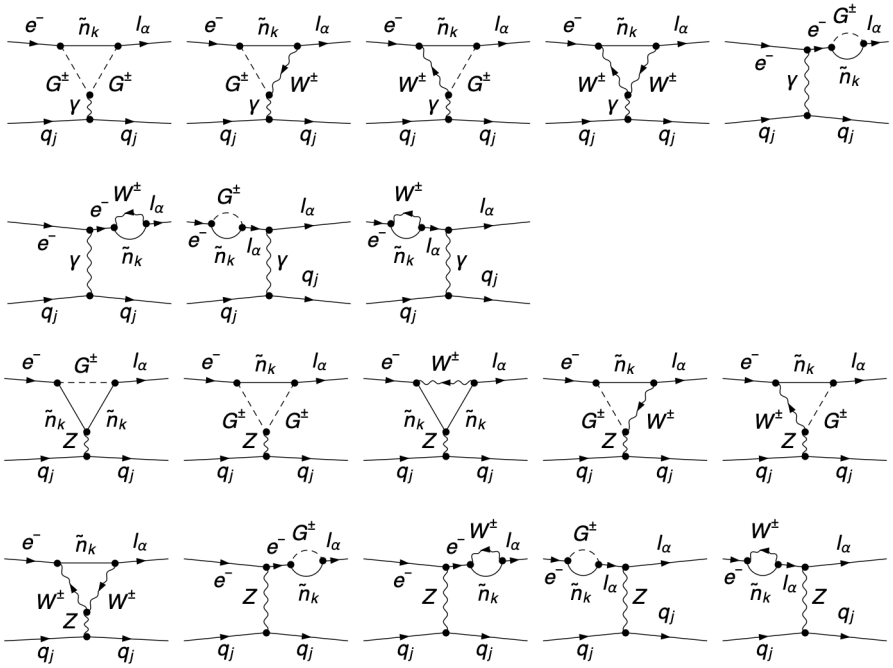

Figure 19: Feynman diagrams generating the effective vertices for $e^- \to \ell_\alpha \gamma$ and $e^- \to \ell_\alpha Z$ in extensions of the SM by heavy neutral leptons. $\tilde{n}_k$ runs over all (light and heavy) neutral lepton mass eigenstates.

dition satisfied, we will apply the effective operator treatment. The amplitudes for the $e-\mu/e-\tau$ conversion processes $pe^- \to \mu^- j / pe^- \to \tau^- j$ are given by

$$\mathcal{M}_{\mathrm{LHeC}} = \mathcal{M}_{\gamma^*} + \mathcal{M}_Z, \tag{152}$$

with $\mathcal{M}_{\gamma^*}$ and $\mathcal{M}_Z$ denoting the amplitudes for virtual photon and Z boson exchange

$$\begin{aligned}
\mathcal{M}_{\gamma^*} &= \bar{u}_{l_\alpha}\left[B^\gamma_{L,R} P_{L,R}\, q^2 \gamma^\nu - i\sigma^{\mu\nu} q_\mu D^\gamma_{L,R} P_{L,R}\right] u_e \left(\frac{-ie\, g_{\mu\nu}}{q^2}\right) \bar{u}_q(-ieQ_q\gamma^\mu)v_q\,, \\
\mathcal{M}_Z &= \bar{u}_{l_\alpha}\left[A^Z_{L,R} P_{L,R}\gamma^\nu + B^Z_{L,R} P_{L,R} q^2\gamma^\nu - i\sigma^{\mu\nu} q_\mu D^Z_{L,R} P_{L,R}\right] u_e \left(\frac{-ig_{\mu\nu}}{q^2 - M_Z^2}\right) \bar{u}_q(\gamma^\mu\, g_{L,R} P_{L,R})v_q.
\end{aligned} \tag{153}$$

Q_q is the quark charge and $g_{L,R}$ are the left and right couplings of the Z boson with quarks (where again expressions like $g_{L,R}P_{L,R}$ stand for the sums, i.e. $g_L P_L + g_R P_R$). $B^\gamma_{L,R}, D^\gamma_{L,R}, A^Z_{L,R}, B^Z_{L,R}$ and $D^Z_{L,R}$ are the effective form factors of the one-loop penguin diagrams in Fig. 19, with results given in the previous subsection.

In the following we will carry out the cLFV sensitivity analysis for the case of muons in the final state, $pe^- \to \mu^- j$, and taus in the final state, $pe^- \to \tau^- j$, separately. These two searches at the LHeC can test the combinations $|\theta_e\theta^*_\mu|$ and $|\theta_e\theta^*_\tau|$ of the flavor-dependent active-sterile mixing angles, respectively, for a given heavy neutrino mass M_N. In the analysis with muons in the final state, we initially fix $|\theta_e\theta^*_\mu| = 10^{-3}$ with $\theta_e = \theta_\mu$ and $\theta_\tau = 0$, and for the analysis with taus in the final state we fix $|\theta_e\theta^*_\tau| = 10^{-3}$ with $\theta_e = \theta_\tau$ and $\theta_\mu = 0$. We then use MadGraph [143] to calculate the total cross section and generate the events, where the form factors and its Lorentz structure have been carefully

implemented as described in [94]. The parton shower and hadronisation are done by Pythia [144]. For fast detector simulation we use Delphes [97]. For event reconstruction and analysis we use MadAnalysis [180, 188].

8.3.4 *Event reconstruction and analysis*

For signal reconstruction (at the reconstructed level after detector simulation), we require at least one muon with $P_T \geqslant 25$ GeV and jets with $P_T \geqslant 5$ GeV. For tau lepton reconstruction, we use an identification efficiency rate of 75% for tau leptons with $P_T \geqslant 25$ GeV and misidentification rate about 1% [189, 190]. For the process with final state taus, we use Pythia for tau decays and then we use the Delphes analysis module to reconstruct the hadronic tau jet with identification efficiency rate of 75% for the signal and identification efficiency rate of 60% for the background. The most relevant backgrounds and their total cross sections are shown in Table 5 for final state taus (left) and final state muons (right).

#	Backgrounds τ final state	$\sigma_{(\mathrm{LHeC})}$[Pb]
bkg1	$pe^- \to Z/\gamma^*(\to \tau^-\tau^+)\, \nu_l\, j$	0.0316
bkg2	$pe^- \to W^\pm(\to \tau^\pm\, \nu_\tau)\, e^-\, j$	0.2657
bkg3	$pe^- \to ZZ(\to \tau^-\tau^+)\, \nu_l\, j$	1.1×10^{-5}
bkg4	$pe^- \to Z(\to \tau^-\tau^+)W^\pm(\to \tau^\pm\, \nu_\tau)\, \nu_l\, j$	2.64×10^{-5}

#	Backgrounds μ final state	$\sigma_{(\mathrm{LHeC})}$[Pb]
bkg1	$pe^- \to Z/\gamma^*(\to \mu^-\mu^+)\, \nu_l\, j$	0.0316
bkg2	$pe^- \to W^\pm(\to \mu^\pm\, \nu_\mu)\, e^-\, j$	0.2657
bkg3	$pe^- \to Z/\gamma^*(\to \tau^-\tau^+ \to \text{leptons})\, \nu_l\, j$	9.1×10^{-4}
bkg4	$pe^- \to W^\pm(\to \tau^\pm\, \nu_\tau \to \text{leptons})\, e^-\, j$	0.0451
bkg5	$pe^- \to ZZ(\to \mu^-\mu^+)\, \nu_l\, j$	1.1×10^{-5}
bkg6	$pe^- \to Z(\to \mu^-\mu^+)W^\pm(\to \mu^\pm\, \nu_\mu)\, \nu_l\, j$	2.64×10^{-5}

Table 5: Dominant background processes considered in our analysis and their total cross sections for final state taus (left) and final state muons (right). The cross sections are obtained from MadGraph, while for the later tau decays we utilize Pythia. The samples have been produced with the following parton level cuts: $P_T(j) \geqslant 5$ GeV, $P_T(l) \geqslant 2$ GeV and $|\eta(l/j)| \leqslant 4.5$.

It is worth mentioning that other backgrounds like $pe^- \to h\nu j$ with the SM Higgs decaying to a lepton pair are suppressed by the small Yukawa couplings, while the process of single top production $pe^- \to \nu t$ is suppressed by the small involved CKM mixing matrix element.

In order to enhance the signal-to-background rate, we reconstruct four variables that can distinguish between the signal and all relevant backgrounds. In Fig. 20, we show the kinematic distributions of the signal with final state muons versus all backgrounds superimposed. The most important variable is the angular distribution of the final state hard leptons (μ/τ). They are mainly detected in the backward region of the detector while all the background processes produce hard leptons (μ/τ) in the forward region of the detector. For the case of signals with hard muons in the final state, the signal events have very low missing energy, while for taus in the final state there is a larger source of missing energy due to the hadronic tau reconstruction. Additionally, the transverse momenta of electrons or μ^+/τ^+ in the signal events are very small since the only source for them is the decay of radiated photons. In order to enhance the signal to background ratio, we optimize the cuts on these reconstructed

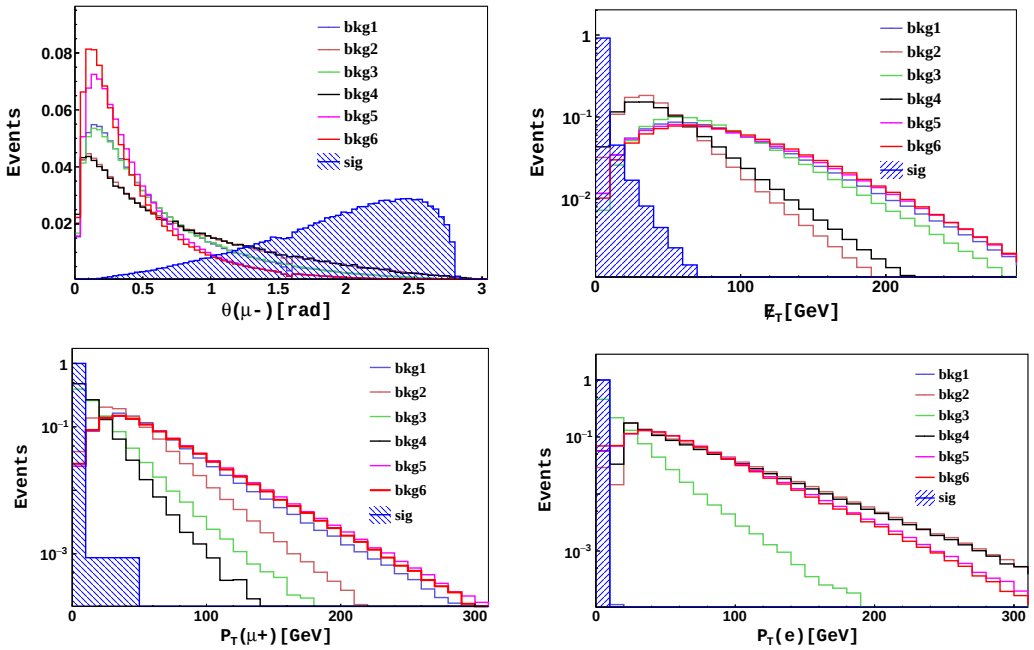

Figure 20: Distributions of kinematic variables (before any cuts applied) for the signal events with $M_N = 1$ TeV, for the process $pe^- \to \mu^- j$ with muons in the final state, and with all relevant background events in Table 5 (right) superimposed and normalized to one. Upper left: angular distribution in radians for hard muons in the final state. Upper right: transverse missing energy. Down left: transverse momentum for anti-muons. Down right: transverse momentum for final state electrons.

kinematic variables as shown in Table 6 (left) for tau final states and (right) for muon final states for the benchmark point with $M_N = 1$ TeV.

8.3.5 *Results: sensitivities to the active-sterile mixing angles at the LHeC*

Given the number of signal events and the number of background events after the optimized cuts, the LHeC sensitivity at 90% confidence level (CL) is obtained for rejecting the signal plus background over the background-only hypothesis and by using the formula [9, 191]

$$\sigma_{sys} = \left[2\left((N_s + N_b)\ln\frac{(N_s + N_b)(N_b + \sigma_b^2)}{N_b^2 + (N_s + N_b)\sigma_b^2} - \frac{N_b^2}{\sigma_b^2}\ln(1 + \frac{\sigma_b^2 N_s}{N_b(N_b + \sigma_b^2)})\right)\right]^{1/2}, \tag{154}$$

with N_s and N_b being the number of signal and background events, and with σ_b being the systematic uncertainty, taken to be 2% [155] for background

Cut	Background events	Signal events
Normalized events (no cut)	297528	8147
$P_T(\tau^+) \leqslant 10$ GeV	137986	8117
$\not{E}_T \leqslant 100$ GeV	132844	8110
$P_T(e) \leqslant 10$GeV	14036	8110
$\theta(\tau^-) \geqslant 1.5$ rad	3561	5302

Cut	Background events	Signal events
Normalized events (no cut)	343600	11639
$P_T(\mu^+) \leqslant 10$ GeV	180114	11596.75
$\not{E}_T \leqslant 50$ GeV	126183	11517.4
$P_T(e) \leqslant 10$ GeV	12705	11517.3
$\theta(\mu^-) \geqslant 1.5$ rad	4822.8	8925.9

Table 6: Cut efficiency, i.e. number of signal events and all backgrounds summed, for the processes $pe^- \to \tau^- j$ (left table) and $pe^- \to \mu^- j$ (right table) at the LHeC with integrated luminosity 3 ab^{-1}. For the signal events with final state taus we fix $\theta_e = \theta_\tau$, $\theta_\mu = 0$ and $|\theta_e \theta_\tau^*| = 10^{-3}$, which corresponds to a total cross section of 0.01173 Pb (before the tau decays). For the signal events with muons in the final state we fix $\theta_e = \theta_\mu$, $\theta_\tau = 0$ and $|\theta_e \theta_\mu^*| = 10^{-3}$, which corresponds to a total cross section of 0.01164 Pb. The heavy neutrino mass parameter M_N has been set to 1 TeV. The numbers of signal and background events without cuts correspond to the above-given total cross sections and integrated luminosity.

events only. For obtaining the current limits from non-collider experiments we use the following experimental constraints at 90% CL:

$$\begin{aligned}
&\mathrm{Br}(\mu \to e\gamma) \leqslant 4.2 \times 10^{-13} \quad [37] \ , \\
&\mathrm{Br}(\tau \to e\gamma) \leqslant 3.3 \times 10^{-8} \ [38] \ , \\
&\mathrm{Br}(\mu \to e^- e^+ e^-) \leqslant 1. \times 10^{-12} \ [181, 182] \ , \\
&\mathrm{Br}(\tau \to e^- e^+ e^-) \leqslant 2.7 \times 10^{-8} \quad [39] \ , \\
&\mathrm{Cr}(\mu - e, {}^{48}_{22}\mathrm{Ti}) \leqslant 4.3 \times 10^{-12} \ [183] \ .
\end{aligned}$$

From the bounds on the branching (or conversion) ratios for $\ell_\alpha \to e\gamma$, $\ell_\alpha \to 3e$ and $\mu - e$ conversion in nuclei, we calculate the limits on the active-sterile neutrino mixing angles using the formulae given in [192]. It is worth mentioning that the processes $\ell_\alpha \to 3e$ and $\mu - e$ conversion in nuclei have an energy scale of $q^2 = M_\alpha^2$ (with $\alpha = \mu, \tau$), which implies that the Z boson contribution is suppressed by the squared mass difference in the propagator due to the small energy transfer [193]. On the other hand, at the LHeC the energy scale is $\sim$ 1.3 TeV and thus the Z boson can have a much larger contribution. The largest contribution indeed comes from the from the effective operator with form factor A_L^Z.

In Fig. 21 we present our results for the LHeC sensitivities to the active-sterile neutrino mixing angles and compare them with the current limits from

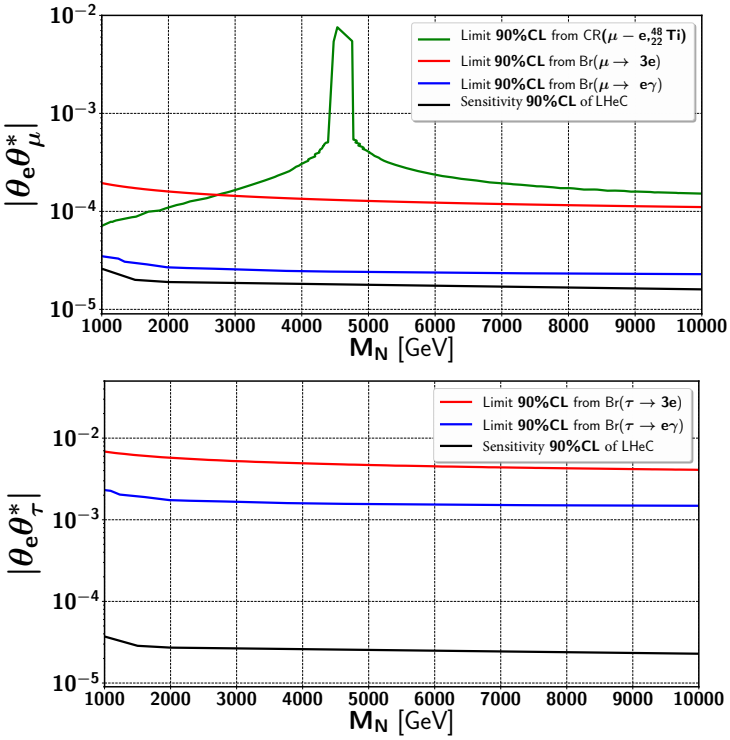

Figure 21: Estimated sensitivities to the active-sterile neutrino mixing angle combinations $|\theta_e\theta^*_\mu|$ (upper panel) and $|\theta_e\theta^*_\tau|$ (lower panel). The black lines show our results for the LHeC sensitivity from the processes $pe^- \to \mu^- j$ and $pe^- \to \tau^- j$, respectively, with 1.3 TeV center-of-mass energy and integrated luminosity of 3 ab^{-1}. The green line in the upper panel corresponds the current limit from $\mu - e$ conversion, the red and blue lines in both panels show the current limits from $\ell_\alpha \to 3e$ and $\ell_\alpha \to e\gamma$ (taken from [192]), respectively.

non-collider experiments. The result with muons in the final state (where the process is sensitive to $|\theta_e\theta^*_\mu|$) is shown in the upper plot, while the one with taus in the final state (sensitive to $|\theta_e\theta^*_\tau|$) is shown in the lower plot. The results show that with sensitivities down to $|\theta_e\theta^*_\mu| \leqslant 2 \times 10^{-5}$ and $|\theta_e\theta^*_\tau| \leqslant 3 \times 10^{-5}$ (for the example of $M_N = 1$ TeV), the LHeC can provide better sensitivity than the current limit in both cases. The sensitivity to the LFV parameters responsible for the conversion of an electron into a tau is better than the current limits by more than an order of magnitude.

8.4 MODEL-INDEPENDENT RESULTS

In this section, we calculate the model independent LHeC sensitivities for the form factors of the FCNC operators inducing cLFV given in section 2.1. The results can be used to estimate the LHeC discovery potential for generic heavy new physics that generates these effective operators. To calculate the LHeC sensitivities, we again analyse the processes $pe^- \to \mu^- j$ and $pe^- \to \tau^- j$, mediated by a cLFV effective coupling to photon, Z boson, and SM Higgs. In

the following, we use the form factors with superscripts to identify the considered boson, i.e. γ, Z or H. To obtain the LHeC sensitivities, we follow the same procedure used in the previous section and perform an analysis at the reconstructed level, switching on only one form factor at a time.

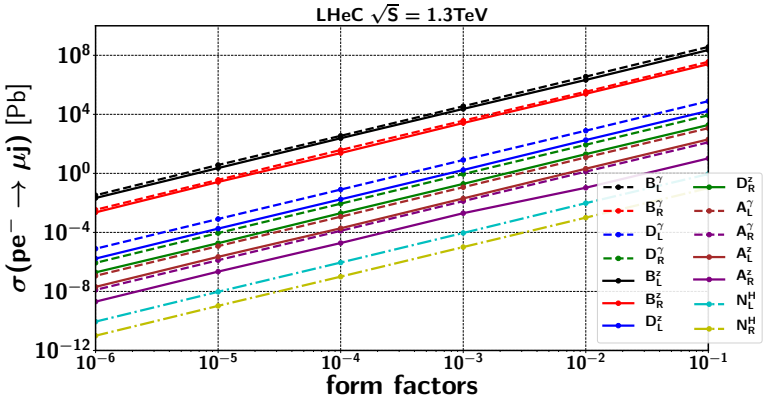

Figure 22: Total cross section for the process $pe^- \to \mu j$ as function of the size of the individual form factors given in Eqs. (169), (144) and (145), for the LHeC with 7 TeV protons and 60 GeV electrons with 80% polarization. For the form factors $B_{L,R}^{Z/\gamma}$ and $D_{L,R}^{Z/\gamma}$, the x-axis shows their size in units of GeV^{-2} and GeV^{-1}, respectively.

In Fig. 22 we show the total cross section of $pe^- \to \mu^- j$ in picobarn as a function of the size of the individual form factors. One can see that the largest cross sections come from the monopole form factors $B_{L,R}^{Z/\gamma}$, which is due to the momentum transfer squared attached to the effective vertex. The dipole form factors, $D_{L,R}^{Z/\gamma}$, also have comparatively large cross section due to the attached q^ν in the effective vertex. The form factors corresponding to the SM Higgs contribution have the lowest cross sections since the coupling of the SM Higgs with the proton beam is suppressed by the small Yukawa couplings. We remark that all considered kinematic distributions of the final state particles, except the angular distribution of the final state lepton, do not change by considering different form factors.

On the other hand, due to the dependence of the monopole and dipole form factors on the momentum of the mediator particle, the angular distributions of the final state leptons are shifted towards the forward direction. In Fig. 23, we show the angular distributions of the final state muons for the process $pe^- \to \mu^- j$, with total event number normalized to one. The shifting of the angular distributions towards the forward direction (in addition to the earlier discussed shifting for the processes with massive mediators compared to the photon-mediated processes) indeed weakens the signal vs. background separation, but still other characteristics such as $P_T(l^+)$, $\not{E}_T$, and $P_T(e)$ can be used to improve the sensitivity.

Our model-independent results are presented in Tables 7 and 8, where we show the LHeC sensitivities to the individual form factors at 90% CL, based on the processes $pe^- \to \mu^- j$ and $pe^- \to \tau^- j$, respectively. For the analysis, we initially fix the values of the considered form factor to 10^{-3}, with all other

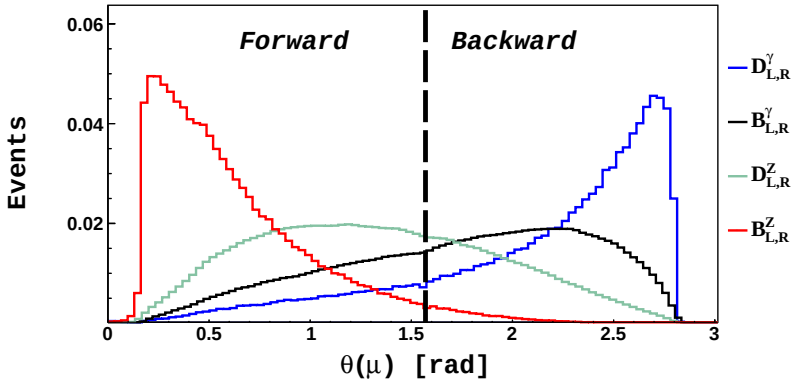

Figure 23: Angular distribution of the muons for the process $pe^- \to \mu^- j$ at the reconstructed level, considering the monopole and dipole form factors for the effective operators that mediate the process via photon and Z boson exchange. The total event numbers are normalized to one. The forward direction is the proton beam direction and the backward direction is the electron beam direction.

form factors set to zero, to calculate the total initial cross section which is used to normalize the generated events with integrated luminosity 3 ab^{-1}. In order to increase the signal over background yield, the cuts have been optimized for each form factor individually. Given the number of signal and background events after each cut we have calculated the LHeC sensitivity at 90% CL for rejecting the signal plus background over the background-only hypothesis using the formula in Eq. (154).

8.5 SUMMARY AND CONCLUSIONS

In this work we have investigated the sensitivity of electron-proton (ep) colliders, in particular of the LHeC, for charged lepton flavor violation (cLFV). In an effective theory approach, we have considered a general effective Lagrangian for the conversion of an electron into a muon or a tau via the effective coupling of the charged leptons to a neutral gauge boson or a neutral scalar field.

For the photon, the Z boson and the Higgs particle of the SM, we have presented the sensitivities of the LHeC (with 3 ab^{-1} integrated luminosity) for the coefficients of the effective operators (cf. section 8.4 and Table 7 for the results with muons and Table 8 for the results with taus in the final state), calculated from an analysis at the reconstructed level.

As an example for a model where such flavor changing neutral current (FCNC) operators are generated at loop level, we have considered the extension of the Standard Model by sterile neutrinos in the context of the SPSS benchmark model. Our results for the sensitivities to the active-sterile neutrino mixing angle combinations $|\theta_e\theta^*_\mu|$ and $|\theta_e\theta^*_\tau|$ are shown in Fig. 21.

Our results show that the LHeC (with 3 ab^{-1} integrated luminosity) could already the LFV conversion of an electron into a muon beyond the current experimental bounds, and could reach more than an order of magnitude higher

Form Factors	Cut	Background events	Signal events	LHeC sensitivity 90% CL
N_L^H/N_R^H	Normalized events (no cut)	343600	274/33	$4.49\times10^{-3}/3.55\times10^{-2}$
N_L^H/N_R^H	$P_T(\mu^+) \leqslant 10$ GeV	180114	274/33	$3.08\times10^{-3}/2.57\times10^{-2}$
N_L^H/N_R^H	$\not{E}_T \leqslant 50$ GeV	126183	269 /32	$2.65\times10^{-3}/2.22\times10^{-2}$
N_L^H/N_R^H	$P_T(e) \leqslant 10$GeV	12705	269/32	$8.41\times10^{-4}/7.05\times10^{-3}$
N_L^H/N_R^H	$\theta(\mu^-) \geqslant 0.5$ rad	9322	232/28	$8.36\times10^{-4}/6.90\times10^{-3}$
Form Factors	Cut	Background events	Signal events	LHeC sensitivity 90% CL
A_L^γ/A_R^γ	Normalized events (no cut)	343600	69000/7875	$1.75\times10^{-5}/1.50\times10^{-4}$
A_L^γ/A_R^γ	$P_T(\mu^+) \leqslant 10$ GeV	180114	68700/7840	$1.31\times10^{-5}/1.09\times10^{-4}$
A_L^γ/A_R^γ	$\not{E}_T \leqslant 50$ GeV	126183	68673/7837	$1.11\times10^{-5}/9.12\times10^{-5}$
A_L^γ/A_R^γ	$P_T(e) \leqslant 10$GeV	12705	68673/7837	$4.93\times10^{-6}/3.12\times10^{-5}$
A_L^γ/A_R^γ	$\theta(\mu^-) \geqslant 1.5$ rad	4823	67586/7713	$3.94\times10^{-6}/2.16\times10^{-5}$
Form Factors	Cut	Background events	Signal events	LHeC sensitivity 90% CL
D_L^γ/D_R^γ [GeV^{-1}]	Normalized events (no cut)	343600	$2.41\times10^7/2.66\times10^6$	$1.58\times10^{-7}/1.42\times10^{-6}$
D_L^γ/D_R^γ [GeV^{-1}]	$P_T(\mu^+) \leqslant 10$ GeV	180114	$2.39\times10^7/2.65\times10^6$	$1.46\times10^{-7}/1.31\times10^{-6}$
D_L^γ/D_R^γ [GeV^{-1}]	$\not{E}_T \leqslant 50$ GeV	126183	$2.37\times10^7/2.63\times10^6$	$1.41\times10^{-7}/1.27\times10^{-6}$
D_L^γ/D_R^γ [GeV^{-1}]	$P_T(e) \leqslant 10$GeV	12705	$2.37\times10^7/2.63\times10^6$	$1.12\times10^{-7}/1.01\times10^{-6}$
D_L^γ/D_R^γ [GeV^{-1}]	$\theta(\mu^-) \geqslant 0.3$ rad	10935	$2.37\times10^7/2.63\times10^6$	$1.05\times10^{-7}/9.44\times10^{-7}$
Form Factors	Cut	Background events	Signal events	LHeC sensitivity 90% CL
B_L^γ/B_R^γ [GeV^{-2}]	Normalized events (no cut)	343600	$9.52\times10^{10}/9.99\times10^9$	$1.35\times10^{-9}/1.28\times10^{-8}$
B_L^γ/B_R^γ [GeV^{-2}]	$P_T(\mu^+) \leqslant 10$ GeV	180114	$9.52\times10^{10}/9.99\times10^9$	$1.31\times10^{-9}/1.25\times10^{-8}$
B_L^γ/B_R^γ [GeV^{-2}]	$\not{E}_T \leqslant 50$ GeV	126183	$9.26\times10^{10}/9.74\times10^9$	$1.31\times10^{-9}/1.25\times10^{-8}$
B_L^γ/B_R^γ [GeV^{-2}]	$P_T(e) \leqslant 10$GeV	12705	$9.26\times10^{10}/9.74\times10^9$	$1.21\times10^{-9}/1.15\times10^{-8}$
B_L^γ/B_R^γ [GeV^{-2}]	$\theta(\mu^-) \geqslant 0.1$ rad	11898	$9.25\times10^{10}/9.73\times10^9$	$1.20\times10^{-9}/1.14\times10^{-8}$
Form Factors	Cut	Background events	Signal events	LHeC sensitivity 90% CL
A_L^Z/A_R^Z	Normalized events (no cut)	343600	17458/2182	$6.77\times10^{-5}/5.37\times10^{-4}$
A_L^Z/A_R^Z	$P_T(\mu^+) \leqslant 10$ GeV	180114	17394/2174	$5.00\times10^{-5}/3.91\times10^{-4}$
A_L^Z/A_R^Z	$\not{E}_T \leqslant 50$ GeV	126183	17276/2159	$4.20\times10^{-5}/3.30\times10^{-4}$
A_L^Z/A_R^Z	$P_T(e) \leqslant 10$GeV	12705	17276/2159	$1.54\times10^{-5}/1.07\times10^{-4}$
A_L^Z/A_R^Z	$\theta(\mu^-) \geqslant 1.5$ rad	4823	13389/1674	$1.36\times10^{-5}/8.74\times10^{-5}$
Form Factors	Cut	Background events	Signal events	LHeC sensitivity 90% CL
D_L^Z/D_R^Z [GeV^{-1}]	Normalized events (no cut)	343600	$3.69\times10^6/4.22\times10^5$	$5.66\times10^{-7}/4.95\times10^{-6}$
D_L^Z/D_R^Z [GeV^{-1}]	$P_T(\mu^+) \leqslant 10$ GeV	180114	$3.68\times10^6/4.21\times10^5$	$4.96\times10^{-7}/4.33\times10^{-6}$
D_L^Z/D_R^Z [GeV^{-1}]	$\not{E}_T \leqslant 50$ GeV	126183	$3.55\times10^6/4.06\times10^5$	$4.75\times10^{-7}/4.15\times10^{-6}$
D_L^Z/D_R^Z [GeV^{-1}]	$P_T(e) \leqslant 10$GeV	12705	$3.55\times10^6/4.06\times10^5$	$3.48\times10^{-7}/3.04\times10^{-6}$
D_L^Z/D_R^Z [GeV^{-1}]	$\theta(\mu^-) \geqslant 0.1$ rad	11898	$3.55\times10^6/4.06\times10^5$	$3.45\times10^{-7}/3.01\times10^{-6}$
Form Factors	Cut	Background events	Signal events	LHeC sensitivity 90% CL
B_L^Z/B_R^Z [GeV^{-2}]	Normalized events (no cut)	343600	$6.99\times10^{10}/5.42\times10^9$	$1.60\times10^{-9}/2.07\times10^{-8}$
B_L^Z/B_R^Z [GeV^{-2}]	$P_T(\mu^+) \leqslant 10$ GeV	180114	$6.96\times10^{10}/5.39\times10^9$	$1.56\times10^{-9}/2.01\times10^{-8}$
B_L^Z/B_R^Z [GeV^{-2}]	$\not{E}_T \leqslant 50$ GeV	126183	$6.95\times10^{10}/5.39\times10^9$	$1.53\times10^{-9}/1.97\times10^{-8}$
B_L^Z/B_R^Z [GeV^{-2}]	$P_T(e) \leqslant 10$GeV	12705	$6.95\times10^{10}/5.39\times10^9$	$1.41\times10^{-9}/1.82\times10^{-8}$

Table 7: LHeC sensitivities and cut efficiencies for the individual form factors (cf. section 2.1) of the FCNC operators inducing cLFV $e-\mu$ conversion, from the process $pe^- \to \mu^- j$ and with an integrated luminosity of 3 ab^{-1}.

sensitivity than the present limits for the LFV conversion of an electron into a tau.

We have argued that the very high sensitivities at the LHeC for some of the form factors are possible because the converted charged lepton is dominantly emitted in the backward direction, enabling an efficient separation of the signal from the background. The LHeC reach we obtained is in fact mainly statistics limited, and higher sensitivities could be achieved with higher integrated luminosity.

Form Factors	Cut	Background events	Signal events	LHeC sensitivity 90% CL
N_L^H/N_R^H	Normalized events (no cut)	297528	148/17	$8.62\times10^{-3}/3.17\times10^{-2}$
N_L^H/N_R^H	$P_T(\tau^+)\leqslant 10$ GeV	137986	148/17	$5.12\times10^{-3}/2.12\times10^{-2}$
N_L^H/N_R^H	$\not{E}_T\leqslant 100$ GeV	132844	147/16	$5.09\times10^{-3}/2.01\times10^{-2}$
N_L^H/N_R^H	$P_T(e)\leqslant 10$ GeV	14036	147/16	$1.61\times10^{-3}/1.48\times10^{-2}$
N_L^H/N_R^H	$\theta(\tau^-)\geqslant 0.5$ rad	8641	126/14	$1.47\times10^{-3}/1.32\times10^{-2}$
Form Factors	Cut	Background events	Signal events	LHeC sensitivity 90% CL
A_L^γ/A_R^γ	Normalized events (no cut)	297528	37260/4252	$2.98\times10^{-5}/2.57\times10^{-4}$
A_L^γ/A_R^γ	$P_T(\tau^+)\leqslant 10$ GeV	137986	37098/4234	$2.09\times10^{-5}/1.76\times10^{-4}$
A_L^γ/A_R^γ	$\not{E}_T\leqslant 100$ GeV	132844	37096/4234	$2.05\times10^{-5}/1.73\times10^{-4}$
A_L^γ/A_R^γ	$P_T(e)\leqslant 10$ GeV	14036	37096/4234	$8.30\times10^{-6}/5.86\times10^{-5}$
A_L^γ/A_R^γ	$\theta(\tau^-)\geqslant 1.5$ rad	3561	36504/4166	$5.75\times10^{-6}/3.33\times10^{-5}$
Form Factors	Cut	Background events	Signal events	LHeC sensitivity 90% CL
D_L^γ/D_R^γ [GeV^{-1}]	Normalized events (no cut)	297528	$1.30\times10^7/1.44\times10^6$	$2.31\times10^{-7}/2.08\times10^{-6}$
D_L^γ/D_R^γ [GeV^{-1}]	$P_T(\tau^+)\leqslant 10$ GeV	137986	$1.29\times10^7/1.43\times10^6$	$2.07\times10^{-7}/1.86\times10^{-6}$
D_L^γ/D_R^γ [GeV^{-1}]	$\not{E}_T\leqslant 100$ GeV	132844	$1.29\times10^7/1.43\times10^6$	$2.06\times10^{-7}/1.85\times10^{-6}$
D_L^γ/D_R^γ [GeV^{-1}]	$P_T(e)\leqslant 10$ GeV	14036	$1.29\times10^7/1.43\times10^6$	$1.62\times10^{-7}/1.45\times10^{-6}$
D_L^γ/D_R^γ [GeV^{-1}]	$\theta(\tau^-)\geqslant 0.3$ rad	11993	$1.29\times10^7/1.43\times10^6$	$1.61\times10^{-7}/1.45\times10^{-6}$
Form Factors	Cut	Background events	Signal events	LHeC sensitivity 90% CL
B_L^γ/B_R^γ [GeV^{-2}]	Normalized events (no cut)	297528	$5.14\times10^{10}/5.41\times10^9$	$1.88\times10^{-9}/1.79\times10^{-8}$
B_L^γ/B_R^γ [GeV^{-2}]	$P_T(\tau^+)\leqslant 10$ GeV	137986	$5.14\times10^{10}/5.41\times10^9$	$1.82\times10^{-9}/1.73\times10^{-8}$
B_L^γ/B_R^γ [GeV^{-2}]	$\not{E}_T\leqslant 100$ GeV	132844	$5.10\times10^{10}/5.43\times10^9$	$1.81\times10^{-9}/1.72\times10^{-8}$
B_L^γ/B_R^γ [GeV^{-2}]	$P_T(e)\leqslant 10$ GeV	14036	$5.10\times10^{10}/5.43\times10^9$	$1.67\times10^{-9}/1.59\times10^{-8}$
B_L^γ/B_R^γ [GeV^{-2}]	$\theta(\tau^-)\geqslant 0.1$ rad	12993	$5.10\times10^{10}/5.43\times10^9$	$1.66\times10^{-9}/1.58\times10^{-8}$
Form Factors	Cut	Background events	Signal events	LHeC sensitivity 90% CL
A_L^Z/A_R^Z	Normalized events (no cut)	297528	12221/1222	$9.00\times10^{-5}/9.01\times10^{-4}$
A_L^Z/A_R^Z	$P_T(\tau^+)\leqslant 10$ GeV	137986	12176/1218	$6.19\times10^{-5}/6.18\times10^{-4}$
A_L^Z/A_R^Z	$\not{E}_T\leqslant 100$ GeV	132844	12165/1217	$6.08\times10^{-5}/6.07\times10^{-4}$
A_L^Z/A_R^Z	$P_T(e)\leqslant 10$ GeV	14036	12165/1217	$2.19\times10^{-5}/2.18\times10^{-4}$
A_L^Z/A_R^Z	$\theta(\tau^-)\geqslant 1.5$ rad	3561	7953/795	$1.89\times10^{-5}/1.88\times10^{-4}$
Form Factors	Cut	Background events	Signal events	LHeC sensitivity 90% CL
D_L^Z/D_R^Z [GeV^{-1}]	Normalized events (no cut)	297528	$1.99\times10^6/2.28\times10^5$	$8.64\times10^{-7}/5.33\times10^{-6}$
D_L^Z/D_R^Z [GeV^{-1}]	$P_T(\tau^+)\leqslant 10$ GeV	137986	$1.98\times10^6/2.27\times10^5$	$7.24\times10^{-7}/3.95\times10^{-6}$
D_L^Z/D_R^Z [GeV^{-1}]	$\not{E}_T\leqslant 100$ GeV	132844	$1.97\times10^6/2.25\times10^5$	$7.22\times10^{-7}/3.92\times10^{-6}$
D_L^Z/D_R^Z [GeV^{-1}]	$P_T(e)\leqslant 10$ GeV	14036	$1.97\times10^6/2.25\times10^5$	$5.05\times10^{-7}/2.10\times10^{-6}$
D_L^Z/D_R^Z [GeV^{-1}]	$\theta(\tau^-)\geqslant 0.1$ rad	12993	$1.97\times10^6/2.25\times10^5$	$5.00\times10^{-7}/2.07\times10^{-6}$
Form Factors	Cut	Background events	Signal events	LHeC sensitivity 90% CL
B_L^Z/B_R^Z [GeV^{-2}]	Normalized events (no cut)	297528	$3.78\times10^{10}/2.93\times10^9$	$2.22\times10^{-9}/9.13\times10^{-9}$
B_L^Z/B_R^Z [GeV^{-2}]	$P_T(\tau^+)\leqslant 10$ GeV	137986	$3.77\times10^{10}/2.91\times10^9$	$2.15\times10^{-9}/8.75\times10^{-9}$
B_L^Z/B_R^Z [GeV^{-2}]	$\not{E}_T\leqslant 100$ GeV	132844	$3.77\times10^{10}/2.91\times10^9$	$2.18\times10^{-9}/8.88\times10^{-9}$
B_L^Z/B_R^Z [GeV^{-2}]	$P_T(e)\leqslant 10$ GeV	14036	$3.77\times10^{10}/2.91\times10^9$	$2.00\times10^{-9}/7.94\times10^{-9}$

Table 8: LHeC sensitivities and cut efficiencies for the individual form factors (cf. section 2.1) of the FCNC operators inducing cLFV $e-\tau$ conversion, from the process $pe^-\to\tau^-j$ and with an integrated luminosity of 3 ab^{-1}.

In summary, ep colliders such as the proposed LHeC would be excellent facilities for probing cLFV. Especially for the case of cLFV electron-tau conversion, they could reach the best sensitivities among all currently envisioned experiments, opening up a great discovery potential for new physics beyond the SM.

ACKNOWLEDGMENTS

This work has been supported by the Swiss National Science Foundation under the project number 200020/175502. A.R. acknowledges the hospitality of the Department of Physics, University of Basel, where the visit was supported through the SU-FPDC Grant Program. A.H. thanks Oliver Fischer for useful discussions.

9

PROSPECTS FOR HEAVY SCALAR SEARCHES AT THE LHEC

Published in: 10.1142/S0217751X19501276 [7]

Prospects for Heavy Scalar Searches at the LHeC

Luigi Delle Rose*, Oliver Fischer†, A. Hammad°

* INFN, Sezione di Firenze, and Department of Physics and Astronomy, University of Florence, Via G. Sansone 1, 50019 Sesto Fiorentino, Italy

† Institute for Nuclear Physics, Karlsruhe Institute of Technology, Hermann-von-Helmholtz-Platz 1, D-76344 Eggenstein-Leopoldshafen, Germany

° Department of Physics, University of Basel, Klingelbergstr. 82, CH-4056 Basel, Switzerland

ABSTRACT

In this article we study the prospects of the proposed Large Hadron electron Collider (LHeC) in the search for heavy neutral scalar particles. We consider a minimal model with one additional complex scalar singlet that interacts with the Standard Model (SM) via mixing with the Higgs doublet, giving rise to a SM-like Higgs boson h_1 and a heavy scalar particle h_2. Both scalar particles are produced via vector boson fusion and can be tested via their decays into pairs of SM particles, analogously to the SM Higgs boson. Using multivariate techniques we show that the LHeC is sensitive to h_2 with masses between 200 and 800 GeV down to scalar mixing of $\sin^2\alpha \sim 10^{-3}$.

9.1 INTRODUCTION

One of the most important tasks of high-energy particle physics of our time is the detailed measurement of the couplings of the recently discovered Higgs boson. Thanks to the recent progress at the Large Hadron Collider (LHC) some of the Higgs boson properties are known with ~ 5% precision. After the high-luminosity LHC most of the so-called κ parameters, which quantify the Higgs signal strength in terms of its Standard Model (SM) prediction, may be known with a precision between 3% and 5% with mostly equal contribution from statistical and systematic uncertainty [194]. Since the Higgs boson provides a notorious portal to new physics, these measurements leave plenty of room for physics beyond the SM in the scalar sector.

A new generation of machines is presently discussed, which are to measure the Higgs boson properties with high precision. Among others it is worth mentioning the so-called Higgs factories, the high-luminosity electron-positron colliders at 250 GeV [195–197].

It is possible, however, to improve the precision of many Higgs boson measurements at the LHC already, by upgrading the collider with a new linear electron recovery linac [158], and colliding one of the proton beams with the new electron beam at about 60 GeV. The resulting facility is the Large Hadron electron Collider (LHeC) [154] which can be operated concurrently to the LHC at ~1.2 TeV centre-of-mass energy with a total integrated luminosity of 1 ab^{-1}. One of its prime objectives is the improvement of the PDF sets which would ameliorate many LHC studies [156]. This can be expected to significantly reduce the PDF-associated systematic uncertainties of LHC Higgs precision studies and also provide a very important input for many exotic BSM studies [156]. Also a measurement of the main decay mode of Higgs boson into the $b\bar{b}$ final state could be improved from ~ 6% to about 1% level precision. Moreover, fig. 3 of ref. [157] shows that the κ_Z and κ_W measurements can be improved from the 2 to 3 percent level at the HL-LHC to the subpercent level when combined with LHeC measurements. The LHeC also has been shown to be more than competitive with Higgs boson measurements, cf. [198–201] and to bring unique opportunities with respect to Beyond the SM (BSM) physics, cf. e.g. [111, 160, 163–165].

Owing to the importance of measuring the Higgs sector, many LHC analyses are searching for additional neutral scalar bosons which can be produced and decay via their mixing with the SM Higgs boson. Like most BSM studies at the LHC, these searches have to deal with very high rates of SM backgrounds.[1] These analyses can access the squared scalar mixing angle on the order of 10% and are particularly sensitive to heavy scalars with masses above a few hundred GeV. It is interesting to note that there are some hints in the LHC data that can be interpreted as a 270 GeV neutral heavy scalar [85–87] which was referred to as the "Madala hypothesis" [88]. These observations, together with the background-related limitations of the LHC, represent our main motivation

1 Even BSM searches with clean signatures like, e.g., multi-lepton, or same-sign dilepton final states, have to contend with large additional background sources due to pile up, mis identification, and towering QCD background rates.

to study the prospects of searches for heavy neutral scalars at the LHeC. A similar study on a preparatory level, motivated by the "Madala hypothesis", has been performed in [202].

In this paper we present a detailed study for searching a heavy Higgs-like at the LHeC via its dominant decays into SM gauge bosons, i.e, *WW* or ZZ, which in turn give rise to the final states 4l, 2l2j or νl2j, among others. Compared with existing analyses at LHC, (cf. [203]) we find plenty of room for a discovery.

9.2 THE MODEL

Extended Higgs sectors are ubiquitous in many BSM scenarios and, as such, represent a very strong case for experimental searches. In particular, extra scalars that are singlets under the SM gauge group are envisaged in some of the most natural extensions of the SM, ranging from Supersymmetry to Composite Higgs models and to GUT extensions (in which the new scalar sector provides the mass to the extra massive gauge bosons). Moreover, in some scenarios the SM singlet scalars can act as a portal to SM neutral fields in dark sectors which otherwise would remain completely unobserved. Extra scalar singlets also play a major role in models of electroweak baryogenesis as they represent one of the most economical possibilities to realize a first-order electroweak phase transition.

Motivated by the aforementioned scenarios, we consider a simple extension of the SM with a complex neutral scalar boson S, singlet under the SM gauge group. The scalar sector is thus described by the potential

$$V(H,S) = m_1^2 H^\dagger H + m_2^2 S^\dagger S + \lambda_1 (H^\dagger H)^2 + \lambda_2 (S^\dagger S)^2 + \lambda_3 (H^\dagger H)(S^\dagger S), \quad (155)$$

which is the most general renormalizable scalar potential of the SM $SU(2)$ Higgs doublet H and the complex scalar S. The mass eigenstates from the resulting mass matrix correspond to the physical fields $h_{1,2}$, which are given by

$$\begin{pmatrix} h_1 \\ h_2 \end{pmatrix} = \begin{pmatrix} \cos\alpha & -\sin\alpha \\ \sin\alpha & \cos\alpha \end{pmatrix} \begin{pmatrix} H \\ S \end{pmatrix}, \quad (156)$$

where the scalar mixing angle α and the masses of the physical scalars are defined in terms of the original parameters of the potential as

$$\tan 2\alpha = \frac{\lambda_3 \nu x}{\lambda_1 \nu^2 - \lambda_2 x^2}, \quad (157)$$

$$m^2_{h_{1,2}} = \lambda_1 \nu^2 + \lambda_2 x^2 \mp \sqrt{(\lambda_1 \nu^2 - \lambda_2 x^2)^2 + (\lambda_3 \nu x)^2}, \quad (158)$$

with $m_{h_2} > m_{h_1}$ and h_1 identified with the 125 GeV Higgs boson. In the previous equations, $\nu = 246.22$ GeV and x are the vacuum expectation values of the H and S fields, respectively.

After mass mixing, the mass eigenstate h_1 corresponds to the SM-like Higgs, by which we mean that in the limit of the scalar mixing angle $\alpha \to 0$ we

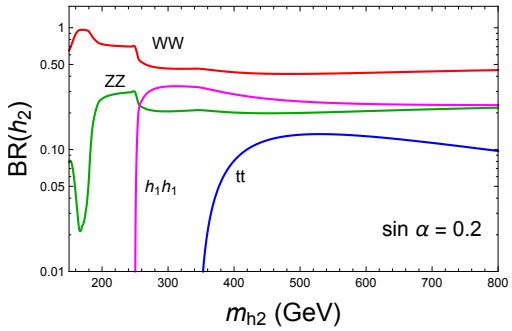

Figure 24: Dominant branching ratios of the heavy Higgs boson h_2 as a function of its mass for a fixed value of the scalar mixing angle, $\sin\alpha = 0.2$.

recover the Higgs boson with the interactions and properties as predicted by the SM. The scalar mixing yields couplings between the mass eigenstate h_2 and the SM fermions and gauge bosons proportional to those of a SM Higgs boson of the same mass, with a rescaling factor given by $\sin\alpha$. On top of the SM-like interactions, the last term in eq. (155) proportional to λ_3 gives rise to a coupling between h_1 and h_2, which yields e.g. the additional decay channel $h_2 \to 2h_1$ if $m_{h_2} > 2m_{h_1}$. If no other decay modes are available for the h_2, as it is the case for our simple setup, the phenomenology of the h_2 below the h_1h_1 threshold is similar to that of the SM Higgs with $m_h = m_{h_2}$, with same the branching ratios and a total decay width simply rescaled by $\sin^2\alpha$. Above the threshold, the branching ratios of h_2 into SM final states is given by

$$\mathrm{BR}(h_2 \to \mathrm{SM}) = \mathrm{BR}_{\mathrm{SM}}(h_2 \to \mathrm{SM})(1 - \mathrm{BR}(h_2 \to h_1h_1)) \tag{159}$$

with $\mathrm{BR}_{\mathrm{SM}}(h_2 \to \mathrm{SM})$ being the SM one. The branching ratio $\mathrm{BR}(h_2 \to h_1h_1)$ is computed from the corresponding partial decay width which can be expressed explicitly as

$$\Gamma(h_2 \to h_1h_1) = \left(\frac{\sin 2\alpha}{v}(\cos\alpha + \frac{v}{x}\sin\alpha)(\frac{m_{h_2}^2}{2} + m_{h_1}^2)\right)^2 \frac{1}{32\pi\, m_{h_2}} \left(1 - \frac{4m_{h_1}^2}{m_{h_2}^2}\right)^{1/2} \tag{160}$$

The main branching ratios of the heavy scalar h_2 are shown in fig. 24 as a function of m_{h_2} for a scalar mixing angle $\sin\alpha = 0.2$ and $x \gg v$. In BSM scenarios in which the SM gauge group is extended by extra abelian gauge factors as in the $B - L$ models, or unified into a larger simple group as in GUT extensions, the vev x of the extra scalar participates in the spontaneous symmetry breaking patterns and sets the scale of the mass of the extra gauge bosons. As the void LHC searches of such states have pushed the corresponding masses to the TeV range or above, it is reasonable to assume a large separation between x and the electroweak scale.

In electron-proton collisions at the LHeC, the heavy Higgs boson h_2 can be produced through vector boson fusion (VBF), via the charged (CC) or neutral currents (NC), cf. the left panel of fig. 25. The resulting cross sections for this process, normalised by $\sin^2\alpha$, are shown in the right panel of fig. 25. It is worth pointing out that the CC cross section is larger by about an order of magnitude, as expected due to the small coupling of the Z boson to the charged leptons, which affects the choice of final states for the search strategies below.

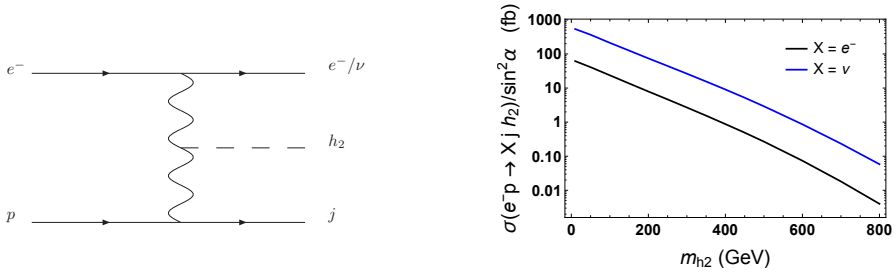

Figure 25: Heavy Higgs production cross section from the process $e^- p \to X\,j\,h_2$ at the LHeC. The final state X being an electron (e^-) and a neutrino (ν) denotes the neutral current (NC) and charged current (CC) interaction, respectively.

9.3 HEAVY HIGGS SEARCH STRATEGY

In the following we investigate the prospects of the LHeC in the search for a heavy Higgs h_2 in the mass region $m_{h_2} > m_{h_1}$ by focusing on its leading decay modes into SM weak gauge bosons, *WW* and ZZ. It is worth mentioning that the other interesting decay channels which would be extremely useful to characterise the phenomenology of the extra scalar, and to eventually discriminate among different models, are the di-higgs and di-top decay modes. Nevertheless, here we consider only those search channels which will most likely represent the priorities of the research program for heavy scalars at the LHeC.

9.3.1 *Signatures and analysis*

In particular, the following signatures will be studied:

1. $\mu^Z_{\ell\ell} := h_2 \to ZZ \to 4\ell$
2. $\mu^Z_{\ell q} := h_2 \to ZZ \to 2\ell 2q$
3. $\mu^W_{\ell q} := h_2 \to WW \to \nu\ell 2j$

As already stated above, further channels exist, which are not expected to add significantly to the final sensitivity of the LHeC to heavy Higgses but are also very interesting in their own right. Examples for these channels are the boosted mono-Z ($h_2 \to Z_{qq} Z_{inv}$), di-top ($h_2 \to t\bar{t}$) and di-Higgs ($h_2 \to 2h_1$), and $\ell\ell' + \not{E}_{miss}$. The all hadronic final state $V_{qq}V_{qq} \to 4j$ adds significantly to the signal statistics, but it brings complication via the nature of the jet reconstruction and the additional combinatorics that are necessary to identify the beam remnant jet. Since we expect the complications to cancel out the advantage in statistics (at least partially) we omit studying this channel here.

Since the signal channels 1, 2, and 3 consist of two vector bosons of high invariant mass, we consider diboson processes in the SM as our primary background. Additional backgrounds exist in the form of processes with initial- and final state radiation of electrons and gluons. These can have large cross sections and mimic the signal final state. Due to the typically small momenta (particularly in the transverse direction) we neglect those contributions in the

following. Furthermore, we also consider signal and background processes only at the leading order and neglect corrections at higher order, which may lead to small modifications in the cross sections and also in the kinematic shapes of the observables.

The background processes considered here and the corresponding cross sections are listed in tab. 9. For these backgrounds we use a systematic uncertainty of 2% [154].

The centre-of-mass at the LHeC is boosted with respect to the laboratory system due to the asymmetric beam energies which pushes the final states towards positive η values. Accordingly, for heavy h_2, which requires larger parton energies, the decay products are strongly forward boosted with large (positive) η values. This provides a good handle to separate signal from background events. For h_2 masses that become comparable to the centre-of-mass energy of ~ 1.2 TeV this good separability is countered by the reduction of the total cross section due to the restricted phase space.
For the reconstruction of the signal we require that the beam-remnant jet from the deep inelastic scattering (DIS) off the proton has a transverse momentum of $P_T(j) > 10$ GeV and a pseudo rapidity of $|\eta(j)| < 4.5$ for geometric acceptance, while for leptons we require $P_T(l) > 2$ GeV and $|\eta(l)| < 4.5$, with l accounts for electrons and muons. These threshold values are representative for studies at the LHeC.

For the simulation of the signal and background event samples, the Monte Carlo event generator MadGraph5 version 2.4.3 [143] is employed. As usual, parton shower and hadronisation is taken care of by Pythia6 [144] while the fast detector simulation is carried out by Delphes [97]. We use the Delphes detector card from the LHeC collaboration. We note that Pythia needs to be patched [172] in order to achieve a reasonable event generation efficiency and that it is crucial that the first (second) beam, as inputted in the MadGraph run card, corresponds to the proton (electron) to correctly match the asymmetric detector setup implemented in the Delphes card. We use an electron beam of 60 GeV with 80% polarisation, the proton beam with energy of 7 TeV and we consider a total integrated luminosity of 1/ab. It is important to notice, that a smaller electron beam energy would result in a smaller production cross section of the h_2 and it would also reduce the LHeC reach with respect to the heavy Higgs mass due to the more restricted phase space.

We perform the analysis for five benchmark masses m_{h_2} from 200 GeV to 800 GeV and, for illustrative purposes, we present detailed results for a specific benchmark point, allowed by current LHC searches [204], defined by $m_{h_2} = 500$ GeV and $\sin\alpha = 0.2$. For larger heavy Higgs masses, the number of events drops significantly and, consequently, the error bands highly enlarge over the expected median preventing us from reaching a reasonable statistical conclusion. All the backgrounds from tab. 9 with all possible decay channels were included for each of the three signal channels, 4ℓ, $2\ell + 2j$, $\ell + 2j + \not{E}_T$. A total of 10^7 events for each signal and background sample was simulated.
From the available visible final states, a number of observables are constructed that are then input into the TMVA package [145], which handles a Multi-Variate Analysis (MVA). Among the different analysis techniques, we em-

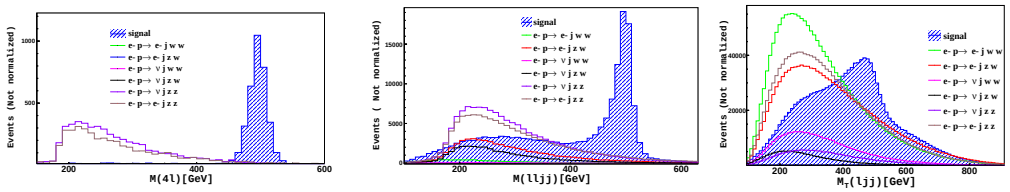

Figure 26: The most relevant observables as ranked by the BDT analysis for the three signal channels $\mu^Z_{\ell\ell}$ (left), $\mu^Z_{\ell q}$ (middle) and $\mu^W_{\ell q}$ (right) with a signal benchmark point defined by $m_{h_2} = 500$ GeV and $\sin\alpha = 0.2$. The variable in the left plot is the invariant mass of four final state leptons. The variable in the middle plot is the invariant mass of two final state jets and two final state leptons. The variable in the right plot is the transverse mass of the lepton and the two jets in the final state.

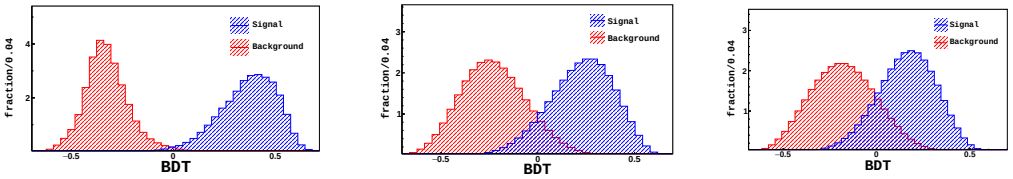

Figure 27: The BDT distributions for the three signal channels $\mu^Z_{\ell\ell}$ (left), $\mu^Z_{\ell q}$ (middle), and $\mu^W_{\ell q}$ (right) with $m_{h_2} = 500$ GeV and $\sin\alpha = 0.2$.

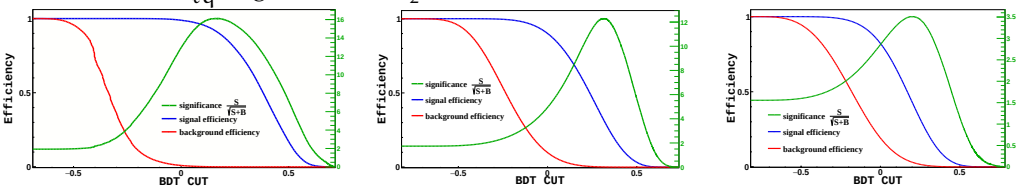

Figure 28: Cut efficiency and the relevant significance distributions for the three signal channels $\mu^Z_{\ell\ell}$ (left), $\mu^Z_{\ell q}$ (middle), and $\mu^W_{\ell q}$ (right) with $m_{h_2} = 500$ GeV and $\sin\alpha = 0.2$.

ployed the Boosted Decision Tree (BDT) which is largely used by the LHC experimental collaborations.

THE FULLY LEPTONIC FINAL STATE, $\mu^Z_{\ell\ell}$: This signal channel consists of two lepton pairs $\ell^+_\alpha \ell^-_\alpha \ell^+_\beta \ell^-_\beta$ with the lepton flavours $\alpha, \beta \in \{e, \mu\}$. Conservatively, we considered here only electrons and muons but, in principle, reconstructing tau leptons is also possible and may enhance the significance of this channel. We observed that the final state events are characterized by a highly boosted beam-remnant jet with large positive η values.

The mass of h_2 in the range investigated here is always larger than $2m_Z$, thus we can require the two Z bosons to be produced on shell and to decay leptonically. From the possible combinations of same flavour and opposite sign leptons, one should recover the invariant masses of both pairs compatibly with m_Z. Nevertheless, for our pre-selection before the actual MVA, we do not explicitly require the lepton pairs to reconstruct the Z boson peaks within a given mass window but simply collect, among all possible leptons in the events, the electron or muon pairs that are closest to the Z rest mass. Final state leptons are thus grouped into three categories: 4μ, $2e2\mu$ or $4e$. The main

source of irreducible backgrounds in this case is given by νjZZ and $e^- jZZ$, while the other backgrounds that contain W bosons are suppressed during the MVA process by exploiting the different positions of the peaks in the invariant mass distributions of the lepton pairs.
We take advantage of the full power of BDT algorithm in distinguishing between signal and background events, feeding it with 42 kinematical observables. The most relevant observables according to the BDT ranking are, as expected, the invariant mass of h_2 from 4μ, $2e2\mu$ and $4e$ respectively, as well the reconstructed invariant mass of Z boson. As an example, the four-lepton invariant mass distribution for the signal and the background samples is shown in fig. 26 for the benchmark point defined by $m_{h_2} = 500$ GeV and $\sin\alpha = 0.2$. We checked that changing the pre-selection cut of the beam remnant jet P_T from 10 GeV to 20 GeV affects the final result for the leptonic channel, which is statistically dominant, only by about 3%.

THE SEMILEPTONIC FINAL STATE, $\mu^Z_{\ell q}$: In this channel the two leptons and two jets can be paired up to the Z boson mass. The invariant mass of the two Z boson candidates in turn reconstructs to m_{h_2}. The analysis strategy follows quite closely the one of the fully leptonic final state described above. In particular, we collect among all possible leptons and jets in the events, the lepton and jet pairs that are closest to the Z mass and we further organize the events into two categories according to the flavour of the lepton pair. The most relevant irreducible background for this channel stems from νjZZ and $e^- jZZ$ but further sizable contributions exist from processes with at least one W boson. The reconstructed invariant mass of the h_2, the pseudo rapidity distribution of leptons and the angular separation between the leptons and the reconstructed Z, $\Delta R(Z, \ell)$, are classified by the BDT algorithm as the most relevant observables in distinguishing signal from backgrounds. The invariant mass distribution of the lepton-jet system for the signal and the background samples is shown in fig. 26 for the benchmark point defined by $m_{h_2} = 500$ GeV and $\sin\alpha = 0.2$.

Differently from the $\mu^Z_{\ell\ell}$ above, the larger cross section allows to access heavier masses with respect to the fully leptonic final state and, as such, makes this process suitable for searches of heavy scalars with larger masses.

THE SEMILEPTONIC FINAL STATE, $\mu^W_{\ell q}$: This signal channel is much more difficult to reconstruct compared to the first two due to the final state neutrino which escapes from the detector and makes it impossible to fully reconstruct the h_2 system.
For our pre-selection we select in each event, among all jets with highest momentum, the two jets with the reconstructed invariant mass that is closest to the W boson mass, and, among all possible leptons, that with the highest momentum that together with the missing energy reconstructs more closely the transverse mass of the second W. The main discriminating variable here is the transverse mass of h_2 which is peaked around the rest mass of h_2 and has a flat tail, due to the missing energy contribution. This distribution is shown if fig. 26 for a particular benchmark point. Further relevant observables are the

Nr.	final state	σ_{LHeC} [fb]
1	e^-jWW	23.0
2	e^-jZW^+	4.16
3	e^-jZZ	0.1
4	νjWW	10.4
5	νjZW^-	8.0
6	νjZZ	2.4

Table 9: The SM background processes considered in this analysis. The samples have been produced with the following cuts: $P_T(j) > 10$ GeV, $P_T(l) > 2$ GeV and $|\eta(j/l)| < 4.5$.

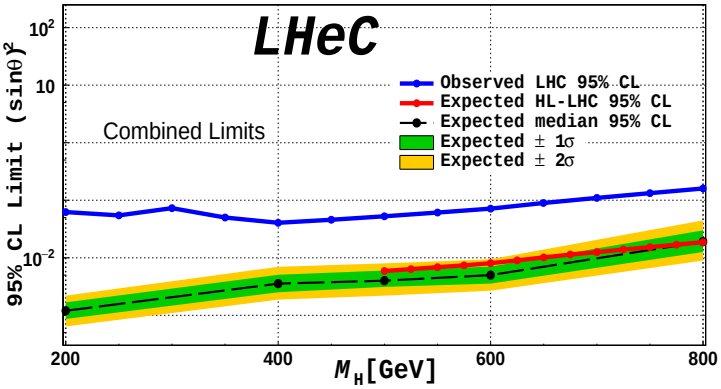

Figure 29: Combined limit for the three signal channels, including a systematic uncertainty of 2%. The blue line represents the current LHC limit at 95% CL as extracted from [204], the red line the forecast of the HL-LHC sensitivity via $h_2 \to ZZ$ searches from ref. [205].

invariant mass of the $(W + l)$ system, the $\eta(W, l)$ and $\eta(\ell)$ distributions. Here the usage of MVA, and especially the BDT, is found to be extremely useful, with respect to standard cut-based analysis, in exploiting the differences between signal and background distributions.

9.3.2 *Results*

We employ the BDT method to perform the multivariate analysis. The discriminating power of the BDT relies on the fact that the signal and the background may be characterised by different features that can be entangled together into several distributions. When these features are not clearly manifest in some specific observables, it could be difficult, in principle, to identify the most relevant distributions able to efficiently separate the signal events from the background ones. This machine learning technique is based on a set of decision trees where each tree yields a binary output depending on the fact that an event is classified as signal-like or background-like during the training session. The main advantage of the algorithm consists on the possibility to combine together sev-

eral discriminating variables (in our study we have employed 42 kinematical observables for both signal and background events) into a single and more effective discriminator, the BDT variable, and thus to reach a higher significance with respect to standard methods.

Figure 27 shows the BDT distributions for the three channels $\mu^Z_{\ell\ell}$ (left), $\mu^Z_{\ell q}$ (middle), and $\mu^W_{\ell q}$ (right) for the benchmark point given by $m_{h_2} = 500$ GeV and $\sin\alpha = 0.2$. The BDT discriminator ranges from -1 to 1: the events with discriminant value near 1 are classified as signal-like events (blue distribution) and those near -1 are considered as background-like events (red distribution). The optimization of the signal/background cut, as a function of the BDT variable, has been performed using the TMVA and expressed in terms of the significance $\frac{S}{\sqrt{S+B}}$. Figure 28 shows the cut efficiency for the three channels $\mu^Z_{\ell\ell}$ (left), $\mu^Z_{\ell q}$ (middle), and $\mu^W_{\ell q}$ (right) for $m_{h_2} = 500$ GeV and $\sin\alpha = 0.2$. For $\mu^Z_{\ell\ell}$ channel, by requiring BDT > 0.163, we can reach significance $\frac{S}{\sqrt{S+B}} = 16.1\sigma$ with signal efficiency 0.91 and background rejection efficiency of 6.4×10^{-4}, for the channel $\mu^Z_{\ell q}$ with BDT> 0.313 we obtain a significance of 12.28σ with signal efficiency 0.4 and background efficiency 1.2×10^{-3}. Finally, for the channel $\mu^W_{\ell q}$, with BDT> 0.23 one can get a significance of 3.5σ with signal efficiency 0.43 and background efficiency 0.034.

The combined sensitivity is derived from the BDT distributions of the above described analyses and for each benchmark mass. As stated above, we included a the systematic uncertainty on the background of 2% and we used the Higgs Analysis-Combined Limit tool [146]. To extract the limit we preformed a frequentist test which uses the profile likelihood as test statistics. In addition to the parameters of interest, such as the total cross section and the integrated luminosity, we include a nuisance parameter for background only of 2% as a logarithmic-normal distribution to account for the unknown systematic uncertainty of the future LHeC. In fig. 29 we show the 95% CL expected median limit on the squared sine of the mixing angle, as well the error bands for 1 and 2 sigma. Due to the different efficiencies, branching fractions and the relevant backgrounds, each final state contributes differently depending on the mass of the heavy scalar. As an example, we find that the $\mu^Z_{\ell\ell}$ channel is the most sensitive one in the mass range $200 - 500$ GeV, while the $\mu^Z_{\ell q}$ channel is sensitive in the higher mass regime. The current LHC limit (red dashed line) at 95% CL has been extracted from [204], where the search has been performed for heavy scalars over the mass range of 130 GeV to 3 TeV at a centre of mass energy of 13 TeV and 35.9/fb of integrated luminosity. In particular, the Z boson pair decay channel has been investigated in the final state objects $4l, 2l2j$ and $2l2\nu$. It is clear that the sensitivity of the LHeC is better than the current LHC one by about two orders of magnitude in the low mass regime up to one order of magnitude in the high mass region. As an example, the expected 2σ median sensitivity of the LHeC to $\sin^2\alpha$ for the mass $m_{h2} = 500$ GeV can be as small as 4×10^{-3}.

For masses up to about 1 TeV this sensitivity is comparable to the forecast of the HL-LHC sensitivity via $h_2 \to ZZ$, which we extract from ref. [205]. It is worthy of note that the LHeC's higher sensitivity for heavy scalars with

masses of only a few hundred GeV is complementary to the higher sensitivity of the HL-LHC at masses on the TeV scale.

9.4 CONCLUSION

Precision measurements of the Higgs boson properties are very important due to its possible role as portal to BSM sectors. Present searches at the LHC are compatible with additional heavy scalar particles that mix on the percent level with the SM Higgs boson. We have shown that the prospects of discovering such heavy scalars at the LHeC are very promising and complementary to the searches at the LHC, where the notorious SM backgrounds and systematic uncertainties make discovery difficult. Using multivariate techniques and by exploiting three of the most promising decay channels of a heavy Higgs, we find that the LHeC can access heavy scalar bosons with masses between 200 and 800 GeV and scalar mixings as small as $\sin^2\alpha \sim 10^{-3}$.
We also pointed out that many other interesting channels exist that may allow to test the properties and the origin of the heavy Higgs boson. Among these, searches for (semi) invisible decays, di-higgs and the di-top final states may successfully exploit the cleaner environment offered by the promising future LHeC.

The superb reach to small scalar mixings for masses below one TeV makes the LHeC complementary to the possible reach of the HL-LHC for larger masses. We therefore conclude, that this machine is uniquely suited in order to discover and study possible scalar bosons with masses $\mathcal{O}(100)$ GeV.

ACKNOWLEDGEMENTS: The authors acknowledge support from the LHeC Study Group. A. Hammad would like to thank Waleed Esmail and Ashraf Kasem for the fruitful discussions. O. Fischer received funding from the European Unions Horizon 2020 research and innovation program under the Marie Sklodowska-Curie grant agreement No 674896 (Elusives). A.Hammad is supported by the Swiss National Science Foundation.

9.5 APPENDIX: MULTI-VARIATE ANALYSIS WITH A BOOSTED DECISION TREE

For our analysis we employed the TMVA package [145] which incorporates a Boosted Decision Tree (BDT). This algorithm allowed us to exploit several kinematical distributions, listed in tab. 13, for each of the three considered signal channels. The signal and background samples are divided into a training and an analysis set. The BDT is first trained on the training sample in order to construct the classifier that assesses whether an event is from a signal or from a background process. The analysis sample is then used to test the final classifier, which is obtained in the following way:

1. A root node is created from an initial number of sample events.
2. The algorithm finds the optimal threshold for a given kinematical observable that gives the best separation between signal and background After-

wards it separates the node into two branches, one containing mostly signal and the other mostly background events.

3. For events that are neither signal- nor background-like, the BDT continues iterating through the input observables to decide on the nature of the unclear events.

4. Considering each branch as a new node, the algorithm goes through steps 2 and 3 and keeps repeating it until a given number of final branches (called leaves) are obtained, which correspond to true signal or pure background.

A given brach will define a next node according to the purity coefficient

$$P = \frac{signal\ events}{(signal\ events + backgrounds\ events)} \tag{161}$$

and the splitting criterion of a given branch, obtained by maximising the signal/background separation, is defined by the Gini index

$$G_i = \sum_i^n W_i P(1-P)\,, \tag{162}$$

where W_i is the weight of the events i. The observable with the highest discrimination power (of signal from background events) is obtained by maximising the difference between the Gini index of the parent node and the sum of Gini indices of the two daughter nodes.

The training sample is reweighted such that the decision tree starts with a maximal Gini index, where signal events are equal to background events (i.e. $P = 0.5$). A leaf with purity greater than 0.5 is called a signal leaf, otherwise it is a background leaf. Several trees can combined together into a so-called forest and the final BDT output discriminator is chosen such that statistical fluctuations are minimized. The BDT discriminator ranges between -1 and 1 corresponding to pure background and pure signal, respectively.

9.6 APPENDIX: STATISTICAL EVALUATION OF THE BDT OUTPUT

For the statistical treatment of our BDT analysis we used the Higgs Analysis-Combined Limit tool [146], which allows for different statistical procedures. From the available options we chose to use a frequentist test of profile Likelihood ratios as test statistics. Besides the total cross section and the integrated luminosity, we included among the parameters of the test statistics a nuisance parameter for the background with a relative strength of 2% to account for the systematic uncertainties at LHeC as quoted by the Conceptual Design Report [155]. The tool then computes the probability of finding the observed (simulated) data incompatible with the prediction for a given hypothesis, the p-value. The expected value of finding the number of events in the ith bin of the BDT distribution is given by

$$E[n_i] = \mu S_i + B_i\,, \tag{163}$$

where the parameter μ is called the signal strength. The signal is excluded at $(1-\alpha)$ confidence level if

$$CL_s = \frac{P\left(q(\mu)|\mu S + B\right)}{P\left(q(\mu)|B\right)} < \alpha, \tag{164}$$

where $q(\mu)$ is the profile log likelihood. Finally, the error bands can be obtained by

$$\text{Band}_{(1-\alpha)} = \hat{\mu} \pm \frac{\sigma\Phi^{-1}\left(1-\alpha\right)}{N}, \tag{165}$$

where $\hat{\mu}$ is the estimated expected median and Φ^{-1} is the cumulative distribution. If we restrict the number of events for the signal and the background to be large and ignore the correlation effect between bins, the significance can be described by the following formula

$$\sigma_{\text{stat+syst}} = \left[2\left((N_s+N_b)\ln\frac{(N_s+N_b)(N_b+\sigma_b^2)}{N_b^2+(N_s+N_b)\sigma_b^2} - \frac{N_b^2}{\sigma_b^2}\ln(1+\frac{\sigma_b^2 N_s}{N_b(N_b+\sigma_b^2)})\right)\right]^{1/2} \tag{166}$$

with N_s, N_b being the number of signal and background events, respectively, and σ_b parametrising the systematic uncertainty.

9.7 APPENDIX: VARIABLES RANKING

In the tables below the following definitions have been adopted: M is the invariant mass, P_T is the transverse momentum, η is the pesudorapidity, ΔR is the angular separation between two isolated objects and is defined as $\Delta R = \sqrt{\Delta\eta^2 + \Delta\Phi^2}$, M_T is the transverse mass given by
$M_T^2 = \left(\sqrt{M^2(f) + P_T^2(f)} + |P_T^{miss}(f)|\right)^2 - \left(\vec{P_T}(f) + \vec{P}_T^{miss}\right)^2$.

$h_2 \to ZZ \to 4l$		
Ranking	Observable	Importance
1	$M(4\mu)$	6.400
2	$M(2e2\mu)$	5.989
3	$M(4e)$	5.715
4	$P_T(2\mu)$	5.028
5	$\Delta R(e,\mu)$	4.887
6	$\Delta R(\mu,\mu)$	4.342
7	$\Delta R(2\mu,2\mu)$	3.797
8	$P_T(2e)_{Z_1}$	3.703
9	$\Delta R(\mu,\mu)$	3.659
10	$\Delta R(e,e)$	3.659
11	$\eta(4e)$	3.600
12	$P_T(j)_{beam}$	3.382
13	$M(\mu\mu)$	3.374
14	$\eta(2\mu)$	3.274
15	$\Delta R(e,\mu)$	3.031
16	$\eta(2e)$	3.001
17	$P_T(e,\mu)$	2.940
18	$\Delta R(e,e)$ in case of 4e	2.562
19	$P_T(4\mu)$	2.487
20	$\Delta R(4e,j)$	2.404
21	$\eta(2e,2\mu)$	2.404
23	$\Delta R(2e2\mu,j)$	2.207
24	$\eta(4\mu)$	2.199
25	$\Delta R(4\mu,j)$	1.928
26	$\eta(2e)$	1.775
27	$\eta(e,m)$	1.711
28	MET	1.652
29	$\eta(2\mu)$	1.628
30	$P_T(4e)$	1.619
31	$P_T(2e2\mu)$	1.582
32	$\Delta R(2e,2e)$	1.012
33	$\Delta R(2e,2\mu)$	.07312

$h_2 \to ZZ \to 2l2j$		
Ranking	Variable	Importance
1	$M(2\mu2j)$	5.534
2	$M(2e2j)$	4.516
3	$\eta(e^-)$	4.372
4	$P_T(\mu^-\mu^+)$	4.305
5	$P_T(jj)_z$	3.942
6	$\eta(\mu^-\mu^+jj)$	3.885
7	$\Delta R(e^-e^+)_z$	3.850
8	$P_T(e^-e^+)_z$	3.793
9	$\Delta R(\mu^-\mu^+)_z$	3.383
10	$\eta(e^-e^+jj)$	3.302
11	MET	3.261
12	$P_T(j)_{beam}$	2.938
13	$\eta(j)_{beam}$	2.763
14	$M(\mu^-\mu^+)_z$	2.737
15	$P_T(\mu^+)$	2.707
16	$\eta(j_2)_z$	2.696
17	$\eta(jj)_z$	2.585
18	$P_T(\mu^-\mu^+jj)$	2.520
19	$\Delta R(e^-e^+jj, j_{beam})$	2.506
20	$\Delta R(\mu^-\mu^+jj, j_{beam})$	2.397
21	$P_T(\mu^-\mu^+)_z$	2.394
22	$P_T(e^+)$	2.306
23	$M(jj)_z$	2.257
24	$PT(e^-e^+jj)$	2.218
25	$\eta(j_1)_z$	2.171
26	$\eta(\mu^-\mu^+)_z$	2.161
27	$M(e^-e^+)_z$	1.931
28	$P_T(e^-)_z$	1.930
29	$P_T(j_2)_z$	1.920
30	$\eta(e^+)_z$	1.701
31	$P_T(j_1)_z$	1.694
32	$\eta(e^-e^+)_z$	1.639
33	$\eta(\mu^-\mu^+)_z$	1.638
34	$\eta(\mu^+)_z$	1.633
35	$\Delta R(j,j)_z$	1.487
36	$\Delta R(jj,\mu^-\mu^+)$	1.463
37	$\Delta R(jj,e-e^+)$	1.462

$h_2 \to W^\pm W^\mp \to 2jl\nu_l$		
Ranking	Variable	Importance
1	$M_T(\mu j_W j_W)$	18.24
2	$P_T(jj)_W$	17.96
3	$P_T(j_1)_W$	14.66
4	$M(j_W j_W j_{beam})$	13.30
5	$\eta(e)$	12.74
6	$M(\mu j_W j_W)$	11.77
7	$P_T(\mu)$	9.395
8	$M(\mu j_W j_W j_{beam})$	9.285
9	$M_T(ej_W j_W)$	8.865
10	$\eta(ej_W j_W)$	7.830
11	$P_T(j_{beam})$	7.590
12	$P_T(j_2)_W$	5.969
13	$\eta(j_2)_W$	5.740
14	$\eta(\mu j_W j_W)$	5.275
15	MET	4.724
16	$P_T(ej_W j_W j_{beam})$	4.329
17	$\eta(j_W j_W j_{beam})$	4.277
18	$P_T(e)$	4.176
19	$M(ej_W j_W)$	4.137
20	$\eta(\mu j_W j_W j_{beam})$	3.658
21	$M(ej_W j_W j_{beam})$	3.544
22	$\eta(j_{beam})$	3.357
23	$\eta(\mu)$	2.970
24	$\eta(j_1)_W$	2.570
25	$M(jj)_W$	2.527
26	$\eta(ej_W j_W j_{beam})_W$	2.346
27	$P_T(j_W j_W j_{beam})_W$	2.019
28	$P_T(\mu j_W j_W)_W$	2.007
29	$P_T(ej_W j_W)_W$	1.712
30	$P_T(\mu j_W j_W j_{beam})_W$	1.552
31	$\eta(jj)_W$	0.6948

Table 10: Variables ranking for $m_{h_2} = 500$ GeV, the importance is in percent. For the four lepton final states also considered were the 9 observables $M(Z)$, and $P_T(Z)$ for the two different Z boson candidates, and $\eta(j)$, which resulted in a BDT ranking of 0.

10

TESTING CP PROPERTIES OF EXTRA HIGGS STATES AT THE HL-LHC

Published in: 10.1007/JHEP03(2021)200 [1]

Testing CP Properties of Extra Higgs States at the HL-LHC

Stefan Antusch*[1], Oliver Fischer†[2], A. Hammad‡[1], Christiane Scherb§[3]

[1] *Department of Physics, University of Basel, Klingelbergstr. 82, CH-4056 Basel, Switzerland*

[2] *Department of Mathematical Sciences, University of Liverpool Liverpool, L69 7ZL, UK*

[3] *PRISMA$^+$ Cluster of Excellence & Mainz Institute for Theoretical Physics, Johannes Gutenberg University, 55099 Mainz, Germany*

ABSTRACT

Extra Higgs states appear in various scenarios beyond the current Standard Model of elementary particles. If discovered at the LHC or future colliders, the question will arise whether CP is violated or conserved in the extended scalar sector. An unambiguous probe of (indirect) CP violation would be the observation that one of the extra Higgs particles is an admixture of a CP-even and a CP-odd state. We discuss the possibility to discover scalar CP violation in this way at the high-luminosity (HL) phase of the LHC. We focus on the Two-Higgs Doublet Model of type I, where we investigate its currently allowed parameter region. Considering a benchmark point that is compatible with the current constraints but within reach of the HL-LHC, we study the prospects of determining the CP property of an extra neutral Higgs state H via the angular distribution of final states in the decay $H \to \tau\bar{\tau}$. The analysis is performed at the reconstructed level, making use of a Boosted Decision Tree for efficient signal-background separation and a shape analysis for rejecting a purely CP-even or odd nature of H.

10.1 INTRODUCTION

After the discovery of the scalar resonance with a mass of about 125 GeV, the combined measurements are now used to establish the particle's properties [206] and whether or not it is indeed the Higgs boson as predicted by the Standard Model (SM). An important part of this procedure is the test of its spin [207, 208] and CP transformation properties [209], for instance in its top-associated production mode [210]. The latter is of particular interest, as the violation of the CP symmetry is a fundamental ingredient in order to explain the long-standing puzzle of the matter-antimatter asymmetry of the Universe [211], in particular because the CP violation in the SM – observed first in Kaon [212] and recently also in Charmed meson decays [213] – is insufficient. This calls for physics beyond the SM (BSM) explanations with significant amount of CP violation, which can e.g. be introduced in the scalar sector.

According to present analyses, the discovered scalar resonance is compatible with the scalar Higgs boson as predicted by the SM, yet the possibility of a more complex scalar sector that includes CP violation remains. Although no additional scalar resonances have been found to date[1] the scalar sector may include additional scalar bosons, which mix only weakly with the SM-like scalar Higgs boson.

A minimal prototype for an extended scalar sector is the Two Higgs Doublet Model (THDM) where the scalar sector of the Standard Model (SM) is extended by an additional scalar $SU(2)_L$ doublet field [217], which allows for the possibility of spontaneous violation of the CP symmetry in the scalar sector [218], see e.g. ref. [219] for an overview over its phenomenology. In general, additional Higgs doublets are tightly constrained as they may introduce Flavour Changing Neutral Currents (FCNCs) at tree-level, and Electric Dipole Moments (EDM) for SM particles, see e.g. ref. [220].

Scalar particles as in the THDM can be discovered and studied at particle colliders, such as the Large Hadron Collider (LHC) [221, 222]. Once another scalar boson is discovered, its CP properties will be studied, similarly to the Higgs boson, via correlations of the final state leptons from its decays, for instance from sequential gauge boson decays [52], polarisation of tau lepton pairs [53], or top quark associated production [54]. Recently the state-of-the-art experimental constraints on the type II THDM were combined and it was shown that observable CP-violating effects in the neutron EDM and also in $t\bar{t}h$ production at the LHC were still possible [223].

In this paper we go beyond existing studies by investigating in detail the possibility to establish the presence of CP violation in the THDM type I from mixing of heavy neutral scalar particles with different CP transformation properties. To this end we define the model in section 2, discuss present experimental constraints and the allowed parameter space in section 3 and perform a collider analysis of the angular distribution of final states in the decay $H \to \tau\bar{\tau}$ and how it can be used to infer the CP property of extra Higgs states in section

1 There exist anomalies in the multi lepton channels and the di-photon channel at the LHC, which were interpreted as possibly due to scalar resonances in refs. [214, 215] and [216], respectively.

4. We summarise our results and conclude in section 5. In the Appendices A and B we discuss the potential of the alternative decay channel $H \to ZZ \to 4\mu$.

10.2 THE COMPLEX TWO-HIGGS DOUBLET MODEL

The THDM was introduced in ref. [218] to discuss the phenomenon of CP violation in the scalar sector, an effect that can potentially be large. All incarnations of the THDM tend to create tree-level flavor changing neutral currents (FCNCs) that arise from the Yukawa potential. In the THDM the FCNCs can be naturally suppressed when a Z_2 symmetry is imposed on the Lagrangian [91], as discussed below.

10.2.1 *The scalar potential*

In the THDM the scalar sector of the SM is extended by an additional field such that the theory contains two $SU(2)_L$-doublet fields, ϕ_1 and ϕ_2, with identical quantum numbers under the SM gauge symmetry group:

$$\phi_1 = \begin{pmatrix} \eta_1^+ \\ (v_1 + h_1 + i h_3)/\sqrt{2} \end{pmatrix} \quad \text{and} \quad \phi_2 = \begin{pmatrix} \eta_2^+ \\ (v_2 + h_2 + i h_4)/\sqrt{2} \end{pmatrix} . \tag{167}$$

Here we introduced the real neutral fields h_i, $i = 1, ..., 4$, the charged (complex) fields η_i^+, $i = 1, 2$, and the vacuum expectation values (vevs) v_i, $i = 1, 2$. In its most general form the THDM allows for global transformations which mix these fields and change the relative phases. The Lagrangian density for this model can be decomposed as

$$\mathcal{L}_{\text{THDM}} = \mathcal{L}_{\text{SM,kin}} + \mathcal{L}_{\phi,\text{kin}} + V_\phi + Y_\phi , \tag{168}$$

where $\mathcal{L}_{\text{SM,kin}}$ denotes the kinetic terms for SM gauge fields and fermions, $\mathcal{L}_{\phi,\text{kin}}$ denotes the kinetic terms for the two scalar fields ϕ_i, $i = 1, 2$, V_ϕ denotes the scalar potential, and y_ϕ the Yukawa terms which gives rise to the couplings between the SM fermions and the scalar fields.

The most general potential for THDMs can be written as

$$\begin{aligned} V_\phi = {} & m_{11}^2(\phi_1^\dagger \phi_1) + m_{22}^2(\phi_2^\dagger \phi_2) - \left[m_{12}^2(\phi_1^\dagger \phi_2) + h.c \right] \\ & + \lambda_1(\phi_1^\dagger \phi_1)^2 + \lambda_2(\phi_2^\dagger \phi_2)^2 + \lambda_3(\phi_1^\dagger \phi_1)(\phi_2^\dagger \phi_2) + \lambda_4(\phi_1^\dagger \phi_2)(\phi_2^\dagger \phi_1) \\ & + \frac{1}{2}\left[\lambda_5(\phi_1^\dagger \phi_2)^2 + \lambda_6(\phi_1^\dagger \phi_1)(\phi_1^\dagger \phi_2) + \lambda_7(\phi_2^\dagger \phi_2)(\phi_1^\dagger \phi_2) + \text{H.c.} \right] . \end{aligned} \tag{169}$$

To avoid FCNCs interactions, THDMs are often defined with a global Z_2 symmetry [91], which transforms the scalar fields as

$$\phi_1 \to \phi_1, \qquad \phi_2 \to -\phi_2 . \tag{170}$$

In V_ϕ, this symmetry enforces $\lambda_6 = \lambda_7 = m_{12}^2 = 0$. In addition, some of the fermion representations also transform under the symmetry to ensure that only one of the Higgs doublets is involved in each Yukawa matrix. With exact

Z_2 symmetry, there is no CP violation in the scalar sector, because the only complex parameter in V_ϕ would be λ_5, and its effect could be absorbed into global redefinitions of the fields.

To allow for CP violation in the scalar sector of the THDMs, we will consider a softly broken Z_2 symmetry, where in addition to λ_5 also the (complex) parameter m_{12}^2 is present and non-zero. The scalar potential is then given by

$$\begin{aligned} V_\phi = {} & m_{11}^2(\phi_1^\dagger\phi_1) + m_{22}^2(\phi_2^\dagger\phi_2) - \left[m_{12}^2(\phi_1^\dagger\phi_2) + h.c\right] + \lambda_1(\phi_1^\dagger\phi_1)^2 + \lambda_2(\phi_2^\dagger\phi_2)^2 \\ & + \lambda_3(\phi_1^\dagger\phi_1)(\phi_2^\dagger\phi_2) + \lambda_4(\phi_1^\dagger\phi_2)(\phi_2^\dagger\phi_1) + \frac{1}{2}\left[\lambda_5(\phi_1^\dagger\phi_2)^2 + H.c\right]. \end{aligned} \tag{171}$$

We parametrize the two a priory complex-valued parameters as $m_{12}^2 = |m_{12}^2|e^{i\eta(m_{12}^2)}$, $\lambda_5 = |\lambda_5|e^{i\eta(\lambda_5)}$, introducing the two phases $\eta(m_{12}^2)$ and $\eta(\lambda_5)$.

When minimizing the Higgs potential after electroweak symmetry breaking, the tadpole equations require

$$\begin{aligned} \frac{\partial V}{\partial h_1} &= \frac{1}{2}v_1v_2^2\Re(\lambda_5) - v_2\Re(m_{12}^2) + \lambda_1 v_1^3 + m_{11}^2 v_1 + \frac{1}{2}\lambda_3 v_1 v_2^2 + \frac{1}{2}\lambda_4 v_1 v_2^2 = 0\,, \\ \frac{\partial V}{\partial h_2} &= \frac{1}{2}v_1^2v_2\Re(\lambda_5) - v_1\Re(m_{12}^2) + \frac{1}{2}\lambda_3 v_1^2 v_2 + \frac{1}{2}\lambda_4 v_1^2 v_2 + \lambda_2 v_2^3 + m_{22}^2 v_2 = 0\,, \\ \frac{\partial V}{\partial h_3} &= -\frac{1}{2}v_1v_2^2\Im(\lambda_5) + v_2\Im(m_{12}^2) = 0\,, \\ \frac{\partial V}{\partial h_4} &= \frac{\partial V}{\partial h_3} \times \left(-\frac{v_1}{v_2}\right) = 0\,, \end{aligned} \tag{172}$$

with v_1 and v_2 denoting the two (by convention real and positive) vacuum expectation values (vevs) of the two scalar fields ϕ_1 and ϕ_2. The two vevs satisfy $v = \sqrt{v_1^2 + v_2^2}$, with v denoting the SM vev $v \approx 246$ GeV, and we define $\tan\beta := v_2/v_1$.

Solving the first two equations one can eliminate m_{11}^2 and m_{22}^2 while from the third equation we get the condition $\Im(m_{12}^2) = \frac{1}{2}v_1v_2\Im(\lambda_5)$. In the following we will use this relation to remove $\Im(m_{12}^2)$ from all equations, leaving

$$\Re(m_{12}^2) \quad \text{and} \quad \lambda_5 = |\lambda_5|\, e^{i\eta(\lambda_5)}\,, \tag{173}$$

as the remaining independent parameters. In this sense, the phase parameter $\eta(\lambda_5)$ of λ_5 governs CP violation in V_ϕ.

10.2.2 *The mass matrix*

The tree-level mass matrix for the neutral scalars is given by:

$$(\mathcal{M}^2)_{ij} = \left.\frac{\partial^2 V}{\partial h_i \partial h_j}\right|_{h_i=0}, \tag{174}$$

with h_i $(i = 1, 2, 3, 4)$ being the neutral components of the two Higgs doublets including the Goldstone boson to be absorbed by the Z boson after electroweak

symmetry breaking. The mass matrix for the four neutral states in the Higgs basis h_1, h_2, h_3, h_4 is

$$M^2 = \begin{pmatrix} D_1 & O_1 & O_2 & O_3 \\ O_1 & D_2 & O_4 & O_5 \\ O_2 & O_4 & D_3 & O_6 \\ O_3 & O_5 & O_6 & D_4 \end{pmatrix}, \tag{175}$$

with the diagonal elements

$$\begin{aligned} D_1 &= 3\lambda_1 v_1^2 + \tfrac{v_2^2\lambda_3}{2} + \tfrac{v_2^2\lambda_4}{2} + m_{11}^2 + \tfrac{1}{2}v_2^2\Re(\lambda_5)\,, \\ D_2 &= \tfrac{\lambda_3 v_1^2}{2} + \tfrac{\lambda_4 v_1^2}{2} + \tfrac{1}{2}\Re(\lambda_5)v_1^2 + 3v_2^2\lambda_2 + m_{22}^2)\,, \\ D_3 &= \lambda_1 v_1^2 + \tfrac{v_2^2\lambda_3}{2} + \tfrac{v_2^2\lambda_4}{2} + m_{11}^2 - \tfrac{1}{2}v_2^2\Re(\lambda_5)\,, \\ D_4 &= \tfrac{\lambda_3 v_1^2}{2} + \tfrac{\lambda_4 v_1^2}{2} - \tfrac{1}{2}\Re(\lambda_5)v_1^2 + v_2^2\lambda_2 + m_{22}^2\,, \end{aligned} \tag{176}$$

and the off-diagonal elements

$$\begin{aligned} O_1 &= v_1 v_2\lambda_3 + v_1 v_2\lambda_4 + v_1 v_2\Re(\lambda_5) - \Re(m_{12}^2)\,, \\ O_2 &= -\tfrac{1}{2}v_2^2\Im(\lambda_5)\,, \\ O_3 &= \tfrac{1}{2}v_1 v_2\Im(\lambda_5)\,, \\ O_4 &= -O_3\,, \\ O_5 &= \tfrac{1}{2}v_1^2\Im(\lambda_5)\,, \\ O_6 &= v_1 v_2\Re(\lambda_5) - \Re(m_{12}^2)\,. \end{aligned} \tag{177}$$

Diagonalizing the mass matrix in eq. (175) leads to three massive neutral scalar bosons H_1, H_2 and H_3, and one massless neutral field H_0. In this article we will evaluate the mass matrix numerically. An analytical dependence of the mass eigenstates' physical properties on the model parameters can be extracted under certain simplifying assumptions, see e.g. refs. [224, 225].

In general, the mass eigenstates do not conserve the CP symmetry. One can see that with the only source of CP violation coming from $\Im(\lambda_5)$, for $\Im(\lambda_5) \to 0$ one retains the CP conserving THDM (with vanishing off-diagonal entries in the mass matrix, $O_{2,3,4,5} \to 0$). The squared neutral Higgs mass matrix can be diagonalized by a 4×4 matrix R as

$$R^\dagger \mathcal{M}^2 R = \mathcal{M}^2_{diag} = \mathrm{diag}(0, M_{H_1}^2, M_{H_2}^2, M_{H_3}^2)\,. \tag{178}$$

The neutral Higgs mass eigenstates H_i $(i = 0, 1, 2, 3)$ are related to the interaction fields h_i via the rotation

$$h_i = \sum_i R_{ij} H_j\,. \tag{179}$$

In the following we identify H_0 with the Goldstone boson that is absorbed by the Z boson and H_1 with the SM-Higgs-like scalar resonance at ~ 125 GeV. This leaves the neutral bosons H_2 and H_3 as new scalar mass eigenstates yet to be observed. We will assume that the extra Higgs states are heavier than H_1 and, without loss of generality, require the mass ordering $M_{H_1} \leqslant M_{H_2} \leqslant M_{H_3}$. The evaluation of the mass matrix and the rotation matrix R is carried out numerically using SPheno[226, 227].

10.2.3 *The Yukawa sector*

The absence of FCNCs at tree-level is ensured when a basis exists in which the contributions to the mass matrices for each fermion of a given representation stem from a single source [91, 228]. In the Standard Model with left-handed doublets and right-handed singlets, this implies that all right-handed quarks of a given charge must couple to a single Higgs multiplet, which can be ensured via a discrete Z_2 symmetry.

This symmetry transforms the scalar fields as in eq. (170), and allows for different possible Z_2 charge assignments for the SM fermions. Here, we select the Z_2 charge assignment of the type I version of the THDM, where all quarks and charged leptons couple only to one of the scalar doublet fields, conventionally chosen to be ϕ_2.[2]

The Z_2-symmetric Yukawa terms of type I THDM are given by

$$-\mathcal{Y}_\phi = Y_u \bar{Q}_L i\sigma_2 \phi_2^* u_R + Y_d \bar{Q}_L \phi_2 d_R + Y_e \bar{L}_L \phi_2 e_R + \text{H.c.} \tag{180}$$

with the Yukawa coupling matrices Y_u, Y_d, Y_e.

10.2.4 *CP violation*

The scalar potential of eq. (171) in general mixes the interaction states with definite CP transformation properties. This is clearly visible in the mass matrix of eq. (175), which mixes the CP-even h_1, h_2 with the CP-odd h_3, h_4 when at least one of the off-diagonal entries O_i, $i = 2,3,4,5$ is non-zero, i.e. when λ_5 has a non-zero imaginary part. The proposed methods for testing CP violation in the Higgs sector include:

- If an extra Higgs state H_i is discovered, its top quark associated production cross section could be used to determine its CP property [54, 229–231], because it is sensitive to the relative magnitudes of the CP-even and CP-odd coefficients of the $\bar{t}tH_i$ coupling. However, this effect is suppressed by the smaller cross section of a three particle final state.

- The angular momentum correlations of the final state muons in $H_i \to ZZ \to 4\mu$ have been proposed as a method to determine the CP transformation property of H_i [52, 207, 232–237]. We will discuss the applicability of this method in the context of the THDM of type I in Appendix 10.6. We find that at the HL-LHC the loop-induced decay rate of the CP-odd pseudoscalar (or of the CP-odd component of a mixed state) via ZZ into 4μ is too suppressed for successful application of the method.

- When contributions from loop-level decays of the H_i can be neglected, an obvious sign for CP mixing in the THDM is the simultaneous observation of three different Higgs states with interactions that, in the CP conserving

2 In the THDM model of type II, the up-type (down-type) quarks and leptons couple conventionally only to ϕ_2 (ϕ_1). Further variations in the lepton sector exist: the "lepton specific" model, where all quarks couple to ϕ_2 while the leptons couple to ϕ_1, and the "flipped" model, where right-handed leptons couple to ϕ_2 like the up-type quarks [219].

case, are only possible at tree-level for pure CP eigenstates [238]. One example is the scalar decay chain $H_i \to ZZ \to 4\mu$ mentioned above. Since $H_i \to ZZ$ at tree-level is only possible when the H_i has a CP-even component, in the CP conserving THDM only H_1 and either H_2 or H_3 can have this tree-level decay. Observing it for all three H_i one can conclude that the THDM violates CP. We discuss this example in Appendix 10.7. However, it is important to note that the observation of several scalar resonances with decays into ZZ is not an unambiguous signal of CP mixing in general, since the third resonance could stem from additional scalar fields outside the THDM.

- The CP transformation property of the H_i can be inferred from its decays to tau lepton pairs. To be specific, the correlation of the tau lepton polarisation planes are directly linked to the CP properties of the parent, and they can be reconstructed via the hadronic decay modes of the two tau leptons [53, 239–243]. In the following we will focus on this method in the main part of the paper.

10.2.5 *Discovering CP violation via* $H \to \tau\bar{\tau}$

We use the impact parameter method as first presented in ref. [53] to extract transverse spin correlations in the decay chains of a field S which is a mixture of a scalar and a pseudoscalar field. In particular we focus on decay chains of the form $S \to \tau\bar{\tau}$ with $\tau^\pm \to \pi^\pm \bar{\nu}_\tau(\nu_\tau)$ and make use of the impact parameters of the visible decay products of the tau lepton, τ_{had}, to extract an asymmetry in the acoplanarity angle of the two tau leptons. We remark that the method does not depend on the Higgs boson production mechanism, but translates directly into correlations among their decay products.

The Yukawa interaction of S can be written as

$$\mathcal{L}_y = y_{S\tau}\ (\bar{\tau}\,(C_v + C_a\ i\gamma_5)\,\tau)\,S \tag{181}$$

with $y_{S\tau}$ being the effective Yukawa coupling of S and the tau lepton and C_a, C_V being the scalar and pseudoscalar components of the coupling, respectively, with $C_v^2 + C_a^2 = 1$. The effective mixing angle $\theta_{\tau\tau}$, defined as

$$\tan(\theta_{\tau\tau}) = \frac{C_a}{C_v}\,,$$

measures the mixing of CP eigenstates. For example, $\theta_{\tau\tau} = 0\ (\frac{\pi}{2})$ holds for pure scalar (pseudoscalar) coupling.

The $\tau\bar{\tau}$ spin correlation can be inferred from the angle between the tau decay planes. We remark that we consider here only the tau decay mode $\tau^\pm \to \pi^\pm\bar{\nu}_\tau(\nu_\tau)$, which has a branching fraction of 11%. While this limits our statistics it provides a clear signal and can thus serve as a conservative estimate for the sensitivity to distinguish CP properties.

For the tau decay $\tau^{\pm} \to \pi^{\pm}\bar{\nu}_{\tau}(\nu_{\tau})$ the angular correlation in the decay width can be written as [53]:

$$\frac{1}{\Gamma}\frac{d\Gamma}{d\phi} = \frac{1}{2\pi}\left(1 - \frac{\pi^2}{16}\frac{C_v^2 - C_a^2}{C_v^2 + C_a^2}\cos\phi\right) = \frac{1}{2\pi}\left(1 - \frac{\pi^2}{16}\left(\cos^2\theta_{\tau\tau} - \sin^2\theta_{\tau\tau}\right)\cos\phi\right). \tag{182}$$

The angle ϕ between the decay planes is the so-called acoplanarity angle, which is sensitive to the CP properties of the scalar parent S via the coupling parameters C_v and C_a. The angular correlation in eq. 182 is given for the case in which one cannot distinguish ϕ from $2\pi - \phi$ and is obtained by the sum over both cases [53]. The acoplanarity angle (ϕ) can be reconstructed from the tau decay properties, namely the two impact parameter vectors

$$\phi = \arccos(\vec{n}^{-} \cdot \vec{n}^{+}), \tag{183}$$

where we introduced

$$\vec{n}^{\pm} = \frac{\vec{P}_{\pi^{\pm}} \times \vec{P}_{\tau^{-}}}{|\vec{P}_{\pi^{\pm}} \times \vec{P}_{\tau^{-}}|}. \tag{184}$$

The impact parameter is defined as the shortest path between the primary vertex and the pion momentum vector extended in the direction of the tau decay point. Since it is basically impossible to reconstruct the tau lepton momentum due to the presence of tau neutrinos among the decay products, the authors in ref. [53] introduce the so-called "Zero-Momentum-Frame" (ZMF) of the tau decay products, in our case the pions. This does not affect the correlations of the decay planes, such that the exact tau direction does not matter. We find the ZMF by boosting the meson momenta such, that $\vec{P}^{*}_{\pi^{+}} = -\vec{P}^{*}_{\pi^{-}}$, where quantities with an asterisk (*) refer to the ZMF. Then a 4-vector is defined for the normalized impact parameter for each tau lepton in the ZMF as $n^{*\pm} = (0, \vec{n}^{*\pm})$, from which one can extract the acoplanarity angle in the boosted frame:

$$\phi^{*} = \arccos(\vec{n}^{*-}_{\perp} \cdot \vec{n}^{*+}_{\perp}). \tag{185}$$

The resulting distribution for ϕ^{*} between 0 and π allows for a clear distinction of fields that are even or odd eigenstates of CP. Below, in sec. 10.4, we will analyse how well the CP property of an extra Higgs state can be distinguished using this method. Finally, we note that the distribution in eq. (182) remains invariant when switching from $\tau\bar{\tau}$ in the laboratory frame to $\pi^{+}\pi^{-}$ in the ZMF (cf. also ref. [53]):

$$\frac{1}{\Gamma}\frac{d\Gamma}{d\phi^{*}} = \frac{1}{\Gamma}\frac{d\Gamma}{d\phi}\bigg|_{\phi\to\phi^{*}} = \frac{1}{2\pi}\left(1 - \frac{\pi^2}{16}\left(\cos^2\theta_{\tau\tau} - \sin^2\theta_{\tau\tau}\right)\cos\phi^{*}\right). \tag{186}$$

10.3 CONSTRAINTS

The THDM with CP violation is constrained from various observations and measurements at collider and non-collider experiments. Below, we discuss constraints from theoretical considerations, from B-physics measurements, Higgs data (from the LHC, LEP, and the Tevatron) and from measurements of EDMs.

10.3.1 *Theory considerations*

As first condition from theory we impose that it has to be perturbative, which constrains the magnitude of the couplings $|\lambda_i| \lesssim 4\pi$. The second theory condition that each model has to satisfy is the stability of the vacuum. Therefore, the potential should be positive for large values of ϕ, which leads to the constraints [224, 244]:

$$\lambda_1 > 0, \qquad \lambda_2 > 0, \qquad \lambda_3 + \sqrt{\lambda_1 \lambda_2} > 0, \qquad \lambda_3 + \lambda_4 - |\lambda_5| + \sqrt{\lambda_1 \lambda_2} > 0\,. \tag{187}$$

The third condition is that the S-matrix has to be unitary for an elastic two-to-two boson scattering process, which limits the magnitude of λ_i, cf. refs. [224, 244]. The fourth condition stems from the so-called oblique parameters, which are constrained as (cf. the global fit of [245, 246]):

$$S = 0.03 \pm 0.10, \qquad T = 0.05 \pm 0.12, \qquad U = 0.03 \pm 0.10\,. \tag{188}$$

These parameters receive contributions from the THDM at the loop-level, and present an independent important constraint.

10.3.2 *B physics data*

The charged Higgs bosons from the THDM contribute to the decays of B mesons, such that the B-physics data set can be used to constrain the THDM parameters. Since the couplings of the charged Higgs bosons are not sensitive to the parameters of the neutral sector, these constraints are independent of the amount of CP violation in the model.

To evaluate the flavor phenomenology in particular for the B physics processes we use the numerical tool FlavorKit [247], which evaluates many flavor-related observables for every scanned point. The most stringent constraints on our model parameters stem from the process $B \to X_s\gamma$, which limits in particular the charged Higgs mass: $m_H^{\pm} \geqslant 580$ GeV at $\tan\beta = 1$ for the THDM of type II. For the type I THDM, the strongest constraints on the charged Higgs mass apply for $\tan\beta \leqslant 2$, while with increasing $\tan\beta$ the constraints get weaker, see refs. [248, 249]. We use the experimental bounds as reported in [250]:

$$\mathrm{Br}(B \to S\gamma)_{E_\gamma \geqslant 1.6\,\mathrm{GeV}} \leqslant (3.32 \pm 0.15) \times 10^{-4}\,. \tag{189}$$

10.3.3 *Higgs data*

The global data set on the Higgs boson includes results from LEP, the Tevatron and the LHC experiments. The existing data is combined with the numerical tool HiggsBounds[251], which we employ to constrain the THDM parameter space.

HiggsBounds first identifies the most sensitive signal channel for each boson H_i separately and then computes the ratio of this theoretically predicted to the observed signal strength for heavy Higgs bosons as

$$\mathcal{K}_i = \frac{\sigma \times \mathrm{Br}(H_i)_{model}}{\sigma \times \mathrm{Br}(H_i)_{obs}}\,, \tag{190}$$

which we use to obtain an exclusion limit at 95% C.L for parameter space points where at least one observable exists, such that $\mathcal{K}_i > 1$.

In addition to the exclusion of individual parameter points, we employ the numerical tool HiggsSignals [252] to evaluate the statistical compatibility of the lightest SM-like Higgs boson in the model with the observed scalar resonance, as it is observed by the LHC experiments. Also, the SM-like Higgs signal rates and masses are compared with the various signal rate measurements published by the experimental collaborations for a fixed Higgs mass hypothesis. The model is tested at the mass position of the observed Higgs peak in the channels with high mass resolutions like $h \to ZZ^* \to 4\ell$ and $h \to \gamma\gamma$. The signal strength modifier for the model for one channel is calculated as

$$\mu = \frac{(\sigma \times \mathrm{Br})_{model}}{(\sigma \times \mathrm{Br})_{SM}} \times \omega\,, \tag{191}$$

with ω being the SM weight, including the experimental efficiency.

A χ^2 test for the model hypothesis is performed, where a local excess in the observed data at a specified mass is matched by the model. The signal strength modifiers and the corresponding predicted Higgs masses enters the total χ^2 evaluation as

$$\chi^2_{tot} = \chi^2_\mu + \sum_{i=1}^{N_H} \chi^2_{m_{H_i}}\,, \tag{192}$$

where χ^2_μ is the χ-squared measure calculated from the signal strength modifier only and $\chi^2_{m_{H_i}}$ is the χ-squared measure calculated from Higgs bosons mass, with i running over the number of the neutral Higgs bosons in the model. The intrinsic experimental statistical and systematic uncertainties within 1σ for χ^2_μ is given by

$$\chi^2_\mu = (\mu_{obs} - \mu_{model})^T C^{-1}_{ij} (\mu_{obs} - \mu_{model})\,, \tag{193}$$

where C_{ij} is the signal strength covariance matrix that contains the uncorrelated intrinsic experimental statistical and systematic uncertainties in its diagonal entries.

The 1σ and 2σ error can be obtained from the best-fit value as $1(2)\sigma = \Delta\chi^2_{best} + 2.3(5.9)$ with $\Delta\chi^2_{best} = 1.049$. CMS reports the combined best fit value for the SM Higgs signal strength at center of mass energy = 13 TeV and integrated luminosity = $35.9 fb^{-1}$ to be $\mu_{best} = 1.17^{+0.1}_{-0.1}$[253], while the recent ATLAS results at $\sqrt{S} = 13$ TeV and integrated luminosity = $79.8 fb^{-1}$ reports $\mu_{best} = 1.13^{+0.09}_{-0.08}$[254]. These results put strong constraints on the physical properties of H_1 to be close to the ones of the SM Higgs boson. It also limits strongly the possible amount of mixing between H_1 and H_i, $i = 2, 3$.

10.3.4 *Electric Dipole Moments*

The upper limit on the electric dipole moment (EDM) of the electron is $|d_e| < 1.1 \times 10^{-29}$ ecm [255]. The new scalars contribute to the electron EDM via Barr-Zee diagrams as discussed, e.g., in refs. [256] and [257] (for latest two-loop results, see ref. [258]). In particular, the CP violating complex phase is

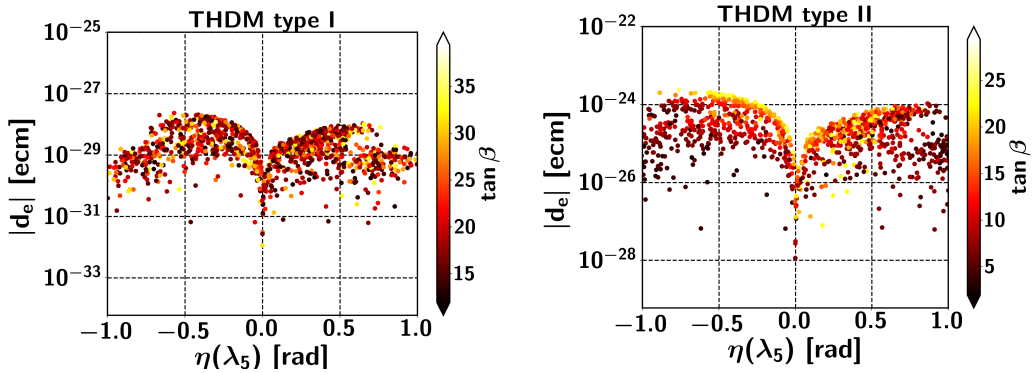

Figure 30: Electron EDM versus $\eta(\lambda_5)$ as a function of $\tan\beta$ for type I and type II THDMs. Points in the plots satisfy all constraints including the Higgs data (at 2σ).

found to strongly affect the magnitude of the EDM, its main source being the modified couplings of the Higgs bosons. In the type II THDM the EDM is enhanced by $\tan\beta$, while in type I the EDM is suppressed by $\frac{1}{\tan\beta}$, cf. ref. [259].

As stated above, the Yukawa couplings can be expressed as a sum of their CP-even and CP-odd part. In general, if a fermion couples to ϕ_1 (ϕ_2) both parts of the coupling are proportional to $\tan\beta$ ($\frac{1}{\tan\beta}$). Thus, in the type I THDM all Yukawa couplings are proportional to $\frac{1}{\tan\beta}$, while in the type II THDM the Yukawa couplings of down-type quarks and leptons are proportional to $\tan\beta$.

In this article we consider large $\tan\beta$, which leads to potentially large couplings and large contributions to the EDM. Therefore, for large $\tan\beta$ the type I THDM with couplings proportional to $\frac{1}{\tan\beta}$ is less constrained, which is one reason for us to focus on this version of THDM. To analyse the EDM constraint, we employ the formulae from refs. [256, 257].

10.3.5 *Scanning the parameter space*

In order to find viable parameter space points that satisfy all constraints we perform a scan over the parameter space. In this scan the full parametric dependence of the physical properties of the scalar particles, like their masses and interaction vertices, are calculated, and the above described constraints are evaluated. For the numerical scan we consider the following ranges of parameters:

$$\begin{aligned} &0.0 \leqslant \lambda_1 \leqslant 10, \quad 0.05 \leqslant \lambda_2 \leqslant 0.2, \quad 0 \leqslant \lambda_3 \leqslant 10, \quad -10 \leqslant \lambda_4 \leqslant 10, \\ &-10 \leqslant |\lambda_5| \leqslant 10, -1.0 \leqslant \eta(\lambda_5) \leqslant 1.0, \quad 2 \leqslant \tan\beta \leqslant 50, \quad -25\ \text{TeV}^2 \leqslant m_{12}^2 \leqslant 25\ \text{TeV}^2. \end{aligned} \tag{194}$$

We obtain 5k parameter space points that satisfy all experimental constraints. We remark that the above parameter ranges are optimised to yield a good efficiency with respect to passing the list of constraints. As we mentioned above we use SPheno to evaluate the mixing matrix numerically.

In fig. 30 we show the contribution to the EDM for our parameter space points as a function of $\tan\beta$ and $\eta(\lambda_5)$ for the type I THDM (left panel). We also show the results for the type II THDM for comparison in the right panel of

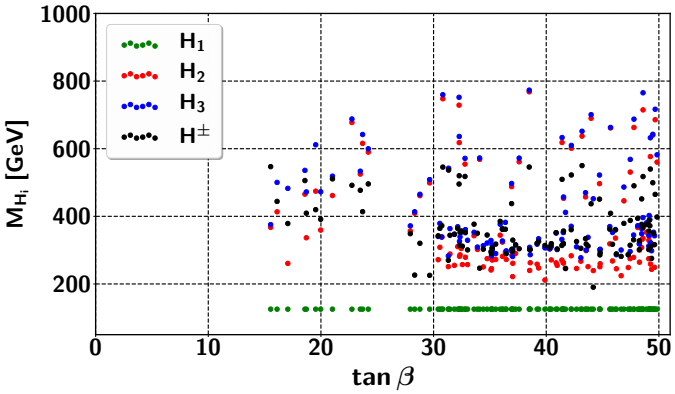

Figure 31: Scatterplot of the allowed parameter space points in the projection of mass m_{H_i} (in GeV) over tan β.

the same figure. One can see that for the THDM of type II low tan β with large η has the smallest EDM values. With the used scan resolution no points below the EDM bound are found. This can be compared with the analysis in ref. [223], wherein a region with small values for tan β was identified that is not excluded by the EDM and the Higgs constraints considering the type II THDM. For the type I version of the THDM allowed parameter space points can be found for all considered values of $\eta(\lambda_5)$. For the parameter space points satisfying all of the above constraints we show the projection of the three neutral scalar masses versus tan β in fig. 31. From this figure we can see that for the viable points we found in our scan, both, H_2 and H_3, have masses between about 200 and 700 GeV, while H_2 has more parameter space points with masses around 200 to 300 GeV, and H_3 tends to be slightly heavier.

10.4 ANALYSIS

In this section we discuss the production mechanism for the scalar bosons of the type I THDM and the currently allowed cross sections. We investigate the process $pp \to H_i \to \tau\bar{\tau}$ that we use to analyse the CP properties of extra Higgs states and evaluate the prospects of finding it in the presence of the considered background processes. Then we perform an analysis of the angular distribution of the final state taus.

10.4.1 *Heavy scalar production rates*

We consider the LHC in its high-luminosity phase (the HL-LHC) with an expected total integrated luminosity of 3 ab^{-1} and a center-of-mass energy of 14 TeV. The dominant production processes for the Higgs bosons at the HL-LHC are gluon-gluon fusion (around 90%) and vector boson fusion. We calculate the effective gluon-gluon-Higgs coupling using SPheno and include the QCD corrections from ref. [260]. The production cross sections are calculated including the effective gluon-Higgs vertex in MadGraph [143].

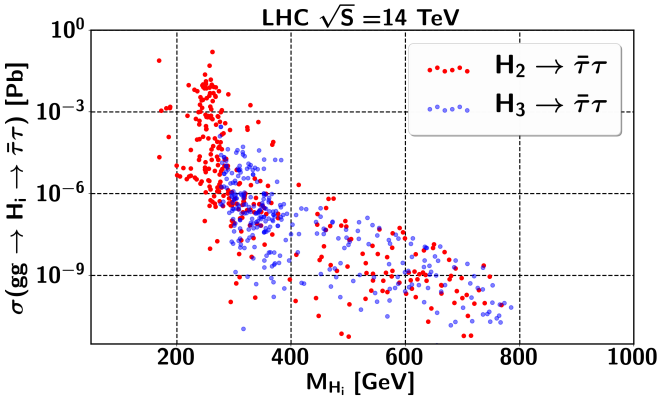

Figure 32: Total cross sections for the process $pp \to H_i \to \tau\bar{\tau}$ at the HL-LHC with $\sqrt{s} = 14$ TeV.

Since the signal for CP violation is encoded in angular correlations of the heavy scalars' decay products, it can only be assessed statistically. Therefore we are interested in how many signal events can be expected, requiring that the parameter point is allowed by the above discussed constraints. For this assessment, we use our parameter space set from the previous section, selecting for parameter points that conform with all constraints. We show the total cross section for the process $pp \to H_i \to \tau\bar{\tau}$ in fig. 32, wherein the blue and red points denote the cross sections for the scalar bosons H_2 and H_3, respectively.

We notice that parameter space points exist with production cross sections larger than a few femtobarn, which would yield more than a few thousand events at the HL-LHC. While this is in principle sufficient for a statistical study of the CP violation signal, it may be difficult in practice due to large backgrounds and reconstruction uncertainties. In the next subsection, we will evaluate a specific benchmark point.

10.4.2 *Signal reconstruction for a benchmark point at the HL-LHC*

In the following we discuss the inclusive signal process

$$pp \to H_i \to \tau\bar{\tau}\,, \tag{195}$$

where we include interference between the H_i. We select a benchmark point with $m_{H_2} = 250$ GeV and $m_{H_3} = 300$ GeV, based on the model parameters $\tan\beta = 31$, $\theta_{\tau\tau} = 0.68 = \frac{\pi}{4.6}$ (which corresponds to $\eta(\lambda_5) = 0.7$), $\lambda_1 = 0.039$, $\lambda_2 = 0.104$, $\lambda_3 = 2.215$, $\lambda_4 = -0.023$, $\Re(\lambda_5) = 0.337$ and $m_{12}^2 = -1.919 \times 10^4$ GeV^2. The parameters m_{11}^2 and m_{22}^2 are then fixed by the previous parameters due to the tadpole equations, cf. eq. (172). It is worth noting that the benchmark point is stable against small changes in the input parameters, e.g changes in the input parameters of $\mathcal{O}(5\%)$ lead to changes in the masses of $\mathcal{O}(0.1\%)$ while still fulfilling all above discussed constraints. Our benchmark point has an electron EDM $|d_e| \approx 7.4 \times 10^{-30}$ ecm and a branching ratio $\mathrm{Br}(B \to X_s\gamma) \approx 3.04 \times 10^{-4}$ leading to possible observable signatures. Therefore both channels can be used as complementary probes of our benchmark point.

Backgrounds	$\sigma_{(\text{HL-LHC})}$[Pb]
$Z \to \tau\bar{\tau}$	1537
QCD jets	$10^8 \times \epsilon^2$
$W + J, W \to \tau\, \nu_\tau$	22
$t\bar{t}$	6
$WW, W \to \tau\, \nu_\tau$	0.9

Table 11: Dominant background processes considered in our analysis and their total cross sections. The samples have been produced with the following cuts: $P_T(j) \geqslant 20$ GeV, $P_T(l) \geqslant 10$ GeV. The efficiency of the QCD jets to be mistagged as tau jet is taken from the CMS paper[262] and we use the fake rate $\epsilon = 5 \times 10^{-3}$ from ref. [262].

The main irreducible SM backgrounds to this process come from $Z \to \tau\bar{\tau}$[261] and from single top and $\bar{t}t$, with tau jet pair produced from the W decay. Other backgrounds arise from the misidentification of light jets as tau jets, for instance W boson plus jet or multijets. The here considered backgrounds are listed, together with their cross sections, in tab. 11

We simulate signal samples including 20 million events and background samples including 30 million events for each background with MadGraph5[143]. The parton shower, hadronisation and spin correlation of the tau lepton decay is taken care of by Pythia8 [95]. We perform a fast detector simulation with Delphes [97]. The tau jets are tagged using the Delphes analysis framework with reconstruction efficiency of 70% and misidentification rate of 5×10^{-3} for the QCD jet, which we implement at the analysis level. For the background we adopt a reconstruction efficiency of 60% (following ref. [189]). For the event reconstruction we require two tau tagged jets with $P_T > 20$ GeV where events with b-tagged jets are rejected.

We find that interference between the H_i bosons has a very small effect for the here chosen benchmark point, namely it increases the total cross section by about 5%. In particular, the interference between H_2 and H_3 is suppressed by the small H_3 total cross section, which is about $1.5 \cdot 10^{-5}$ pb, compared to the total cross section of the H_2, which is 0.3 pb. Therefore, in the next section, we will study an exclusive sample from the process $pp \to H_2 \to \tau\bar{\tau}$.

10.4.3 *Shape analysis for establishing CP violation*

We focus here on the H_2 boson, which in general is more strongly coupled to the SM fermions and thus yields a stronger signal, i.e. more events. To separate the signal from the backgrounds, we train a Boosted Decision Tree (BDT),[3] which we feed with the simulated distributions from the process $pp \to H_2 \to \tau\bar{\tau}$, neglecting the small contributions from H_1 and H_3. As variables we include the invariant mass of the two reconstructed taus, the missing transverse energy and $\Delta R(\tau_{had}, \tau_{had})$.

3 We use the Tool for Multi-Variate Analysis package (TMVA) [145].

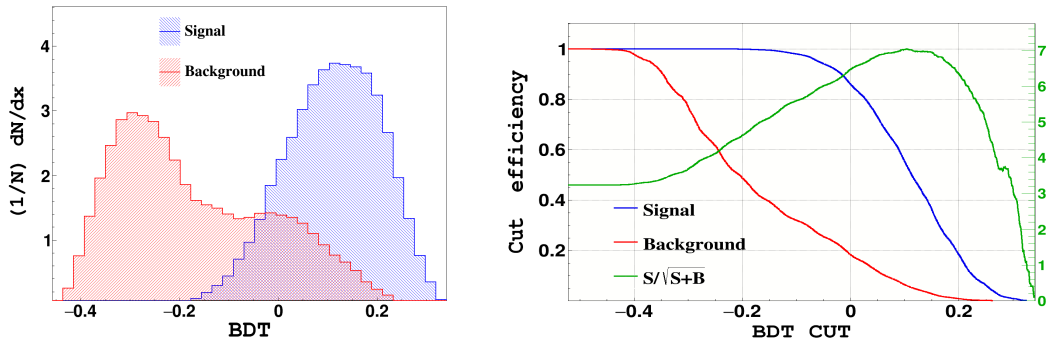

Figure 33: Left: The distribution of the Boosted Decision Tree response to the signal (blue) and to the background (red), superimposed. Right: Cut efficiency that maximizes the BDT cut. For a cut value greater than 0.104 one can get $\frac{S}{\sqrt{S+B}} = 7.04\sigma$ with number of signal events = 2043 and background events = 82212 after the BDT cuts. The cut efficiency for the signal is 0.57 and for the background 0.00059.

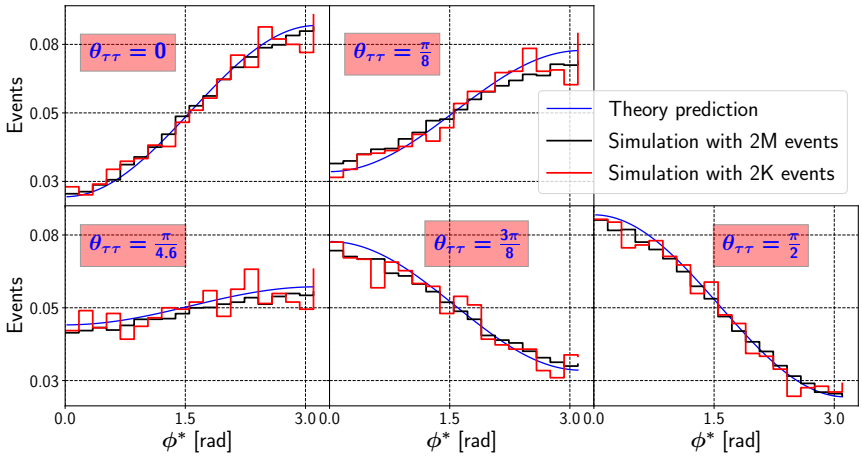

Figure 34: Distributions for the events $pp \to H_2 \to \tau\bar{\tau}$ in the τ-acoplanarity angle ϕ^*, in the zero momentum frame, see sec. 10.2.4 for details. The red lines denote the results from a MonteCarlo simulation with MadGraph5 for the 2043 events, as expected for the chosen benchmark point at the HL-LHC. The black lines are evaluated from samples with 2M events and indicate the infinite statistics limit. Systematic uncertainties stem from hadronisation, detector simulation, and reconstruction. The blue lines were derived from the theory prediction in eq. (182). For all distributions the total number of events is normalised to one.

The BDT algorithm ranks the input variables according to their ability to separate between signal events and background events. The BDT classifier ranges from -1 to 1 and quantifies the separability of signal and background. Events with discriminant value near 1 are classified as signal-like events and those near -1 are considered as background-like events. The BDT response to signal and background events is shown in the left panel of fig. 33 in blue and red, respectively. The optimization of the signal significance as a function of signal and background cut efficiency is shown in the right panel of fig. 33. The

maximum cut efficiency is at BDT classifier $\geqslant 0.193$, corresponding to a signal significance 7σ with signal efficiency 0.57 and background rejection efficiency 0.0059. For the benchmark point with $\theta_{\tau\tau} = 0.68$, the BDT yields 2043 signal events versus 82212 background events.

Additionally, we simulate distributions for the same benchmark point but with different CP-mixing angles $\theta_{\tau\tau} = 0, \pi/8, 3/8\pi, \pi/2$. We remark that we are using the simulations with different $\theta_{\tau\tau}$ values only for comparison, and we do not check that all experimental constraints are satisfied for suitable corresponding parameter points.

As signal we consider the decay $H_2 \to \tau\bar{\tau}$ with subsequent decay of $\tau^\pm \to \nu_\tau \pi^\pm$. As described above we study the tracks inside the tau jets, which carry information about the spin correlation between the tau lepton and $\pi^\pm$, and thus allow us to reconstruct the angle between the decay planes of the two τ leptons, the acoplanarity angle ϕ^* as defined above. A P_T cut on the tagged jets is applied, forcing the transverse momentum to be larger than 20 GeV. Furthermore, we improve the quality of the events with a cut on the track impact parameter: $d_0 \geqslant 50\ \mu m$. (This cut is taken into account during the analysis and the reported numbers after BDT cut assume this cut.) The fourvectors of the pion candidates' track are boosted to the ZMF as described in sec. 10.2.5 above. In the ZMF the new acoplanarity angle ϕ^* is evaluated according to eq. (185).

Now we turn to analysing the shape of the distribution, aiming to infer the CP-mixing angle $\theta_{\tau\tau}$ from the simulated data. First we observe that the simulated distributions after all cuts have a very similar shape to the theory prediction for $\Gamma(\Phi)$ from eq. 182. We thus define the reconstructed distribution in the ZMF frame for our numerical fit to the data, introducing the fit parameters a, b, as:

$$\frac{1}{\Gamma}\frac{d\Gamma}{d\phi^*}(\theta_{\tau\tau}) = a(\theta_{\tau\tau}) - b(\theta_{\tau\tau})\cos\phi^* \,. \tag{196}$$

We find excellent agreement between our fitted values for $a_{\theta_{\tau\tau}}, b_{\theta_{\tau\tau}}$ and the theoretical values in eq. 182, which are $a_{\theta_{\tau\tau}} = 1/(2\pi)$ and $b_{\theta_{\tau\tau}} = \pi/32\left(\cos^2\theta_{\tau\tau} - \sin^2\theta_{\tau\tau}\right)$. We therefore directly compare the reconstructed distributions with the theory predictions from eq. 186.

For our shape analysis we consider the distributions for the samples of 2043 events labelled "2K", corresponding to the expected event yield of the benchmark point at the HL-LHC, and the "infinite statistics" limit labelled "2M", corresponding to 2 million events. The latter have a much smaller statistical uncertainty compared to the systematic one, which stems from uncertainties related to hadronisation, detector simulation, and the reconstruction of tau leptons. We show the distributions for both, the small and large versions of the five signal samples, in fig. 34. In the figure we also show the theory prediction for $1/\Gamma d\Gamma/d\phi^*$ in eq. (186).

The distributions are given for $N_{bins} = 20$ bins from which we create a χ^2 fit for different values of $\theta_{\tau\tau}$ using

$$\chi^2(\theta_{fit}) = \frac{\left(S_i^{\theta_{\tau\tau}} - \frac{n_S}{\Gamma}\frac{d\Gamma}{d\phi_i^*}(\theta_{fit})\right)^2}{(\delta S_i)^2 + \delta_{syst}^2}\,, \tag{197}$$

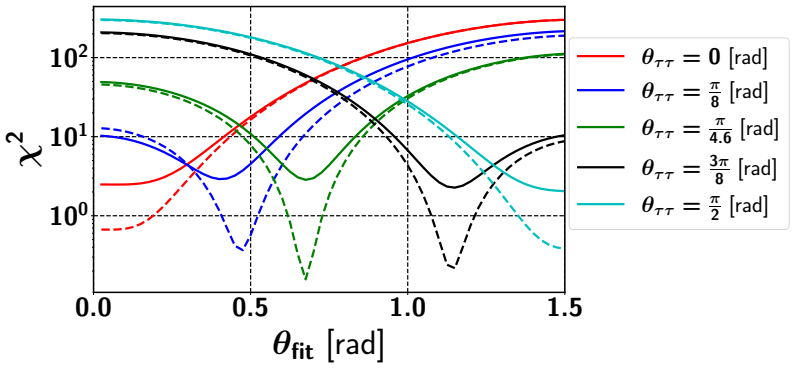

Figure 35: Absolute value of the χ^2 for the five different values of CP-mixing $\theta_{\tau\tau}$ evaluated according to eq. (197) with $\delta_{sys} = 0.5\% \cdot (N_{bkg}/N_{bins})$. The solid and dashed lines correspond to the 2K (HL-LHC) and 2M ("infinite statistics") event samples, respectively, for details see text.

where $\theta_{\tau\tau}$ is the mixing angle of a given benchmark point, θ_{fit} an input of the theoretical distribution, $S_i^{\theta_{\tau\tau}}$ the signal distribution in bin i, $n_S = 2043$ is the total number of signal events, and

$$\delta S_i = \sqrt{S_i}, \qquad \delta_{\text{syst}} = \alpha \frac{N_{\text{bkg}}}{N_{\text{bins}}}\,. \tag{198}$$

The number of background events after the BDT cut is $N_{\text{bkg}} = 82212$ and α is the precision with which the background can be controlled experimentally. The background is completely flat with respect to the signal, which is an outcome of our simulation. In the following we consider the three exemplary values $\alpha = 5\%, 1\%$, and 0.5%, which we assume to be conservative, realistic, and optimistic, respectively.

For both, the distributions from the small and large samples, the above χ^2 fit yields a minimum for θ_{fit} that agrees with the set value $\theta_{\tau\tau}$ with high accuracy. We chose the confidence level (CL) for excluding pure CP-even or CP-odd hypotheses from the $\Delta\chi^2$ distributions at 90%. For our 20 observables (the bins) minus the one parameter (θ_{fit}) this corresponds to $\Delta\chi^2 = 27.2$. We find that for $\alpha = 5\%$ and 1% no statistically meaningful statement on CP violation is possible at the 90% CL for our benchmark point at the HL-LHC. We show the resulting χ^2 distributions for the five considered CP mixing angles in fig. 35 for $\alpha = 0.5\%$. For our benchmark point where the set value is $\theta_{\tau\tau} = \frac{\pi}{4.6}$, and considering the HL-LHC sample with 2043 events, our procedure allows to determine $\theta_{\tau\tau} \simeq \frac{\pi}{4.6} \pm 0.3$ at 90% CL. CP-conservation can therefore be excluded at $\gtrsim 90\%$ CL for this point.

10.5 CONCLUSIONS

The violation of CP symmetry is fundamental to the baryon asymmetry of the Universe. One of the few ways to introduce it is a CP-violating scalar sector, which implies the existence of additional scalar degrees of freedom (i.e. extra Higgs states) with possible observable consequences at the LHC and future colliders. Some of the signatures that indicate the violation of CP in

the scalar sector include: simultaneous observation of specific processes, top-quark associated production modes and angular momentum correlations in sequential decays such as $H_i \to ZZ \to 4\mu$ and $H_i \to \tau\bar{\tau}$.

In this article we consider the type I and II Two Higgs Doublet Models (THDMs) as examples for observable CP violation in the scalar sector. We evaluated the mass eigenbasis numerically, i.e. without assumptions on any of the parameters. We determined a viable parameter space region via a numerical scan over the parameters that are compatible with the present constraints, including theoretical considerations, B-physics measurements, Higgs data, and measurements of electric dipole moments. Our scan shows that the constraints allow for scalar bosons with masses of order a few hundreds of GeV, which can be within reach of the HL-LHC. Moreover, we find that the possible amount of CP violation is much more suppressed in the type II THDM.

In case of CP violation the decay chain $H_i \to ZZ \to 4\mu$ can give rise to three clearly distinct Higgs peaks. This can provide a clear signal for CP violation in the considered THDM (cf. Appendix B), where exactly two of the Higgs fields can decay to ZZ at the tree-level in case of CP conservation. However, this signature is not unambiguous, since the third resonance could stem from additional scalar fields outside the THDM. Using the angular distributions in this decay chain turned out not to be feasible due to the coupling of the CP-odd component to ZZ, occurring only at loop-level, being too strongly suppressed (cf. Appendix A).

Towards finding an unambiguous signal of CP violation in the scalar sector we have analysed the process $pp \to H_2 \to \tau\bar{\tau}$ in the type I THDM at the detector level for a selected benchmark point, using a Boosted Decision Tree (BDT). We included the following SM backgrounds: $Z \to \tau\bar{\tau}$, single top and $t\bar{t}$, and light jet misidentification. For our analysis the decays $\tau \to \nu\tau\pi$ were implemented. The detectability of CP non-conservation was quantified via a χ^2 fit of the theoretically predicted distributions of the reconstructed tau-decay planes to the simulated data. We find that CP conservation in the scalar sector can be excluded at the 90% CL for our selected benchmark point, i.e. when the CP-mixing angle is close to its maximal value ($\pi/4$) and the background can be controlled with a relative accuracy of 0.5%, which could be the accuracy target for future measurements. Our results are conservative, since also other τ-decays (such as $\tau \to \nu_\tau\rho$) can be used to study CP violation.

Acknowledgements

This work has been supported by the Swiss National Science Foundation under the project number 200020/175502. O.F. received funding from the European Unions Horizon 2020 research and innovation program under the Marie Sklodowska-Curie grant agreement No 674896 (Elusives). C.S. was supported by the Cluster of Excellence Precision Physics, Fundamental Interactions, and Structure of Matter (PRISMA+ EXC 2118/1) funded by the German Research Foundation (DFG) within the German Excellence Strategy (Project ID 39083149), and by grant 05H18UMCA1 of the German Federal Ministry for Education and

Research (BMBF). A.H. would like to thank Waleed Esmail for fruitful discussions.

10.6 APPENDIX: ANGULAR CORRELATIONS IN $H_i \to ZZ \to 4\mu$

In this appendix we investigate the process $H_i \to ZZ \to 4\mu$, and the possibility to infer the CP property of H_i from angular correlations in the final state muons. This possibility has been discussed previously, cf. refs. [52, 207, 232–237]. Searches for such processes have been carried out by the ATLAS [221] and CMS [222] collaborations.

The starting point is the observation that CP-odd fields couple to ZZ only at loop-level, dominantly via a loop involving a top quark, cf. fig. 36. The pseudoscalar coupling to the top quark gives rise to specific correlations in the four-fermion final states. In order to determine whether or not these final state correlations can be observed, we investigate the branching ratios of CP-even (H) and CP-odd scalars (A_0) into ZZ.

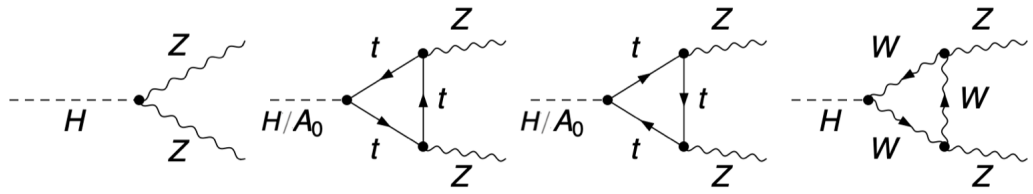

Figure 36: Feynman diagrams for the coupling of CP-even (H) and CP-odd (A_0) Higgs fields to two Z bosons, at tree and one-loop level.

Let us evaluate the size of the effective couplings for H and A_0 from the contributions in fig. 36. The matrix element for Higgs decays to ZZ is given by

$$i\mathcal{M} = i\mathcal{M}^{\text{tree}}_{(H\to ZZ)} + i\mathcal{M}^{\text{one-loop}}_{(H/A_0\to ZZ)} \tag{199}$$

$$= C_1\,\epsilon_1^*\epsilon_2^* + C_2\,(P_2\epsilon_1^*)(P_1\epsilon_2^*) + C_3\,\mathcal{E}_{\mu\nu\alpha\beta}P_1^\mu P_2^\nu \epsilon_1^{*\alpha}\epsilon_2^{*\beta}\,, \tag{200}$$

where $\epsilon_1^*, \epsilon_2^*$ and P_1, P_2 are the polarization vectors and the momenta for the outgoing gauge bosons, and $\mathcal{E}_{\mu\nu\alpha\beta}$ is the totally antisymmetric tensor. The form factors C_2 and C_3 measure the strength of the coupling of the CP-even and CP-odd states to ZZ that arises at one-loop level, while C_1 is the coupling of the CP-even field to ZZ from the tree-level diagram. It is the contraction of the momenta via the antisymmetric tensor $\mathcal{E}_{\mu\nu\alpha\beta}$ in the last term of eq. (200) that gives rise to the different correlations in the four-muon final states of the

process $A_0 \to ZZ \to 4\mu$. We evaluated the coefficients C_i using FeynCalc[263] and Package-X [264]. The tree-level and the one-loop couplings are given by:

$$
\begin{aligned}
C_1 &= \frac{igM_Z \sin(\beta-\alpha)}{\cos\theta_W}, \\
C_2 &= \frac{i \sin\alpha\, g^3 m_t^2}{18\pi^2 m_H^4 \sin\beta \cos\theta_W^2 m_W}\left(3m_H^2 + m_t^2 \ln(\chi_t)^2 + \sqrt{m_H^4 - 4m_H^2 m_t^2}\ln(\chi_t)\right) + \\
&\quad \frac{i \sin(\beta-\alpha)\, g^3 m_W \cos\theta_W^2}{4\pi^2 m_H^4}\left(-30m_H^2 + (m_H^2 - m_W^2)\ln(\chi_W)^2 - 10\sqrt{m_H^4 - 4m_H^2 m_W^2}\ln(\chi_W)\right), \\
C_3 &= \frac{-ig^3 m_t^2}{18\pi^2 m_{A_0}^4 \tan\beta \cos\theta_W^2 m_W} \times \\
&\quad \left(2m_{A_0}^2 + (4\sin\theta_W^4 - 3\sin\theta_W^2)m_{A_0}^2 \ln(\chi_t)^2 - 9\sqrt{m_{A_0}^4 - 4m_{A_0}^2 m_t^2}\ln(\chi_t)\right),
\end{aligned}
\tag{201}
$$

where α is the mixing angle between the CP-even Higgs bosons, θ_W is the weak mixing angle and

$$
\chi_a = \frac{\sqrt{m_\phi^4 - 4m_\phi^2 m_a^2} + 2m_a^2 - m_\phi^2}{2m_a^2},
$$

with m_ϕ and m_a denoting the masses of the decaying Higgs bosons (H or A_0) and of the loop particles, respectively.

It is in principle possible to test the CP transformation property of the extra Higgs state via an asymmetry in the angular distributions of the four fermion final states [233]. For CP-odd fields, this requires the measurement of the final state correlations in the final states from the process $A_0 \to ZZ \to 4\mu$. To infer the CP transformation property sucessfully, a large sample of 4μ from this decay chain is needed, which in turn requires a substantial branching fraction of the process. The dominant pseudoscalar decay modes are e.g. $A_0 \to \bar{t}t \propto (y_t \cos\beta)^2$ and $A_0 \to \bar{b}b \propto (y_b \sin\beta)^2$ and also $A_0 \to H^\pm W^\mp \propto (g_2 \sin 2\beta(P_A - P_W))^2$, $A_0 \to HZ \propto (\sin(\alpha-\beta)\sqrt{g_1^2+g_2^2}(P_A - P_Z))^2$.

Since the dominant decay channels are unsuppressed tree-level decays, it turns out that the branching ratio for $A_0 \to ZZ$ in THDMs is quite small, maximally about 10^{-3} (cf. [265]), and the branching ratio to 4μ leads to a further suppression by $\mathrm{Br}(ZZ \to 4\mu) \simeq 10^{-3}$ We find that the production cross section for A_0 is at most 0.1 pb, which yields a total cross section for the process $pp \to A_0 \to ZZ \to 4\mu$ of $\sim 10^{-7}$ pb, and suppressing backgrounds by introducing cuts will reduce the resulting number of events that can be used for an analysis even further. With the total luminosity at the HL-LHC being 3 $(\mathrm{ab})^{-1}$ it is clear that the loop-suppressed decay $A_0 \to ZZ \to 4\mu$ is too much suppressed to use it for studying the angular correlations of the four muons. Of course the same conclusion also applies to the CP-odd component of an H_i that is an admixture of a CP-even and a CP-odd field.

10.7 APPENDIX: THE HIGGS SPECTRUM FROM $H_i \to ZZ \to 4\mu$

The process $pp \to H_i \to ZZ \to 4\mu$ is a very clear channel that may contribute substantially to the discovery of the scalar H_i.[4] As we discussed in the previ-

4 Another very relevant discovery channel for a scalar boson in the here considered mass range is $H_i \to 2H_1$ [266].

ous section, it is not feasible to use the angular distributions of the final state muons from this process at the HL-LHC for establishing the existence of CP violation in the scalar sector. However, in the context of THDMs, it can still be used to establish a signal of CP violation via the reconstructed Higgs spectrum from the invariant mass distribution of the Higgs decay products.

When the scalars are not pure eigenstates of CP, all of the H_i can have sizeable branching ratios into ZZ, giving rise to three resonances in the 4μ final state, as shown in fig. 37. Measuring three peaks for the invariant masses of the four muon final states is thus a clear signal for CP violation within the complex THDM.

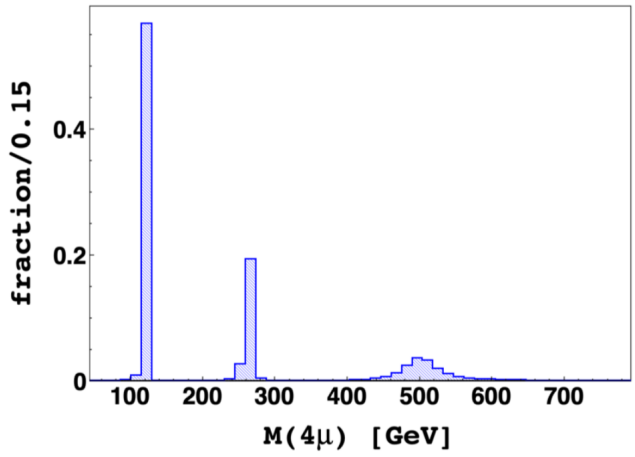

Figure 37: Distribution of the total invariant mass of the four muon final state from the process $pp \to H_i \to ZZ \to 4\mu$, from an inclusive simulation of the signal sample with 20M events, including a fast detector simulation with Delphes.

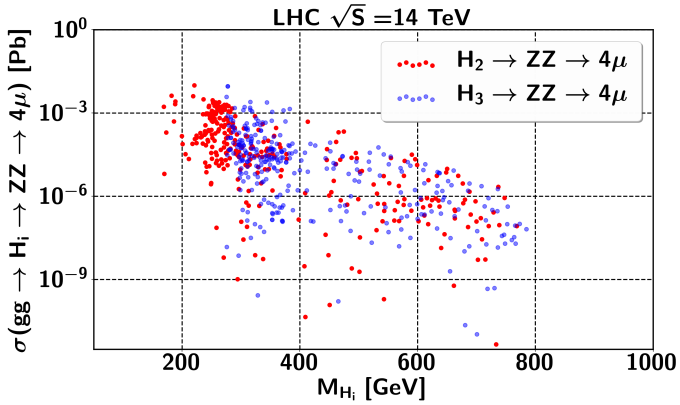

Figure 38: Total cross sections for the process $pp \to H_i \to ZZ \to 4\mu$ at the LHC with $\sqrt{s} = 14$ TeV. The scatter plot uses the results from the parameter space scan in sec. 10.3.5.

To evaluate the observability of this process, we consider a benchmark point with $m_{H_2} = 260$ GeV and $m_{H_3} = 500$ GeV, based on the model parameters $\tan\beta = 4$, $\lambda_1 = 0.172$, $\lambda_2 = 0.0828$, $\lambda_3 = 5.149$, $\lambda_4 = -0.313$, $\Re(\lambda_5) =$

Backgrounds	$\sigma_{(\text{HL-LHC})}$[Pb]
$pp \to ZZ \to 4\mu$	0.0065
$pp \to \bar{t}t$, where $t \to$ leptons	6.7
$pp \to \bar{t}tZ$	0.0002
$pp \to WZ \to 3\mu + \nu_\mu$	0.099
$pp \to tWb$, where $t \to$ leptons	7.1

Table 12: Dominant background processes considered in our analysis and their total cross sections. The samples have been produced with the following cuts: $P_T(j) \geqslant 20$ GeV, $P_T(l) \geqslant 10$ GeV.

$-4.6431, \eta(\lambda_5) = 0.81$ and $m_{12}^2 = 1.091 \times 10^4$ GeV^2. The parameters m_{11}^2 and m_{22}^2 are then fixed by the previous parameters due to the tadpole equations, cf. eq. (172). In fig. 38 we show the total cross section for the process $pp \to H_i \to ZZ \to 4\mu$ for number of scanned points from our scan in sec. 10.3.5.

We consider the following backgrounds: The dominant SM background that contributes to the final state with 4μ is ZZ production. Other reducible backgrounds are *WW* and *WZ* production, where one of the jets is misidentified as a muon. This set of background processes can be sufficiently reduced by the requirement of tight isolation criteria for the hard final state muons. The set of backgrounds with $t\bar{t}$ production and the associated production of top quark with a *W* boson can be reduced by vetoing b-jets. The last set of backgrounds with three gauge boson production is highly suppressed by the large missing energy associated to these processes and will not be included in the analysis. All the considered and included backgrounds are listed with their cross sections in tab. 12.

We constructed all possible kinematic variables for the signal and all relevant backgrounds and used the BDT to optimize the signal to background classifier as shown in fig. 39 (left). According to the BDT ranking, the invariant mass of the four final state muons is the most important variable to separate the signal from the backgrounds. The fact that all three neutral bosons can decay into a pair of Z bosons proofs that our benchmark point has Higgs states with mixed CP properties, since otherwise one of the three bosons would be a pure pseudoscalar which does not interact with ZZ at tree-level.

The signal significance as a function of signal and background cut efficiency is shown in the right panel of fig. 39. The maximum cut efficiency is at BDT $\geqslant 0.193$, corresponding to a signal significance 11σ with signal efficiency 0.187 and background rejection efficiency 0.0004, which demonstrates an excellent discovery potential for our benchmark point in this channel alone.

We emphasize that the observation of three scalar resonances in the 4μ final state is a positive signal for CP violation *only* in the THDM, because there it is absent when CP is conserved. It is not an unambiguous signal of CP violation outside the THDM, since the third resonance could stem from some other CP-even scalar field.

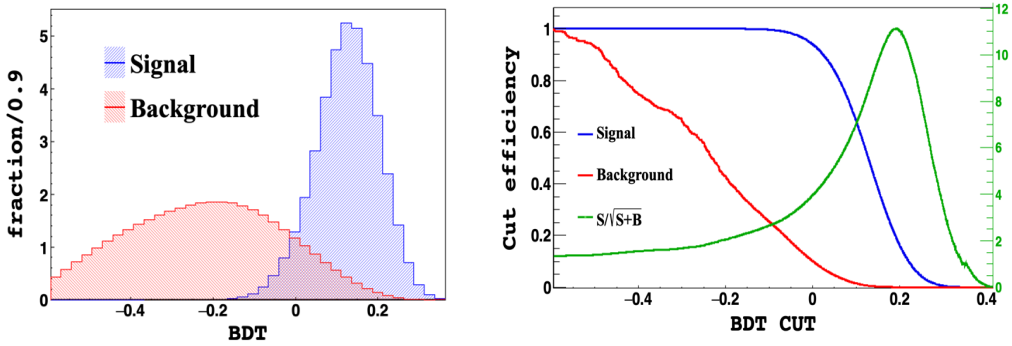

Figure 39: *Left:* The distribution of the Boosted Decision Tree response to the signal (blue) and to the background (red), superimposed. *Right:* Cut efficiency as a function of the BDT cut. For a cut value greater than 0.193 one can get $S/\sqrt{S+B} = 11\sigma$ with number of signal events $= 939$ and background events $= 6185$. The cut efficiency for the signal is 0.187 and for the background 0.0004.

11

LOW SCALE TYPE II SEESAW: PRESENT CONSTRAINTS AND PROSPECTS FOR DISPLACED VERTEX SEARCHES

Published in: 10.1007/JHEP02(2019)157 [6]

Low scale type II seesaw: Present constraints and prospects for displaced vertex searches

Stefan Antusch*[1], Oliver Fischer†[2], A. Hammad‡[1], Christiane Scherb§[1]

[1] *Department of Physics, University of Basel, Klingelbergstr. 82, CH-4056 Basel, Switzerland*

[2] *Institute for Nuclear Physics, Karlsruhe Institute of Technology Hermann-von-Helmholtz-Platz 1, D-76344 Eggenstein-Leopoldshafen, Germany*

ABSTRACT

The type II seesaw mechanism is an attractive way to generate the observed light neutrino masses. It postulates a $SU(2)_L$-triplet scalar field, which develops an induced vacuum expectation value after electroweak symmetry breaking, giving masses to the neutrinos via its couplings to the lepton $SU(2)_L$-doublets. When the components of the triplet field have masses around the electroweak scale, the model features a rich phenomenology. We discuss the current allowed parameter space of the minimal low scale type II seesaw model, taking into account all relevant constraints, including charged lepton flavour violation as well as collider searches. We point out that the symmetry protected low scale type II seesaw scenario, where an approximate "lepton number"-like symmetry suppresses the Yukawa couplings of the triplet to the lepton doublets, is still largely untested by the current LHC results. In part of this parameter space the triplet components can be long-lived, potentially leading to a characteristic displaced vertex signature where the doubly-charged component decays into same-sign charged leptons. By performing a detailed analysis at the reconstructed level we find that already at the current run of the LHC a discovery would be possible for the considered parameter point, via dedicated searches for displaced vertex signatures. The discovery prospects are further improved at the HL-LHC and the FCC-hh/SppC.

11.1 INTRODUCTION

The Standard Model (SM) of elementary particles is successfully describing a plethora of observed phenomena at many different energy scales. However, the observation of neutrino oscillations [267, 268] is evidence that at least two of the neutrinos are massive. Since the SM cannot account for these masses in a renormalizable way, this calls for physics beyond the SM (BSM). An attractive possibility for generating the masses for the neutrino degrees of freedom of the SM consists in adding a scalar $SU(2)_L$-triplet field (a "triplet Higgs field") to the scalar sector of the theory, which obtains an induced vacuum expectation value v_T after electroweak symmetry breaking, giving masses to the neutrinos via its couplings to two lepton $SU(2)_L$-doublets. This mechanism for neutrino mass generation is often referred to as the type-II seesaw mechanism [269–274].

In particular the "low scale" version of the type II seesaw mechanism, where the components of the triplet field have masses around the electroweak scale (or TeV scale), has implications for various well known observables at different energy scales, see e.g. [55, 56]. It may be embedded for instance in left-right symmetric extensions of the SM, with additional interesting phenomenology at the LHC, cf. refs. [275, 276], or studied in its minimal version with only one triplet Higgs added to the SM. Regarding the triplet Higgs field, its doubly charged component is of particular importance for phenomenology, since it can decay into a pair of same-sign charged leptons via the above mentioned lepton number violating Yukawa coupling (matrix) Y_Δ of the triplet to the lepton $SU(2)_L$-doublets. Detailed phenomenological studies of such signatures have been conducted for the LHC, e.g. in refs. [57–60], and also for a 100 TeV proton-proton collider in ref. [277].

Searches for prompt decays to same-sign lepton pairs and pair-produced doubly charged Higgs bosons have been performed at the LHC (for the different center-of-mass energies) [278–283], and similar analyses exist for LEP [61–63], and at the Tevatron [64–67]. Searches for same-sign W boson pairs have recently been performed at LHC in ref. [284]. Without any significant excess of events, the LHC analyses mentioned above presently provide stringent constraints from direct searches, which require the masses of the doubly charged scalars to be above $\sim$ 600 GeV (for the part of parameter space where Y_Δ is not too small). Moreover, searches at future lepton colliders could have the potential to discover doubly charged scalars with masses $\sim$ 1 TeV, provided the center-of-mass energy is 3 TeV, as discussed in ref. [285].

The possibility that the scalar particles do not decay promptly, but can be rather long lived, has important consequences for LHC searches: While the above mentioned strong constraints from prompt same-sign charged leptons can no longer be applied, one might consider them as heavy Stable Charged Particles (HSCPs) if their lifetime is sufficiently long for them to pass through the relevant parts of the detector, i.e. the muon system (or the tracker). The corresponding signature would be, among others, a characteristic energy deposition in the different subdetectors. Searches for HSCPs have been performed by ATLAS [68, 69] and CMS [70]. When the decays of a long lived particle

are non-prompt but occur inside the detector, one might also search for the displaced secondary vertices. This possibility has recently been discussed in ref. [71], where it has been claimed that the high-luminosity (HL) LHC can probe a broad part of the parameter space via such displaced vertex searches, restricted however severely by the HSCP constraints.

In this paper we discuss the current allowed parameter space of the minimal low scale type II seesaw model, taking into account all relevant constraints, including charged lepton flavour violation as well as various (prompt and non-prompt) collider searches. We calculate carefully the constraints from the prompt searches, taking into account only the simulated events which satisfy the "promptness" criteria applied in the experimental analyses. Reconsidering constraints from HSCP searches, we find that the existing analyses cannot be applied to the triplet components of the minimal type II seesaw because their lifetimes are not large enough to pass through a sufficient part of the detector. Finally, for the displaced vertex signature, we perform a detailed analysis at the reconstructed level, for a selected benchmark point. We find that already at the current run of the LHC, a discovery would be possible for the considered parameter point. At a future collider with higher center-of-mass energy like the FCC-hh/SppC [128, 133], the larger Lorentz factors and larger luminosities would further enhance the sensitivity of these displaced vertex searches.

11.2 THE MINIMAL TYPE II SEESAW EXTENSION OF THE STANDARD MODEL

In the minimal type-II seesaw model the scalar sector consists of the SM scalar $\Phi \sim (1,2,\frac{1}{2})$ and an additional triplet scalar field $\Delta \sim (1,3,2)$. Their matrix representation is given by:

$$\Phi = \begin{pmatrix} \Phi^+ \\ \Phi^0 \end{pmatrix} \text{ and } \Delta = \begin{pmatrix} \frac{\Delta^+}{\sqrt{2}} & \Delta^{++} \\ \Delta^0 & -\frac{\Delta^+}{\sqrt{2}} \end{pmatrix}. \tag{202}$$

The $SU(3)_C \times SU(2)_L \times U(1)_Y$ invariant Lagrangian for this scalar sector is

$$\mathcal{L} = (D_\mu \Phi)^\dagger (D^\mu \Phi) + Tr((D_\mu \Delta)^\dagger (D^\mu \Delta)) - V(\Phi, \Delta) - \mathcal{L}_{Yukawa} \tag{203}$$

with the covariant derivaties

$$D_\mu \Phi = \partial_\mu \Phi + i g T^a W_\mu^a \Phi + i \frac{g'}{2} B_\mu \Phi \tag{204}$$

$$D_\mu \Delta = \partial_\mu \Delta + i g [T_\mu^a, \Delta] + i \frac{g'}{2} B_\mu \Delta, \tag{205}$$

the scalar potential

$$\begin{aligned} V(\Phi, \Delta) = {} & \mu^2 \Phi^\dagger \Phi - M_T^2 Tr(\Delta^\dagger \Delta) - \frac{\lambda}{4} |\Phi^\dagger \Phi|^2 \\ & - \lambda_{HT} \Phi^\dagger \Phi Tr(\Delta^\dagger \Delta) - \lambda_T (Tr(\Delta^\dagger \Delta))^2 \\ & - \lambda'_T Tr((\Delta^\dagger \Delta)^2) - \lambda'_{HT} \Phi^\dagger \Delta \Delta^\dagger \Phi \\ & - (\kappa \Phi^\top i\sigma^2 \Delta^\dagger \Phi + h.c.) \end{aligned} \tag{206}$$

and the new Yukawa terms

$$\mathcal{L}_{Y_\Delta} = Y_\Delta \bar{\ell^c} i\sigma^2 \Delta \ell + \text{H.c.}\,. \tag{207}$$

After electroweak symmetry breaking both scalar fields acquire their vacuum expectation values (VEVs)

$$\langle \Phi \rangle = \frac{1}{\sqrt{2}} \begin{pmatrix} 0 \\ v \end{pmatrix} \text{ and } \langle \Delta \rangle = \frac{1}{\sqrt{2}} \begin{pmatrix} 0 & 0 \\ v_T & 0. \end{pmatrix}, \tag{208}$$

where (as we will see later) $v_T \ll v$. Evolving the scalar fields around their VEVs and minimizing the potential leads to seven physical massive eigenstates: $H^{\pm\pm}, H^\pm, h, H, A$. The three massless Goldstone bosons $G^\pm$ and G^0 are absorbed by the SM gauge bosons $W^\pm$ and Z. The masses for the physical Higgs bosons are

$$m^2_{H^{\pm\pm}} = \frac{\kappa v^2}{\sqrt{2} v_T} + \frac{\lambda'_{HT} v^2}{2} + \lambda'_T v_T^2 \tag{209}$$

$$m^2_{H^\pm} = \frac{\kappa v^2}{\sqrt{2} v_T} + \frac{\lambda'_{HT} v^2}{4} + \frac{\lambda'_{HT} v_T^2}{2} + \sqrt{2}\kappa v_T \tag{210}$$

$$m^2_h = \frac{1}{2}(A + C - \sqrt{(A-C)^2 + 4B^2}) \tag{211}$$

$$m^2_H = \frac{1}{2}(A + C + \sqrt{(A-C)^2 + 4B^2}), \tag{212}$$

with $A = -\frac{\lambda}{2} v^2$, $B = -(\lambda_{HT} + \lambda'_{HT}) v_T v - \sqrt{2}\kappa v$ and $C = \frac{\kappa v^2}{\sqrt{2} v_T} - 2(\lambda_T + \lambda'_T) v_T^2$, and

$$m^2_{A^0} = \frac{\kappa v^2}{\sqrt{2} v_T} + 2\sqrt{2}\kappa v_T. \tag{213}$$

PHYSICAL MASSES AND PARAMETER SPACE: The scalar potential and the new Yukawa term contain the following parameters: five coupling parameters λ, λ_{HT}, λ_T, λ'_T and λ'_{HT}, two mass parameters μ and M_T, the seesaw parameter κ (with mass dimension = 1), the VEVs v and v_T and the new Yukawa couplings matrix $(Y_\Delta)_{ij}$. The tadpole equations allow us to express μ and M_T in terms of the couplings and κ:

$$\mu^2 = -\sqrt{2}\kappa v_T + \frac{1}{2}(\lambda_{HT} + \lambda'_{HT}) v_T + \frac{1}{4}\lambda v^2\,, \tag{214}$$

$$M_T^2 = -(\lambda_T + \lambda'_T) v_T^2 - \frac{1}{2}(\lambda_{HT} + \lambda'_{HT}) v^2 + \frac{\kappa v^2}{\sqrt{2} v_T}. \tag{215}$$

In the following we fix the VEV v to the SM value $v \approx 246$ GeV. By solving the tadpole equations and taking the leading order in $\lambda^{(\prime)}_{HT} v_T/\kappa$ we obtain for v_T the relation

$$v_T = \frac{\kappa v^2}{\sqrt{2} M_T^2}\,. \tag{216}$$

Furthermore, we chose h to play the role of the SM Higgs boson (with the requirement that $m_h < m_H$), and we fix λ such that $m_h \sim 125$ GeV. Neglecting the terms in eq. (211) that are proportional to the triplet VEV v_T, we thus use the SM value for λ.

The contributions from the couplings λ_T and λ'_T to all the mass terms are suppressed by the triplet VEV v_T, and we will neglect this contribution in the following discussion. For definiteness, in our analyses we will fix the couplings in the following way: $\lambda_T = 0.1$ and $\lambda'_T = 0.2$. The masses of the singly charged scalar $H^\pm$ and the doubly charged scalar $H^{\pm\pm}$ depend only via the first term in eqs. (210) and (209) on λ'_{HT}, respectively. Their masses are fixed to the same scale by $\kappa v^2/v_T$, with a mass splitting $m_{H^\pm} - m_{H^{\pm\pm}} = -\lambda'_{HT} v^2/4 + \sqrt{2}\kappa v_T$, such that $m_{H^\pm}$ and $m_{H^{\pm\pm}}$ are effectively free parameters.

In the following, we allow in most cases for a non-zero λ'_{HT}, but we keep $\lambda'_{HT} < 0$ such that $H^{\pm\pm}$ is the lightest of the new scalars. The reason for this choice is that when we discuss potentially long-lived $H^{\pm\pm}$ (cf. section 11.4.3) it avoids additional decay modes, but allows to have $m_{H^{\pm\pm}}$ somewhat below m_h. Only for illustrating some of the phenomenological constraints we will make the simplifying assumption that $\lambda'_{HT} = 0$, which leads to nearly degenerate masses for all extra scalars (controlled by the parameters λ_{HT} and κ). We use Sarah [93] and Spheno [226, 227] for the evaluation of the model parameters and for the numerical calculation of the constraints from non-collider experiments in section 3.

11.3 CONSTRAINTS FROM NON-COLLIDER EXPERIMENTS

NEUTRINO MASSES: In the type-II seesaw model the active neutrinos acquire masses after electroweak symmetry breaking via the contributions from the new Yukawa term, yielding

$$m_\nu = Y_\Delta \sqrt{2} v_T = Y_\Delta \frac{\kappa v^2}{M_T^2}. \tag{217}$$

It is referred to as a "seesaw" model, because the light neutrino masses are inversely proportional to the triplet mass (squared).

Via eq. 217, the observed neutrino masses constrain the model parameters $(Y_\Delta)_{ij}$ and v_T. For a given neutrino mass ordering the Yukawa couplings can be obtained via

$$(Y_\Delta)_{ij} = \frac{1}{\sqrt{2} v_T} U^\dagger_{PMNS} m_\nu^{diag} U_{PMNS}, \tag{218}$$

where U_{PMNS} is the Pontecorvo-Maki-Nakagawa-Sakata matrix. In the following, normal hierarchy is assumed and best fit values for U_{PMNS} are used from [286, 287] (with the additional assumption of the Majorana phase being zero). Eq. (218) thus fixes the Yukawa couplings $(Y_\Delta)_{ij}$ for our choice of assumptions.

CONSTRAINTS ON v_T: From electroweak precision measurements the ρ parameter is measured to be $\rho \simeq 1.00037 \pm 0.00023$ [288]. In the model ρ can be written as

$$\rho = \frac{1 + \frac{2v_T^2}{v^2}}{1 + \frac{4v_T^2}{v^2}}, \tag{219}$$

which leads to an upper bound for the triplet VEV $v_T \lesssim 2.1$ GeV.

Z WIDTH: For a doubly charged mass, $m_{H^{\pm\pm}} < \frac{m_Z}{2}$ a new on-shell decay mode $Z \to H^{\pm\pm}H^{\mp\mp}$ is allowed. The LEP experiment constrained the allowed decay width of the Z boson into non-SM particles to be below 2 MeV at 95% CL, which implies the lower limit on the mass $m_{H^{\pm\pm}} > 42.9$ GeV [289].

LEPTON FLAVOR VIOLATING PROCESSES: In the type II seesaw model, lepton flavor violating (LFV) processes $\tau \to \bar{l}_i l_j l_k$ and $\mu \to \bar{e}ee$ can be mediated at tree level via $H^{\pm\pm}$ exchange. The contribution of the doubly charged scalars to the LFV branching ratio $BR(l_i \to l_k l_m l_n)$ is given by[290]:

$$BR(l_i \to \bar{l}_k l_m l_n) = \frac{|(Y_\Delta)_{mn}(Y_\Delta)_{ki}|^2}{64 G_f^2 m_{H^{\pm\pm}}^4}. \tag{220}$$

The most stringent bound arises from $\mu \to \bar{e}ee$ with $BR(\mu \to \bar{e}ee) < 1.0 \times 10^{-12}$ from the SINDRUM experiment [181]. Since the Yukawa couplings are inversely proportional to the triplet VEV, the experimental bounds constitute (for our choice of PMNS parameters and neutrino mass spectrum) a lower limit for v_T, e.g. $v_T > 8.8 \times 10^{-9}$ GeV, $v_T > 5.1 \times 10^{-9}$ GeV and $v_T > 3.1 \times 10^{-9}$ GeV for masses $m_{H^{\pm\pm}} = 150$ GeV, $m_{H^{\pm\pm}} = 300$ GeV and $m_{H^{\pm\pm}} = 600$ GeV respectively.

Also the lepton flavor violating process $\mu \to e\gamma$ receives contributions from loops with virtual H^+, H^-, ν_α or $H^{++}, H^{--} l_\alpha$, where the appearing couplings to the new scalars are inversely proportional to the triplet VEV. The MEG collaboration states the currently most stringent upper bound of $BR(\mu \to e\gamma) < 4.2 \times 10^{-13}$ [37] on the branching ratio of this process, which translates (for our choice of PMNS parameters and neutrino mass spectrum) into a lower limit of the triplet VEV of, e.g., $v_T > 4.8 \times 10^{-9}$ GeV, $v_T > 2.6 \times 10^{-9}$ GeV and $v_T > 1.6 \times 10^{-9}$ GeV for masses $m_{H^{\pm\pm}} = 150$ GeV, $m_{H^{\pm\pm}} = 300$ GeV and $m_{H^{\pm\pm}} = 600$ GeV respectively. A discussion of the dependence of the LFV constraints on the PMNS parameters and neutrino mass spectrum can be found e.g. in ref. [291, 292].

THE ANOMALOUS MAGNETIC MOMENT OF THE MUON: The anomalous magnetic moment of the muon was measured very precisely by the Muon g-2 collaboration [293]:

$$a_\mu^{exp} = 11659208.0(6.3) \times 10^{-10}.$$

The result deviates by about three standard deviations from the SM predicted value, given by [288]:

$$a_\mu^{SM} = 11659183 \times 10^{-10}.$$

The type II seesaw model modifies the theory prediction for this amplitude: At one loop level the amplitude receives new contributions from both $H^{\pm\pm}$ and $H^{\pm}$ as

$$\delta a_\mu(H^{\pm\pm}) = -\frac{2\left|(Y_\Delta)_{ij}(Y_\Delta)_{ij}\right|^2 m_\mu^2}{12\pi^2 m_{H^{\pm\pm}}^2},$$

$$\delta a_\mu(H^{\pm}) = -\frac{2\left|(Y_\Delta)_{ij}(Y_\Delta)_{ij}\right|^2 m_\mu^2}{96\pi^2 m_{H^{\pm}}^2}.$$

We notice that, in principle, the modified theory prediction could explain the observed value of a_μ for some range of the triplet mass and $v_T \lesssim 10^{-10}$ GeV. This region is, however, already excluded by the LFV experiments.

11.4 SIGNATURES FROM DOUBLY CHARGED SCALARS AT THE LHC

In the following, we will focus on the doubly charged scalar $H^{\pm\pm}$, which has the clearest collider signatures. Under our assumptions (cf. section 2), it is the lightest of the new scalars and can decay to two same-sign leptons, $H^{\pm\pm} \to l_\alpha^\pm l_\beta^\pm$, to two on-shell W-bosons, $H^{\pm\pm} \to W^\pm W^\pm$ or into the three body final states $H^{\pm\pm} \to W^\pm (W^\pm)^* \to W^\pm f\bar{f}'$, depending on the triplet VEV and the mass $m_{H^{\pm\pm}}$. For $v_T < 10^{-4}$ GeV the decay to two same-sign leptons is dominant, cf. e.g. [294]. The production cross sections for all production modes of the triplet components are shown in fig. 40 for $\sqrt{s} = 13$ TeV and the example value $v_T = 0.1$ GeV, fixing $\lambda'_{HT} = 0$ for illustration (such that $m_{H^\pm} = m_{H^{\pm\pm}}$). The corresponding Feynman diagrams are shown in fig. 41.

As one can see from fig. 40, the production cross section for the s-channel charged current process $pp \to W^\pm \to H^{\pm\pm}H^\mp$ is twice the production through the neutral current process $pp \to Z^*/\gamma^* \to H^{++}H^{--}$. In comparison, the t-channel production cross section is subdominant for small $m_{H^{\pm\pm}}$, but falls off less strongly with $m_{H^{\pm\pm}}$ such that $pp \to W^\pm W^\mp \to H^{++}H^{--}$ dominates above about 300 GeV. The t-channel production of a single $H^{\pm\pm}$ is suppressed by the triplet VEV (which in the plot is chosen as $v_T = 0.1$).

We remark that, although we will focus on searches for doubly charged scalars, also the singly charged scalars are subject to LHC searches. Here, due to the large backgrounds from single top, $t\bar{t}$, and multi-vector bosons, these searches are not as stringent compared to those for the doubly charged scalars, see e.g. ref. [295] and references therein.

11.4.1 *Impact on the Higgs-to-diphoton rate*

The decay of the (SM-like) Higgs boson into two photons is introduced at the one-loop level in the SM, and it is dominated by the contribution from top quarks and the gauge bosons $W^\pm$. In the SM the contribution of $W^\pm$ is dominant, the contribution from top quarks is smaller and has opposite sign.

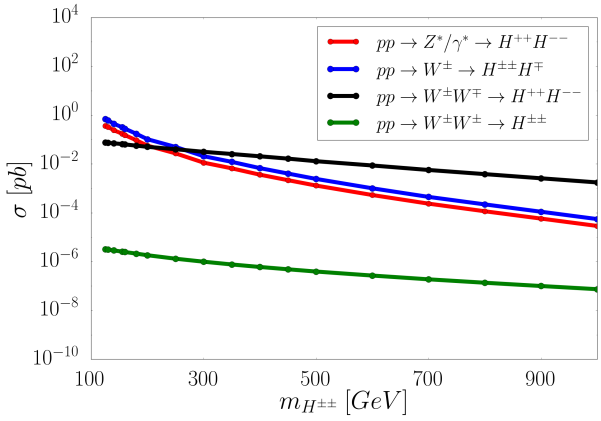

Figure 40: Production cross section for the dominant production channels at the LHC with $\sqrt{s} = 13$ TeV, the example values $v_T = 0.1$ GeV for the triplet Higgs vev and $\lambda'_{HT} = 0$.

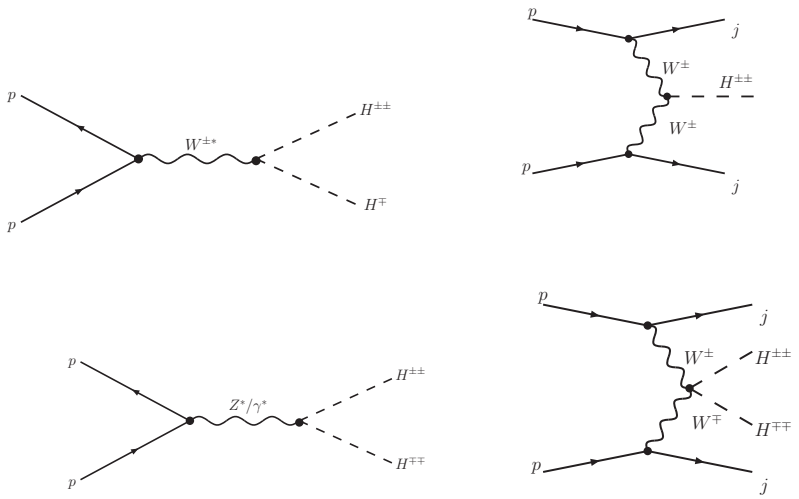

Figure 41: Dominant Feynman diagrams for the production of doubly charged scalers $H^{\pm\pm}$ (i.e. the doubly charged components of the triplet Higgs field Δ in the minimal type II seesaw mechanism) via neutral and charged current interactions.

The contributions from the doubly and singly charged scalars are proportional to the couplings

$$g_{hH^{++}H^{--}} \approx \frac{v^2}{m^2_{H^{\pm\pm}}}\lambda_{HT}\,, \quad g_{hH^{+}H^{-}} \approx \frac{v^2}{m^2_{H^{\pm}}}(\lambda_{HT} + \tfrac{1}{2}\lambda'_{HT})\,, \tag{221}$$

where we neglected a suppressed dependency on the mixing angle of the CP-even components from the doublet and triplet scalar fields, which is assumed to be small.

The currently reported signal strength from CMS in terms of the SM prediction is given by $\mu = \frac{\sigma^{exp}(h\to\gamma\gamma)}{\sigma^{SM}(h\to\gamma\gamma)} = 1.1^{+0.32}_{-0.3}$ [296], which limits the contribution from the doubly and singly charged scalars to be less than 100% of the SM predicted value. There is a broad region of parameters λ_{HT} and λ'_{HT} where this is satisfied (cf. e.g. [297]).

11.4.2 *LHC searches for prompt $H^{\pm\pm}$ decays*

SEARCHES FOR SAME-SIGN LEPTON PAIRS: At the LHC, searches for decays to same-sign leptons have been performed at center-of-mass energies $\sqrt{s} = 7$ TeV, 8 TeV and 13 TeV [278–283]. For $m_{H^{\pm\pm}} > 300$ GeV, the strongest constraints stem from the data sets with 36.1/fb at $\sqrt{s} = 13$ TeV for same-sign ee, $\mu\mu$, $e\mu$ pairs from decaying $H^{++}H^{--}$ pairs. In the following we use the bounds from the ATLAS analyses. Their negative search results put stringent bounds on the production cross section of the doubly charged Higgs bosons. When $H^{\pm\pm} \to l^{\pm}_{\alpha} l^{\pm}_{\beta}$ is the dominant decay mode, i.e. as long as Y_Δ is not too small (or v_T is below $\sim 10^{-4}$ GeV), the cross section depends only on $m_{H^{\pm\pm}}$, and values of $m_{H^{\pm\pm}}$ below about 620 GeV can be excluded.

It is important to stress that the analyses mentioned above require the $H^{\pm\pm}$ to decay promptly to three different modes, same-sign ee, $\mu\mu$ and $e\mu$. The most stringent constraint for $m_{H^{\pm\pm}} < 300$ GeV comes from the di-muon final state searches with 8 TeV (e.g. from the ATLAS analysis in ref. [280]), where the "promptness" condition is defined via the longitudinal impact parameter z_0 and the (transverse) impact parameter d_0 of the reconstructed track as

$$\begin{aligned} &|z_0 \times \sin\theta| < 1 \text{ mm} \text{ and} \\ &|d_0| < 0.2 \text{ mm}\,. \end{aligned} \tag{222}$$

When we apply the constraints on the cross section from prompt same-sign lepton pair searches where the $H^{\pm\pm}$ might be comparatively long-lived, we take only the fraction of events into account which satisfy these "promptness" criteria. We will discuss this in detail in the next section.

SEARCHES FOR SAME-SIGN W PAIRS: In ref. [284] a search for pairs of W bosons has been performed at ATLAS with 36.1/fb. Only the region where the W decays are dominant and the W bosons are on-shell has been considered. No excess above the SM predictions has been found. This leads to an exclusion of the mass region where $m_{H^{\pm\pm}}$ lies between 200 and 220 GeV for $BR(H^{\pm\pm} \to W^{\pm}W^{\pm}) \sim 1$, which is satisfied for $v_T \gtrsim 3 \times 10^{-4}$ GeV.

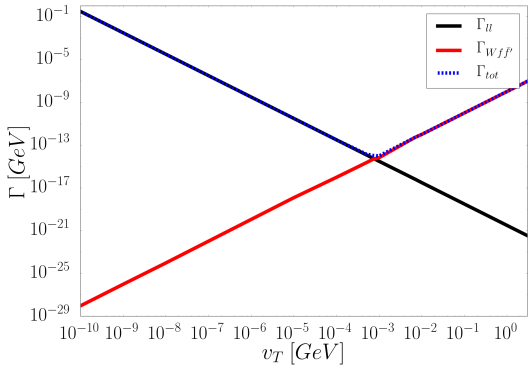

Figure 42: Total decay width of the doubly charged scalar field $H^{\pm\pm}$ as a function of the triplet VEV v_T for $m_{H^{\pm\pm}} = 130$ GeV (blue). Red and black lines are partial decay widths for $H^{\pm\pm} \to l^{\pm}l^{\pm}$ and $H^{\pm\pm} \to W^{\pm}(W^{\pm})^* \to W^{\pm}ff'$ respectively.

11.4.3 *Signatures of long-lived* $H^{\pm\pm}$

LIFETIME OF THE DOUBLY CHARGED SCALARS AT THE LHC: For parameter values of the triplet VEV $v_T \lesssim 10^{-4}$ GeV, the decay of $H^{\pm\pm}$ into a pair of same-sign leptons is dominant (since $Y_\Delta \propto 1/v_T$). For larger v_T and the scalar mass $m_{H^{\pm\pm}} \lesssim 160$ GeV, the dominant decay to on-shell $W^{\pm}W^{\pm}$ is kinematically forbidden and the $H^{\pm\pm}$ decays mainly via $H^{\pm\pm} \to W^{\pm}(W^{\pm})^* \to W^{\pm}f\bar{f}'$, where f' is the isospin partner of the fermion f. The decay into a pair of same-sign leptons is proportional to Y_Δ and dominates for smaller value of v_T. The rate of three body decays $H^{\pm\pm} \to W^{\pm}(W^{\pm})^* \to W^{\pm}f\bar{f}'$ is proportional to v_T [298],

$$\Gamma(H^{\pm\pm} \to W^{\pm}(W^{\pm})^* \to W^{\pm}f\bar{f}') = \frac{g^6 v_T^2 m_{H^{\pm\pm}}}{6144\pi^3}\left(3 + N_c \sum_{q,q'} |V_{q,q'}|^2\right) F\left(\frac{m_W^2}{m_{H^{\pm\pm}}^2}\right), \tag{223}$$

with N_c being the color factor and the factor of 3 stems from the sum over the three lepton generations. The function $F(m_W^2/m_{H^{\pm\pm}}^2)$ is given in Ref. [298]. For the numerical analysis, we use the decay rate calculated with MadGraph [92]. Fig. 42 shows the total decay width (blue dotted line) as a function of v_T for $m_{H^{\pm\pm}} = 130$ GeV, where the red and black lines are the partial decay width for three body and same-sign di-leptons respectively. One can get a minimal total decay width (and hence a maximal lifetime) at the point where the two lines cross, which (for $m_{H^{\pm\pm}} = 130$ GeV) is at $v_T \sim 10^{-3}$ GeV.

The resulting small total decay width gives rise to lifetimes for the $H^{\pm\pm}$ particles that can be macroscopic for certain parameter choices. We show the proper lifetime as a function of $m_{H^{\pm\pm}}$ and v_T in fig. 43. It can be seen that between $v_T \sim 1 \times 10^{-4}$ GeV and $v_T \sim 1 \times 10^{-3}$ GeV and $m_{H^{\pm\pm}} < 155$ GeV a proper decay length above 1 mm is possible.

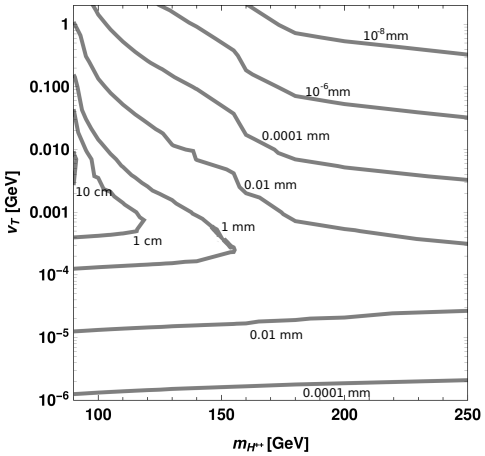

Figure 43: Contours of proper lifetime of the doubly charged scalar particle $H^{\pm\pm}$ as a function of its mass and the triplet VEV v_T.

DISPLACED VERTEX PROBABILITIES: The number of displaced $H^{\pm\pm}$ decays for a given parameter point can be expressed as:

$$N(x_1, x_2, \sqrt{s}, \mathcal{L}) = P(x_1, x_2)\sigma_{H^{\pm\pm}}(\sqrt{s})\mathcal{L}, \tag{224}$$

with $\sigma_{H^{\pm\pm}}(\sqrt{s})$ being the inclusive production cross section of a single $H^{\pm\pm}$, and $\mathcal{L}$ being the considered integrated luminosity. $P(x_1, x_2)$ is the probability for a particle with a given proper lifetime τ to decay within given boundaries in the detector, defined by the range $x_1 \leqslant x \leqslant x_2$. It is given by:

$$P(x_1, x_2) = \int_{x_1}^{x_2} dx \frac{1}{c\tau\sqrt{\gamma^2 - 1}} e^{\left(-\frac{x}{c\tau\sqrt{\gamma^2-1}}\right)} = e^{-\frac{x_1}{\Delta x_{lab}}} - e^{-\frac{x_2}{\Delta x_{lab}}}. \tag{225}$$

where Δx_{lab} is the decay length in the laboratory frame given by (with the Lorentz factor γ)

$$\Delta x_{lab} = |\vec{v}|\,\tau_{lab} = c\tau\sqrt{\gamma^2 - 1}\,, \tag{226}$$

and $\tau = \hbar/\Gamma$ with the total decay width Γ. For the Lorentz factor γ of $H^{\pm\pm}$ we use average values obtained from simulations with MadGraph [143]. For the current LHC run at center-of-mass energy 13 TeV, the HL-LHC at a center-of-mass energy 14 TeV, and for the FCC-hh with center-of-mass energy 100 TeV the average γ is shown as a function of $m_{H^{\pm\pm}}$ in fig. 44.

For a first look at the prospects for displaced vertex searches, we consider the HL-LHC with $\sqrt{s} = 14$ TeV and the FCC-hh with 100 TeV, and integrated luminosities of 3000 fb^{-1} and 20 ab^{-1}. We use eq. (224) with the average Lorentz factors from fig. 44, and the boundaries $x_1 = 1$ mm and $x_2 = 1$ m. The numbers of displaced events are shown in fig. 45 as a function of $m_{H^{\pm\pm}}$ and v_T. We remark that this first look is on the parton level and serves illustrative purposes only.

In the next section we will describe a possible LHC analysis to search for long lived doubly charged scalar bosons with $v_T = 5\times10^{-4}$ GeV and $m_{H^{\pm\pm}} = 130$ GeV, where $c\tau \approx 1$ cm. We will consider the pair production of doubly

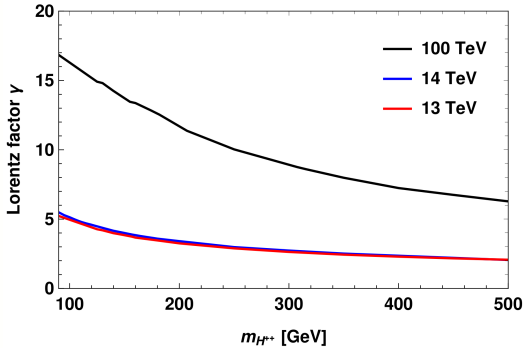

Figure 44: Average Lorentz factor γ as a function of $m_{H^{\pm\pm}}$ for $\sqrt{s} = 13$ TeV, 14 TeV and 100 TeV.

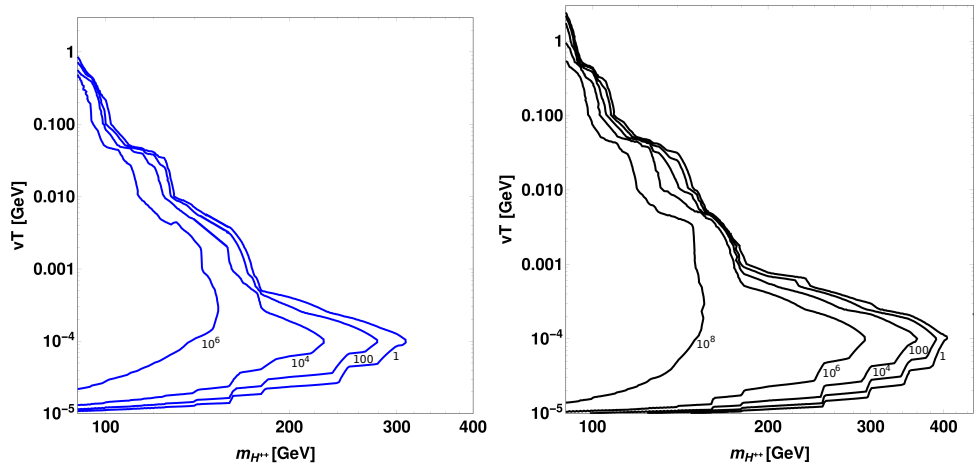

Figure 45: Total number of doubly charged Higgs bosons decaying with a displacement between the boundaries $x_1 = 1$ mm and $x_2 = 1$ m, for the HL-LHC (left) and the FCC-hh (right). For this figure we consider the production channel $pp \to \gamma^*/Z^* \to H^{\pm\pm}H^{\mp\mp}$ only.

charged scalar through the neutral current $pp \to \gamma^*/Z^* \to H^{\pm\pm}H^{\mp\mp}$ with two pairs of same sign di-lepton in the final state.

We like to note that although the single production of a $H^{\pm\pm}$ in association with a single charged Higgs boson has a larger cross section (by a factor 2), it is not expected to significantly increase the prospects for a displaced vertex discovery. The reason is that the reconstruction of the single charged $H^{\pm}$ is not efficient since it decays mainly to a tau lepton and missing energy. We will therefore focus on the production channel $pp \to \gamma^*/Z^* \to H^{\pm\pm}H^{\mp\mp}$.

APPLICATION OF CONSTRAINTS FROM PROMPT SEARCHES TO POTENTIALLY LONG-LIVED $H^{\pm\pm}$: As mentioned in the previous section, when applying the constraints on the $H^{\pm\pm}$ production cross section we have to take care that we only count the events where the "promptness" criteria of eq. 222 are satisfied. We did this by simulating samples of events for the relevant parameter points to obtain the fraction of events which (for the given parameter point) satisfy the "promptness" criteria. This fraction is then multiplied with the total production cross section to obtain the "effective" production cross section

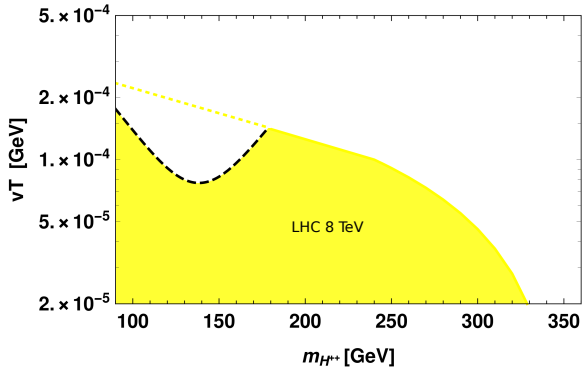

Figure 46: Parameter space constraints from prompt LHC ($\sqrt{s} = 8$ TeV) searches for same-sign dileptons at 95% confidence level [280], taking the possible displacement into account. The dashed black line indicates where the effective cross section is smaller than the observed limit. The dotted yellow line shows where the limit from the prompt search would be if all decays were prompt.

to be compared with the constraints from the experimental analysis [280]. To simulate samples for a wide range of parameter points, we performed a fast detector simulation using the same cuts as in [280], and extracted $|z_0 \times \sin\theta|$ as well as the impact parameter d_0. The resulting excluded region from prompt searches for decays $H^{\pm\pm} \to l^{\pm}_{\alpha} l^{\pm}_{\beta}$ is shown in fig. 46 as a function of $m_{H^{\pm\pm}}$ and v_T.

SEARCHES FOR HEAVY STABLE CHARGED PARTICLES AT THE LHC: Searches for heavy stable charged particles (HSCPs) have been performed by ATLAS (cf. e.g. [68, 69]) and CMS (cf. e.g. [70]). They require that the HSCP candidate are stable on collider scales, i.e. they pass the relevant parts of the detector. For the ATLAS analysis, the HSCP candidate has to pass the muon system, while the CMS performed two versions of the analysis, one where the tracks have to pass the muon system, and a "tracker only" analysis where they only have to pass through the tracker (such that multiple hits in the tracker can be recorded). However, while the ATLAS analysis goes down to 50 GeV, the CMS analysis only starts at 100 GeV, and for HSCP candidates with $Q = 2e$, they assume the candidate to be a lepton-like fermion (not a scalar as in our case). For a well reconstructed track the signature is a characteristic ionization energy loss (dE/dx).

To evaluate the constraint on the production cross section for $H^{\pm\pm}$ from HSCP searches, we must only count the events where the $H^{\pm\pm}$ actually pass through the relevant parts of the detector. This means, we have to use the "effective" cross section $P(x_1, x_2)\sigma$ (cf. eq. (225)) with x_1 being the outer radius of the respective detector part, and $x_2 = \infty$, i.e. the probability

$$P(x_1, \infty) = e^{-\frac{x_1}{\Delta x_{\text{lab}}}} . \tag{227}$$

For example, for $\gamma \sim 4$, $m_{H^{\pm\pm}} = 130$ GeV, $v_T = 5 \times 10^{-4}$ GeV, i.e. the benchmark point we will consider in the next section, we roughly get $P(1\,\text{m}, \infty) \sim 10^{-47}$ (for passing the tracker) and $P(11\,\text{m}, \infty) \sim 10^{-182}$ (for passing the muon sys-

tem). This clearly means that HSCP constraints cannot exclude this parameter point (in contrast to what has been claimed recently in [71]). On the other hand, for $m_{H^{\pm\pm}} = 90$ GeV, $v_T = 7.5 \times 10^{-4}$ GeV, where $c\tau \sim 35$ cm and $\gamma \sim 5$, one obtains $P(1\,\mathrm{m}, \infty) \sim 0.56$ and $P(11\,\mathrm{m}, \infty) \sim 10^{-3}$. Also this parameter point is not excluded by the ATLAS analysis which requires a track that passes the muon system, whereas a "tracker only" analysis (as performed by CMS) could quite likely exclude it. So far, however, this analysis does not exist for such low masses and for doubly charged scalars. It would therefore be highly desirable to extend the search to scalars with lower masses, and ideally also to the case of finite lifetimes.

Finally, we note that HSCPs can be searched for very well in the particularly clean environment of a lepton collider. At LEP, these searches have been done, cf. refs. [299–301] (cf. also ref. [61] for prompt searches). They put stringent limits on the production cross section of heavy charged particles that manage to escape from the detector and exclude them for masses up to the kinematic limit of ~ 90 GeV. For finite lifetimes one may also reconsider these limits, however we expect that in the cleaner environment of a lepton collider a $H^{\pm\pm}$ with $m_{H^{\pm\pm}} \lesssim 90$ GeV would not have been missed. In the following, we will therefore focus on $H^{\pm\pm}$ masses above this value.

11.5 SUMMARY OF PRESENT CONSTRAINTS

We summarise the present constraints on doubly charged scalars $H^{\pm\pm}$ in the low scale type II seesaw scenario (under the simplifying assumptions discussed in section 2) in fig. 47. The various constraints have been discussed in the previous sections.

- We find that for 10^{-5} GeV $\lesssim v_T \lesssim 10^{-1}$ GeV and $m_{H^{\pm\pm}} \lesssim 200$ GeV there exists an allowed region where the $H^{\pm\pm}$ is long-lived and not excluded by neither prompt searches at LHC nor by the constraints from the existing HSCP analyses.
- When the triplet vacuum expectation value is $v_T > 10^{-4}$ GeV, the decays $H^{\pm\pm} \to W^{\pm}W^{\pm}$ start to dominate the branching ratio, and the number of prompt decays $H^{\pm\pm} \to l^{\pm}_{\alpha} l^{\pm}_{\beta}$ is suppressed. Searches for di-W bosons are efficient only in the narrow range of $200\,\mathrm{GeV} \lesssim m_{H^{\pm\pm}} \lesssim 220\,\mathrm{GeV}$ [284], which is shown by the purple area in fig. 47.
- Finally, for $m_{H^{\pm\pm}} \gtrsim 620$ GeV, constraints from LFV processes are the most powerful, constraining v_T to be above about $\mathcal{O}(10^{-9})$ GeV for $m_{H^{\pm\pm}} \sim 700$ GeV.

It is striking that the part of parameter space where $v_T > 10^{-4}$ GeV is still largely untested by current experiments. However, this is the region where the low type II seesaw mechanism could be motivated by an approximate "lepton number"-like symmetry. The symmetry would suppress the Yukawa couplings of the triplet to the lepton doublets and can thus provide a "natural" explanation for the smallness of the observed neutrino masses (in the t'Hooft sense that neutrino masses go to zero when the approximate symmetry is

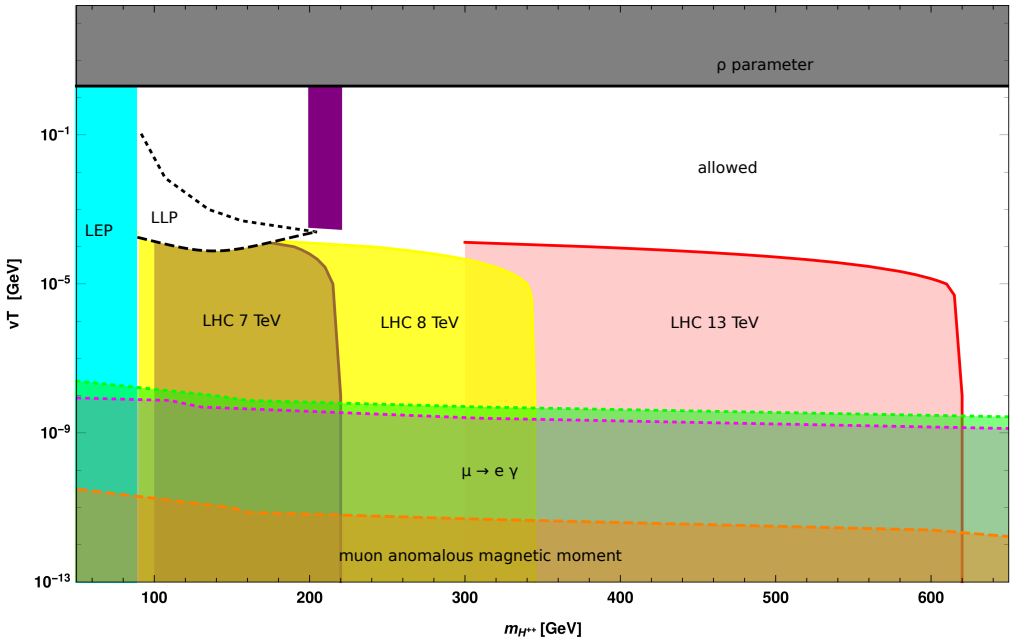

Figure 47: Parameter space of the type-II seesaw model. The black area in top is excluded because of the ρ parameter. The cyan vertical area is the estimate for the excluded region by searches at LEP. The orange region on the bottom is excluded by the experimental measurement for the muon anomalous magnetic moment. The magenta area is excluded by $\mu \to e\gamma$ (for our example choice of PMNS parameters and neutrino mass spectrum) and the green area is excluded by constraints on $\mu \to \bar{e}ee$. The red, yellow and brown areas are excluded by the LHC searches for same sign di-lepton final states at 7, 8 and 13 TeV. The purple area is excluded by LHC searches for same-sign W bosons. Finally, the white area is allowed. The part of the white area inside the dashed and dotted black lines on the left (denoted by LLP) features displaced decays from long-lived $H^{\pm\pm}$. The lower dashed line is obtained from the limit on the prompt decays as described in the main text. The upper dotted line (where no experimental constraints exist to date) shows the region where $c\tau > 1$ mm. Above this line the dominant decay is the three-body decay to $W^{\pm} f \bar{f}'$.

restored).[1] Searches for displaced vertex signatures, as discussed in the next section, can help to probe part of this physically well-motivated parameter space.

11.6 DISPLACED VERTEX SIGNATURE: ANALYSIS FOR A BENCHMARK POINT

To study in detail the prospect for displaced vertex searches from $H^{\pm\pm}$ decays, we perform an analysis at the reconstructed level. As benchmark point we consider $v_T = 5\times10^{-4}$ GeV and $m_{H^{\pm\pm}} = 130$ GeV, and for definiteness $\lambda'_{HT} = 0$ and the other parameters fixed as discussed in section 2. For this benchmark point with $c\tau \approx 1$ cm, we consider the three different hadron colliders: the LHC with 13 TeV center-of-mass energy and integrated luminosity 100 fb^{-1}, the HL-LHC with 14 TeV center-of-mass energy and integrated luminosity 3000 fb^{-1}, and the FCC-hh with 100 TeV center-of-mass energy and integrated luminosity 20 ab^{-1}. For each of these colliders we generate a Monte Carlo event sample with 10^6 events, using pileup events = 50 per vertex. The Monte Carlo simulations of signal and background is carried out with the event generator MadGraph5 version 2.4.3 [143]. For parton shower and hadronisation we use Pythia6 [144], while the fast detector simulation is carried out by Delphes [97].

EVENT RECONSTRUCTION EFFICIENCY: For lifetimes as small as for the here considered benchmark point the $H^{\pm\pm}$ decays dominantly within the first (few) layers of the pixel tracker, and we consider the corresponding reconstruction efficiency to be equal to those of prompt signatures. We note that the track-only analysis is not sufficient to probe parameter points with such small lifetimes.

In general, for benchmark points with larger lifetimes the $H^{\pm\pm}$ decays may occur anywhere in the detector system, e.g. in the ECAL or in the muon system. The particle ID algorithms, which depend on the full detector information, are thus non-trivially affected by the displacement of each event. Since our parent particle is electrically charged and has a very characteristic dE/dx we assume, however, that 100% of its decays can be detected and identified, provided they are being caught by the triggers and the analysis selection requirements.

SELECTION REQUIREMENTS: For signal event selection we require at least one pair of charged tracks for the final state leptons, with lepton transverse momenta $P_T(\mu) > 25$ GeV and $|\eta(\mu)| < 2.5$. We consider here only muons for simplicity, also in parts because it is not clear to us what kind of signal an electron would cause that appears inside the HCAL or muon system. We use a muon isolation cone radius of 0.1 and we impose a cut of $\Delta R > 0.2$ between two same sign muons to ensure their separation. To increase the cut efficiency we impose further a cut on the invariant dimuon mass to be $M_{\mu\mu} = m_{H^{\pm\pm}} \pm 20$ GeV.

1 An alternative option consists in assigning lepton number to the triplet Higgs field. Then the parameter κ for the coupling to the Higgs doublets would be suppressed by the approximate symmetry. This part of parameter space for the low type II seesaw mechanism is strongly constrained by LFV bounds.

Furthermore, we require at least one displaced decay with same sign dimuons with a displacement in the XY plane $L_{xy} > 8$ mm and the impact parameter $d_0 > 4$ mm. This is expected to remove possible SM backgrounds and detector effects [10, 302, 303]. Finally, a matching condition between our reconstructed events and generator level events is imposed to ensure that the reconstructed tracks stem from the $H^{\pm\pm}$ candidate. Therefore we require the difference $\Delta R(H^{\pm\pm})$ of reconstructed and generator events to be $\Delta R(H^{\pm\pm}) < 0.1$ [10].

RESULTS: From the simulated event samples we reconstruct the $H^{\pm\pm}$ track and its displacement parameters from the observed distribution of the same-sign lepton pairs on an event-by-event basis. Fig 48 shows the resulting displacement of the secondary vertex (defined by the $H^{\pm\pm}$ decay) and the transverse momentum of the $H^{\pm\pm}$ candidate. In fig. 49 we show the invariant mass of the lepton pair (here two muons) and the transverse displacement of the secondary vertex. All histograms are normalized to the expected number of events at the LHC, HL-LHC and FCC-hh, considering the corresponding integrated luminosity, before applying any cuts.

After applying the selection cuts, the cut flow of which is shown in tab. 13, we find that about 13 events remain in the LHC data set, while for the HL-LHC and FCC-hh as many as ~ 500 and ~ 32000 events remain that are conform with our selection criteria. It is worth mentioning that, while the same benchmark point is used for different detector simulation and normalization factors (cross section$\times$ integrated luminosity), the detector dimensions as well the different value of the Lorentz factor γ affect the analysis, greatly enhancing the number of signal events at the FCC-hh.

Table 13: Cut flow of simulated signal samples for displaced decays of the $H^{\pm\pm}$ to same sign dimuons. For this table, the benchmark point with $v_T = 5\times10^{-4}$ GeV and $m_{H^{\pm\pm}} = 130$ GeV was considered. For the LHC, HL-LHC, and FCC-hh we use 13, 14, and 100 TeV center-of-mass energy and an integrated luminosity of 100 fb^{-1}, 3000 fb^{-1}, and 20 ab^{-1}, respectively. In our analysis we consider the production channel $pp \to \gamma^* Z^* \to H^{\pm\pm}H^{\mp\mp}$ only.

Cuts	LHC	HL-LHC	FCC-hh
Expected events (detector level)	280	10640	345323
Two same sign muons	220	8135	244050
$P_T(\mu) > 25$ GeV&$\lvert\eta(\mu)\rvert < 2.5$&$\Delta R(\mu,\mu) > 0.2$	180	6508	209883
110 GeV$< m_{H^{\pm\pm}} <$ 150 GeV	175	6332	203586
$L_{xy} > 8$ mm	76	2749	105864
$d0 > 4$ mm	13.6	467	31759

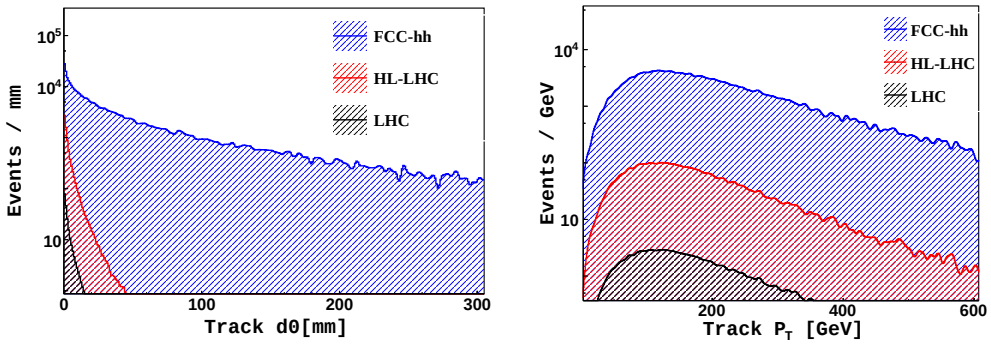

Figure 48: Results from our simulations before applying any cuts. Left: impact parameter of the reconstructed track of $H^{\pm\pm}$ decaying to di-muons. Right: transverse momentum of the reconstructed track.

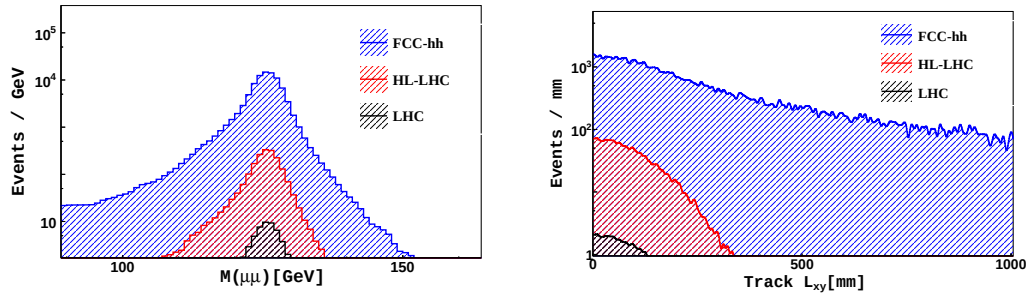

Figure 49: Results from our simulations before applying any cuts. Left: invariant mass of $H^{\pm\pm}$ decaying to two muons final state. Right: longitudinal length of $H^{\pm\pm}$ decaying to two muons.

11.7 CONCLUSIONS

In this paper we have investigated present constraints and displaced vertex signature prospects in the low scale type II seesaw mechanism, which is an attractive way to generate the observed light neutrino masses. It postulates a $SU(2)_L$-triplet scalar field, which obtains an induced vacuum expectation value after electroweak symmetry breaking, giving masses to the neutrinos via its couplings to two lepton $SU(2)_L$-doublets.

Taking into account all relevant present constraints, including charged lepton flavour violation as well as collider searches, we have discussed the current allowed parameter space of the minimal low scale type II seesaw model. We investigated the possibility that the triplet components can be long lived, and calculated carefully the constraints from the prompt searches, taking into account only the simulated events which satisfy the "promptness" criteria applied in the experimental analyses.

We have also reconsidered constraints from present HSCP searches. We find that for most of the relevant parameter space for the long lived doubly charged scalars they cannot be applied because the lifetimes are not large enough to pass through the relevant parts of the detector. Nevertheless, such searches could test the part of the parameter space with lifetimes above a few cm via a

"tracker only" analysis. Such analyses applicable to long lived doubly charged scalars do not exist but would be very desirable.

For 10^{-5} GeV $\lesssim v_T \lesssim 10^{-1}$ GeV and $m_{H^{\pm\pm}} \lesssim 200$ GeV, there exists an allowed region where the $H^{\pm\pm}$ is long-lived and not excluded by neither prompt searches at LHC nor by the constraints from the existing HSCP analyses.

For the characteristic displaced vertex signature where the doubly-charged component decays into same-sign charged leptons, we have performed a detailed analysis at the reconstructed level for a selected benchmark, which has a lifetime about 1 cm such that "tracker only" analyses are not efficient and additional information from secondary vertex reconstruction is necessary. We found that already in present LHC data with 100 fb^{-1} about 13 events may be detected in this way. Furthermore, the HL-LHC and FCC-hh have prospects to discover up to $\sim$ 500 and $\sim$ 32000 events in their final data sets, respectively. Aside from the enhanced production cross sections and luminosities, the larger Lorentz factors at the FCC-hh/SppC [128, 133] would lead to discovery prospects in an enlarged part of parameter space.

Finally, we like to point out that the symmetry protected low scale type II seesaw scenario, where an approximate "lepton number"-like symmetry suppresses the Yukawa couplings of the triplet to the lepton doublets, is still largely untested by the current LHC results. Searches for displaced vertex signatures can help to probe part of this physically well-motivated parameter space.

Acknowledgements

We are thankful to the organizers and participants the LHC LLP workshops for the stimulating atmosphere and many useful discussions. This work has been supported by the Swiss National Science Foundation. O.F. received funding from the European Unions Horizon 2020 research and innovation program under the Marie Sklodowska-Curie grant agreement No 674896 (Elusives).

Part IV

SUMMARY AND CONCLUSION

12

SUMMARY AND CONCLUSION

The standard model successfully describes an impressive amount of data, but there are experimental and theoretical reasons that call for extensions. Experimentally, the SM is inadequate for describing the observed pattern of neutrino oscillation. If we insist to sustain the SM field contents, the simplest way to account for neutrino mass is to add right-handed neutrinos forming the seesaw mechanism. Low scale seesaw scenarios give a natural explanation for the smallness of neutrino masses in terms of symmetries. If the lepton number like symmetry is protected, it allows for sizable active-sterlie mixing angles which make this scenario testable at the current and future colliders. In this dissertation, we investigated the widely discussed signatures from sterile neutrinos at colliders. The dominating production processes of the sterile neutrinos feature unambiguous signals for lepton number violation at proton-proton and electron-proton colliders. We investigated the sensitivity of electron-proton colliders for charged lepton flavor violation in an effective theory approach. We considered a general effective Lagrangian for the conversion of an electron into a muon or a tau via the effective coupling to a neutral gauge boson or a neutral scalar field. As an example model where such flavor changing neutral current operators are generated at loop level, we considered the low scale seesaw scenario to test the LHeC sensitivity to the active-sterile mixing parameters.

On the other hand, the hierarchy problem and possible improvement of the meta-stable SM vacuum motivate an extension to the SM scalar sector. The easiest way is to extend the SM scalar sector by a $SU(2)_L$ singlet, doublet or triplet. So far, all measurements of the observed Higgs boson properties are in agreement with the SM Higgs boson characteristics where the mixing between the SM Higgs boson and the extra scalar is highly suppressed. Thus, the features of the additional scalars can be easily captured at colliders due to the modification of the SM Higgs boson properties or even via direct search for extra scalar signatures at colliders. Accordingly, we studied the prospects of the proposed LHeC in the search for heavy neutral singlet scalar particles. Also, we investigated the sensitivity of the high luminosity phase of the LHC for probing various signatures of the additional $SU(2)_L$ doublet and triplet components.

In this dissertation, we presented various studies for sterile neutrinos and heavy scalars at different current and future colliders which we summarize as follows:

In chapter 6, we investigated one of the most promising sterile neutrino signatures at the proton-proton colliders, the Lepton Number Violation (LFV) but Lepton Number conservation (LNC) final states $e^{\pm}\mu^{\mp}jj$. One of the main advantages of this process is that it is not contaminated from the SM background, such that the signal and the backgrounds can be distinguished via multivariate

analysis utilizing the BDT. For event generation, we assumed that the active-sterile mixings $|\theta_e|^2 = |\theta_\mu|^2$ and $|\theta_\tau|^2 = 0$. We remark that the signature of the process under consideration is sensitive to $|\theta_e\theta_\mu|^2/|\theta|^2$. We considered the High Luminosity phase of the LHC (HL-LHC) and the Future Circular Collider (FCC-hh) with $\sqrt{s} = 14$ and 100 TeV and total integrated luminosity of 3 and 20 ab^{-1}. Kinematic observables are constructed from each event and fed into a multivariate analysis tool to perform a BDT analysis. In this study, we derived the 1,2,3 and 5 σ limits on the total production cross section and recast it as limit on the active-sterile mixing parameters. We found that the systematic uncertainties affect smaller sterile neutrino masses more than the larger ones. In particular, this effect is relevant when $M_N < 400$ (600) GeV at the HL-LHC (FCC-hh). For 200 GeV mass, the limits can be weakened greatly by adding a 10% systematic uncertainty on the background. Therefore, controlling the systematic uncertainty at the future proton-proton colliders will be very important to enhance the discovery potential for sterile neutrinos with small masses. Our analysis reported the 5 σ sensitivity on the active-sterile mixing parameters for fixed sterile neutrino mass $M_N = 500$ GeV, down to 1.7×10^{-2} for the HL-LHC and 1.9×10^{-4} for the FCC-hh.

In chapter 7, we have analyzed two of the most promising signatures of heavy neutrinos at ep colliders: the LFV lepton-trijet signature $pe^- \to \mu^- + 3j$ and the displaced vertex signature. The latter is particularly relevant for heavy neutrino masses below m_W , where the heavy neutrinos can have macroscopic lifetimes. Considering the symmetry protected low scale seesaw scenario we have performed our analysis for the choice of the active-sterile mixing parameters as $\theta_e = \theta_\mu$ and $\theta_\tau = 0$. However, for the signal under consideration, by replacing $|\theta_e\theta_\mu|$ with $2|\theta_e|^2|\theta_\mu|^2/|\theta|^2$ one can easily recover the full parameters dependence. The results of the displaced vertex search shown that LHeC and FCC-he can reach exclusion sensitivities down to $\mathcal{O}(10^{-8})$ and $\mathcal{O}(10^{-9})$ for the active-sterile mixing parameters $|\theta_e\theta_\mu|$, respectively at 95% confidence level. For the sterile neutrino prompt decays to lepton-trijet signature at ep colliders, we have improved our previous estimates by including SM background processes and separating signal from background signatures at the reconstructed level with a BDT analysis. Our statistical evaluation shows that this channel can reach exclusion sensitivities to active-sterile mixing parameters $|\theta_e\theta_\mu|$ down to 10^{-7} for FCC-he and 2×10^{-7} for the LHeC at 95% confidence level. It is worth mentioning that the analysis shows that the LHeC and the FCC-he are excellent facilities for discovering heavy neutrinos in a large mass window around the electroweak scale.

In chapter 8, we investigated the LHeC sensitivity for charged lepton flavor violation search in an effective theory apprach with an effective Lagrangian that allows for the conversion of an electron into a muon or a tau lepton via effective coupling to neutral gauge bosons or neutral scalar field. We have found that the LHeC would be an excellent facility for probing the charged lepton flavor violation, which could reach the best sensitivities among all currently envisioned experiments, opening up a great discovery potential for new

physics beyond the SM. The study presented the sensitivities of the LHeC search for the coefficients of the effective operators with final state muon and tau lepton calculated from a cut based analysis at the reconstructed level. Considering the Symmetry Protected Seesaw (SPSS) as an example model that can generate flavor changing neutral currents at one loop level, our results report the sensitivities to the active-sterile neutrino mixing angle combinations $|\theta_e\theta_\mu^*|$ and $|\theta_e\theta_\tau^*|$ down to 2×10^{-5} and 3×10^{-5} for sterile neutrino masses $\sim 1TeV$. We have argued that the very high sensitivities at the LHeC to the active-sterile mixing parameters are possible because the converted charged lepton is dominantly emitted in the backward direction, enabling an efficient separation of the signal from the background. Comparing our results with the future upgrade of the current experiments looking for LFV, we show that the LHeC could be sensitive to the LFV conversion of an electron into a muon beyond the current experimental bounds, and could reach more than an order of magnitude higher sensitivity than the present limits for the LFV conversion of an electron into a tau.

In general, our results demonstrated that ep colliders, such as the LHeC and the FCC-he, are excellent facilities for discovering sterile neutrinos in a large mass window compared to all proposed future colliders. The LHeC is very sensitive to sterile neutrino search in mass window ranging from few GeV up to $\mathcal{O}(10^5)$ GeV. Indeed, the LHeC is sensitive to beyond SM physics in general not only the sterile neutrinos. The prospects of discovering heavy scalars at the LHeC are very promising and complementary to the searches at the LHC, where the notorious SM backgrounds and systematic uncertainties make a discovery difficult. Thus, the superb reach of the LHeC to very small mixing between the extra scalars and the SM Higgs boson for scalar masses below one TeV makes this machine uniquely suited to discover and study possible scalar bosons with masses $\mathcal{O}(100)$ GeV. In the following we summarize our results for extra scalar searches at current and future colliders.

In chapter 9, we investigated the prospects of the LHeC in the search for heavy neutral scalar particles. We considered a minimal model with one additional complex scalar singlet that interacts with the SM via mixing with the Higgs doublet field, giving rise to a SM-like Higgs boson and a heavy scalar boson. Using multivariate techniques and exploiting three of the most promising decay channels of a heavy Higgs, we found that the LHeC can access heavy scalar bosons with masses between 200 and 800 GeV and scalar mixing as small as $\sim 10^{-3}$. We also pointed out that many other interesting channels exist that may allow to test the properties and the origin of the heavy Higgs boson. Among these, searches for (semi) invisible decays, di-higgs and the di-top final states may successfully exploit the cleanest environment offered by the promising future LHeC.

In chapter 10, we considered the scalar doublet extending the SM Lagrangian taking the two Higgs doublet model as an example to test the HL-LHC sensitivity for probing the CP violation signature in the scalar sector. We evalu-

ated the mass eigenbasis numerically, i.e. without assumptions on any of the parameters. We determined a viable parameter space region via a numerical scan over the parameters that are compatible with the present constraints, including theoretical considerations, B-physics measurements, Higgs data, and measurements of electric dipole moments. Our scan shows that the constraints allow for scalar bosons with masses of a few hundreds of GeV, which can be within the reach of the HL-LHC. We found that the CP violation can be probed within the framework of the THDM by observing three sequential decays for $H_i \to ZZ \to \mu$. This can provide a clear signal for CP violation in the considered THDM, where exactly two of the Higgs fields can decay to Z boson pair at the tree-level in case of CP conservation. However, this signature is not unambiguous, since the third resonance could stem from additional scalar fields outside the THDM. For an unambiguous spontaneous CP violation we have studied the angular correlation between the tau lepton pair in the process $pp \to H_2 \to \tau\bar{\tau}$ at the reconstructed level. While it is impossible to reconstruct the tau lepton plane at the reconstructed level we used the impact parameter method with the hadronic decays of tau leptons, $\tau^{\pm} \to \nu\pi^{\pm}$. The impact parameter method is based on the fact that tau lepton is a long lived particle. Thus, independently of its final state neutrino, constructing the impact parameter of the tau lepton with the momentum of the charged pion one can construct the tau lepton plane at the reconstructed level. Measuring the angular correlation between the tau lepton pair is used to test the CP property of H_2. The detectability of CP non-conservation was quantified via a χ^2 fit of the theoretically predicted distributions of the reconstructed tau-decay planes to the simulated data. We found that CP conservation in the scalar sector can be excluded at the 90% CL for our selected benchmark point, i.e. when the CP-mixing angle is close to its maximal value$(\pi/4)$ and the background can be controlled with a relative accuracy of 0.5%, which could be the accuracy target for future measurements.

In chapter 11, we investigated the signatures of the doubly charged component of $SU(2)_L$ scalar triplet field at the current LHC and its future upgrade, HL-LHC and the FCC-hh. we focused on the possibility that the triplet components can be long lived, and calculated carefully the constraints from the prompt searches, taking into account only the simulated events which satisfy the promptness criteria applied in the experimental analyses and satisfied the constraints from the current heavy stable charged particles direct searches. We found that most of the relevant parameter space for the long lived doubly charged scalars they can not be applied because the lifetimes are not large enough to pass through the relevant parts of the detector. Nevertheless, such searches could test the part of the parameter space with displaced distances about few cm. Our study reported that with long lived doubly charged Higgs with displaced distance $\sim$ 1 cm, there exists an allowed region not excluded by neither the prompt searches at the LHC nor by the constraints from the existing charged heavy stable or tack only searches. Focusing on this parameter region, we have performed a detailed analysis at the reconstructed level for a selected benchmark, which has a displaced distance about 1 cm such that

"tracker only" analyses are not efficient and additional information from secondary vertex reconstruction is necessary. We found that already in present LHC data with 100fb^{-1} about 13 events may be detected in this way. Furthermore, the HL-LHC and FCC-hh have prospects to discover up to ~ 500 and ~ 32000 events in their final data sets, respectively.

Finally, the various collider types are complementary in many ways such as providing various testable signatures for new particles at different center-of-mass energies. The current LHC provide an energy of 13 TeV that can be used to prob massive particles. Although, the analysis for new physics suffer from the large QCD contamination and the Pile Up effect but it can still test the LNV signatures from the heavy neutrino decays. For the LHeC which is present in almost every search discussed in this dissertation. It provides probes for LFV, displaced vertices and also for heavy Higgs boson search. But the sensitivities to the sterile neutrino parameters might be a bit weaker compared to the corresponding searches at e^+e^- and pp colliders except for LFV which they can be well suited for.
The collider searches are one of the many aspects of the sterile neutrino and heavy Higgs phenomenology, which should be used to their fullest is these future colliders are built. The future collider experiments are powerful tools not only to prob the active-sterile mixings and masses of the heavy neutrinos but also to provide precise test for heavy scalars at masses above the current LHC.

13 AUTHOR CONTRIBUTION TO THE PUBLISHED PAPERS

This dissertation based on papers that have been published in different peer reviewed journals. The dissertation author is a co-author of these papers and his contribution to the published work done as follows:

- In chapters 6,7 and 9, the author did the full simulation of the events, preselection analysis, machine learning analysis based on the Boosted Decision Trees (BDT) and the statistical evaluation for the BDT classifier based on the maximum log likelihood method.

- In chapter 8, the author did the calculation of electron to muon or tau conversion processes at one loop level using Peng4BSM@LO with double check from FeynCalc program. Also, the implementation of the effective vertices, with their Lorantz structure, in MadGraph with full simulation of events at the LHeC and the statistical evaluation of the cut efficiency to provide limits on the active-sterile mixings have been done by the author.

- In chapter 10, the author has created the model files for the complex THDM and scanned over the allowed parameter space by automating wide set of programs to test the scanned points over the current measurements. In collaboration with Dr. Oliver Fischer, the analysis for spin correlation of Higgs boson decays based on the impact parameter method has been done for the first time for simulated events at the reconstructed level. Full simulation of the events, preselection analysis, machine learning analysis and the statistical evaluation for the final classifier based on the maximum log likelihood method has been done by the author.

- In chapter 11, in collaboration with Christane Schreb, the model files for type II seesaw mechanism has been created using SARAH program and implemented in MadGraph for full simulation. The scan over the allowed parameter space has been done by a private code written by the author. The displaced vertex analysis has been done by the author.

BIBLIOGRAPHY

[1] Stefan Antusch, Oliver Fischer, A. Hammad, and Christiane Scherb. "Testing CP Properties of Extra Higgs States at the HL-LHC." In: *JHEP* 03 (2021), p. 200. DOI: 10.1007/JHEP03(2021)200. arXiv: 2011.10388 [hep-ph].

[2] Stefan Antusch, A. Hammad, and Ahmed Rashed. "Searching for charged lepton flavor violation at ep colliders." In: *JHEP* 03 (2021), p. 230. DOI: 10.1007/JHEP03(2021)230. arXiv: 2010.08907 [hep-ph].

[3] Stefan Antusch, A. Hammad, and Ahmed Rashed. "Probing Z′ mediated charged lepton flavor violation with taus at the LHeC." In: *Phys. Lett. B* 810 (2020), p. 135796. DOI: 10.1016/j.physletb.2020.135796. arXiv: 2003.11091 [hep-ph].

[4] Stefan Antusch, Oliver Fischer, and A. Hammad. "Lepton-Trijet and Displaced Vertex Searches for Heavy Neutrinos at Future Electron-Proton Colliders." In: *JHEP* 03 (2020), p. 110. DOI: 10.1007/JHEP03(2020)110. arXiv: 1908.02852 [hep-ph].

[5] W. Abdallah, A. Hammad, S. Khalil, and S. Moretti. "Dark matter spin characterization in mono-Z channels." In: *Phys. Rev. D* 100.9 (2019), p. 095006. DOI: 10.1103/PhysRevD.100.095006. arXiv: 1907.08358 [hep-ph].

[6] Stefan Antusch, Oliver Fischer, A. Hammad, and Christiane Scherb. "Low scale type II seesaw: Present constraints and prospects for displaced vertex searches." In: *JHEP* 02 (2019), p. 157. DOI: 10.1007/JHEP02(2019)157. arXiv: 1811.03476 [hep-ph].

[7] Luigi Delle Rose, Oliver Fischer, and A. Hammad. "Prospects for Heavy Scalar Searches at the LHeC." In: *Int. J. Mod. Phys. A* 34.23 (2019), p. 1950127. DOI: 10.1142/S0217751X19501276. arXiv: 1809.04321 [hep-ph].

[8] W. Abdallah, A. Hammad, S. Khalil, and S. Moretti. "Searching for Charged Higgs Bosons in the B − L Supersymmetric Standard Model at the High Luminosity Large Hadron Collider." In: *Phys. Lett. B* 788 (2019), pp. 65–69. DOI: 10.1016/j.physletb.2018.10.065. arXiv: 1806.03585 [hep-ph].

[9] Stefan Antusch, Eros Cazzato, Oliver Fischer, A. Hammad, and Kechen Wang. "Lepton Flavor Violating Dilepton Dijet Signatures from Sterile Neutrinos at Proton Colliders." In: *JHEP* 10 (2018), p. 067. DOI: 10.1007/JHEP10(2018)067. arXiv: 1805.11400 [hep-ph].

[10] W. Abdallah, A. Hammad, A. Kasem, and S. Khalil. "Long-lived B-L symmetric SSM particles at the LHC." In: *Phys. Rev. D* 98.9 (2018), p. 095019. DOI: 10.1103/PhysRevD.98.095019. arXiv: 1804.09778 [hep-ph].

[11] Guido Altarelli. "Introduction to the Terascale." In: *34th SLAC Summer Institute on Particle Physics: The Next Fronterier: Exploring with the LHC*. Nov. 2006. arXiv: hep-ph/0611025.

[12] Riccardo Barbieri. *Ten Lectures on the ElectroWeak Interactions*. Scuola Normale Superiore, 2007. ISBN: 978-88-7642-311-6. arXiv: 0706.0684 [hep-ph].

[13] Antonio Pich. "The Standard model of electroweak interactions." In: *2006 European School of High-Energy Physics*. May 2007. arXiv: 0705.4264 [hep-ph].

[14] Guido Altarelli and Ferruccio Feruglio. "Phenomenology of neutrino masses and mixings." In: *10th International Workshop on Neutrino Telescopes*. June 2003. arXiv: hep-ph/0306265.

[15] Alessandro Strumia and Francesco Vissani. "Neutrino masses and mixings and..." In: (June 2006). arXiv: hep-ph/0606054.

[16] M. D. Messier. "Review of neutrino oscllations experiments." In: *eConf* C060409 (2006), p. 018. arXiv: hep-ex/0606013.

[17] M. Tanabashi et al. "Review of Particle Physics." In: *Phys. Rev. D* 98.3 (2018), p. 030001. DOI: 10.1103/PhysRevD.98.030001.

[18] Rabindra N. Mohapatra and Goran Senjanovic. "Neutrino Mass and Spontaneous Parity Nonconservation." In: *Phys. Rev. Lett.* 44 (1980), p. 912. DOI: 10.1103/PhysRevLett.44.912.

[19] R. N. Mohapatra. "Seesaw mechanism and its implications." In: *SEESAW25: International Conference on the Seesaw Mechanism and the Neutrino Mass*. Dec. 2004, pp. 29–44. DOI: 10.1142/9789812702210_0003. arXiv: hep-ph/0412379.

[20] Junya Hashida, Takuya Morozumi, and Agus Purwanto. "Neutrino mixing in seesaw model." In: *Prog. Theor. Phys.* 103 (2000). [Erratum: Prog.Theor.Phys. 103, 865 (2000)], pp. 379–391. DOI: 10.1143/PTP.103.379. arXiv: hep-ph/9909208.

[21] Zurab Berezhiani and Anna Rossi. "Flavor structure, flavor symmetry and supersymmetry." In: *Nucl. Phys. B Proc. Suppl.* 101 (2001). Ed. by K. A. Olive, S. Rudaz, and Mikhail A. Shifman, pp. 410–420. DOI: 10.1016/S0920-5632(01)01527-4. arXiv: hep-ph/0107054.

[22] K. S. Babu, Q. Y. Liu, and A. Yu. Smirnov. "Solar neutrinos and grand unification." In: *Phys. Rev. D* 57 (1998), pp. 5825–5835. DOI: 10.1103/PhysRevD.57.5825. arXiv: hep-ph/9707457.

[23] T. Yanagida and J. Sato. "Large lepton mixing in seesaw models: Coset space family unification." In: *Nucl. Phys. B Proc. Suppl.* 77 (1999). Ed. by Y. Suzuki and Y. Totsuka, pp. 293–298. DOI: 10.1016/S0920-5632(99)00431-4. arXiv: hep-ph/9809307.

[24] Ernest Ma, D. P. Roy, and Utpal Sarkar. "A Seesaw model for atmospheric and solar neutrino oscillations." In: *Phys. Lett. B* 444 (1998), pp. 391–396. DOI: 10.1016/S0370-2693(98)01395-1. arXiv: hep-ph/9810309.

[25] M. Jezabek and Y. Sumino. "Neutrino masses and bimaximal mixing." In: *Phys. Lett. B* 457 (1999), pp. 139–146. DOI: 10.1016/S0370-2693(99)00517-1. arXiv: hep-ph/9904382.

[26] Kazuo Koike. "Seesaw mechanism and possible generation structure." In: (Sept. 1999). arXiv: hep-ph/9909219.

[27] D. Falcone. "Neutrino masses and mixings in a seesaw framework." In: *Phys. Rev. D* 61 (2000), p. 097302. DOI: 10.1103/PhysRevD.61.097302. arXiv: hep-ph/9909207.

[28] Qaisar Shafi and Zurab Tavartkiladze. "Bimaximal neutrino mixings and proton decay in SO(10) with anomalous flavor U(1)." In: *Phys. Lett. B* 487 (2000), pp. 145–150. DOI: 10.1016/S0370-2693(00)00807-8. arXiv: hep-ph/9910314.

[29] R. Arnold et al. "First results of the search of neutrinoless double beta decay with the NEMO 3 detector." In: *Phys. Rev. Lett.* 95 (2005), p. 182302. DOI: 10.1103/PhysRevLett.95.182302. arXiv: hep-ex/0507083.

[30] A. S. Barabash. "Precise half-life values for two neutrino double beta decay." In: *Phys. Rev. C* 81 (2010), p. 035501. DOI: 10.1103/PhysRevC.81.035501. arXiv: 1003.1005 [nucl-ex].

[31] P. S. Bhupal Dev, Srubabati Goswami, Manimala Mitra, and Werner Rodejohann. "Constraining Neutrino Mass from Neutrinoless Double Beta Decay." In: *Phys. Rev. D* 88 (2013), p. 091301. DOI: 10.1103/PhysRevD.88.091301. arXiv: 1305.0056 [hep-ph].

[32] Bernhard Schwingenheuer. "Status and prospects of searches for neutrinoless double beta decay." In: *Annalen Phys.* 525 (2013), pp. 269–280. DOI: 10.1002/andp.201200222. arXiv: 1210.7432 [hep-ex].

[33] Julien Lesgourgues and Sergio Pastor. "Neutrino mass from Cosmology." In: *Adv. High Energy Phys.* 2012 (2012), p. 608515. DOI: 10.1155/2012/608515. arXiv: 1212.6154 [hep-ph].

[34] Julien Lesgourgues, Gianpiero Mangano, Gennaro Miele, and Sergio Pastor. *Neutrino Cosmology*. Cambridge University Press, Feb. 2013. ISBN: 978-1-108-70501-1, 978-1-139-60341-6.

[35] Martina Gerbino. "Neutrino properties from cosmology." In: *Prospects in Neutrino Physics*. Mar. 2018, pp. 52–52. arXiv: 1803.11545 [astro-ph.CO].

[36] Julien Lesgourgues and Sergio Pastor. "Neutrino cosmology and Planck." In: *New J. Phys.* 16 (2014), p. 065002. DOI: 10.1088/1367-2630/16/6/065002. arXiv: 1404.1740 [hep-ph].

[37] A. M. Baldini et al. "Search for the lepton flavour violating decay $\mu^+ \to e^+\gamma$ with the full dataset of the MEG experiment." In: *Eur. Phys. J. C* 76.8 (2016), p. 434. DOI: 10.1140/epjc/s10052-016-4271-x. arXiv: 1605.05081 [hep-ex].

[38] Bernard Aubert et al. "Searches for Lepton Flavor Violation in the Decays tau+- —> e+- gamma and tau+- —> mu+- gamma." In: *Phys. Rev. Lett.* 104 (2010), p. 021802. DOI: 10.1103/PhysRevLett.104.021802. arXiv: 0908.2381 [hep-ex].

[39] K. Hayasaka et al. "Search for Lepton Flavor Violating Tau Decays into Three Leptons with 719 Million Produced Tau+Tau- Pairs." In: *Phys. Lett. B* 687 (2010), pp. 139–143. DOI: 10.1016/j.physletb.2010.03.037. arXiv: 1001.3221 [hep-ex].

[40] K. Arndt et al. "Technical design of the phase I Mu3e experiment." In: (Sept. 2020). arXiv: 2009.11690 [physics.ins-det].

[41] Alberto Lusiani. "Search for Lepton-Flavor-Violating Tau Decays at the B-factories." In: *PoS* HQL2010 (2010). Ed. by Luigi Benussi, Stefano Bianco, Davide Piccolo, and Daniela Rebuzzi, p. 054. DOI: 10.22323/1.128.0054. arXiv: 1012.3733 [hep-ex].

[42] A. M. Baldini et al. "The design of the MEG II experiment." In: *Eur. Phys. J. C* 78.5 (2018), p. 380. DOI: 10.1140/epjc/s10052-018-5845-6. arXiv: 1801.04688 [physics.ins-det].

[43] W. Altmannshofer et al. "The Belle II Physics Book." In: *PTEP* 2019.12 (2019). Ed. by E. Kou and P. Urquijo. [Erratum: PTEP 2020, 029201 (2020)], p. 123C01. DOI: 10.1093/ptep/ptz106. arXiv: 1808.10567 [hep-ex].

[44] M. Bona et al. "SuperB: A High-Luminosity Asymmetric e+ e- Super Flavor Factory. Conceptual Design Report." In: (May 2007). arXiv: 0709.0451 [hep-ex].

[45] John Leslie Almond. "Search for heavy neutrinos at CMS." In: *PoS* ICHEP2018 (2019), p. 640. DOI: 10.22323/1.340.0640.

[46] Albert M Sirunyan et al. "Search for heavy Majorana neutrinos in same-sign dilepton channels in proton-proton collisions at $\sqrt{s} = 13$ TeV." In: *JHEP* 01 (2019), p. 122. DOI: 10.1007/JHEP01(2019)122. arXiv: 1806.10905 [hep-ex].

[47] Dehua Zhu. "Search for Long-Lived Heavy Neutral Leptons and Detector Modules for the CMS Pixel Phase 1 Upgrade." PhD thesis. Zurich, ETH, 2020. DOI: 10.3929/ethz-b-000447851.

[48] Federico Scutti. "Search for heavy neutrinos with the ATLAS detector." In: *PoS* NuFact2019 (2020), p. 094. DOI: 10.22323/1.369.0094.

[49] Georges Aad et al. "Combined Measurement of the Higgs Boson Mass in pp Collisions at $\sqrt{s} = 7$ and 8 TeV with the ATLAS and CMS Experiments." In: *Phys. Rev. Lett.* 114 (2015), p. 191803. DOI: 10.1103/PhysRevLett.114.191803. arXiv: 1503.07589 [hep-ex].

[50] E. A. Reyes Rojas. "The Higgs Boson at LHC and the Vacuum Stability of the Standard Model." PhD thesis. Colombia, U. Natl., 2015. arXiv: 1511.03651 [hep-ph].

[51] Mark Trodden. "Electroweak baryogenesis: A Brief review." In: *33rd Rencontres de Moriond: Electroweak Interactions and Unified Theories*. 1998. arXiv: hep-ph/9805252.

[52] Darwin Chang, Wai-Yee Keung, and Ivan Phillips. "CP odd correlation in the decay of neutral Higgs boson into Z Z, W+ W-, or t anti-t." In: *Phys. Rev. D* 48 (1993), pp. 3225–3234. DOI: 10.1103/PhysRevD.48.3225. arXiv: hep-ph/9303226.

[53] Stefan Berge and Werner Bernreuther. "Determining the CP parity of Higgs bosons at the LHC in the tau to 1-prong decay channels." In: *Phys. Lett. B* 671 (2009), pp. 470–476. DOI: 10.1016/j.physletb.2008.12.065. arXiv: 0812.1910 [hep-ph].

[54] John F. Gunion and Xiao-Gang He. "Determining the CP nature of a neutral Higgs boson at the LHC." In: *Phys. Rev. Lett.* 76 (1996), pp. 4468–4471. DOI: 10.1103/PhysRevLett.76.4468. arXiv: hep-ph/9602226.

[55] A. Abada, C. Biggio, F. Bonnet, M. B. Gavela, and T. Hambye. "Low energy effects of neutrino masses." In: *JHEP* 12 (2007), p. 061. DOI: 10.1088/1126-6708/2007/12/061. arXiv: 0707.4058 [hep-ph].

[56] P. S. Bhupal Dev, Michael J. Ramsey-Musolf, and Yongchao Zhang. "Doubly-Charged Scalars in the Type-II Seesaw Mechanism: Fundamental Symmetry Tests and High-Energy Searches." In: *Phys. Rev. D* 98.5 (2018), p. 055013. DOI: 10.1103/PhysRevD.98.055013. arXiv: 1806.08499 [hep-ph].

[57] A. G. Akeroyd and Mayumi Aoki. "Single and pair production of doubly charged Higgs bosons at hadron colliders." In: *Phys. Rev. D* 72 (2005), p. 035011. DOI: 10.1103/PhysRevD.72.035011. arXiv: hep-ph/0506176.

[58] Pavel Fileviez Perez, Tao Han, Gui-yu Huang, Tong Li, and Kai Wang. "Neutrino Masses and the CERN LHC: Testing Type II Seesaw." In: *Phys. Rev. D* 78 (2008), p. 015018. DOI: 10.1103/PhysRevD.78.015018. arXiv: 0805.3536 [hep-ph].

[59] Alejandra Melfo, Miha Nemevsek, Fabrizio Nesti, Goran Senjanovic, and Yue Zhang. "Type II Seesaw at LHC: The Roadmap." In: *Phys. Rev. D* 85 (2012), p. 055018. DOI: 10.1103/PhysRevD.85.055018. arXiv: 1108.4416 [hep-ph].

[60] Robert Foot, H. Lew, X. G. He, and Girish C. Joshi. "Seesaw Neutrino Masses Induced by a Triplet of Leptons." In: *Z. Phys. C* 44 (1989), p. 441. DOI: 10.1007/BF01415558.

[61] G. Abbiendi et al. "Search for doubly charged Higgs bosons with the OPAL detector at LEP." In: *Phys. Lett. B* 526 (2002), pp. 221–232. DOI: 10.1016/S0370-2693(01)01474-5. arXiv: hep-ex/0111059.

[62] J. Abdallah et al. "Search for doubly charged Higgs bosons at LEP-2." In: *Phys. Lett. B* 552 (2003), pp. 127–137. DOI: 10.1016/S0370-2693(02)03125-8. arXiv: hep-ex/0303026.

[63] P. Achard et al. "Search for doubly charged Higgs bosons at LEP." In: *Phys. Lett. B* 576 (2003), pp. 18–28. DOI: 10.1016/j.physletb.2003.09.082. arXiv: hep-ex/0309076.

[64] D. Acosta et al. "Search for doubly-charged Higgs bosons decaying to dileptons in $p\bar{p}$ collisions at $\sqrt{s} = 1.96$ TeV." In: *Phys. Rev. Lett.* 93 (2004), p. 221802. DOI: 10.1103/PhysRevLett.93.221802. arXiv: hep-ex/0406073.

[65] T. Aaltonen et al. "Search for Doubly Charged Higgs Bosons with Lepton-Flavor-Violating Decays involving Tau Leptons." In: *Phys. Rev. Lett.* 101 (2008), p. 121801. DOI: 10.1103/PhysRevLett.101.121801. arXiv: 0808.2161 [hep-ex].

[66] V. M. Abazov et al. "Search for pair production of doubly-charged Higgs bosons in the $H^{++}H^{--} \to \mu^+\mu^+\mu^-\mu^-$ final state at Do." In: *Phys. Rev. Lett.* 101 (2008), p. 071803. DOI: 10.1103/PhysRevLett.101.071803. arXiv: 0803.1534 [hep-ex].

[67] Victor Mukhamedovich Abazov et al. "Search for doubly-charged Higgs boson pair production in $p\bar{p}$ collisions at $\sqrt{s} = 1.96$ TeV." In: *Phys. Rev. Lett.* 108 (2012), p. 021801. DOI: 10.1103/PhysRevLett.108.021801. arXiv: 1106.4250 [hep-ex].

[68] Georges Aad et al. "Search for long-lived, multi-charged particles in pp collisions at $\sqrt{s}$=7 TeV using the ATLAS detector." In: *Phys. Lett. B* 722 (2013), pp. 305–323. DOI: 10.1016/j.physletb.2013.04.036. arXiv: 1301.5272 [hep-ex].

[69] Georges Aad et al. "Search for heavy long-lived multi-charged particles in pp collisions at $\sqrt{s} = 8$ TeV using the ATLAS detector." In: *Eur. Phys. J. C* 75 (2015), p. 362. DOI: 10.1140/epjc/s10052-015-3534-2. arXiv: 1504.04188 [hep-ex].

[70] Vardan Khachatryan et al. "Search for long-lived charged particles in proton-proton collisions at $\sqrt{s} = 13$ TeV." In: *Phys. Rev. D* 94.11 (2016), p. 112004. DOI: 10.1103/PhysRevD.94.112004. arXiv: 1609.08382 [hep-ex].

[71] P. S. Bhupal Dev and Yongchao Zhang. "Displaced vertex signatures of doubly charged scalars in the type-II seesaw and its left-right extensions." In: *JHEP* 10 (2018), p. 199. DOI: 10.1007/JHEP10(2018)199. arXiv: 1808.00943 [hep-ph].

[72] A. Abada et al. "FCC Physics Opportunities: Future Circular Collider Conceptual Design Report Volume 1." In: *Eur. Phys. J. C* 79.6 (2019), p. 474. DOI: 10.1140/epjc/s10052-019-6904-3.

[73] A. Abada et al. "HE-LHC: The High-Energy Large Hadron Collider: Future Circular Collider Conceptual Design Report Volume 4." In: *Eur. Phys. J. ST* 228.5 (2019), pp. 1109–1382. DOI: 10.1140/epjst/e2019-900088-6.

[74] A. Abada et al. "FCC-hh: The Hadron Collider: Future Circular Collider Conceptual Design Report Volume 3." In: *Eur. Phys. J. ST* 228.4 (2019), pp. 755–1107. DOI: 10.1140/epjst/e2019-900087-0.

[75] A. Abada et al. "FCC-ee: The Lepton Collider: Future Circular Collider Conceptual Design Report Volume 2." In: *Eur. Phys. J. ST* 228.2 (2019), pp. 261–623. DOI: 10.1140/epjst/e2019-900045-4.

[76] P. Agostini et al. "The Large Hadron-Electron Collider at the HL-LHC." In: (July 2020). arXiv: 2007.14491 [hep-ex].

[77] Ettore Majorana. "Teoria simmetrica dell'elettrone e del positrone." In: *Nuovo Cim.* 14 (1937), pp. 171–184. DOI: 10.1007/BF02961314.

[78] Steven Weinberg. "Baryon and Lepton Nonconserving Processes." In: *Phys. Rev. Lett.* 43 (1979), pp. 1566–1570. DOI: 10.1103/PhysRevLett.43.1566.

[79] Herbi K. Dreiner, Howard E. Haber, and Stephen P. Martin. "Two-component spinor techniques and Feynman rules for quantum field theory and supersymmetry." In: *Phys. Rept.* 494 (2010), pp. 1–196. DOI: 10.1016/j.physrep.2010.05.002. arXiv: 0812.1594 [hep-ph].

[80] Claudio Giganti, Stéphane Lavignac, and Marco Zito. "Neutrino oscillations: The rise of the PMNS paradigm." In: *Prog. Part. Nucl. Phys.* 98 (2018), pp. 1–54. DOI: 10.1016/j.ppnp.2017.10.001. arXiv: 1710.00715 [hep-ex].

[81] Nuno Rosa Agostinho, O. J. P. Eboli, and M. C. Gonzalez-Garcia. "LHC Run I Bounds on Minimal Lepton Flavour Violation in Type-III See-saw: A Case Study." In: *JHEP* 11 (2017), p. 118. DOI: 10.1007/JHEP11(2017)118. arXiv: 1708.08456 [hep-ph].

[82] O. J. P. Eboli, J. Gonzalez-Fraile, and M. C. Gonzalez-Garcia. "Neutrino Masses at LHC: Minimal Lepton Flavour Violation in Type-III See-saw." In: *JHEP* 12 (2011), p. 009. DOI: 10.1007/JHEP12(2011)009. arXiv: 1108.0661 [hep-ph].

[83] J. A. Aguilar-Saavedra, P. M. Boavida, and F. R. Joaquim. "Flavored searches for type-III seesaw mechanism at the LHC." In: *Phys. Rev. D* 88 (2013), p. 113008. DOI: 10.1103/PhysRevD.88.113008. arXiv: 1308.3226 [hep-ph].

[84] Chian-Shu Chen and Ya-Juan Zheng. "LHC signatures for the cascade seesaw mechanism." In: *PTEP* 2015 (2015), 103B02. DOI: 10.1093/ptep/ptv134. arXiv: 1312.7207 [hep-ph].

[85] Stefan von Buddenbrock, Nabarun Chakrabarty, Alan S. Cornell, Deepak Kar, Mukesh Kumar, Tanumoy Mandal, Bruce Mellado, Biswarup Mukhopadhyaya, and Robert G. Reed. "The compatibility of LHC Run 1 data with a heavy scalar of mass around 270\,GeV." In: (June 2015). arXiv: 1506.00612 [hep-ph].

[86] Stefan von Buddenbrock, Nabarun Chakrabarty, Alan S. Cornell, Deepak Kar, Mukesh Kumar, Tanumoy Mandal, Bruce Mellado, Biswarup Mukhopadhyaya, Robert G. Reed, and Xifeng Ruan. "Phenomenological signatures of additional scalar bosons at the LHC." In: *Eur. Phys. J. C* 76.10 (2016), p. 580. DOI: 10.1140/epjc/s10052-016-4435-8. arXiv: 1606.01674 [hep-ph].

[87] Stefan von Buddenbrock, Alan S. Cornell, Abdualazem Fadol, Mukesh Kumar, Bruce Mellado, and Xifeng Ruan. "Multi-lepton signatures of additional scalar bosons beyond the Standard Model at the LHC." In: *J. Phys. G* 45.11 (2018), p. 115003. DOI: 10.1088/1361-6471/aae3d6. arXiv: 1711.07874 [hep-ph].

[88] Stefan von Buddenbrock, Alan S. Cornell, Mukesh Kumar, and Bruce Mellado. "The Madala hypothesis with Run 1 and 2 data at the LHC." In: *J. Phys. Conf. Ser.* 889.1 (2017), p. 012020. DOI: 10.1088/1742-6596/889/1/012020. arXiv: 1709.09419 [hep-ph].

[89] Albert M Sirunyan et al. "Search for a standard model-like Higgs boson in the mass range between 70 and 110 GeV in the diphoton final state in proton-proton collisions at $\sqrt{s} = 8$ and 13 TeV." In: *Phys. Lett. B* 793 (2019), pp. 320–347. DOI: 10.1016/j.physletb.2019.03.064. arXiv: 1811.08459 [hep-ex].

[90] Ahmed Ali Abdelalim, Biswaranjan Das, Shaaban Khalil, and Stefano Moretti. "Di-photon decay of a light Higgs state in the BLSSM." In: (Dec. 2020). arXiv: 2012.04952 [hep-ph].

[91] Sheldon L. Glashow and Steven Weinberg. "Natural Conservation Laws for Neutral Currents." In: *Phys. Rev. D* 15 (1977), p. 1958. DOI: 10.1103/PhysRevD.15.1958.

[92] Johan Alwall, Claude Duhr, Benjamin Fuks, Olivier Mattelaer, Deniz Gizem Öztürk, and Chia-Hsien Shen. "Computing decay rates for new physics theories with FeynRules and MadGraph 5_aMC@NLO." In: *Comput. Phys. Commun.* 197 (2015), pp. 312–323. DOI: 10.1016/j.cpc.2015.08.031. arXiv: 1402.1178 [hep-ph].

[93] Florian Staub. "SARAH 4 : A tool for (not only SUSY) model builders." In: *Comput. Phys. Commun.* 185 (2014), pp. 1773–1790. DOI: 10.1016/j.cpc.2014.02.018. arXiv: 1309.7223 [hep-ph].

[94] Celine Degrande, Claude Duhr, Benjamin Fuks, David Grellscheid, Olivier Mattelaer, and Thomas Reiter. "UFO - The Universal FeynRules Output." In: *Comput. Phys. Commun.* 183 (2012), pp. 1201–1214. DOI: 10.1016/j.cpc.2012.01.022. arXiv: 1108.2040 [hep-ph].

[95] Torbjorn Sjostrand, Stephen Mrenna, and Peter Z. Skands. "A Brief Introduction to PYTHIA 8.1." In: *Comput. Phys. Commun.* 178 (2008), pp. 852–867. DOI: 10.1016/j.cpc.2008.01.036. arXiv: 0710.3820 [hep-ph].

[96] Matteo Cacciari, Gavin P. Salam, and Gregory Soyez. "FastJet User Manual." In: *Eur. Phys. J. C* 72 (2012), p. 1896. DOI: 10.1140/epjc/s10052-012-1896-2. arXiv: 1111.6097 [hep-ph].

[97] J. de Favereau, C. Delaere, P. Demin, A. Giammanco, V. Lemaître, A. Mertens, and M. Selvaggi. "DELPHES 3, A modular framework for fast simulation of a generic collider experiment." In: *JHEP* 02 (2014), p. 057. DOI: 10.1007/JHEP02(2014)057. arXiv: 1307.6346 [hep-ex].

[98] S. Gariazzo, C. Giunti, M. Laveder, Y. F. Li, and E. M. Zavanin. "Light sterile neutrinos." In: *J. Phys. G* 43 (2016), p. 033001. DOI: 10.1088/0954-3899/43/3/033001. arXiv: 1507.08204 [hep-ph].

[99] André de Gouvêa and Andrew Kobach. "Global Constraints on a Heavy Neutrino." In: *Phys. Rev. D* 93.3 (2016), p. 033005. DOI: 10.1103/PhysRevD.93.033005. arXiv: 1511.00683 [hep-ph].

[100] Georges Aad et al. "Search for heavy Majorana neutrinos with the ATLAS detector in pp collisions at $\sqrt{s} = 8$ TeV." In: *JHEP* 07 (2015), p. 162. DOI: 10.1007/JHEP07(2015)162. arXiv: 1506.06020 [hep-ex].

[101] Vardan Khachatryan et al. "Search for heavy Majorana neutrinos in $e^{\pm}e^{\pm}$+ jets and $e^{\pm}$ $\mu^{\pm}$+ jets events in proton-proton collisions at $\sqrt{s} = 8$ TeV." In: *JHEP* 04 (2016), p. 169. DOI: 10.1007/JHEP04(2016)169. arXiv: 1603.02248 [hep-ex].

[102] M. Agostini et al. "Background-free search for neutrinoless double-β decay of ^{76}Ge with GERDA." In: *Nature* 544 (2017), p. 47. DOI: 10.1038/nature21717. arXiv: 1703.00570 [nucl-ex].

[103] Marco Drewes. "The Phenomenology of Right Handed Neutrinos." In: *Int. J. Mod. Phys. E* 22 (2013), p. 1330019. DOI: 10.1142/S0218301313300191. arXiv: 1303.6912 [hep-ph].

[104] D. Wyler and L. Wolfenstein. "Massless Neutrinos in Left-Right Symmetric Models." In: *Nucl. Phys. B* 218 (1983), pp. 205–214. DOI: 10.1016/0550-3213(83)90482-0.

[105] R. N. Mohapatra and J. W. F. Valle. "Neutrino Mass and Baryon Number Nonconservation in Superstring Models." In: *Phys. Rev. D* 34 (1986), p. 1642. DOI: 10.1103/PhysRevD.34.1642.

[106] Mikhail Shaposhnikov. "A Possible symmetry of the nuMSM." In: *Nucl. Phys. B* 763 (2007), pp. 49–59. DOI: 10.1016/j.nuclphysb.2006.11.003. arXiv: hep-ph/0605047.

[107] Jörn Kersten and Alexei Yu. Smirnov. "Right-Handed Neutrinos at CERN LHC and the Mechanism of Neutrino Mass Generation." In: *Phys. Rev. D* 76 (2007), p. 073005. DOI: 10.1103/PhysRevD.76.073005. arXiv: 0705.3221 [hep-ph].

[108] M. B. Gavela, T. Hambye, D. Hernandez, and P. Hernandez. "Minimal Flavour Seesaw Models." In: *JHEP* 09 (2009), p. 038. DOI: 10.1088/1126-6708/2009/09/038. arXiv: 0906.1461 [hep-ph].

[109] Michal Malinsky, J. C. Romao, and J. W. F. Valle. "Novel supersymmetric SO(10) seesaw mechanism." In: *Phys. Rev. Lett.* 95 (2005), p. 161801. DOI: 10.1103/PhysRevLett.95.161801. arXiv: hep-ph/0506296.

[110] Frank F. Deppisch, Lukas Graf, Julia Harz, and Wei-Chih Huang. "Neutrinoless Double Beta Decay and the Baryon Asymmetry of the Universe." In: *Phys. Rev. D* 98.5 (2018), p. 055029. DOI: 10.1103/PhysRevD.98.055029. arXiv: 1711.10432 [hep-ph].

[111] Stefan Antusch, Eros Cazzato, and Oliver Fischer. "Sterile neutrino searches at future e^-e^+, pp, and e^-p colliders." In: *Int. J. Mod. Phys. A* 32.14 (2017), p. 1750078. DOI: 10.1142/S0217751X17500786. arXiv: 1612.02728 [hep-ph].

[112] K. Moffat, S. Pascoli, and C. Weiland. "Equivalence between massless neutrinos and lepton number conservation in fermionic singlet extensions of the Standard Model." In: (Dec. 2017). arXiv: 1712.07611 [hep-ph].

[113] Stefan Antusch, Eros Cazzato, and Oliver Fischer. "Resolvable heavy neutrino–antineutrino oscillations at colliders." In: *Mod. Phys. Lett. A* 34.07n08 (2019), p. 1950061. DOI: 10.1142/S0217732319500615. arXiv: 1709.03797 [hep-ph].

[114] F. del Aguila, J. A. Aguilar-Saavedra, and R. Pittau. "Neutrino physics at large colliders." In: *J. Phys. Conf. Ser.* 53 (2006). Ed. by K. Anagnostopoulos, I. Antoniadis, G. Fanourakis, A. Kehagias, A. Savoy-Navarro, J. Wess, and G. Zoupanos, pp. 506–527. DOI: 10.1088/1742-6596/53/1/032. arXiv: hep-ph/0606198.

[115] Tao Han and Bin Zhang. "Signatures for Majorana neutrinos at hadron colliders." In: *Phys. Rev. Lett.* 97 (2006), p. 171804. DOI: 10.1103/PhysRevLett.97.171804. arXiv: hep-ph/0604064.

[116] F. del Aguila, J. A. Aguilar-Saavedra, and R. Pittau. "Heavy neutrino signals at large hadron colliders." In: *JHEP* 10 (2007), p. 047. DOI: 10.1088/1126-6708/2007/10/047. arXiv: hep-ph/0703261.

[117] F. del Aguila and J. A. Aguilar-Saavedra. "Distinguishing seesaw models at LHC with multi-lepton signals." In: *Nucl. Phys. B* 813 (2009), pp. 22–90. DOI: 10.1016/j.nuclphysb.2008.12.029. arXiv: 0808.2468 [hep-ph].

[118] Anupama Atre, Tao Han, Silvia Pascoli, and Bin Zhang. "The Search for Heavy Majorana Neutrinos." In: *JHEP* 05 (2009), p. 030. DOI: 10.1088/1126-6708/2009/05/030. arXiv: 0901.3589 [hep-ph].

[119] Wei Chao, Zong-guo Si, Ya-juan Zheng, and Shun Zhou. "Testing the Realistic Seesaw Model with Two Heavy Majorana Neutrinos at the CERN Large Hadron Collider." In: *Phys. Lett. B* 683 (2010), pp. 26–32. DOI: 10.1016/j.physletb.2009.11.059. arXiv: 0907.0935 [hep-ph].

[120] Arindam Das and Nobuchika Okada. "Inverse seesaw neutrino signatures at the LHC and ILC." In: *Phys. Rev. D* 88 (2013), p. 113001. DOI: 10.1103/PhysRevD.88.113001. arXiv: 1207.3734 [hep-ph].

[121] Arindam Das and Nobuchika Okada. "Improved bounds on the heavy neutrino productions at the LHC." In: *Phys. Rev. D* 93.3 (2016), p. 033003. DOI: 10.1103/PhysRevD.93.033003. arXiv: 1510.04790 [hep-ph].

[122] Arindam Das, Partha Konar, and Swapan Majhi. "Production of Heavy neutrino in next-to-leading order QCD at the LHC and beyond." In: *JHEP* 06 (2016), p. 019. DOI: 10.1007/JHEP06(2016)019. arXiv: 1604.00608 [hep-ph].

[123] Daniel Alva, Tao Han, and Richard Ruiz. "Heavy Majorana neutrinos from $W\gamma$ fusion at hadron colliders." In: *JHEP* 02 (2015), p. 072. DOI: 10.1007/JHEP02(2015)072. arXiv: 1411.7305 [hep-ph].

[124] Claudio O. Dib, C. S. Kim, Kechen Wang, and Jue Zhang. "Distinguishing Dirac/Majorana Sterile Neutrinos at the LHC." In: *Phys. Rev. D* 94.1 (2016), p. 013005. DOI: 10.1103/PhysRevD.94.013005. arXiv: 1605.01123 [hep-ph].

[125] Claudio O. Dib, C. S. Kim, and Kechen Wang. "Search for Heavy Sterile Neutrinos in Trileptons at the LHC." In: *Chin. Phys. C* 41.10 (2017), p. 103103. DOI: 10.1088/1674-1137/41/10/103103. arXiv: 1703.01936 [hep-ph].

[126] Claudio O. Dib, C. S. Kim, Kechen Wang, and Jue Zhang. "Distinguishing Dirac/Majorana Sterile Neutrinos at the LHC." In: *Phys. Rev. D* 94.1 (2016), p. 013005. DOI: 10.1103/PhysRevD.94.013005. arXiv: 1605.01123 [hep-ph].

[127] E. Arganda, M. J. Herrero, X. Marcano, and C. Weiland. "Exoticμτjjevents from heavy ISS neutrinos at the LHC." In: *Phys. Lett. B* 752 (2016), pp. 46–50. DOI: 10.1016/j.physletb.2015.11.013. arXiv: 1508.05074 [hep-ph].

[128] Jingyu Tang et al. "Concept for a Future Super Proton-Proton Collider." In: (July 2015). arXiv: 1507.03224 [physics.acc-ph].

[129] Stefan Antusch and Oliver Fischer. "Testing sterile neutrino extensions of the Standard Model at future lepton colliders." In: *JHEP* 05 (2015), p. 053. DOI: 10.1007/JHEP05(2015)053. arXiv: 1502.05915 [hep-ph].

[130] E. Fernandez-Martinez, M. B. Gavela, J. Lopez-Pavon, and O. Yasuda. "CP-violation from non-unitary leptonic mixing." In: *Phys. Lett. B* 649 (2007), pp. 427–435. DOI: 10.1016/j.physletb.2007.03.069. arXiv: hep-ph/0703098.

[131] Stefan Antusch, Mattias Blennow, Enrique Fernandez-Martinez, and Jacobo Lopez-Pavon. "Probing non-unitary mixing and CP-violation at a Neutrino Factory." In: *Phys. Rev. D* 80 (2009), p. 033002. DOI: 10.1103/PhysRevD.80.033002. arXiv: 0903.3986 [hep-ph].

[132] G Apollinari, I Béjar Alonso, O Brüning, M Lamont, and L Rossi. *High-Luminosity Large Hadron Collider (HL-LHC): Preliminary Design Report*. CERN Yellow Reports: Monographs. Geneva: CERN, 2015. DOI: 10.5170/CERN-2015-005. URL: https://cds.cern.ch/record/2116337.

[133] T. Golling et al. "Physics at a 100 TeV pp collider: beyond the Standard Model phenomena." In: (June 2016). DOI: 10.23731/CYRM-2017-003.441. arXiv: 1606.00947 [hep-ph].

[134] M. L. Mangano et al. "Physics at a 100 TeV pp Collider: Standard Model Processes." In: (July 2016). DOI: 10.23731/CYRM-2017-003.1. arXiv: 1607.01831 [hep-ph].

[135] R. Contino et al. "Physics at a 100 TeV pp collider: Higgs and EW symmetry breaking studies." In: (June 2016). DOI: 10.23731/CYRM-2017-003.255. arXiv: 1606.09408 [hep-ph].

[136] Ian Hinchliffe, Ashutosh Kotwal, Michelangelo L. Mangano, Chris Quigg, and Lian-Tao Wang. "Luminosity goals for a 100-TeV pp collider." In: *Int. J. Mod. Phys. A* 30.23 (2015), p. 1544002. DOI: 10.1142/S0217751X15440029. arXiv: 1504.06108 [hep-ph].

[137] Celine Degrande, Olivier Mattelaer, Richard Ruiz, and Jessica Turner. "Fully-Automated Precision Predictions for Heavy Neutrino Production Mechanisms at Hadron Colliders." In: *Phys. Rev. D* 94.5 (2016), p. 053002. DOI: 10.1103/PhysRevD.94.053002. arXiv: 1602.06957 [hep-ph].

[138] Richard Ruiz, Michael Spannowsky, and Philip Waite. "Heavy neutrinos from gluon fusion." In: *Phys. Rev. D* 96.5 (2017), p. 055042. DOI: 10.1103/PhysRevD.96.055042. arXiv: 1706.02298 [hep-ph].

[139] Yi Cai, Tao Han, Tong Li, and Richard Ruiz. "Lepton Number Violation: Seesaw Models and Their Collider Tests." In: *Front. in Phys.* 6 (2018), p. 40. DOI: 10.3389/fphy.2018.00040. arXiv: 1711.02180 [hep-ph].

[140] Janusz Gluza and Tomasz Jeliński. "Heavy neutrinos and the pp →lljj CMS data." In: *Phys. Lett. B* 748 (2015), pp. 125–131. DOI: 10.1016/j.physletb.2015.06.077. arXiv: 1504.05568 [hep-ph].

[141] G. Anamiati, M. Hirsch, and E. Nardi. "Quasi-Dirac neutrinos at the LHC." In: *JHEP* 10 (2016), p. 010. DOI: 10.1007/JHEP10(2016)010. arXiv: 1607.05641 [hep-ph].

[142] Arindam Das, P. S. Bhupal Dev, and Rabindra N. Mohapatra. "Same Sign versus Opposite Sign Dileptons as a Probe of Low Scale Seesaw Mechanisms." In: *Phys. Rev. D* 97.1 (2018), p. 015018. DOI: 10.1103/PhysRevD.97.015018. arXiv: 1709.06553 [hep-ph].

[143] J. Alwall, R. Frederix, S. Frixione, V. Hirschi, F. Maltoni, O. Mattelaer, H. S. Shao, T. Stelzer, P. Torrielli, and M. Zaro. "The automated computation of tree-level and next-to-leading order differential cross sections, and their matching to parton shower simulations." In: *JHEP* 07 (2014), p. 079. DOI: 10.1007/JHEP07(2014)079. arXiv: 1405.0301 [hep-ph].

[144] Torbjorn Sjostrand, Stephen Mrenna, and Peter Z. Skands. "PYTHIA 6.4 Physics and Manual." In: *JHEP* 05 (2006), p. 026. DOI: 10.1088/1126-6708/2006/05/026. arXiv: hep-ph/0603175.

[145] A. Hoecker et al. *TMVA - Toolkit for Multivariate Data Analysis*. 2007. arXiv: physics/0703039 [physics.data-an].

[146] Higgs Analysis Combined-Limit. *https://twiki.cern.ch/twiki/bin/viewauth/CMS/SWGuideHiggsAnalysisCombinedLimit*.

[147] Frank F. Deppisch, P. S. Bhupal Dev, and Apostolos Pilaftsis. "Neutrinos and Collider Physics." In: *New J. Phys.* 17.7 (2015), p. 075019. DOI: 10.1088/1367-2630/17/7/075019. arXiv: 1502.06541 [hep-ph].

[148] Toshinori Mori. "Final Results of the MEG Experiment." In: *Nuovo Cim. C* 39.4 (2017), p. 325. DOI: 10.1393/ncc/i2016-16325-7. arXiv: 1606.08168 [hep-ex].

[149] Stefan Antusch and Oliver Fischer. "Non-unitarity of the leptonic mixing matrix: Present bounds and future sensitivities." In: *JHEP* 10 (2014), p. 094. DOI: 10.1007/JHEP10(2014)094. arXiv: 1407.6607 [hep-ph].

[150] Higgs Analysis Combined-Limit. *https://twiki.cern.ch/twiki/bin/viewauth/CMS/SWGuideHiggsAnalysisCombinedLimit*.

[151] P. Abreu et al. "Search for neutral heavy leptons produced in Z decays." In: *Z. Phys. C* 74 (1997). [Erratum: Z.Phys.C 75, 580 (1997)], pp. 57–71. DOI: 10.1007/s002880050370.

[152] Albert M Sirunyan et al. "Search for heavy neutral leptons in events with three charged leptons in proton-proton collisions at $\sqrt{s} = 13$ TeV." In: *Phys. Rev. Lett.* 120.22 (2018), p. 221801. DOI: 10.1103/PhysRevLett.120.221801. arXiv: 1802.02965 [hep-ex].

[153] Georges Aad et al. "Search for heavy neutral leptons in decays of W bosons produced in 13 TeV pp collisions using prompt and displaced signatures with the ATLAS detector." In: *JHEP* 10 (2019), p. 265. DOI: 10.1007/JHEP10(2019)265. arXiv: 1905.09787 [hep-ex].

[154] Oliver Bruening and Max Klein. "The Large Hadron Electron Collider." In: *Mod. Phys. Lett. A* 28.16 (2013), p. 1330011. DOI: 10.1142/S0217732313300115. arXiv: 1305.2090 [physics.acc-ph].

[155] J.L. Abelleira Fernandez et al. "A Large Hadron Electron Collider at CERN: Report on the Physics and Design Concepts for Machine and Detector." In: *J. Phys. G* 39 (2012), p. 075001. DOI: 10.1088/0954-3899/39/7/075001. arXiv: 1206.2913 [physics.acc-ph].

[156] Max Klein. "Deep inelastic scattering at the energy frontier." In: *Annalen Phys.* 528 (2016), pp. 138–144. DOI: 10.1002/andp.201500252.

[157] Oliver Bruning and Max Klein. "Exploring the Energy Frontier with Deep Inelastic Scattering at the LHC A contribution to the update of the European Strategy on Particle Physics." In: (2018). URL: https://cds.cern.ch/record/2652313.

[158] D. Angal-Kalinin et al. "PERLE. Powerful energy recovery linac for experiments. Conceptual design report." In: *J. Phys. G* 45.6 (2018), p. 065003. DOI: 10.1088/1361-6471/aaa171. arXiv: 1705.08783 [physics.acc-ph].

[159] G. Ingelman and J. Rathsman. "Heavy majorana neutrinos at ep colliders." In: *Zeitschrift fur Physik C Particles and Fields* 60.2 (June 1993), pp. 243–254. DOI: 10.1007/BF01474620.

[160] Han Liang, Xiao-Gang He, Wen-Gan Ma, Shao-Ming Wang, and Ren-You Zhang. "Seesaw Type I and III at the LHeC." In: *JHEP* 09 (2010), p. 023. DOI: 10.1007/JHEP09(2010)023. arXiv: 1006.5534 [hep-ph].

[161] Carl Blaksley, Mattias Blennow, Florian Bonnet, Pilar Coloma, and Enrique Fernandez-Martinez. "Heavy Neutrinos and Lepton Number Violation in lp Colliders." In: *Nucl. Phys. B* 852 (2011), pp. 353–365. DOI: 10.1016/j.nuclphysb.2011.06.021. arXiv: 1105.0308 [hep-ph].

[162] Subhadeep Mondal and Santosh Kumar Rai. "Probing the Heavy Neutrinos of Inverse Seesaw Model at the LHeC." In: *Phys. Rev. D* 94.3 (2016), p. 033008. DOI: 10.1103/PhysRevD.94.033008. arXiv: 1605.04508 [hep-ph].

[163] O. Cakir, A. Senol, and A. T. Tasci. "Single Production of Fourth Family t-prime Quarks at LHeC." In: *EPL* 88.1 (2009), p. 11002. DOI: 10.1209/0295-5075/88/11002. arXiv: 0905.4347 [hep-ph].

[164] Zhiqing Zhang. "Top and EW Physics at the LHeC." In: *PoS* EPS-HEP2015 (2015), p. 342. DOI: 10.22323/1.234.0342. arXiv: 1511.05399 [hep-ex].

[165] David Curtin, Kaustubh Deshpande, Oliver Fischer, and José Zurita. "New Physics Opportunities for Long-Lived Particles at Electron-Proton Colliders." In: *JHEP* 07 (2018), p. 024. DOI: 10.1007/JHEP07(2018)024. arXiv: 1712.07135 [hep-ph].

[166] Georges Azuelos, Monica D'Onofrio, Oliver Fischer, and Jose Zurita. "BSM physics at the LHeC and the FCC-eh." In: *PoS* DIS2018 (2018), p. 190. DOI: 10.22323/1.316.0190. arXiv: 1807.01618 [hep-ph].

[167] A. Abada et al. "FCC Physics Opportunities: Future Circular Collider Conceptual Design Report Volume 1." In: *Eur. Phys. J. C* 79.6 (2019), p. 474. DOI: 10.1140/epjc/s10052-019-6904-3.

[168] Max Klein. "The Large Hadron Electron Collider Project." In: *17th International Workshop on Deep-Inelastic Scattering and Related Subjects*. Aug. 2009. arXiv: 0908.2877 [hep-ex].

[169] F. Zimmermann, M. Benedikt, D. Schulte, and J. Wenninger. "Challenges for Highest Energy Circular Colliders." In: *Proc. 5th International Particle Accelerator Conference (IPAC'14), Dresden, Germany, June 15-20, 2014*. (Dresden, Germany). International Particle Accelerator Conference 5. https://doi.org/10.18429/JACoW-IPAC2014-MOXAA01. Geneva, Switzerland: JACoW, 2014, pp. 1–6. ISBN: 978-3-95450-132-8. DOI: https://doi.org/10.18429/JACoW-IPAC2014-MOXAA01. URL: http://jacow.org/ipac2014/papers/moxaa01.pdf.

[170] M. Klein and R. Yoshida. "Collider Physics at HERA." In: *Prog. Part. Nucl. Phys.* 61 (2008), pp. 343–393. DOI: 10.1016/j.ppnp.2008.05.002. arXiv: 0805.3334 [hep-ex].

[171] J. B. Dainton, M. Klein, P. Newman, E. Perez, and F. Willeke. "Deep inelastic electron-nucleon scattering at the LHC." In: *JINST* 1 (2006), P10001. DOI: 10.1088/1748-0221/1/10/P10001. arXiv: hep-ex/0603016.

[172] Uta Klein. *private communication.*

[173] E. Barberio et al. "Averages of b–hadron properties at the end of 2005." In: (Mar. 2006). arXiv: hep-ex/0603003.

[174] Stefan Antusch, Eros Cazzato, and Oliver Fischer. "Sterile neutrino searches via displaced vertices at LHCb." In: *Phys. Lett. B* 774 (2017), pp. 114–118. DOI: 10.1016/j.physletb.2017.09.057. arXiv: 1706.05990 [hep-ph].

[175] J. Adam et al. "New constraint on the existence of the $\mu^+ \to e^+\gamma$ decay." In: *Phys. Rev. Lett.* 110 (2013), p. 201801. DOI: 10.1103/PhysRevLett.110.201801. arXiv: 1303.0754 [hep-ex].

[176] Stefano Miscetti. "Status of the Mu2e experiment at Fermilab." In: *EPJ Web Conf.* 234 (2020). Ed. by G. D'Ambrosio, M. Iacovacci, S. Mastroianni, M. Passera, and G. Venanzoni, p. 01010. DOI: 10.1051/epjconf/202023401010.

[177] Sudip Jana, Nobuchika Okada, and Digesh Raut. "Displaced Vertex and Disappearing Track Signatures in type-III Seesaw." In: (Nov. 2019). arXiv: 1911.09037 [hep-ph].

[178] O. Flores-Sánchez, J. Hernández-Sánchez, C.G. Honorato, S. Moretti, and S. Rosado. "Light charged Higgs boson production at futures ep colliders." In: *PoS* DIS2019 (2019), p. 094. DOI: 10.22323/1.352.0094. arXiv: 1908.09405 [hep-ph].

[179] Georges Azuelos, Monica D'Onofrio, Sho Iwamoto, and Kechen Wang. "Search for the SUSY electroweak sector at ep colliders." In: *Phys. Rev. D* 101.9 (2020), p. 095015. DOI: 10.1103/PhysRevD.101.095015. arXiv: 1912.03823 [hep-ph].

[180] Eric Conte, Benjamin Fuks, and Guillaume Serret. "MadAnalysis 5, A User-Friendly Framework for Collider Phenomenology." In: *Comput. Phys. Commun.* 184 (2013), pp. 222–256. DOI: 10.1016/j.cpc.2012.09.009. arXiv: 1206.1599 [hep-ph].

[181] U. Bellgardt et al. "Search for the Decay mu+ —> e+ e+ e-." In: *Nucl. Phys.* B299 (1988), pp. 1–6. DOI: 10.1016/0550-3213(88)90462-2.

[182] V.A. Baranov et al. "Search for mu+ —> e+ e+ e- decay." In: *Sov. J. Nucl. Phys.* 53 (1991), pp. 802–807.

[183] C. Dohmen et al. "Test of lepton flavor conservation in mu —> e conversion on titanium." In: *Phys. Lett.* B317 (1993), pp. 631–636. DOI: 10.1016/0370-2693(93)91383-X.

[184] Alexander Vadimovich Bednyakov and ŞüKrü Hanif TanyıLdıZı. "A Mathematica Package for Calculation of One-Loop Penguins in FCNC Processes." In: *Int. J. Mod. Phys. C* 26.04 (2014), p. 1550042. DOI: 10.1142/S0129183115500424. arXiv: 1311.5546 [hep-ph].

[185] J. Bernabeu, G.A. Gonzalez-Sprinberg, and J. Vidal. "Weak dipole moments at e^+e^- colliders." In: *Ringberg Workshop on Perspectives for Electroweak Interactions in e+ e- Collisions*. Feb. 1995, pp. 0329–342. arXiv: hep-ph/9505223.

[186] Robert Budny, Boris Kayser, and Joel Primack. "Weak Electric and Magnetic Dipole Moment Effects in e+ e- –> Lepton+ Lepton-." In: *Phys. Rev.* D15 (1977), p. 1222. DOI: 10.1103/PhysRevD.15.1222.

[187] A. Gutiérrez-Rodríguez, M.A. Hernández-Ruíz, C.P. Castañeda Almanza, A. Espinoza-Garrido, and A. Chubykalo. "Limits on the electromagnetic and weak dipole moments of the tau-lepton in a 331 model." In: *Nucl. Phys. B Proc. Suppl.* 253-255 (2014). Ed. by Kiyoshi Hayasaka and Toru Iijima, pp. 202–203. DOI: 10.1016/j.nuclphysbps.2014.09.049.

[188] Eric Conte, Béranger Dumont, Benjamin Fuks, and Chris Wymant. "Designing and recasting LHC analyses with MadAnalysis 5." In: *Eur. Phys. J. C* 74.10 (2014), p. 3103. DOI: 10.1140/epjc/s10052-014-3103-0. arXiv: 1405.3982 [hep-ph].

[189] Giuseppe Bagliesi. "Tau tagging at Atlas and CMS." In: *17th Symposium on Hadron Collider Physics 2006 (HCP 2006)*. July 2007. arXiv: 0707.0928 [hep-ex].

[190] S. Gennai, F. Moortgat, L. Wendland, A. Nikitenko, S. Wakefield, G. Bagliesi, S. Dutta, A. Kalinowski, M. Konecki, and D. Kotlinski. "Tau jet reconstruction and tagging at high level trigger and off-line." In: *Eur. Phys. J. C* 46S1 (2006), pp. 1–21. DOI: 10.1140/epjcd/s2006-02-001-y.

[191] Tomohiro Abe et al. "LHC Dark Matter Working Group: Next-generation spin-0 dark matter models." In: *Phys. Dark Univ.* 27 (2020), p. 100351. DOI: 10.1016/j.dark.2019.100351. arXiv: 1810.09420 [hep-ex].

[192] R. Alonso, M. Dhen, M.B. Gavela, and T. Hambye. "Muon conversion to electron in nuclei in type-I seesaw models." In: *JHEP* 01 (2013), p. 118. DOI: 10.1007/JHEP01(2013)118. arXiv: 1209.2679 [hep-ph].

[193] Benjamin W. Lee and Robert E. Shrock. "Natural Suppression of Symmetry Violation in Gauge Theories: Muon - Lepton and Electron Lepton Number Nonconservation." In: *Phys. Rev.* D16 (1977), p. 1444. DOI: 10.1103/PhysRevD.16.1444.

[194] M. Cepeda et al. "Report from Working Group 2: Higgs Physics at the HL-LHC and HE-LHC." In: *CERN Yellow Rep. Monogr.* 7 (2019). Ed. by Andrea Dainese, Michelangelo Mangano, Andreas B. Meyer, Aleandro Nisati, Gavin Salam, and Mika Anton Vesterinen, pp. 221–584. DOI: 10.23731/CYRM-2019-007.221. arXiv: 1902.00134 [hep-ph].

[195] M. Bicer et al. "First Look at the Physics Case of TLEP." In: *JHEP* 01 (2014). Ed. by Norman A. Graf, Michael E. Peskin, and Jonathan L. Rosner, p. 164. DOI: 10.1007/JHEP01(2014)164. arXiv: 1308.6176 [hep-ex].

[196] "The International Linear Collider Technical Design Report - Volume 2: Physics." In: (June 2013). Ed. by Howard Baer et al. arXiv: 1306.6352 [hep-ph].

[197] Muhammd Ahmad et al. "CEPC-SPPC Preliminary Conceptual Design Report. 1. Physics and Detector." In: (Mar. 2015).

[198] Tao Han and H. C. Liu. "PRODUCTION OF CHARGED AND NEUTRAL HIGGS BOSONS IN HIGH-ENERGY LEPTON NUCLEON INTERACTIONS." In: *Z. Phys. C* 28 (1985), pp. 295–301. DOI: 10.1007/BF01575738.

[199] Tao Han and Bruce Mellado. "Higgs Boson Searches and the H b anti-b Coupling at the LHeC." In: *Phys. Rev. D* 82 (2010), p. 016009. DOI: 10.1103/PhysRevD.82.016009. arXiv: 0909.2460 [hep-ph].

[200] Mukesh Kumar, Xifeng Ruan, Rashidul Islam, Alan S. Cornell, Max Klein, Uta Klein, and Bruce Mellado. "Probing anomalous couplings using di-Higgs production in electron–proton collisions." In: *Phys. Lett. B* 764 (2017), pp. 247–253. DOI: 10.1016/j.physletb.2016.11.039. arXiv: 1509.04016 [hep-ph].

[201] Yi-Lei Tang, Chen Zhang, and Shou-hua Zhu. "Invisible Higgs Decay at the LHeC." In: *Phys. Rev. D* 94.1 (2016), p. 011702. DOI: 10.1103/PhysRevD.94.011702. arXiv: 1508.01095 [hep-ph].

[202] Chuene Mosomane, Mukesh Kumar, Alan S. Cornell, and Bruce Mellado. "Exploring CP-even scalars of a Two Higgs-doublet model in future e^- p colliders." In: *J. Phys. Conf. Ser.* 889.1 (2017), p. 012004. DOI: 10.1088/1742-6596/889/1/012004. arXiv: 1707.05997 [hep-ph].

[203] Vardan Khachatryan et al. "Search for a Higgs boson in the mass range from 145 to 1000 GeV decaying to a pair of W or Z bosons." In: *JHEP* 10 (2015), p. 144. DOI: 10.1007/JHEP10(2015)144. arXiv: 1504.00936 [hep-ex].

[204] Albert M Sirunyan et al. "Search for a new scalar resonance decaying to a pair of Z bosons in proton-proton collisions at $\sqrt{s} = 13$ TeV." In: *JHEP* 06 (2018). [Erratum: JHEP 03, 128 (2019)], p. 127. DOI: 10.1007/JHEP06(2018)127. arXiv: 1804.01939 [hep-ex].

[205] *Search for a new scalar resonance decaying to a pair of Z bosons at the High-Luminosity LHC*. Tech. rep. CMS-PAS-FTR-18-040. Geneva: CERN, 2019. URL: https://cds.cern.ch/record/2658263.

[206] Georges Aad et al. "Measurements of the Higgs boson production and decay rates and constraints on its couplings from a combined ATLAS and CMS analysis of the LHC pp collision data at $\sqrt{s} = 7$ and 8 TeV." In: *JHEP* 08 (2016), p. 045. DOI: 10.1007/JHEP08(2016)045. arXiv: 1606.02266 [hep-ex].

[207] S. Y. Choi, D. J. Miller, M. M. Muhlleitner, and P. M. Zerwas. "Identifying the Higgs spin and parity in decays to Z pairs." In: *Phys. Lett. B* 553 (2003), pp. 61–71. DOI: 10.1016/S0370-2693(02)03191-X. arXiv: hep-ph/0210077.

[208] Yanyan Gao, Andrei V. Gritsan, Zijin Guo, Kirill Melnikov, Markus Schulze, and Nhan V. Tran. "Spin Determination of Single-Produced Resonances at Hadron Colliders." In: *Phys. Rev. D* 81 (2010), p. 075022. DOI: 10.1103/PhysRevD.81.075022. arXiv: 1001.3396 [hep-ph].

[209] Joseph R. Dell'Aquila and Charles A. Nelson. "P or CP Determination by Sequential Decays: V1 V2 Modes With Decays Into $\bar{\ell}$epton (A) ℓ(B) And/or $\bar{q}$ (A) q(B)." In: *Phys. Rev. D* 33 (1986), p. 80. DOI: 10.1103/PhysRevD.33.80.

[210] Matthew R. Buckley and Dorival Goncalves. "Boosting the Direct CP Measurement of the Higgs-Top Coupling." In: *Phys. Rev. Lett.* 116.9 (2016), p. 091801. DOI: 10.1103/PhysRevLett.116.091801. arXiv: 1507.07926 [hep-ph].

[211] A. D. Sakharov. "Violation of CP Invariance, C asymmetry, and baryon asymmetry of the universe." In: *Pisma Zh. Eksp. Teor. Fiz.* 5 (1967), pp. 32–35. DOI: 10.1070/PU1991v034n05ABEH002497.

[212] J. H. Christenson, J. W. Cronin, V. L. Fitch, and R. Turlay. "Evidence for the 2π Decay of the K_2^0 Meson." In: *Phys. Rev. Lett.* 13 (1964), pp. 138–140. DOI: 10.1103/PhysRevLett.13.138.

[213] Roel Aaij et al. "Observation of CP Violation in Charm Decays." In: *Phys. Rev. Lett.* 122.21 (2019), p. 211803. DOI: 10.1103/PhysRevLett.122.211803. arXiv: 1903.08726 [hep-ex].

[214] W. Abdallah, S. Khalil, and S. Moretti. "Double Higgs peak in the minimal SUSY B-L model." In: *Phys. Rev. D* 91.1 (2015), p. 014001. DOI: 10.1103/PhysRevD.91.014001. arXiv: 1409.7837 [hep-ph].

[215] Stefan Buddenbrock, Alan S. Cornell, Yaquan Fang, Abdualazem Fadol Mohammed, Mukesh Kumar, Bruce Mellado, and Kehinde G. Tomiwa. "The emergence of multi-lepton anomalies at the LHC and their compatibility with new physics at the EW scale." In: *JHEP* 10 (2019), p. 157. DOI: 10.1007/JHEP10(2019)157. arXiv: 1901.05300 [hep-ph].

[216] T. Biekötter, M. Chakraborti, and S. Heinemeyer. "The "96 GeV excess" at the LHC." In: Mar. 2020. arXiv: 2003.05422 [hep-ph].

[217] H. E. Haber, Gordon L. Kane, and T. Sterling. "The Fermion Mass Scale and Possible Effects of Higgs Bosons on Experimental Observables." In: *Nucl. Phys. B* 161 (1979), pp. 493–532. DOI: 10.1016/0550-3213(79)90225-6.

[218] T. D. Lee. "A Theory of Spontaneous T Violation." In: *Phys. Rev. D* 8 (1973). Ed. by G. Feinberg, pp. 1226–1239. DOI: 10.1103/PhysRevD.8.1226.

[219] G. C. Branco, P. M. Ferreira, L. Lavoura, M. N. Rebelo, Marc Sher, and Joao P. Silva. "Theory and phenomenology of two-Higgs-doublet models." In: *Phys. Rept.* 516 (2012), pp. 1–102. DOI: 10.1016/j.physrep.2012.02.002. arXiv: 1106.0034 [hep-ph].

[220] Vernon D. Barger, J. L. Hewett, and R. J. N. Phillips. "New Constraints on the Charged Higgs Sector in Two Higgs Doublet Models." In: *Phys. Rev. D* 41 (1990), pp. 3421–3441. DOI: 10.1103/PhysRevD.41.3421.

[221] Georges Aad et al. "Study of the spin and parity of the Higgs boson in diboson decays with the ATLAS detector." In: *Eur. Phys. J. C* 75.10 (2015). [Erratum: Eur.Phys.J.C 76, 152 (2016)], p. 476. DOI: 10.1140/epjc/s10052-015-3685-1. arXiv: 1506.05669 [hep-ex].

[222] Vardan Khachatryan et al. "Combined search for anomalous pseudoscalar HVV couplings in VH(H $\to$ b$\bar{\text{b}}$) production and H $\to$ VV decay." In: *Phys. Lett. B* 759 (2016), pp. 672–696. DOI: 10.1016/j.physletb.2016.06.004. arXiv: 1602.04305 [hep-ex].

[223] Kingman Cheung, Adil Jueid, Ying-Nan Mao, and Stefano Moretti. "Two-Higgs-doublet model with soft CP violation confronting electric dipole moments and colliders." In: *Phys. Rev. D* 102.7 (2020), p. 075029. DOI: 10.1103/PhysRevD.102.075029. arXiv: 2003.04178 [hep-ph].

[224] Ilya F. Ginzburg and Maria Krawczyk. "Symmetries of two Higgs doublet model and CP violation." In: *Phys. Rev. D* 72 (2005), p. 115013. DOI: 10.1103/PhysRevD.72.115013. arXiv: hep-ph/0408011.

[225] Duarte Fontes, Margarete Mühlleitner, Jorge C. Romão, Rui Santos, João P. Silva, and Jonas Wittbrodt. "The C2HDM revisited." In: *JHEP* 02 (2018), p. 073. DOI: 10.1007/JHEP02(2018)073. arXiv: 1711.09419 [hep-ph].

[226] Werner Porod. "SPheno, a program for calculating supersymmetric spectra, SUSY particle decays and SUSY particle production at e+ e- colliders." In: *Comput. Phys. Commun.* 153 (2003), pp. 275–315. DOI: 10.1016/S0010-4655(03)00222-4. arXiv: hep-ph/0301101.

[227] W. Porod and F. Staub. "SPheno 3.1: Extensions including flavour, CP-phases and models beyond the MSSM." In: *Comput. Phys. Commun.* 183 (2012), pp. 2458–2469. DOI: 10.1016/j.cpc.2012.05.021. arXiv: 1104.1573 [hep-ph].

[228] E. A. Paschos. "Diagonal Neutral Currents." In: *Phys. Rev. D* 15 (1977), p. 1966. DOI: 10.1103/PhysRevD.15.1966.

[229] Fawzi Boudjema, Rohini M. Godbole, Diego Guadagnoli, and Kirtimaan A. Mohan. "Lab-frame observables for probing the top-Higgs interaction." In: *Phys. Rev. D* 92.1 (2015), p. 015019. DOI: 10.1103/PhysRevD.92.015019. arXiv: 1501.03157 [hep-ph].

[230] Dorival Goncalves and David Lopez-Val. "Pseudoscalar searches with dileptonic tops and jet substructure." In: *Phys. Rev. D* 94.9 (2016), p. 095005. DOI: 10.1103/PhysRevD.94.095005. arXiv: 1607.08614 [hep-ph].

[231] S. Amor Dos Santos et al. "Probing the CP nature of the Higgs coupling in t$\bar{\text{t}}$h events at the LHC." In: *Phys. Rev. D* 96.1 (2017), p. 013004. DOI: 10.1103/PhysRevD.96.013004. arXiv: 1704.03565 [hep-ph].

[232] C. P. Buszello, I. Fleck, P. Marquard, and J. J. van der Bij. "Prospective analysis of spin- and CP-sensitive variables in H —> Z Z —> l(1)+ l(1)- l(2)+ l(2)- at the LHC." In: *Eur. Phys. J. C* 32 (2004), pp. 209–219. DOI: 10.1140/epjc/s2003-01392-0. arXiv: hep-ph/0212396.

[233] Rohini M. Godbole, D. J. Miller, and M. Margarete Muhlleitner. "Aspects of CP violation in the H ZZ coupling at the LHC." In: *JHEP* 12 (2007), p. 031. DOI: 10.1088/1126-6708/2007/12/031. arXiv: 0708.0458 [hep-ph].

[234] Felipe Ferreira, Benjamin Fuks, Verónica Sanz, and Dipan Sengupta. "Probing CP-violating Higgs and gauge-boson couplings in the Standard Model effective field theory." In: *Eur. Phys. J. C* 77.10 (2017), p. 675. DOI: 10.1140/epjc/s10052-017-5226-6. arXiv: 1612.01808 [hep-ph].

[235] A. De Rujula, Joseph Lykken, Maurizio Pierini, Christopher Rogan, and Maria Spiropulu. "Higgs Look-Alikes at the LHC." In: *Phys. Rev. D* 82 (2010), p. 013003. DOI: 10.1103/PhysRevD.82.013003. arXiv: 1001.5300 [hep-ph].

[236] Sara Bolognesi, Yanyan Gao, Andrei V. Gritsan, Kirill Melnikov, Markus Schulze, Nhan V. Tran, and Andrew Whitbeck. "On the spin and parity of a single-produced resonance at the LHC." In: *Phys. Rev. D* 86 (2012), p. 095031. DOI: 10.1103/PhysRevD.86.095031. arXiv: 1208.4018 [hep-ph].

[237] P. Artoisenet et al. "A framework for Higgs characterisation." In: *JHEP* 11 (2013), p. 043. DOI: 10.1007/JHEP11(2013)043. arXiv: 1306.6464 [hep-ph].

[238] Duarte Fontes, Jorge C. Romão, Rui Santos, and João P. Silva. "Undoubtable signs of CP-violation in Higgs boson decays at the LHC run 2." In: *Phys. Rev. D* 92.5 (2015), p. 055014. DOI: 10.1103/PhysRevD.92.055014. arXiv: 1506.06755 [hep-ph].

[239] Roni Harnik, Adam Martin, Takemichi Okui, Reinard Primulando, and Felix Yu. "Measuring CP Violation in $h \to \tau^+\tau^-$ at Colliders." In: *Phys. Rev. D* 88.7 (2013), p. 076009. DOI: 10.1103/PhysRevD.88.076009. arXiv: 1308.1094 [hep-ph].

[240] Stefan Berge, Werner Bernreuther, and Sebastian Kirchner. "Prospects of constraining the Higgs boson's CP nature in the tau decay channel at the LHC." In: *Phys. Rev. D* 92 (2015), p. 096012. DOI: 10.1103/PhysRevD.92.096012. arXiv: 1510.03850 [hep-ph].

[241] Akanksha Bhardwaj, Partha Konar, Pankaj Sharma, and Abhaya Kumar Swain. "Exploring CP phase in τ-lepton Yukawa coupling in Higgs decays at the LHC." In: *J. Phys. G* 46.10 (2019), p. 105001. DOI: 10.1088/1361-6471/ab2ee5. arXiv: 1612.01417 [hep-ph].

[242] K. Lasocha, E. Richter-Was, M. Sadowski, and Z. Was. "Deep neural network application: Higgs boson CP state mixing angle in $H \to \tau\tau$ decay and at the LHC." In: *Phys. Rev. D* 103.3 (2021), p. 036003. DOI: 10.1103/PhysRevD.103.036003. arXiv: 2001.00455 [hep-ph].

[243] Abhaya Kumar Swain. "M_{T2} as a probe of CP phase in $h \to \tau\tau$ at the LHC." In: (Aug. 2020). arXiv: 2008.11127 [hep-ph].

[244] A. Arhrib, E. Christova, H. Eberl, and E. Ginina. "CP violation in charged Higgs production and decays in the Complex Two Higgs Doublet Model." In: *JHEP* 04 (2011), p. 089. DOI: 10.1007/JHEP04(2011)089. arXiv: 1011.6560 [hep-ph].

[245] M. Baak, M. Goebel, J. Haller, A. Hoecker, D. Kennedy, R. Kogler, K. Moenig, M. Schott, and J. Stelzer. "The Electroweak Fit of the Standard Model after the Discovery of a New Boson at the LHC." In: *Eur. Phys. J. C* 72 (2012), p. 2205. DOI: 10.1140/epjc/s10052-012-2205-9. arXiv: 1209.2716 [hep-ph].

[246] M. Baak, M. Goebel, J. Haller, A. Hoecker, D. Ludwig, K. Moenig, M. Schott, and J. Stelzer. "Updated Status of the Global Electroweak Fit and Constraints on New Physics." In: *Eur. Phys. J. C* 72 (2012), p. 2003. DOI: 10.1140/epjc/s10052-012-2003-4. arXiv: 1107.0975 [hep-ph].

[247] Werner Porod, Florian Staub, and Avelino Vicente. "A Flavor Kit for BSM models." In: *Eur. Phys. J. C* 74.8 (2014), p. 2992. DOI: 10.1140/epjc/s10052-014-2992-2. arXiv: 1405.1434 [hep-ph].

[248] Mikolaj Misiak and Matthias Steinhauser. "Weak radiative decays of the B meson and bounds on $M_{H^\pm}$ in the Two-Higgs-Doublet Model." In: *Eur. Phys. J. C* 77.3 (2017), p. 201. DOI: 10.1140/epjc/s10052-017-4776-y. arXiv: 1702.04571 [hep-ph].

[249] Tetsuya Enomoto and Ryoutaro Watanabe. "Flavor constraints on the Two Higgs Doublet Models of Z_2 symmetric and aligned types." In: *JHEP* 05 (2016), p. 002. DOI: 10.1007/JHEP05(2016)002. arXiv: 1511.05066 [hep-ph].

[250] Yasmine Sara Amhis et al. "Averages of b-hadron, c-hadron, and τ-lepton properties as of 2018." In: (Sept. 2019). arXiv: 1909.12524 [hep-ex].

[251] Philip Bechtle, Oliver Brein, Sven Heinemeyer, Oscar Stål, Tim Stefaniak, Georg Weiglein, and Karina E. Williams. "HiggsBounds – 4: Improved Tests of Extended Higgs Sectors against Exclusion Bounds from LEP, the Tevatron and the LHC." In: *Eur. Phys. J. C* 74.3 (2014), p. 2693. DOI: 10.1140/epjc/s10052-013-2693-2. arXiv: 1311.0055 [hep-ph].

[252] Philip Bechtle, Sven Heinemeyer, Oscar Stål, Tim Stefaniak, and Georg Weiglein. "HiggsSignals: Confronting arbitrary Higgs sectors with measurements at the Tevatron and the LHC." In: *Eur. Phys. J. C* 74.2 (2014), p. 2711. DOI: 10.1140/epjc/s10052-013-2711-4. arXiv: 1305.1933 [hep-ph].

[253] *Combined measurements of the Higgs boson's couplings at* $\sqrt{s} = 13$ *TeV*. Tech. rep. CMS-PAS-HIG-17-031. Geneva: CERN, 2018. URL: http://cds.cern.ch/record/2308127.

[254] *Combined measurements of Higgs boson production and decay using up to 80* fb^{-1} *of proton–proton collision data at* $\sqrt{s} = 13$ *TeV collected with the ATLAS experiment*. Tech. rep. ATLAS-CONF-2018-031. Geneva: CERN, 2018. URL: https://cds.cern.ch/record/2629412.

[255] V. Andreev et al. "Improved limit on the electric dipole moment of the electron." In: *Nature* 562.7727 (2018), pp. 355–360. DOI: 10.1038/s41586-018-0599-8.

[256] Tomohiro Abe, Junji Hisano, Teppei Kitahara, and Kohsaku Tobioka. "Gauge invariant Barr-Zee type contributions to fermionic EDMs in the two-Higgs doublet models." In: *JHEP* 01 (2014). [Erratum: JHEP 04, 161 (2016)], p. 106. DOI: 10.1007/JHEP01(2014)106. arXiv: 1311.4704 [hep-ph].

[257] Eung Jin Chun, Jongkuk Kim, and Tanmoy Mondal. "Electron EDM and Muon anomalous magnetic moment in Two-Higgs-Doublet Models." In: *JHEP* 12 (2019), p. 068. DOI: 10.1007/JHEP12(2019)068. arXiv: 1906.00612 [hep-ph].

[258] Wolfgang Altmannshofer, Stefania Gori, Nick Hamer, and Hiren H. Patel. "Electron EDM in the complex two-Higgs doublet model." In: *Phys. Rev. D* 102 (2020), p. 115042. DOI: 10.1103/PhysRevD.102.115042. arXiv: 2009.01258 [hep-ph].

[259] Daniel Egana-Ugrinovic and Scott Thomas. "Higgs Boson Contributions to the Electron Electric Dipole Moment." In: (Oct. 2018). arXiv: 1810.08631 [hep-ph].

[260] Alexander Belyaev, Neil D. Christensen, and Alexander Pukhov. "CalcHEP 3.4 for collider physics within and beyond the Standard Model." In: *Comput. Phys. Commun.* 184 (2013), pp. 1729–1769. DOI: 10.1016/j.cpc.2013.01.014. arXiv: 1207.6082 [hep-ph].

[261] Georges Aad et al. "Evidence for the Higgs-boson Yukawa coupling to tau leptons with the ATLAS detector." In: *JHEP* 04 (2015), p. 117. DOI: 10.1007/JHEP04(2015)117. arXiv: 1501.04943 [hep-ex].

[262] *Analysis of the CP structure of the Yukawa coupling between the Higgs boson and τ leptons in proton-proton collisions at $\sqrt{s} = 13$ TeV*. Tech. rep. CMS-PAS-HIG-20-006. Geneva: CERN, 2020. URL: https://cds.cern.ch/record/2725571.

[263] Vladyslav Shtabovenko, Rolf Mertig, and Frederik Orellana. "FeynCalc 9.3: New features and improvements." In: *Comput. Phys. Commun.* 256 (2020), p. 107478. DOI: 10.1016/j.cpc.2020.107478. arXiv: 2001.04407 [hep-ph].

[264] Hiren H. Patel. "Package-X: A Mathematica package for the analytic calculation of one-loop integrals." In: *Comput. Phys. Commun.* 197 (2015), pp. 276–290. DOI: 10.1016/j.cpc.2015.08.017. arXiv: 1503.01469 [hep-ph].

[265] Werner Bernreuther, Patrick Gonzalez, and Martin Wiebusch. "Pseudoscalar Higgs Boson Decays into W and Z Bosons Revisited." In: (Sept. 2009). arXiv: 0909.3772 [hep-ph].

[266] A. Hammad, S. Khalil, and S. Moretti. "LHC signals of a B-L supersymmetric standard model CP -even Higgs boson." In: *Phys. Rev. D* 93.11 (2016), p. 115035. DOI: 10.1103/PhysRevD.93.115035. arXiv: 1601.07934 [hep-ph].

[267] Q. R. Ahmad et al. "Direct evidence for neutrino flavor transformation from neutral current interactions in the Sudbury Neutrino Observatory." In: *Phys. Rev. Lett.* 89 (2002), p. 011301. DOI: 10.1103/PhysRevLett.89.011301. arXiv: nucl-ex/0204008.

[268] Y. Fukuda et al. "Evidence for oscillation of atmospheric neutrinos." In: *Phys. Rev. Lett.* 81 (1998), pp. 1562–1567. DOI: 10.1103/PhysRevLett.81.1562. arXiv: hep-ex/9807003.

[269] W. Konetschny and W. Kummer. "Nonconservation of Total Lepton Number with Scalar Bosons." In: *Phys. Lett. B* 70 (1977), pp. 433–435. DOI: 10.1016/0370-2693(77)90407-5.

[270] M. Magg and C. Wetterich. "Neutrino Mass Problem and Gauge Hierarchy." In: *Phys. Lett. B* 94 (1980), pp. 61–64. DOI: 10.1016/0370-2693(80)90825-4.

[271] J. Schechter and J. W. F. Valle. "Neutrino Masses in SU(2) x U(1) Theories." In: *Phys. Rev. D* 22 (1980), p. 2227. DOI: 10.1103/PhysRevD.22.2227.

[272] T. P. Cheng and Ling-Fong Li. "Neutrino Masses, Mixings and Oscillations in SU(2) x U(1) Models of Electroweak Interactions." In: *Phys. Rev. D* 22 (1980), p. 2860. DOI: 10.1103/PhysRevD.22.2860.

[273] Rabindra N. Mohapatra and Goran Senjanovic. "Neutrino Masses and Mixings in Gauge Models with Spontaneous Parity Violation." In: *Phys. Rev. D* 23 (1981), p. 165. DOI: 10.1103/PhysRevD.23.165.

[274] George Lazarides, Q. Shafi, and C. Wetterich. "Proton Lifetime and Fermion Masses in an SO(10) Model." In: *Nucl. Phys. B* 181 (1981), pp. 287–300. DOI: 10.1016/0550-3213(81)90354-0.

[275] Alessio Maiezza, Miha Nemevšek, and Fabrizio Nesti. "Lepton Number Violation in Higgs Decay at LHC." In: *Phys. Rev. Lett.* 115 (2015), p. 081802. DOI: 10.1103/PhysRevLett.115.081802. arXiv: 1503.06834 [hep-ph].

[276] Miha Nemevšek, Fabrizio Nesti, and Juan Carlos Vasquez. "Majorana Higgses at colliders." In: *JHEP* 04 (2017), p. 114. DOI: 10.1007/JHEP04(2017)114. arXiv: 1612.06840 [hep-ph].

[277] Yong Du, Aaron Dunbrack, Michael J. Ramsey-Musolf, and Jiang-Hao Yu. "Type-II Seesaw Scalar Triplet Model at a 100 TeV pp Collider: Discovery and Higgs Portal Coupling Determination." In: *JHEP* 01 (2019), p. 101. DOI: 10.1007/JHEP01(2019)101. arXiv: 1810.09450 [hep-ph].

[278] Georges Aad et al. "Search for doubly-charged Higgs bosons in like-sign dilepton final states at $\sqrt{s} = 7$ TeV with the ATLAS detector." In: *Eur. Phys. J. C* 72 (2012), p. 2244. DOI: 10.1140/epjc/s10052-012-2244-2. arXiv: 1210.5070 [hep-ex].

[279] *Inclusive search for doubly charged higgs in leptonic final states at sqrt s=7 TeV*. Tech. rep. CMS-PAS-HIG-11-007. Geneva: CERN, 2011. URL: http://cds.cern.ch/record/1369542.

[280] Georges Aad et al. "Search for anomalous production of prompt same-sign lepton pairs and pair-produced doubly charged Higgs bosons with $\sqrt{s} = 8$ TeV pp collisions using the ATLAS detector." In: *JHEP* 03 (2015), p. 041. DOI: 10.1007/JHEP03(2015)041. arXiv: 1412.0237 [hep-ex].

[281] "Search for a doubly-charged Higgs boson with $\sqrt{s} = 8$ TeV pp collisions at the CMS experiment." In: (2016).

[282] Morad Aaboud et al. "Search for doubly charged Higgs boson production in multi-lepton final states with the ATLAS detector using proton–proton collisions at $\sqrt{s} = 13$ TeV." In: *Eur. Phys. J. C* 78.3 (2018), p. 199. DOI: 10.1140/epjc/s10052-018-5661-z. arXiv: 1710.09748 [hep-ex].

[283] "A search for doubly-charged Higgs boson production in three and four lepton final states at $\sqrt{s} = 13$ TeV." In: (2017).

[284] Morad Aaboud et al. "Search for doubly charged scalar bosons decaying into same-sign W boson pairs with the ATLAS detector." In: *Eur. Phys. J. C* 79.1 (2019), p. 58. DOI: 10.1140/epjc/s10052-018-6500-y. arXiv: 1808.01899 [hep-ex].

[285] Pankaj Agrawal, Manimala Mitra, Saurabh Niyogi, Sujay Shil, and Michael Spannowsky. "Probing the Type-II Seesaw Mechanism through the Production of Higgs Bosons at a Lepton Collider." In: *Phys. Rev. D* 98.1 (2018), p. 015024. DOI: 10.1103/PhysRevD.98.015024. arXiv: 1803.00677 [hep-ph].

[286] Ivan Esteban, M. C. Gonzalez-Garcia, Michele Maltoni, Ivan Martinez-Soler, and Thomas Schwetz. "Updated fit to three neutrino mixing: exploring the accelerator-reactor complementarity." In: *JHEP* 01 (2017), p. 087. DOI: 10.1007/JHEP01(2017)087. arXiv: 1611.01514 [hep-ph].

[287] NuFIT 3.2 (2018). "www.nu-fit.org." In: ().

[288] M. Tanabashi et al. "Review of Particle Physics." In: *Phys. Rev. D* 98.3 (2018), p. 030001. DOI: 10.1103/PhysRevD.98.030001.

[289] Shinya Kanemura, Kei Yagyu, and Hiroshi Yokoya. "First constraint on the mass of doubly-charged Higgs bosons in the same-sign diboson decay scenario at the LHC." In: *Phys. Lett. B* 726 (2013), pp. 316–319. DOI: 10.1016/j.physletb.2013.08.054. arXiv: 1305.2383 [hep-ph].

[290] Mitsuru Kakizaki, Yoshiteru Ogura, and Fumitaka Shima. "Lepton flavor violation in the triplet Higgs model." In: *Phys. Lett. B* 566 (2003), pp. 210–216. DOI: 10.1016/S0370-2693(03)00833-5. arXiv: hep-ph/0304254.

[291] A. G. Akeroyd, Mayumi Aoki, and Hiroaki Sugiyama. "Lepton Flavour Violating Decays tau —> anti-l ll and mu —> e gamma in the Higgs Triplet Model." In: *Phys. Rev. D* 79 (2009), p. 113010. DOI: 10.1103/PhysRevD.79.113010. arXiv: 0904.3640 [hep-ph].

[292] P. S. Bhupal Dev, Clara Miralles Vila, and Werner Rodejohann. "Naturalness in testable type II seesaw scenarios." In: *Nucl. Phys. B* 921 (2017), pp. 436–453. DOI: 10.1016/j.nuclphysb.2017.06.007. arXiv: 1703.00828 [hep-ph].

[293] G. W. Bennett et al. "Final Report of the Muon E821 Anomalous Magnetic Moment Measurement at BNL." In: *Phys. Rev. D* 73 (2006), p. 072003. DOI: 10.1103/PhysRevD.73.072003. arXiv: hep-ex/0602035.

[294] P. S. Bhupal Dev, Dilip Kumar Ghosh, Nobuchika Okada, and Ipsita Saha. "125 GeV Higgs Boson and the Type-II Seesaw Model." In: *JHEP* 03 (2013). [Erratum: JHEP 05, 049 (2013)], p. 150. DOI: 10.1007/JHEP03(2013)150. arXiv: 1301.3453 [hep-ph].

[295] Morad Aaboud et al. "Search for charged Higgs bosons decaying via $H^{\pm} \to \tau^{\pm}\nu_{\tau}$ in the τ+jets and τ+lepton final states with 36 fb^{-1} of pp collision data recorded at $\sqrt{s} = 13$ TeV with the ATLAS experiment." In: *JHEP* 09 (2018), p. 139. DOI: 10.1007/JHEP09(2018)139. arXiv: 1807.07915 [hep-ex].

[296] "Updated measurements of the Higgs boson at 125 GeV in the two photon decay channel." In: (Mar. 2013).

[297] A. Arhrib, R. Benbrik, M. Chabab, G. Moultaka, and L. Rahili. "Higgs boson decay into 2 photons in the type~II Seesaw Model." In: *JHEP* 04 (2012), p. 136. DOI: 10.1007/JHEP04(2012)136. arXiv: 1112.5453 [hep-ph].

[298] Zhaofeng Kang, Jinmian Li, Tianjun Li, Yandong Liu, and Guo-Zhu Ning. "Light Doubly Charged Higgs Boson via the WW^* Channel at LHC." In: *Eur. Phys. J. C* 75.12 (2015), p. 574. DOI: 10.1140/epjc/s10052-015-3774-1. arXiv: 1404.5207 [hep-ph].

[299] R. Barate et al. "Search for pair production of longlived heavy charged particles in e+ e- annihilation." In: *Phys. Lett. B* 405 (1997), pp. 379–388. DOI: 10.1016/S0370-2693(97)00715-6. arXiv: hep-ex/9706013.

[300] P. Abreu et al. "Search for heavy stable and longlived particles in e+ e- collisions at s**(1/2) = 189-GeV." In: *Phys. Lett. B* 478 (2000), pp. 65–72. DOI: 10.1016/S0370-2693(00)00265-3. arXiv: hep-ex/0103038.

[301] G. Abbiendi et al. "Search for stable and longlived massive charged particles in e+ e- collisions at s**(1/2) = 130-GeV to 209-GeV." In: *Phys. Lett. B* 572 (2003), pp. 8–20. DOI: 10.1016/S0370-2693(03)00639-7. arXiv: hep-ex/0305031.

[302] David G. Cerdeño, Victor Martín-Lozano, and Osamu Seto. "Displaced vertices and long-lived charged particles in the NMSSM with right-handed sneutrinos." In: *JHEP* 05 (2014), p. 035. DOI: 10.1007/JHEP05(2014)035. arXiv: 1311.7260 [hep-ph].

[303] Georges Aad et al. “Search for long-lived, heavy particles in final states with a muon and multi-track displaced vertex in proton-proton collisions at $\sqrt{s} = 7$ TeV with the ATLAS detector.” In: *Phys. Lett. B* 719 (2013), pp. 280–298. DOI: 10.1016/j.physletb.2013.01.042. arXiv: 1210.7451 [hep-ex].